CLIMATE TRANSITIONS ACROSS THE CENOZOIC: INSIGHT FROM ELEMENTAL

RATIOS IN BENTHIC FORAMINIFERA AND MARINE GASTROPODS

by

SINDIA MARIA SOSDIAN

A Dissertation submitted to the

Graduate School-New Brunswick

Rutgers, The State University of New Jersey

in partial fulfillment of the requirements

for the degree of

Doctor of Philosophy

Graduate Program in Oceanography

written under the direction of

Yair Rosenthal

and approved by

Yair Rosenthal_____

Anthony Broccoli_____

Ken Miller_____

Jim Wright_____

Maureen Raymo_____

New Brunswick, New Jersey

[October, 2008]

ABSTRACT OF THE DISSERTATION

CLIMATE TRANSITIONS ACROSS THE CENOZOIC: INSIGHT FROM

ELEMENTRAL RATIOS IN BENTHIC FORAMINIFERA AND MARINE

GASTROPODS

By SINDIA MARIA SOSDIAN

Dissertation Director:
Yair Rosenthal

The Cenozoic climate record derived from the oxygen isotope ratios of benthic

foraminifera ($\delta^{18}O_b$) displays several, short term steps signifying the glaciation of

Antarctica (~33.7 Ma) and the development (~2.7 Ma) and intensification (~0.9 Ma) of

large-scale northern hemisphere glaciation (NHG), termed hereafter the late Pliocene

transition (LPT) and mid-Pleistocene transition (MPT), respectively. The interpretation

of the $\delta^{18}O_b$ record, which is controlled by both temperature and the oxygen isotopic

composition of seawater (δ_{ω}), is, however, not straightforward.

In the work presented here, I:(1) used Mg/Ca benthic foraminiferal

paleothermometry paired with $\delta^{18}O_b$ to construct high resolution records of deep ocean

temperature and global ice volume to understand the underlying mechanisms of Pliocene-

Pleistocene climate transitions and (2) developed a new salinity independent

paleothermometer based on Sr/Ca ratios in marine gastropods and examined its potential

for Cenozoic low-latitude sea surface temperature reconstructions and

I constructed and applied a new regional Mg/Ca-temperature calibration based on

downcore Mg/Ca variations to encompass changes in temperature and carbonate

saturation in deep Atlantic Ocean. The new, high resolution bottom water temperature record from North Atlantic Deep Sea Drilling Project site 607 indicates that the deep ocean cooled across both the LPT and MPT. The cooling across the MPT preconditioned the high latitudes for ice-sheet growth by modifying heat transport through changes in meridional temperature gradients. Across the LPT, the mean trend in sea level decreased by 20±25m whereas the MPT is associated with an increase in glacial-interglacial amplitude of sea level. I propose that the MPT is related to a change in ice sheet dynamics, specifically growth of thicker ice sheets, and that a threshold response to high-latitude cooling is not sufficient to explain the MPT.

The Sr/Ca- temperature calibration study, based on the marine gastropod *Conus ermineus*, shows that strontium incorporation into the aragonitic gastropod shell is most likely driven by a temperature influence on growth rate. To minimize the ontogenetic effect, I separated the Sr/Ca-temperature calibration into juvenile and adult growth stages. The application of the new low-latitude paleothermometer to fossil specimens shows that the low latitudes cooled along with high latitudes throughout the Cenozoic.

Acknowledgements

Table of Contents

Lists of tables

List of Figures

Chapter 1

1. Introduction

Fundamental to reconstructing past climate and understanding Cenozoic climate transitions is our ability to extract paleotemperatures from marine carbonates. The oxygen isotope composition of marine carbonates has been the most quantitative proxy of Cenozoic climate change. Oxygen isotope ratios in marine carbonates, developed as a paleotemperature proxy in the 1950s, provided the first glimpse into the temperature evolution of Earth's climate (Urey, 1947; Epstein, 1953; Emiliani, 1995). A decade later, Shackleton (1967) determined that the Pleistocene sedimentary oxygen isotope record, in actuality, mainly reflects variations in the oxygen isotope composition of sea water, largely determined by changes in global ice volume. Since the discovery of Shackleton, the $\delta^{18}O$ record has primarily been interpreted as a record of changes in global ice volume.

The benthic foraminiferal oxygen isotope record ($\delta^{18}O_b$), a benchmark tool, has been used to understand the nature and timing of Cenozoic climate transitions. Benthic foraminifera are insulated from regional and latitudinal changes in temperature and salinity which makes them a valuable recorder of global climate change. The utility of this established proxy has enabled paleoceanographers to document the evolution of global glaciations over the past 65 Myrs (Fig 1.1) (Miller et al., 1987; Zachos et al., 2001). However, the $\delta^{18}O_b$ record is not solely a signal of global ice volume variations as proposed by Shackleton; it is controlled by temperature and the isotopic composition of the seawater (δ_ω) from which marine carbonates were formed.

Prior to the end of the Eocene (~34 Ma), the Earth was possibly ice free and the variations in $\delta^{18}O_b$ record primarily reflect temperature during this time (Lear et al., 2000). Following the Eocene, however, major ice sheet expansion in Antarctica occurred (Miller et al., 1991; Zachos et al., 1992) which complicated the interpretation of the $\delta^{18}O_b$ record. Without the assumption of an ice free world, it is difficult to determine the partitioning of the $\delta^{18}O_b$ between temperature and ice volume across major climate transitions, such as growth of a large ice sheet on Antarctica across the Eocene/Oligocene boundary and intensification of northern hemisphere glaciation during the late Pliocene. Therefore, an independent temperature proxy is necessary to separate the temperature and ice-volume components and understand the relationship between development of the cryosphere and the mean climate state. Paired with the $\delta^{18}O_b$ record, a salinity-independent paleothermometer would allow determination of both past temperatures and changes in local and global δ_ω (i.e. local salinity and continental ice volume).

Trace metals incorporated into the shells of calcium carbonate secreting organisms provide a useful suite of geochemical tracers for reconstruction of past environments. Past changes in seawater temperature have been documented by changes in trace metal to calcium ratios of calcite and aragonite. Inorganic precipitation experiments show that strontium uptake into inorganic aragonite decreases with increasing temperature (Kinsman and Holland, 1969). Likewise, laboratory experiments show that magnesium uptake into inorganic calcite increases with increasing temperature (Katz, 1973; Hartley and Mucci, 1996). Empirical and culture studies have shown this relationship between Sr/Ca and Mg/Ca ratios and temperature in mollusks and foraminifera, respectively (Dodd, 1965; Nurnberg et al., 1996). Mollusks, due to their

fast growth rates, have the potential to a high-resolution archive of past surface ocean temperature. In chapter four, I highlight the potential of marine gastropods as a powerful archive of low-latitude temperature variations.

Gastropods are long-lived, deposit their shells at high rates, and are ubiquitous in the tropical surface water. *Conus sp.* are present in the fossil record throughout the Cenozoic and thus may provide information on the tropical surface ocean response to Cenozoic climate change. Geochemical analysis of growth bands provides a high resolution window into changes in mean annual temperature with replication and temperature seasonality, in contrast to planktonic foraminifera. Previously, the stable isotope composition of *Conus sp.* have been used to document a cooling and increase in seasonality in association with the transition from greenhouse to icehouse (Kobashi et al., 2001; Kobashi and Grossman, 2003; Kobashi et al., 2004). However, previous studies may be biased by estimates of changes in the oxygen isotopic composition of seawater. Sr/Ca ratios in marine gastropods, an independent temperature proxy, would allow for determination of local temperature and δ_ω changes. Several studies on calcitic and aragonitic mollusks have documented a relationship between Sr/Ca ratios and temperature (Dodd, 1965; Palacios et al., 1994). However, it has been suggested that biological effects, such as growth rate and ontogeny, play a role in strontium incorporation into the mollusk shell (Gillikin et al., 2005). In chapter four, I explore the utility of Sr/Ca ratios in the marine gastropod, *Conus ermineus*, as an independent low latitude paleothermometer.

Trace metal ratios in foraminifera, specifically Mg/Ca, have been utilized as temperature proxy to aid in interpretation of the oxygen isotope record. The use of

Mg/Ca ratios as a paleotemperature proxy was first established in the planktonic foraminifera through core-top, sediment trap, and culturing studies (Nurnberg et al., 1996; Lea et al., 1999; Anand et al., 2003). Over the last ten years, Mg/Ca ratios in benthic foraminifera have emerged as powerful deep ocean temperature proxy. This proxy has been successfully used in Quaternary and Cenozoic climate studies to investigate glacial-interglacial changes in deep ocean temperature, changes in ocean circulation and long-term shifts in global ice volume (Martin et al., 2002; Lear et al., 2000; Lear et al., 2003). Global core-top calibrations show that relationship between Mg/Ca and temperature is best explained with an exponential fit (Rosenthal et al., 1997; Lear et al., 2002). However, recent advances suggest that a linear approximation best describes the relationship between Mg/Ca and temperature in benthic foraminifera (Marchitto et al., 2007). Although temperature exerts a primary control on Mg incorporation into foraminiferal shells, changes in carbonate saturation have been shown to exert a secondary influence on shell Mg/Ca (Martin et al., 2002; Rosenthal et a., 2006; Elderfield et al., 2006; Jordan, 2008). In chapter two, I examine downcore Mg/Ca records from Atlantic and Pacific Oceans to construct a regional specific Mg/Ca-temperature calibration that reflects both changes in temperature and carbonate saturation. I apply the new Mg/Ca-temperature calibration to reconstruct changes in deep ocean temperature, and paired with $\delta^{18}O_b$, changes in global ice volume across the Pliocene-Pleistocene.

The benthic foraminiferal oxygen isotope record ($\delta^{18}O_b$) displays a pronounced shift from 3.2 to 2.7 Ma which marks the late-Pliocene transition (LPT) where glaciations intensified evident by a substantial increase in ice rafted debris in the northern North

Atlantic at 2.7 Ma (Fig. 1.1). From the late Pliocene to early Pleistocene (2.7 to 1.25 Ma), the cyclical waxing and waning of ice sheets was dictated primarily by orbitally driven changes in insolation at the 41-kyr period. The mid-Pleistocene transition (Schrag et al.), from 1.2 to 0.75 Ma represents the switch from 41-kyr, small amplitude to 100-kyr, large amplitude glacial-interglacial cycles. Following the MPT, from 0.7 Ma to the present, ice sheets varied predominately at the 100-kyr period and the amplitude of $\delta^{18}O_b$ variability increased implying growth of larger ice sheets during glacial maxima.

The development of large-scale northern hemisphere glaciation has been linked to a threshold response to a global cooling driven by tectonic drawdown of pCO_2, emergence of the Panama Isthmus, and polar ocean stratification (Ruddiman et al., 1988; Haug and Tiedemann, 1998; Sigman et al., 2004). Mechanisms to explain the MPT invoke a threshold response to a global cooling attributed to a secular decrease in atmospheric pCO_2, changes in sea ice growth, and/or ice sheet dynamics (Clark et al., 1998; Raymo, 1997; Ruddiman et al., 1988; Tziperiman et al., 2003).

Understanding the mechanisms to explain climate transitions across the Pliocene-Pleistocene, specifically the late Pliocene and mid-Pleistocene transition, relies on separation of the benthic oxygen isotope record into its temperature and ice volume components. Here, I construct a deep ocean temperature record from Mg/Ca ratios in benthic foraminifera from Deep Sea Drilling Project site 607 located in the subpolar North Atlantic which monitors surface conditions in the polar latitudes and deep water circulation. I examine the evolution of deep ocean temperature and ice volume and their temporal relationships on orbital and long-time scales to understand the causes of both transitions. In Chapter three, I compare the new, orbitally resolved records with

paleoclimatic records to gain more perspective on the mechanisms behind the mid-

Pleistocene transition.

1.1 References

Anand, P., Elderfield, H. and Conte, M.H., 2003. Calibration of Mg/Ca thermometry in planktonic foraminifera from a sediment trap time series. *Paleoceanography*, 18: 1050, doi:10.1029/2002PA000846.

Clark, P.U., Archer, D., D. Pollard, J.D. Blum, J.A. Rial, V. Brovkin, A.C. Mix, N.G. Pisias, and M. Roy, 2006. The Middle Pleistocene transition: Characteristics, mechanisms, and implications for long-term changes in atmospheric pCO2. *Quaternary Science Reviews*, 25: 3150-3184.

Clark, P.U. and Pollard, D., 1998. Origin of the Middle Pleistocene transition by ice sheet erosion of regolith. *Paleoceanography*, 13: 1-9.

Dodd, J.R., 1965. Environmental control of strontium and magnesium in Mytilus. *Geochim. Cosmochim. Acta*, 29: 385-398.

Elderfield, H., Yu, J., Anand, P., Kiefer, T. and Nyland, B., 2006. Calibrations for benthic foraminiferal Mg/Ca paleothermometry and the carbonate ion hypothesis. *Earth and Planetary Science Letters*, 250(3-4): 633-649.

Emiliani, C., 1955. Pleistocene temperatures. *J. Geol.*, 63: 538-578.

Epstein, S., Buchsbaum, R., Lowenstam, H.A. and Urey, H.C., 1953. Revised carbonate-water isotopic temperature scale. *Geol. Soc. Am. Bull*, 64: 1315-1325.

Gillikin, D.P. et al., 2005. Strong biological controls on Sr/Ca ratios in aragonitic marine bivalve shells. *Geochemistry Geophysics Geosystems*, 6.

Hartley, G. and Mucci, A., 1996. The influence of pCO2 on the partitioning of magnesium in calcite overgrowths precipitated from artificial seawater at 25° and 1atm total pressure. *Geochimica et Cosmochimica Acta*, 60: 315-324.

Haug, G. and Tiedemann, R., 1998. Effect of the formation of the isthmus of panama on the Atlantic Ocean thermohaline circulation. *Nature,* 393: 673-676.

Jordan, K., 2008. Mg/Ca-Temperature Calibration, Master's thesis, Oceanography. Rutgers, The State University of New Jersey, New Brunswick.

Katz, A., 1973. The interaction of magnesium with calcite during crystal growth at 25-90°C and one atmosphere. *Geochimica et Cosmochimica Acta*, 37: 1563-1586.

Kinsman, D.J. and Holland, H.D., 1969. The co-precipitation of cations with CaCO3: IV. The co-precipitation of Sr2þ with aragonite between 168 and 96 8C. *Geochimica et Cosmochimica Acta*, 33: 1-17.

Kobashi, T. and Grossman, E.L., 2003. The oxygen isotopic record of seasonality in Conus shells and its application to understanding Late Middle Eocene (38 Ma) climate. *Paleontological Research*, 7(4): 343-355.

Kobashi, T., Grossman, E.L., Dockery, D.T. and Ivany, L.C., 2004. Water mass stability reconstructions from greenhouse (Eocene) to icehouse (Oligocene) for the northern Gulf Coast continental shelf (USA). *Paleoceanography*, 19(1).

Kobashi, T., Grossman, E.L., Yancey, T.E. and Dockery, D.T., 2001. Reevaluation of conflicting Eocene tropical temperature estimates: Molluskan oxygen isotope evidence for warm low latitudes. *Geology*, 29(11): 983-986.

Lea, D.W., Mashiotta, T.A. and Spero, H., 1999. Controls on magnesium and strontium uptake in planktonic foraminifera determined by live culturing. *Geochimica et Cosmochimica Acta*, 63: 2369-2379.

Lear, C.H., Y. Rosenthal, and N. Slowey, 2002. Benthic foraminiferal Mg/Capaleothermometry: A revised core-top calibration. *Geochimica et Cosmochimica Acta*, 66: 3375-3387.

Lear, C.H., Rosenthal, Y. and Wright, J.D., 2003. The closing of a seaway: Ocean water masses and global climate change. *Earth Planetary Science Letters*, 210: 425-436.

Martin, P.A. et al., 2002. Quaternary deep sea temperature histories derived from benthic foraminiferal Mg/Ca. *Earth and Planetary Science Letters*, 198(1-2): 193-209.

Marchitto, T.M., Bryan, S.P., Curry, W.B. and McCorkle, D.C., 2007. Mg/Ca temperature calibration for the benthic foraminifer Cibicidoides pachyderma. *Paleoceanography*, 22(1): doi:10.1029/2006PA001287.

Miller, K.G., Fairbanks, R.G., and Mountain, G.S., 1987. Tertiary oxygen isotope synthesis, sea level history, and continental margin erosion. *Paleoceanography*, 2: 1-19.

Miller, K.G. et al., 2005. The Phanerozoic record of global sea-level change. *Science*, 312: 1293-1298.

Nürnberg, D., Bijma, J. and Hemleben, C., 1996. Assessing the reliability of magnesium in foraminiferal calcite as a proxy for water mass temperature. *Geochimica et Cosmochimica Acta*, 60: 803–814.

Palacios, R., Orensanz, J.M. and Armstrong, D.A., 1994. Seasonal and lifelong variation of Sr/Ca ratio in shells of Mya arenaria from Grays Harbor- an ancillary criterion in demographic studies. *Estuarine Coastal and Shelf Science*, 39(4): 313-327.

Raymo, M.E., Ruddiman, W.F. and Froelich, P.N., 1988. Influence of Late Cenozoic Mountain Building on Ocean Geochemical Cycles. *Geology,* 16: 649-653.

Raymo, M.E., Ruddiman, W.F., Backman, J., Clement, B.M. and Martinson, D.G., 1989. Late Pliocene variation in Northern Hemisphere ice sheets and North Atlantic deep circulation. *Paleoceanography*, 4: 413-446.

Raymo, M.E., 1997. The timing of major climate terminations. *Paleoceanography*, 12: 577-585.

Rosenthal, Y., Boyle, E.A. and Slowey, N., 1997. Environmental controls on the incorporation of Mg, Sr, F and Cd into benthic foraminiferal shells from Little Bahama Bank: prospects for thermocline paleoceanography. *Geochimica et Cosmochimica Acta*, 61: 3633-3643.

Rosenthal, Y., Lear, C.H., Oppo, D.W. and Linsley, B.K., 2006. Temperature and Carbonate Ion Effects on Mg/Ca and Sr/Ca Ratios in Benthic Foraminifera: The Aragonitic Species Hoeglundina elegan. *Paleoceanography*, 21: doi: 10.1029/2005PA001158.

Ruddiman, W.F., M.E. Raymo, D.G. Martinson, B.M. Clement, and J. Backman, 1989. Mid-Pleistocene evolution of Northern Hemisphere climate. *Paleoceanography*, 4: 353-412.

Ruddiman, W.F. and Raymo, M.E., 1988. Northern hemisphere climate regimes during the past 3 Ma: possible tectonic connections. In: N.J. Shackleton, R.G. West, and D.Q. Bowen (Editor), The Past Three Million Years: Evolution of Climatic Variability in the North Atlantic Region. University Press, Cambridge, pp. 227-234.

Shackleton, N.J., 1967. Oxygen isotope analyses and Pleistocene temperatures re-assessed. *Nature,* 215: 15-17.

Sigman, D.M., Jaccard, S.L. and Haug, G.H., 2004. Polar ocean stratification in a cold climate. *Nature*, 428: 59-63.

Tziperiman, E. and Gildor, H., 2003. On the mid-Pleistocene transition to 100- kyr glacial cycles and the asymmetry between glaciation and deglaciation times. *Paleoceanography*, 18.

Urey, H.C., 1947. The thermodynamic properties of isotopic substances. *J. Chem. Soc*: 562-581.

Zachos, J., Pagani, M., Sloan, L., Thomas, E. and Billups, K., 2001. Trends, rhythms, and aberrations in global climate 65 Ma to present. *Science*, 292(5517): 686-693.
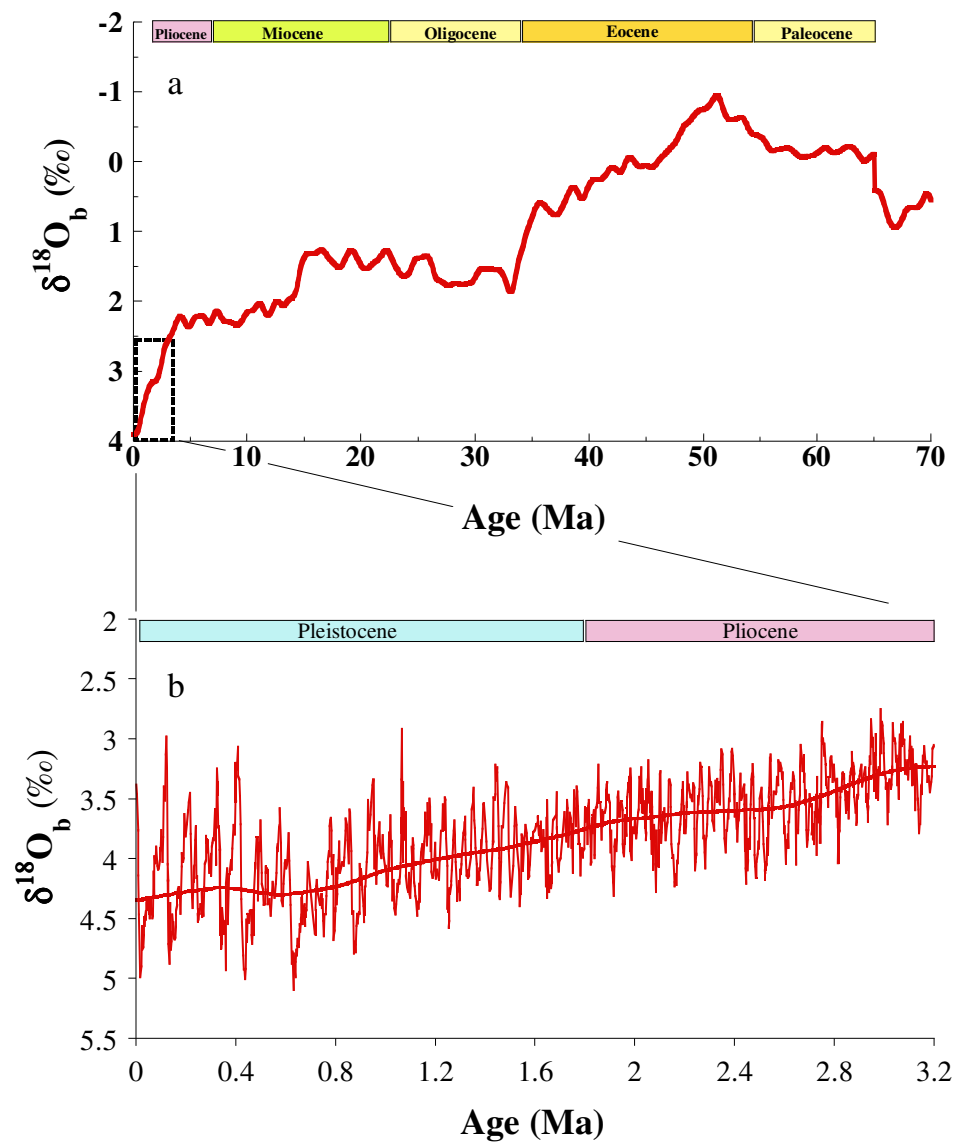
Figure 1.1 (a) Cenozoic global stacked benthic foraminiferal oxygen isotope record as presented by Miller et al., (2005). (b) Pliocene-Pleistocene ODP site 846 benthic foraminiferal oxygen isotope record, data from Shackleton et al., (1995) and Mix et al., (1995).

Chapter 2

2. Deep Sea Temperature and Ice Volume Changes across Pliocene-Pleistocene Climate Transitions

2.1. Abstract

During the Plio-Pleistocene, Earth underwent profound changes which led to the development (~2700 ka) and intensification (~900 ka) of large-scale northern hemisphere glaciation recorded in benthic foraminiferal oxygen isotope ($\delta^{18}O_b$) record as an increase in the mean trend, amplitude of glacial cycles, and the late Pleistocene shift in periodicity. The late Pliocene transition (LPT) has been postulated to be a threshold response to a long-term global cooling, attributed to tectonic drawdown of pCO_2, and the mid-Pleistocene transition (Schrag et al.) has been hypothesized to be either a function of a similar threshold response to a global cooling or a change in ice sheet dynamics. Here we present a new, high-resolution record of deep ocean temperature derived from benthic foraminiferal Mg/Ca from North Atlantic DSDP site 607 to examine temporal changes in temperature and global ice volume. Our record shows that temperature variations are a significant portion of the $\delta^{18}O_b$ signal and that the deep ocean cooled across the LPT and MPT by 2°C and 1.3°C, respectively. The nature of ice-volume response to each transition is markedly different. Across the LPT, the Mg/Ca-derived sea level record shows a decline by 20±25 m whereas across the MPT there is no discernible change in the mean trend but rather an increase in the glacial-interglacial amplitude of sea level. Our data indicate that the LPT is related to a glaciation threshold response to a global cooling. The cooling across the MPT preconditioned the high latitude climate for entry

into the 100-kyr climate regime but is not sufficient to explain the MPT which requires

an additional shift in ice sheet dynamics.

2.2. Introduction

The Plio-Pleistocene represents an epoch when Earth's climate underwent dramatic

changes. The benchmark tool paleoceanographers use to understand the timing and

nature of climate transitions is variations in oxygen isotopes recorded in calcitic tests of

benthic foraminifera ($\delta^{18}O_b$). Benthic oxygen foraminiferal isotope records however

reflect a combination of in situ changes in ocean temperature and global changes in the

$\delta^{18}O$ composition of seawater (δ_ω) resulting primarily from growth and decay of

continental ice sheets. However, resolving the relative contributions of each of these

components to the $\delta^{18}O_b$ is not straightforward. A pronounced shift in the $\delta^{18}O_b$, from

3200 to 2700 ka, marks the LPT from warm, relatively ice free conditions to a cooler,

more glaciated climate in the northern hemisphere linked to a threshold response to

global cooling (Ruddiman et al., 1988) (Fig. 2.1). Following major ice-sheet expansion,

41-kyr glacial-interglacial cycles, paced by obliquity driven changes in insolation,

dominated the climate system. Across the mid-Pleistocene, from 1200 to 700 ka, the

$\delta^{18}O_b$ record exhibits a shift in the dominant periodicity from 41-kyr to ~100-kyr and an

increase in amplitude representing intensification of northern hemisphere glaciation

(NHG) and/or a deep-ocean cooling (Shackleton and Opdyke, 1976). The development

of large-scale NHG has been linked to a threshold response to a shift in background

climate state driven by a decrease in pCO_2 (Raymo et al., 1988), uplift of the isthmus of

Panama (Haug and Tiedemann, 1998), and polar ocean stratification (Haug et al., 1998;

Ruddiman et al., 1988). Mechanisms to explain the MPT invoke a threshold response to

a global cooling attributed to a secular decrease in atmospheric pCO_2 (Raymo, 1997), changes in sea ice growth (Tziperiman and Gildor, 2003), and/or ice sheet dynamics (Clark et al., 1998; Raymo, 1997; Ruddiman et al., 1988; Tziperiman et al., 2003). Explanations for development and intensification of large-scale NHG hinge on the separation of the benthic oxygen isotope record into its temperature and ice volume components. The LPT hypotheses suggest that a global cooling accompanied the manifestation of glacial-interglacial variability in ice volume. The MPT hypotheses propose that the areal extent of ice sheets increased in association with a decrease in mean temperature across the MPT whereas the ice sheet dynamics supports the contention that ice sheets grew in height with a subsequent decrease in mean temperature. An independent deep ocean temperature record would allow us to understand the trajectory of temperature and ice volume in context of the proposed hypotheses.

Attempts to evaluate deep ocean temperature change derive mainly from oxygen isotope records (Emiliani, 1955; Shackleton, 1967; Labeyrie et al., 1987; Shackleton, 2000; Waelbroeck et al., 2002). An independent deep North Atlantic bottom water temperature (BWT) record, from Ostracod Mg/Ca shows an increase in average glacial-interglacial amplitude (Δ(G-I)) from 3.6°C during the late Pliocene 41-kyr glaciations to 4.5°C during the late Pleistocene 100-kyr glaciations in the deep North Alantic (Dwyer et al., 1995). The increase in Δ(G-I) reflects mainly a decrease in glacial temperatures which suggests that Pleistocene deep water was cooler than during the Pliocene. However, this BWT record is not continuous and covers only the late Pleistocene (0-220 ka) and the late Pliocene (2300 to 3200 ka). A continuous BWT record through the Plio-

Pleistocene, with the same resolution of the $\delta^{18}O_b$ record, is required to understand the trajectory of deep ocean temperature and its coherency and phase to $\delta^{18}O_b$.

Here I present the first continuous, high resolution deep sea temperature record of the late Pliocene-Pleistocene, using Mg/Ca ratios in benthic foraminifera. We use this record to deconvolve changes in the oxygen isotopic composition of seawater (δ_ω) and estimate ice volume variations and its temporal relationship with deep ocean temperature. Our record shows that temperature variations are a significant portion of the $\delta^{18}O_b$ signal and that the deep ocean cooled across both climate transitions. The nature of ice volume response to each transition is markedly different with a 20±25 m increase in the mean sea level across the LPT. The MPT represents an increase in the glacial-interglacial sea level amplitude (i.e. shift towards stronger glaciation and deglaciation cycles).

2.3. Methods

2.3.1. Anaytical Methods

Mg/Ca measurements were done at Rutgers University (New Brunswick, NJ), using Finnigan Element-XR inductively coupled plasma mass spectrometry (ICP-MS) following the analytical protocol detailed in Rosenthal et al., 1999. Repeated analysis of standard solutions with same elemental ratios (El/Ca) but changing Ca concentration ([Ca]=1.5 mM to 8 mM) were used to quantify and correct for matrix changes. Typical sample size included 3-15 benthic foraminifera specimens with sample weights ranging from 200-400 μg. However, in some intervals due to low abundance of benthic foraminifera sample weights were as low as 100 μg. Samples were chemically cleaned using the Cd-cleaning protocol from Boyle and Keigwin (1985/6) method modified for small sample analysis. To accommodate small sample sizes (<150 μg), the protocol was

modified slightly as follows: i) during the reducing step, the reducing reagent was diluted 1:2 and only 25 µl was added to small samples and 100 µl to all other samples, since $CaCO_3$ is slightly soluble in it and ii) small samples were omitted from the oxidizing step to prevent further dissolution. The reducing agent was prepared by adding 750 ul of anhydrous hydrazine to 10 ml of a citric acid/ammonia solution and then diluted with ammonium hydroxide to 20 ml.

A cleaning test was performed to determine whether modifying the reducing agent for small samples affects the absolute Mg/Ca values. Previously, it has been suggested that a stronger reducing agent dissolved the tests more vigorously and preferentially leaches Mg/Ca (Barker et al., 2003; Yu et al., 2006). Initially samples from intervals during 1.5 to 1.8 Myr were cleaned using a 1:4 dilution in the reducing step. The core was re-sampled during several intervals and samples were re-cleaned using a stronger reducing agent (1:2) to account the possible presence of an offset in Mg/Ca. This interval was chosen because a large amount of the samples analyzed were <.200 ug. There was a slight offset in Mg/Ca between samples measured with a strong (1:2) and weak (1:4) reducing solution (Table 2.1). To correct for a cleaning offset due to low sample weights, Mg/Ca data from the interval 1503 to 1801 kyr were adjusted by +0.1 mmol mol^{-1}.

Mn/Ca, Fe/Ca, Al/Ca, and Ti/Ca were used to screen samples for contamination due to diagenetic coating or detrital materials; Mn/Ca values exceeded the typical threshold of ~100 umol mol^{-1} (Boyle, 1983) for the entirety of the record (range 100 to 500 umol mol^{-1} depending on species) but do not covary with Mg/Ca. Samples with elevated values of Fe/Ca, Al/Ca and Ti/Ca (i.e. >2σ) were removed from the record. The

long-term reproducibility of Mg/Ca analysis was about 1% as determined by repeated

measurements of three consistency standards with Mg/Ca ratios ranging from 1.24 to

7.51 mmol mol-1. The precision of consistency standard with Mg/Ca of 1.25 mmol mol^{-1}

was ±1.24% (r.s.d); the precisions of consistency standards with Mg/Ca of 3.32 and 7.51

mmol mol^{-1} were ±1.16% and ±0.57%, respectively (Table 2.2; Fig. 2.2). Isotopic

measurements for *Chain* 82-24-23PC and DSDP site 607 were done at Rutgers

University, using an Optima mass spectrometer. Values are reported versus V-PDB

through the analysis of NBS19 with values of 1.95‰ and −2.20‰ for $\delta^{13}C$ and $\delta^{18}O$,

respectively. The precision of the isotope analyses is better than ±0.06‰ for $\delta^{13}C$ and

better than ±0.08‰ for $\delta^{18}O$.

2.3.2. Age Model and Time Series Analysis

DSDP site 607 sample depths have been converted to age by alignment of the benthic

oxygen isotope record to the LRO4 stacked $\delta^{18}O_b$ record giving a sampling resolution of

~3 ky (Lisiecki et al., 2005). For CHN82-23PC, sample depths taken every 5 cm have

been converted to age using a new *C. wuellerstorfi* oxygen isotope record from this core

(sampling resolution of ~2 ky). Core CHN82-23PC provides 165-kyr history with a

sedimentation rate of ~2 cm/kyr**.** Alignment of the benthic oxygen isotope record from

core CHN82-23PC to the LRO4 stacked benthic oxygen isotope record (Lisiecki et al.,

2005). Alignment was done visually by establishing ties points at peak interglacial and

glacial events.

The long-term trend was determined by applying a Gaussian filter with a cut-off

frequency of 400 kyr to all proxy records. To compute the average amplitude of glacial-

interglacial variability in temperature and δ_ω, I first defined the marine isotope stages (MIS) using the $\delta^{18}O_b$ record. Then I averaged downcore values in each MIS during three time intervals from the late Pliocene to present. The amplitude of glacial-interglacial variability was calculated by subtracting the interglacial from the glacial temperature estimates. Spectral analyses were completed on linearly detrended time series using the Arand software package from Brown University (available online at http://www.ngdc.noaa.gov/paleo/softlib/).

2.3.3. Oxygen Isotopes

Stable oxygen isotope records in benthic foraminifera are routinely used to reconstruct past changes in deep ocean temperature and continental ice volume. The Pleistocene benthic oxygen isotope record from DSDP site 607, a composite record of two benthic foraminifera species *Uvigerina* and *Cibicidoides*, was originally published by Ruddiman et al. (1989) and Raymo et al. (1989) and used to investigate changes in North Atantic climate. Ideally, each isotopic record is reconstructed from a single benthic foraminifera species, but due insufficient specimens of a single species available in time intervals, composite records consisting of species from different micro-habitats were utilized in the construction of DSDP site 607 $\delta^{18}O_b$ record. Foraminiferal shells can be offset from equilibrium due to vital effects and micro-habitat differences and an isotopic adjustment is applied to calibrate each species to isotopic equilibrium (Shackleton, 1974).

Since the original analysis of the oxygen isotope record, M. Raymo (*per. comm.*) noted that re-analysis of foraminiferal samples from DSDP site 607 results in a 0.2-0.3‰ offset (typically lighter than the original dataset). Part of this offset is attributable to

instrumentation, specifically reference gas contamination when measuring isotopes on the

Finnigan MAT 251 at Lamont-Doherty Earth Observatory (Ostermann and Curry, 2000)

and cannot be corrected at this late date. Additionally, part of the offset in the $\delta^{18}O_b$

record might also be related to the isotopic adjustment used in constructing a composite

$\delta^{18}O_b$ record from two species. The benthic foraminifera used in the original $\delta^{18}O_b$ record

dwell in different microhabitats, specifically within and on top of the sediments. The

epifaunal species, Cibicidoides, has been calibrated to equilibrium a constant 0.64 ‰

offset in $\delta^{18}O_b$. These inter-species corrections rely on assuming that the offsets are

constant in the temporal and spatial domain.

To determine the offset with time between the original dataset and the

foraminiferal shells used to reconstruct the Mg/Ca-deep ocean temperature record,

presented here, I re-analyzed certain intervals from the Pleistocene DSDP site 607 record.

Plotted in figure 2.3 is a comparison between the original and new stable isotope data

which shows that re-analysis of DSDP site 607 is offset from the original data. In certain

intervals, such as MIS 11 to 8, the offset is larger and more constant than the interval

from 500 to 2000 ka. For example, MIS 13-14 displays no offset between the original

and new data set, whereas across MIS 11 to 8 there is a systematic offset. This original

$\delta^{18}O_b$ record is offset, in the MIS 11 to 8 when comparing to other $\delta^{18}O_b$ records as well

(Fig. 2.4) which suggests that original data are offset due to reference gas contamination

and isotopic adjustment between species.

2.3.4. Mg/Ca-Temperature Calibration

The published calibration from Lear et al., (2002) indicated that there was an

exponential relationship (Mg/Ca=$0.867e^{.109*BWT}$) between *Cibicidoides* Mg/Ca and

temperature. However, the calibration relies heavily on *Cibicidiodes* Mg/Ca data from core-top Mg/Ca data that may be elevated due to authigenic processes or downslope transport (Marchitto et al., (2007). Recently, Marchitto et al., (2007) re-evaluated the calibration from 5 to 19°C with new core-top Mg/Ca data to determine the relationship, (exponential or linear) and sensitivity, between Mg/Ca and temperature. They proposed that a linear approximation best describes the Mg/Ca-temperature relationship following the equation Mg/Ca=1.2 + 0.116 *BWT for the benthic foraminifera *Cibicidoides pachyderma*.

The expected range of glacial-interglacial variability in BWT at DSDP site 607 is from -2 to 4°C based on results from previous studies (Dwyer et al., 1995; Adkins et al., 2002). Extrapolation of the Marchitto et al., (2007) calibration to the -2 to 4 temperature range predicts values for shell Mg/Ca from 1.0 to 1.7 mmol mol-1. Is the Marchitto et al., (2007) calibration applicable below the temperature calibration range (<5°C)? The *Cibicidoides* Mg/Ca core-top value from this study falls close to the value predicted by the Marchitto calibration (Fig. 2.5). Additionally, core-top Mg/Ca data from the Norwegian Seas and Gulf of Mexico fall along the Marchitto calibration which suggest that calibration captures the Mg/Ca-low temperature relationship (Jordan, 2008).

Below 5°C, in the low temperature end of the calibration, Martin et al., (2002) showed that non-temperature related effects, specifically carbonate saturation, affect shell Mg/Ca. Ceara rise core top data, which transects a large range in carbonate ion and small range in temperature, fall along a steeper trend than predicted from the calibration (Martin et al., 2002; Rosenthal et al., 1997; Russell, 1995). Elderfield et al., (2006) identified this relationship in a global calibration analysis and showed shell Mg/Ca

decreases with decreasing carbonate saturation following a 0.0086 mmol mol^{-1} change in Mg/Ca per umol kg^{-1} of ΔCO_3^{2-}. For purpose of this study, we construct a regional calibration that encompasses both changes in temperature and carbonate saturation.

To construct a regional calibration, we examine *Cibicidoides wuellerstorfi* and *Oridorsalis umbonatus* core-top and glacial Mg/Ca data from cores CHN82-23PC and ODP Site 846 (this study) and a previously published record Core M16772 (Martin et al., 2002) located in the western north Atlantic, eastern equatorial Pacific, and eastern equatorial Atlantic, respectively (Table 2.3). Amongst these sites, there is a large difference in carbonate saturation (~30 umol kg^{-1}) and a small offset in bottom water temperature (BWT) (~1.0ºC). We determine last glacial maximum (LGM) paleotemperatures by combining estimates of the oxygen isotope composition of seawater (δ_ω) derived from modeling pore-water fluids and benthic $\delta^{18}O$ data at each study site (δ_ωAtlantic=1.2‰ and δ_ωPacific=0.9‰ are assumed for the LGM, following Fairbanks and Matthews (1978) and Adkins et al. (2002).

We measured *Cibicidoides* Mg/Ca values from Holocene and LGM time intervals for all locations. However, the abundance of *Oridorsalis* in the most recent glacial-interglacial cycle is low in core *Chain* 82-24-23PC, thus Mg/Ca values from Marine Isotope Stage (MIS) 5e and 6 are used. In contrast, abundance of this species in ODP site 846 is high across the last glacial cycle and Mg/Ca values from the HL (Holocene) and LGM are used. *Cibicidoides* and *Oridorsalis sp.* interglacial Mg/Ca values decrease from the Atlantic to the Pacific by ~0.6 mmol mol^{-1} (Fig. 2.6). In the Atlantic, *Cibicidoides* CHN82-23PC Mg/Ca is offset from M16772 Mg/Ca by ~0.34 mmol mol^{-1} which reflects the difference in temperature (ΔT=1.2°C) and carbonate saturation (d(ΔCO_3^{2-})=28 umol

kg^{-1}) between sites. The offset in Mg/Ca (ΔMg/Ca) is the sum of Mg/Ca attributable to temperature (ΔMg/Ca$_{BWT}$=0.05, assuming 0.12 change in Mg/Ca per °C using the calibration of Marchitto et al., (2007)) and to carbonate saturation (ΔMg/Ca$_{\Delta CO32}$=0.16, assuming 0.0086 change in Mg/Ca per ΔCO_3^{2-} umol kg^{-1} from Elderfield et al., (2006)) which combined, does not account for the total change in Mg/Ca by ~0.1 mmol mol^{-1} or ~1°C temperature equivalent. A comparable offset is evident between the Atlantic (M16772) and Pacific (846) intergalcial Mg/Ca data for both *Cibicidoides* and *Oridorsalis* which is related to a similar combination of temperature and carbonate saturation. The total interglacial Mg/Ca offset of 0.1 mmol mol^{-1} that is unaccounted for between sites is related to differences in analytical method, standardization, and foraminifera cleaning and reflects the temperature uncertainty of the calibration; the uncertainty (±1°C) of the downcore Mg/Ca-temperature calibration gives an uncertainty of ±25 m (1SD) when calculating sea level variations.

The Ceara Rise Mg/Ca core-top data (Martin et al., 2002; Rosenthal et al., 1997; Russell, 1995), plotted in figure 2.6, transects the difference in interglacial Mg/Ca between sites. The Ceara Rise core-tops are bathed in similar water masses as the core sites, specifically upper limb NADW (*Chain* 82-24-23PC), lower limb NADW (M16772), and southern source waters (ODP site 846), and hence span different carbonate saturation states and a small temperature range. The correspondence in difference between ΔCO_3^{2-} and Mg/Ca between Ceara Rise core-top data and CHN82-23PC, M16772, and 846 interglacial data supports the idea that changes in carbonate saturation are causing the offset in Mg/Ca between sites.

Linear equations based on *Cibicidoides* Holocene and LGM Mg/Ca values at each site were calculated and have a range of slopes (0.09-.15 mmol mol^{-1} per ºC). In the Atlantic, both cores CHN82-23PC and M16772 give steeper slopes than in the Pacific. During glacial cycles, at sites CHN82-23PC and M16772, changes in water mass variability and deep ocean carbon sequestration have been hypothesized to decrease the carbonate saturation of the deep North Atlantic Ocean (Boyle, 1985/6; Crowley, 1985). A decrease in the seawater calcite saturation state is predicted to lower the glacial Mg/Ca (Elderfield et al., 2006; Martin et al., 2002). Evidence from $CaCO_3$ preservation, foraminiferal shell weight, planktonic Mg/Ca, benthic Mg/Ca, Zn/Ca, and B/Ca studies indicate that the glacial deep North Atlantic ocean (>3 km) was more undersaturated by about 15-25 umol kg^{-1} than the Holocene, whereas the deep Pacific ocean (>3 km) was more saturated by about 5 umol kg^{-1} (Barker et al., 2002; Elderfield et al., 2006; Marchitto et al., 2002). In the Atlantic, the decrease in ΔCO_3^{2-} acts to decrease LGM Mg/Ca values and then increase the slope associated with the linear equations, wheras the Pacific slope is closer to published calibrations (Lear, 2002; Marchitto et al., 2007).

Expected LGM Mg/Ca values, derived from assuming a 0.12 change in Mg/Ca per °C (from Marchitto et al., 2007) to convert BWT to Mg/Ca, fall higher than the observed Mg/Ca (Table 2.2). Linear equations between interglacial and expected Mg/Ca values gives a shallower slope which is in close agreement with the *C*. pachyderma Mg/Ca-temperature calibration (Mg/Ca=0.116*BWT+1.20) from Marchitto et al., (2007). Core-top data from two locations, the Norwegian Seas (~-1°C) and Gulf of Mexico (~4°C), homothermal sections where only $\Delta CO3$ varies in a saturated range, generated by Kate Jordan (2008) fall along the linear equation for the western north Atlantic

suggesting that a regional calibration for this site is applicable to reconstruct paleotemperatures.

The offset between observed and expected Mg/Ca is the change in Mg/Ca due to carbonate saturation changes. In core *Chain* 82-24-23PC, the offset between expected and observed Mg/Ca of 0.10 mmol mol^{-1} corresponds to a change of ~12 umol kg^{-1} in ΔCO_3^{2-} during the LGM which is slightly lower than the expected minimum value of 15 umol kg-1. The offset in Mg/Ca equates into 0.007 per umol kg^{-1} ΔCO_3^{2-} which is slightly lower than the carbonate ion correction (0.0086 mmol mol^{-1} per umol kg^{-1} ΔCO_3^{2-}) proposed by Elderfield et al., (2006) to account for the influence of carbonate saturation on Mg/Ca-temperature calibration for *C. wuellerstorfi.*

The downcore Mg/Ca record presented here is a composite of two species, *C. wuellerstorfi* and *O.umbonatus*, thus below we assess the *O. umbonatus* calibration in a similar manner. Glacial BWT estimates were determined in the same manner as above, assuming that the change in BWT across MIS 5e-6 is similar to MIS 1-2 in the North Atlantic. Linear equations between interglacial and glacial Atlantic Mg/Ca values give a steeper slope than the Pacific similar to *Cibicidoides* Mg/Ca data set. The offset in interglacial Mg/Ca values and slopes is related to the difference in temperature and carbonate saturation. Core-top calibrations from Lear et al., (2002) and Rathman et al., (2004) suggest a lower temperature sensitivity (11%) than from the observed data. The Atlantic slope which is based on Mg/Ca values from MIS 5e and 6 may be overestimated due to the substitute of H-LGM estimates of BWT change. For the downcore Mg/Ca record, we assume that the temperature sensitivity of *Cibicidoides* and *Oridorsalis*

Mg/Ca-temperature calibrations are similar, as previously thought from published core-top calibrations.

For the study site used here, I applied a *Cibicidoides* linear Mg/Ca-temperature calibration Mg/Ca=0.15*BWT + 1.15 based on the relationship from core-top and LGM Mg/Ca analysis. To convert Mg/Ca to temperature I applied a species adjustment determined from analysis of co-existing samples, to the Mg/Ca data by normalizing *O. umbonatus* to *C. wuellerstorfi*, and then using a single calibration to calculate the down-core temperature record similar to the approach applied to $\delta^{18}O_b$ data. The difference in Mg/Ca between species 0.16 mmol mol-1 (p<0.001) is determined by calculating the difference in the whole-core mean (Fig. 2.7).

To validate the application of the regional calibration and species adjustment, I applied the *ad hoc* Mg/Ca-temperature calibration to the downcore composite Mg/Ca record from CHN82-23PC and DSDP site 607. The BWT and $\delta^{18}O_b$ record are coherent in both trend and frequency which suggests that the Mg/Ca-BWT record is reproducing high latitude climate variability (Fig. 2.1). The range of glacial-interglacial temperature variability falls within the observed estimates from Mg/Ca in ostracodes (Dwyer et al., 1995) and oxygen isotope studies (Labeyrie et al., 1987; Lisiecki et al., 2005; Schrag, 2002; Waelbroeck et al., 2002). Using the Mg/Ca-BWT estimates, I calculated the δ_ω record and convert to sea level. I compared the Mg/Ca-derived bottom water temperature and sea level records to previously published records across the last 4 glacial-interglacial cycles. The Mg/Ca-derived sea level record resolves the glacial-interglacial variability, periodicity, and asymmetric pattern associated with large-scale glaciations (Fig. 2.8). The average glacial-interglacial amplitude from the 607 sea level record is ~140 m which

falls within a reasonable range of previously published records (90 to 140 m) (Dwyer et al., 1995; Lea et al., 2002; Peltier et al., 2006; Shackleton, 2000; Siddall et al., 2003; Waelbroeck et al., 2002; Yokoyama et al., 2000). The agreement of the Mg/Ca-derived BWT and sea level record with the current proxy evidence across late Pleistocene glacial-interglacial validates the use of a regional specific Mg/Ca-temperature calibration to reconstruct temperatures across the Pliocene-Pleistocene.

The construction of the new Mg/Ca-temperature calibration for the western North Atlantic encompass both changes in temperature and variations in carbonate saturation on glacial-interglacial timescales. However, long-term changes in deep ocean carbonate saturation across the Pliocene-Pleistocene might impact variations in the benthic foraminiferal Mg/Ca record. The Mg/Ca-bottom water temperature record shows a long-term cooling trend across the Pliocene-Pleistocene with two distinct cooling phases during the LPT (3.2 to 2.7 Ma) and MPT (1.2 to 0.8 Ma). To investigate whether variations in deep ocean carbonate saturation played a role in the long-term Mg/Ca variations, I compare a carbonate preservation record, based on planktonic foraminiferal preservation, to the Mg/Ca record, specifically focusing on the two cooling phases. Plotted in figure 2.9 is percentage whole test foraminifera (%WTF), an indicator of the corrosiveness of deep water masses from ODP site 927, located at the northeastern flank of the Ceara Rise at a 3300-m water depth. The Ceara Rise is an ideal site to monitor changes in past deep ocean carbonate saturation because it is sensitive to variations in deep ocean circulation. Across the LPT (from 3.1 to 2.7 Ma), the % WTF record shows no large swings and stays above 75% which suggests that carbonate saturation changes did not drive the decrease in Mg/Ca-BWT associatied with the development of large-

scale NH glaciation. Across the MPT (from 1.2 to 0.8 Ma), there is an increase in the amplitude of %WTF variations, mainly represented by a decrease in glacial values. The interglacial %WTF values remain relatively constant indicating that the interglacial Mg/Ca values were not affected by carbonate saturation values. The interglacial Mg/Ca-BWT trend shows ~1.0°C cooling which suggests that the high latitudes cooled in association with intensification of NH glaciation. However, the glacial cooling trend might be partially attributable to changes in carbonate saturation due to water mass variability. The glacial-interglacial variability of the %WTF records ranges from 60 to 25% during the late Pleistocene 100-kyr cycles. Previously, I highlighted that from the holocene to LGM carbonate saturation decreased by ~15 umol/kg. Thus a 35% decrease in %WTF during G-I cycles corresponds to a 15 umol/kg change in carbonate saturation of 15 umol/kg. Across the MPT, glacial %WTF values decreases from 50 to 20% which would equate to a decrease in carbonate saturation of ~13 umol/kg. Using the Mg/Ca-carbonate ion sensitivity proposed by Elderfield et al. (2006), this change in carbonate saturation corresponds to a decrease in Mg/Ca of 0.1 mmol/mol or ~0.7°C cooling. Part of the total glacial cooling of 1.5°C, across the MPT, is attributable to a decrease in carbonate saturation due to increased influence of AABW. The ad hoc calibration used in this study accounts for changes in carbonate saturation due to water mass variability and thus the cooling represents a temperature signal. Therefore, carbonate saturation variations partially affect the long-term Mg/Ca record but do not primarily drive the primary two cooling phases.

2.4.Results

BWTs in the deep North Atlantic Ocean were determined using Mg/Ca ratios in benthic foraminifera, epifaunal *Cibicidoides wuellerstorfi* and epi/infaunal *Oridorsalis umbonatus*. *Cibicidoides* and *Oridorsalis* species were previously used to determine Cenozoic deep-sea temperatures (Lear et al., 2000). The late Pliocene to late Pleistocene record (165-3200 ka) derives from Deep Sea Drilling Project (DSDP) site 607 (41°N, 32°W, 3427-m water depth) and for the late Quaternary interval the record is supplemented with measurements from nearby core *Chain* 82-24-23PC (43°N, 31°W, 3406-m water depth) (Fig.2.1). Continuous high-resolution stable isotope records from DSDP site 607 are available from Ruddiman et al. (1989) and Raymo et al. (1989). The age model for *Chain* 82-24-23PC is based on visual alignment to the $\delta^{18}O_b$ record from *Chain* 82-24-4PC (Boyle, 1985/6). Both sites are currently bathed in North Atlantic Deep Water (NADW, T=2.6°C, S=34.1‰$_o$) and are directly linked to the hydrographic conditions in the high latitudes (where NADW forms) which are potentially influenced by variations in NH glaciation. The relatively high sedimentation rate and location makes DSDP site 607 an ideal candidate to evaluate Pliocene-Pleistocene climate evolution at orbital scale resolution (3-ky).

Benthic foraminiferal Mg/Ca has been successfully applied downcore to reconstruct deep water temperatures on long (e.g. Cenozoic) and short (e.g. millennial-orbital) timescales using *Cibicidoides sp., Oridorsalis sp.,* and *Uvigerina sp.* (Billups, 2003; Billups et al., 2002; Lear et al., 2000; Marchitto et al., 2003; Martin et al., 2002). However, new Mg/Ca-temperature calibrations suggest that the sensitivity of the low-temperature end is distinct from the entire calibration range likely due to secondary

effects, such as the influence of carbonate saturation on shell Mg/Ca (Bryan et al., 2008; Elderfield et al., 2006; Lear, 2002; Marchitto et al., 2007; Martin et al., 2002; Raitzsch et al., 2008). To convert Mg/Ca ratios to paleotemperature, I apply a newly developed regional (i.e. western North Atlantic) Mg/Ca-temperature calibration (Mg/Ca=0.15*BWT+1.15) based on downcore variations in Mg/Ca that encompass both temperature and carbonate saturation effects.

The temperature record shows two major cooling events during the Plio-Pleistocene associated with late Pliocene and mid-Pleistocene climate transitions. These generally covary and are coherent with the $\delta^{18}O_b$ record in average trend, frequency, and amplitude (Fig. 2.1). In the late Pliocene, from 3200 to 2700ka, average Mg/Ca-derived BWT decreases from 4.5°C to 2.5°C into the early Pleistocene (Table 2.4). Concomitantly, the Δ(G-I) in BWT increases across the LPT from 2.0 to 3.3°C reflecting a decrease in both average interglacial (I) and glacial (G) temperatures. Spectral analysis of the BWT record from 1000-2500 ka shows a dominant 41-kyr peak, coherent with the $\delta^{18}O_b$ record signaling the development of obliquity paced G-I variability in the NH (Fig. 2.10).

The MPT is documented in the BWT record by a significant cooling from 1150 to 850ka, where average BWT decreases by from 2.5 to 1.2°C, and an increase in Δ(G-I) from 3.3°C to 3.9°C, at 900 ka, reflecting a decrease in average I and G temperatures. The dominant frequency shifts from 41-kyr to 100-kyr at the culmination of the cooling trend, around 700 ka. The fact that the cooling and amplitude increase preceeds the frequency shift suggests that the cooling might not solely drive the MPT (Fig. 2.1, 2.10). Across the last 450 ka, G-I BWT variability resembles the asymmetric, sawtooth pattern

of the $\delta^{18}O_b$ record with gradual cooling into glacial periods followed by abrupt warming across the deglaciation. The BWT shifts from present-day values during the late Holocene to near freezing temperatures during the last glacial maximum (LGM).

2.5.Discussion

The BWT record demonstrates that the increase in $\delta^{18}O_b$ at both transitions, previously thought to primarily reflect an increase in ice volume, is also a deep ocean cooling signal. Across the LPT, the cooling accounts for more than half of the positive isotopic shift wheras across the MPT it accounts for the entire shift in $\delta^{18}O_b$. The change in $\Delta(G-I)$ of deep water temperature, from 3.3 to 4.9°C, across the MPT corresponds with the increase in $\delta^{18}O_b$ amplitude, from 1.2 to 1.9 ‰. This means that the relative contributions of temperature and ice volume to the $\delta^{18}O_b$ record is about half of each signal which suggests that substantial portion of 100-kyr cycle in the $\delta^{18}O_b$ record is a deep-water temperature signal. The temperature signal is a significant portion of the $\delta^{18}O_b$ signal in the average trend and amplitude and implies that interpreting the $\delta^{18}O_b$ as exclusively an ice volume proxy is incorrect. These findings support the view from Emiliani (1955) and Shackleton (2000) that a significant portion of the Pleistocene $\delta^{18}O_b$ variability is related to deep ocean temperature changes.

Cross-spectral analysis between $\delta^{18}O_b$ and Mg/Ca-derived BWT reveals that BWT leads $\delta^{18}O_b$ in the late Pliocene-early Pleistocene by 3±2kyr in the obliquity band and in the late Pleistocene by 11±5 kyr in the eccentricity band (Fig. 2.11). Around 700 ka, the lead increases in association with the appearance of narrow band of low-frequency BWT variability. The lead, evident in the BWT record in the late Pleistocene, is in agreement with other deep ocean temperature studies (Dwyer et al., 1995; Martin et al.,

2002; Shackleton, 2000). The phase relationship between Mg/Ca-BWT and $\delta^{18}O_b$ represents the response time constant of ice-volume response to changes insolation. An increase in the phase relationship, coincident with the emergence of 100-kyr cycles, indicates there is a switch in the response time of the NH ice sheets related to a change in size of ice sheets (i.e. from smaller, stable to larger, unstable ice sheets). Prior to the MPT, ice sheets were smaller and responded linearily to summer insolation forcing; however, after 700 ka with the entry in the 100-kyr climate regime, ice sheets may have grown larger which delayed the response time, observed in the downcore record as a larger lead in Mg/Ca-BWT over $\delta^{18}O_b$.

The BWT record at DSDP site 607 reflects a combination of temporal changes in the temperature of source waters and water mass variability (Boyle, 1985/6; Ruddiman, 1989). During glacial periods, DSDP 607 is sensitive to water mass changes, specifically the influence of Antarctic Bottom Water (AABW), a relatively cold, fresh water mass while during interglacial periods NADW resides at DSDP 607 and is mainly reflecting high latitude temperature variations. The relative proportions of NADW (T=2.7°C) and AABW (T=0°C), plotted in figure 2.1 as %NADW at site 607 (2), vary on both long and orbital time scales. From 3100 to 2700 ka, NADW primarily resided at site 607 and the surface ocean temperature was higher due to strong meridional overturning circulation (Raymo, 1996). The decrease in BWT, across the LPT, which is evident in both interglacial and glacial temperatures, mainly reflects NH polar surface ocean temperature cooling related to initiation of NH glaciations. Following 2700 ka, NADW production decreased but AABW did not completely replace NADW and thus the increase in BWT amplitude primarily reflects the influence of waxing and waning of NH ice sheets. The

trend of LPT cooling contrasts with the results of Dwyer et al., (1995) who suggested that BWT did not change across the LPT. Furthermore, based on alkenone derived sea surface temperature record from the eastern equatorial Pacific, Lawrence et al., (2006) suggest that the tropics cooled monotonically from the Pliocene to the late Pleistocene in contrast to the results from the BWT record. The difference may stem from the variable response to NHG in the high and low latitudes.

From 1150 to 850 ka, the variability in BWT Δ(G-I) reflects a combination of high-latitude cooling and water mass variability. During glacial periods, %NADW at DSDP 607 decreases to less than 20% in some time intervals indicating the increased influence of AABW. The cooling in BWT across the MPT, reflects mainly high latitude variations and to a lesser extent NADW suppression. Both interglacial and glacial temperatures decreased across the MPT, which suggests that the cooling is a high-latitude signal. The larger decrease in glacial temperatures is likely related to an increase in AABW influence. The initial decrease in BWT precedes the decrease in %NADW by ~200 kyr and only contributes <0.5°C, assuming the glacial decrease of 1.3°C is a combination of high-latitude cooling and water mass changes and the interglacial decrease of 0.9°C is solely a high latitude cooling. The MPT cooling is in accord with surface ocean records from high latitudes and upwelling regimes which suggesting that it is capturing a global climate shift (Becquey et al., 2002; Lawrence et al., 2006; Marlow et al., 2000; McClymont et al., 2005; Ruddiman et al., 1988; Schefus et al., 2004).

Here, I show that to the first order changes in the Mg/Ca-BWT represent high latitude temperature variations and provide a means to extract the δ_ω component of the $\delta^{18}O_b$ record and evaluate global ice volume variations across the MPT and LPT. I use

the paleotemperature equation ($T=16.9-4.0(\delta^{18}O_b - \delta_\omega)$) from Shackleton (Shackleton, 1974) and assume that variations in δ_ω mainly reflect variations in global ice volume and a 10 m change in sea level equates to a 0.1‰ change in δ_ω (Fairbanks, 1989; Shackleton et al., 1973). To estimate sea level variability from the Mg/Ca-temperature and $\delta^{18}O_b$ record, I use the new $\delta^{18}O_b$ data for the interval from MIS 11 to 9 and assume a minimal offset in the rest of the original record. Propagation of uncertainties of this method derived from the Mg/Ca-benthic foraminiferal paleothermometry technique and stable isotope measurements allows determination of limitations of reconstructed changes in sea level. The regional Mg/Ca-temperature calibration constructed here has roughly a ±1°C uncertainty and the precision on $\delta^{18}O_b$ analyses is ±0.5°C. Propagation of the above uncertainties implies an uncertainty in the reconstructed sea level record of ±25 m.

To evaluate long-term and glacial-interglacial changes in sea level, I apply a 3-point moving average to the raw sea level data (Fig. 2.12). The long term record shows an increase in glacial-interglacial amplitude towards the late Pleistocene, as discussed earlier, and is comparable to the sea level record from Miller et al., (2005). Smoothing of the raw data minimizes variability due to interspecific oxygen isotope normalization or small sample size for Mg/Ca analysis. Note there is a divergence following the MPT in the records, however the Miller et al., (2005) sea level record, based on benthic oxygen isotope records, is not corrected for changes in deep ocean temperature. Interpretation of large scale changes in sea level is valid even with an uncertainty of ±25 m. From the 41-kyr to 100-kyr world, G-I amplitude increased, in both glacial and interglacial values, and is reproduced amongst several G-I cycles within each time interval minimizing the uncertainty associated with this major finding. With a standard deviation of ±25 m, the

1σ standard error on analysis of n samples (0.2/n) is such that an increase in the sample size would almost halve the 1σ standard error. Therefore, the long-term shift across the two major climate transitions represents an interpretable observation from the sea level record.

However, interpretation of individual glacial and interglacial absolute values for the last 4 G-I cycles is limited by the uncertainty of the technique. Plotted in figure 2.13 is a comparison between the DSDP site 607 sea level record and other proxy sea level records. The expected G-I sea level range, derived from other proxy records, is from -10 to 125 m. The sea level record, from this study, encompasses the range of expected sea level variability within the ±25-m uncertainty and resolves similar G-I variability. However, MIS 11 is considerably higher than the expected interglacial highstand values from other sea level records. Thus, combining Mg/Ca-temperature estimates and $\delta^{18}O_b$ record to evaluate changes in sea level is useful for interpreting long-term changes but not absolute lowstand and highstand values.

The δ_ω record shows a gradual increase in ice volume from the mid- to late Pliocene, corresponding to an overall ~20±25 m decrease in sea level. From the late Pliocene to the early Pleistocene, Δ(G-I) in sea level fluctuated from 60-80 m on average which is comparable, within errors, with the 40-70 m estimate from inferred sea level studies (Cronin et al., 1994; Dwyer et al., 1995). The LPT estimate of average sea level decrease is smaller, than previous estimates (Cronin et al., 1994; Dowsett et al., 1990; Mudelsee et al., 2005) which determined an decrease of 30-35 m in sea level associated with NH glaciation. Large estimates of sea level change (>20m) across the LPT cannot be explained by purely NH ice sheet growth and thus requires an additional increase in

ice volume in the southern hemisphere which is not supported by proxy evidence (Kennett et al., 1993).

Across the MPT, the δ_ω record remains stable (average 0.4‰ for the early and late Pleistocene) indicating no significant increase in ice volume (0 ± 25 m) associated with the MPT. The isotopic shift in the $\delta^{18}O_b$ record across the MPT is related to a deep ocean cooling rather than an increase in NH ice volume. The MPT is represented in the δ_ω record by a 0.6 to 0.7 ‰ increase in amplitude which indicates that glacial-interglacial periods became more extreme during the late Pleistocene. Following the MPT, less NH ice persisted in interglacial periods in despite of the cooler climate while more ice persisted in the glacial periods.

The lack of discernible trend in ice volume across the MPT is in agreement with δ_ω records from the western equatorial Pacific (de Garidel-Thoron et al., 2005; Medina-Elizalde et al., 2005), but inconsistent with sea-level estimates based on depositional sequences from shallow marine sediments (Kitamura et al., 2006) (who found a 20-30 m decrease across from 1000 to 900 ka). The latter may, however, reflect uncertainties in quantifying local uplift in the Japanese study. Quaternary estimates of G-I sea level variability, derived from this study, range from 120-150m in an asymmetric pattern with gradual ice sheet growth and abrupt decay similar to the $\delta^{18}O_b$ record. The last 400 ka in sea level variabiliy is similar in trend and within the upper limit of the G-I range (~145 m) suggested by numerous sea level records (Fairbanks, 1989; Lea et al., 2002; Schrag et al., 1996; Schrag, 2002; Waelbroeck et al., 2002; Yokoyama et al., 2000).

The divergence in sea level and similarity in deep ocean temperature history across the LPT and MPT suggest that each transition may be responding to different sets

of forcings (Fig.2.13). A substantial increase in ice volume across the LPT but not across

the MPT promotes the idea that each climate shift is unique and mechanistically different.

The global cooling of the deep ocean and concomitant increase in ice volume across the

LPT may be related to a high latitude response to a secular decrease in atmospheric

carbon dioxide (pCO_2) as previously proposed by (Ruddiman et al., 1988). SST records

from upwelling regimes show a similar cooling trend which supports the idea that the

BWT cooling is a global trend in temperature. Additionally, the global cooling, which

acted to increase vertical stratification in the polar ocean following Sigman et al., (2004),

played a role in increasing moisture supply to the NH which acts to promote ice sheet

growth. Following Haug et al., (2005), a global cooling would have increased

seasonality, in response to polar ocean stratification, and provided a moisture supply to

the NH for growth of glacial ice.   As the climate cooled, in the late Pliocene, ice sheets

might have developed in the NH as a response to the changing glaciation threshold and

preconditioning due an increased moisture transport to the high latitudes.

The deep ocean cooling associated with the MPT has been highlighted as a

similar threshold response to radiative forcing; however ice core records of pCO_2 show

no discernible long term trend, though the record does not extend across the full MPT

(Luthi et al., 2008; Siegenthaler et al., 2005). Sea surface temperature records from

western tropical Pacific, a region primarily influenced by varying pCO_2, show no long-

term cooling across the MPT which suggests that the shift in mean climate state

potentially is not driven by pCO_2 variability (de Garidel-Thoron et al., 2005).   The

cooling, from 1150 to 825 ka, however, precedes the major expansion of ice sheets and

the frequency shift from 41-ky to 100-ky at 700 ka. The increase in glacial ice volume

and decrease in interglacial ice volume and increase in the phase relationship which occurs following cooling, points to a fundamental change in ice sheets dynamics rather than a threshold response to global cooling.

Recently Huybers and Tziperiman (2008), using an ice sheet model, proposed that in the 41-kyr world ice sheets were much thinner relative to late Pleistocene thicker, unstable ice sheets, building upon the regolith hypothesis of Clark and Pollard (1998). We propose that the increase in phase lead of BWT over $\delta^{18}O_b$ and increase in G-I sea level amplitude across the MPT represents a fundamental change in ice sheet dynamics with the growth of thicker, more unstable ice sheets, as suggested by Clark and Pollard (1998) that fully deglaciate during interglacial periods. The cooling associated with the MPT might have preconditioned the NH to allow the growth of taller glacial ice sheets, but cannot account for the shift in frequency or sea level history.

2.6 References

Adkins, J. F., K. McIntyre, et al. (2002). "The salinity, temperature and d18O content of the glacial deep ocean." Science, 298: 1769-1773.

Barker, S. and H. Elderfield (2002). "Foraminiferal calcification response to glacial-interglacial changes in atmospheric CO_2." Science, 297: 833-836.

Becquey, S. and R. Gersonde (2002). "Past hydrographic and climatic changes in the Subantarctic Zone of the South Atlantic: the Pleistocene record from ODP Site 1090." Palaeogeography, Palaeoclimatology, Palaeoecology 182: 221-239.

Billups, K., and D.P. Schrag (2003). "Application of foraminiferal Mg/Ca ratios to questions of Cenozoic climate change." Earth and Planetary Science Letters 209(1-2): 181-195.

Billups, K. and D. P. Schrag. (2002). "Paleotemperatures and Ice-Volume of the Past 27 myr Revisited with Paired Mg/Ca and Stable Isotope Measurements on Benthic Foraminifera." Paleoceanography 17, 10.1029/2000PA000567(1).

Boyle, E. A., and L.D. Keigwin. (1985/6). "Comparison of Atlantic and Pacific paleochemical records for the last 215,000 years: Changes in deep ocean circulation and chemical inventories." Earth and Planetary Science Letters 76: 135-150.

Bryan, S. P. and T. M. Marchitto (2008). "The Mg/Ca - temperature proxy in benthic foraminifera: New calibrations from the Florida Straits and a hypothesis regarding Mg/Li." Paleoceanography.

Clark, P. U., Archer, D., D. Pollard, J.D. Blum, J.A. Rial, V. Brovkin, A.C. Mix, N. G. Pisias, and M. Roy (2006). "The Middle Pleistocene transition: Characteristics, mechanisms, and implications for long-term changes in atmospheric pCO2." Quaternary Science Reviews 25: 3150-3184.

Clark, P. U. and D. Pollard (1998). "Origin of the Middle Pleistocene transition by ice sheet erosion of regolith." Paleoceanography 13: 1-9.

Cronin, T. M., A. Kitamura, et al. (1994). "Late Pliocene climate change 3.4–2.3 Ma: paleoceanographic record from the Yabuta Formation, Sea of Japan." Palaeogeography, Palaeoclimatology, Palaeoecology 108: 437-455.

Crowley, T. J. (1985). Late Quaternary carbonate changes in the North Atlantic and Atlantic/Pacific comparisons. The Carbon Cycle and Atmospheric CO_2: Natural Variations Archean to Present. E. Sundquist, and W.S. Broecker. Washington, DC, Geophysical Monograph Series, AGU: 271-284.

de Garidel-Thoron, T., Y. Rosenthal, et al. (2005). "Stable sea surface temperatures in the western Pacific warm pool over the past 1.75 million years." Nature 433: 294-298.

Dowsett, H. J. and T. M. Cronin (1990). "High eustatic sea level during the middle Pliocene: evidence from southeastern U.S. Atlantic coastal plain." Geology 18: 435-438.

Dwyer, G. S., T. M. Cronin, et al. (1995). "North Atlantic deepwater temperature change during late Pliocene and late Quaternary climatic cycles." Science 270: 1347-1351.

Elderfield, H., J. Yu, et al. (2006). "Calibrations for benthic foraminiferal Mg/Ca paleothermometry and the carbonate ion hypothesis." Earth and Planetary Science Letters 250(3-4): 633-649.

Fairbanks, R. G. (1989). "A 17,000-year glacio-eustatic sea level record: influence of glacial melting rates on the Younger Dryas event and deep-ocean circulation." Nature 342: 637-642.

Fairbanks, R. G. (1989). "17,000 year glacio-eustatic sea level record: influence of glacial melting rates on the Younger Dryas event and deep ocean circulation." Nature 342: 637-642.

Fairbanks, R. G. and R. K. Matthews (1978). "The oxygen isotope stratigraphy of the Plesitocene reef tracts of Barbados, West Indies." Quaternary Research 10(1): 181-196.

Gröger, M., Henrich, R. and Bickert, T., 2003. Variability of silt grain size and planktonic foraminiferal preservation in Plio/Pleistocene sediments from the western equatorial Atlantic and Caribbean. Marine Geology, 201: 307-320.

Haug, G. and R. Tiedemann (1998). "Effect of the formation of the isthmus of panama on the Atlantic Ocean thermohaline circulation." Nature 393: 673-676.

Kennett, J. P. and D. A. Hodell (1993). "Evidence for relative climatic stability of Antarctica during the early Pliocene: A marine perspective." Geografiska Annaler 75: 205-220.

Kitamura, A. and T. Kawagoe (2006). "Eustatic sea-level change at the Mid- Pleistocene climate transition: new evidence from the shallow-marine sediment record of Japan." Quaternary Science Reviews 25: 323–335.

Labeyrie, L. D., J. C. Duplessy, et al. (1987). "Variations in mode of formation and temperature of oceanic deep waters over the past 125,000 years." Nature 327: 477-482.

Lawrence, K. T., Z. Liu, et al. (2006). "Evolution of the Eastern Tropical Pacific Through Plio-Pleistocene Glaciation." Science 312: 79-83.

Lea, D. W., P. A. Martin, et al. (2002). "Reconstructing a 350 ky history of sea level using planktonic Mg/Ca and oxygen isotope records from a Cocos Ridge core." Reconstructing a 350 ky history of sea level using planktonic Mg/Ca and oxygen isotope records from a Cocos Ridge core 21: 283-293.

Lear, C. H., H. Elderfield, et al. (2000). "Cenozoic deep-sea temperatures and global ice volumes from Mg/Ca in benthic foraminiferal calcite." 287: 269-272.

Lear, C. H., Y. Rosenthal, and N. Slowey (2002). "Benthic foraminiferal Mg/Capaleothermometry: A revised core-top calibration." Geochimica et Cosmochimica Acta 66: 3375-3387.

Lisiecki, L. E. and M. E. Raymo (2005). "A Pliocene-Pleistocene stack of 57 globally distributed benthic d18O records." Paleoceanography 20, PA1003, doi:10.1029/2004PA001071.

Luthi, D., M. Le Floch, et al. (2008). "High-resolution carbon dioxide concentration record 650,000-800,000 years before present." Nature 453: 379-382.

Marchitto, T. M., S. P. Bryan, et al. (2007). "Mg/Ca temperature calibration for the benthic foraminifer Cibicidoides pachyderma." Paleoceanography 22(1): doi:10.1029/2006PA001287.

Marchitto, T. M. and P. B. deMenocal (2003). "Late Holocene variability of upper North Atlantic Deep Water temperature and salinity." Geochemistry, Geophysics, Geosystems 4(12).

Marchitto, T. M., D. W. Oppo, et al. (2002). "Paired benthic foraminiferal Cd/Ca and Zn/Ca evidence for a greatly increased presence of Southern Ocean Water in the glacial North Atlantic." Paleoceanography 17, doi:10.1029/2000PA000598.

Marlow, J. R., C. B. Lange, et al. (2000). "Upwelling intensification as part of the Pliocene–Pleistocene climate transition." Science 290: 2288–2291.

Martin, P. A., D. W. Lea, et al. (2002). "Quaternary deep sea temperature histories derived from benthic foraminiferal Mg/Ca." Earth and Planetary Science Letters 198(1-2): 193-209.

McClymont, E. L. and A. Rossel-Mele (2005). "Links between the onset of modern Walker circulation and the mid-Pleistocene climate transition." Geology 33: 389-392.

Medina-Elizalde, M. and D. W. Lea (2005). "The mid-Pleistocene transition in the tropical Pacific." Science 310: 1009–1012.

Mudelsee, M. and M. E. Raymo (2005). "Slow dynamics of the Northern Hemisphere Glaciation." Paleoceanography 20, PA4022, doi:10.1029/2005PA001153.

Peltier, W. R. and R. G. Fairbanks (2006). "Global glacial ice volume and Last Glacial Maximum duration from an extended Barbados sea level record." Quaternary Science Reviews 25: 3322-3337.

Raitzsch, M., H. Kuhnert, et al. (2008). "Benthic foraminifer Mg/Ca anomalies in South Atlantic core top sediments and their implications for paleothermometry." Geochemistry, Geophysics, Geosystems 9: doi:10.1029/2007GC001788.

Raymo, M. E., B. Grant, M. Horowitz, and G. H. Rau (1996). "Mid-Pliocene warmth: stronger greenhouse and stronger conveyor." Marine Micropaleontology 27: 313-326.

Raymo, M. E., D. W. Oppo, and W. Curry (1997). "The mid-Pleistocene climate transition: a deep sea carbon isotopic perspective." Paleoceanography 12: 546–559.

Rosenthal, Y., E. A. Boyle, et al. (1997). "Temperature control on the incorporation of Mg, Sr, F and Cd into benthic foraminiferal shells from Little Bahama Bank: prospects for thermocline paleoceanography." Geochimica et Cosmochimica Acta 61: 3633-3643.

Ruddiman, W. F., M.E. Raymo, D.G. Martinson, B.M. Clement, and J. Backman (1989). "Mid-Pleistocene evolution of Northern Hemisphere climate." Paleoceanography 4: 353-412.

Ruddiman, W. F. and M. E. Raymo (1988). Northern hemisphere climate regimes during the past 3 Ma: possible tectonic connections. The Past Three Million Years: Evolution of Climatic Variability in the North Atlantic Region. N. J. Shackleton, R.G. West, and D.Q. Bowen. Cambridge, University Press: 227-234.

Russell, A. D., S. Emerson, B.K. Nelson, J. Erez, and D.W. Lea, D.W., P. A. Martin, D. K. Pak, and H. J. Spero (1995). "Uranium in foraminiferal calcite as a recorder of seawater uranium concentrations." Geochimica et Cosmochimica Acta 58: 671-681.

Schefus, E., J. S. S. Damste, et al. (2004). "Forcing of tropical Atlantic sea surface temperatures during the mid-Pleistocene transition." Paleoceanography 19, PA4029, doi:10.1029/2003PA000892.

Schrag, D. P., G. Hampt, et al. (1996). "Pore fluid constraints on the temperature and oxygen isotopic composition of the glacial ocean." Science 272: 1930-1932.

Schrag, D. P., J. F. Adkins, K. McIntyre, J. L. Alexander, D. A. Hodell, C. D. Charles, and J. F. McManus (2002). "The oxygen isotopic composition of seawater during the Last Glacial Maximum." Quaternary Science Reviews 21: 331-342.

Shackleton, N. J. (1974). "Attainment of isotopic equilibrium between ocean water and the benthonic foraminifera genus Uvigerina: isotopic changes in the ocean during the last glacia." Colloques Internationaux du Centre National du Recherche Scientifique 219: 203-210.

Shackleton, N. J. (2000). "The 100,000-year ice-age cycle identified and found to lag temperature, carbon dioxide, and orbital eccentricity." Science 289: 1897-1902.

Shackleton, N. J. and N. D. Opdyke (1973). "Oxygen isotope and paleomagnetic stratigraphy of Equatorial Pacific core V28-238: oxygen isotope temperatures and ice volumes on a 10^5 and 10^6 year scale." Quaternary Research 3: 39-55.

Siddall, M., E. J. Rohling, et al. (2003). "Sea-level fluctuations during the last glacial cycle." Nature 423: 853-858.

Siegenthaler, U. and e. al (2005). "Stable carbon cycle–climate relationship during the late Pleistocene." Science 310: 1313-1317.

Tziperiman, E. and H. Gildor (2003). "On the mid-Pleistocene transition to 100- kyr glacial cycles and the asymmetry between glaciation and deglaciation times." Paleoceanography 18.

Waelbroeck, C., L. Labeyrie, et al. (2002). "Sea-level and deep water temperature changes derived from benthic foraminifera isotopic records." Quaternary Science Reviews 21: 295-305.

Yokoyama, Y., K. Lambeck, et al. (2000). "Timing of the last glacial maximum from observed sea-level minima." Nature 406: 713-716.
.
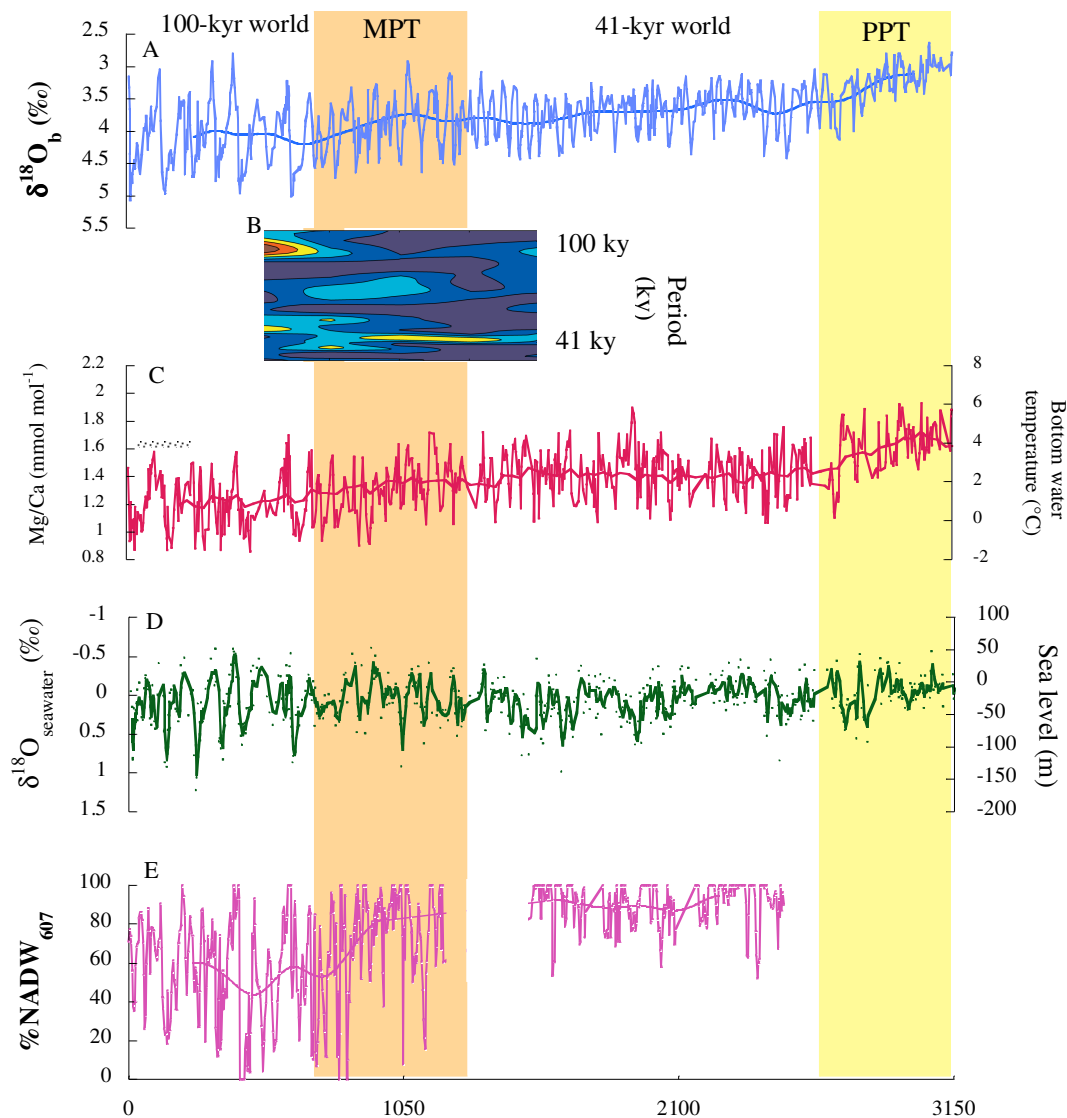
Figure 2.1 Western North Atlantic DSDP site 607 records based on the benthic foraminifera. (a) Previous reconstruction of benthic oxygen isotope record from Raymo et al., (1989) and Ruddiman et al., (1989); (b) Evolutionary spectral analysis plot of BWT from 500 to 1500 ka. The spectra reveals that the BWT record is dominated by 41-kyr cycles prior to the MPT and by 100-kyr cycles following the transition. (c) Mg/Ca-derived BWT record. To convert Mg/Ca ratios to bottom water temperature the following equation was used: Mg/Ca=0.15*BWT+1.15; (d) δ_{ω} record, calculated by extracting the component in benthic $\delta^{18}O$ explained by the Mg/Ca-derived BWT using the paleotemperature equation from Shackleton (1973) relative to SMOW; The curve also represents a reconstruction of sea level relative to today calculated with the assumption that a 0.1‰ shift in δ_{sw} results from a 10-m change in sea level (Fairbanks et al, 1989). (e) Percent NADW at DSDP 607 calculated as described by Raymo et al., (1997). MPT and LPT refer to mid-Pleistocene transition and late Pliocene transition, respectively.
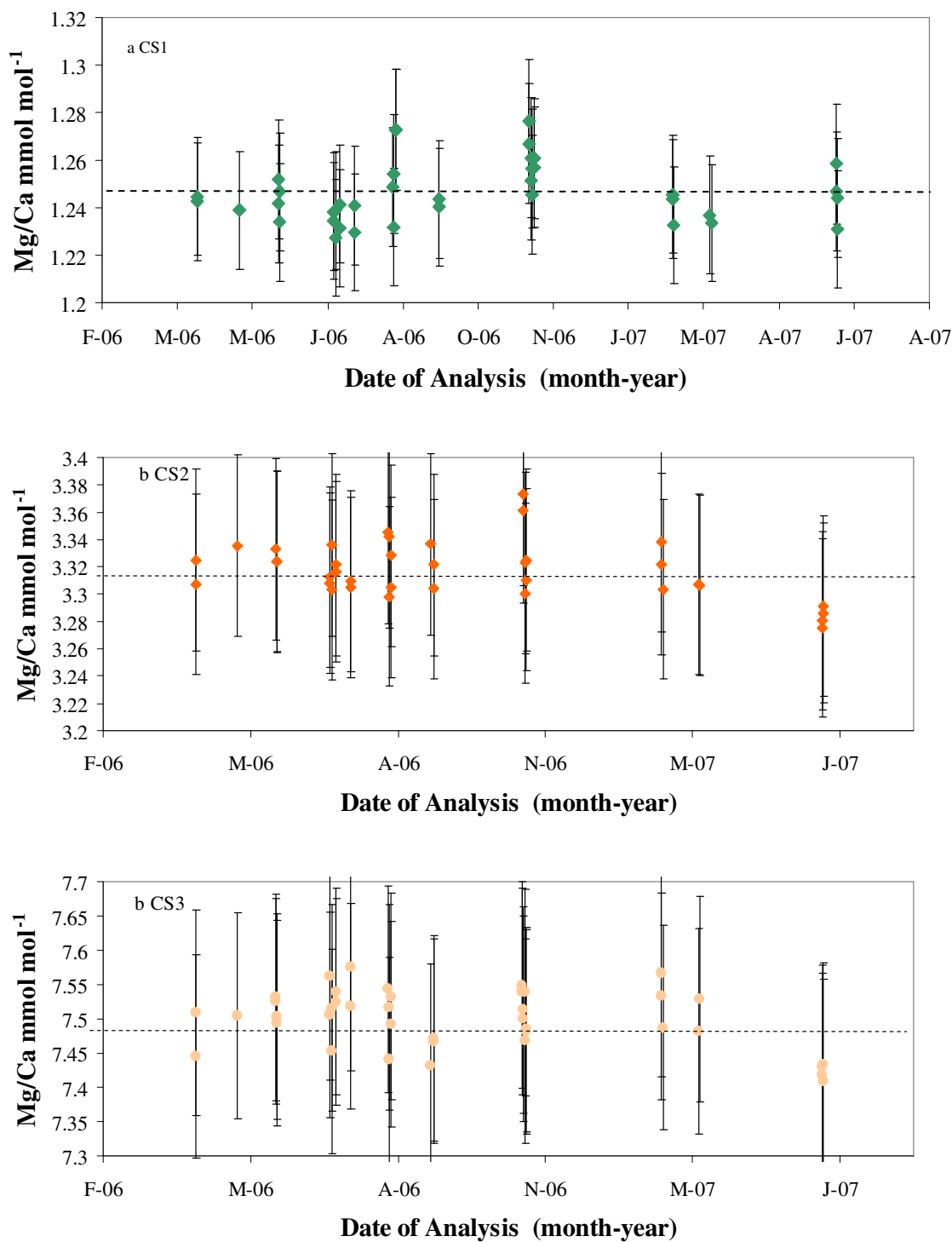
Figure 2.2. Long-term precision of consistency standards with varying Mg/Ca ratios. Dashed lines represent expected Mg/Ca values. Plotted are 2% error bars.
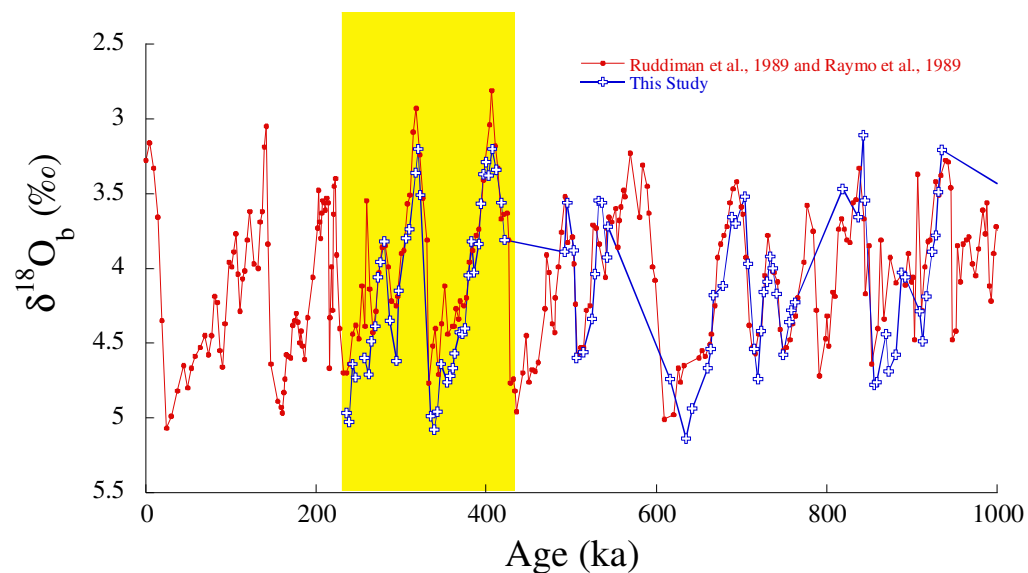
Figure 2.3 Benthic foraminiferal stable isotope data from original analysis of DSDP site 607 from Ruddiman et al. (1989) and Raymo et al. (1989) and re-analysis of new samples from this study. Note the offset in marine isotope stage 9 and 11 (shaded region) between the original and new oxygen isotope data.
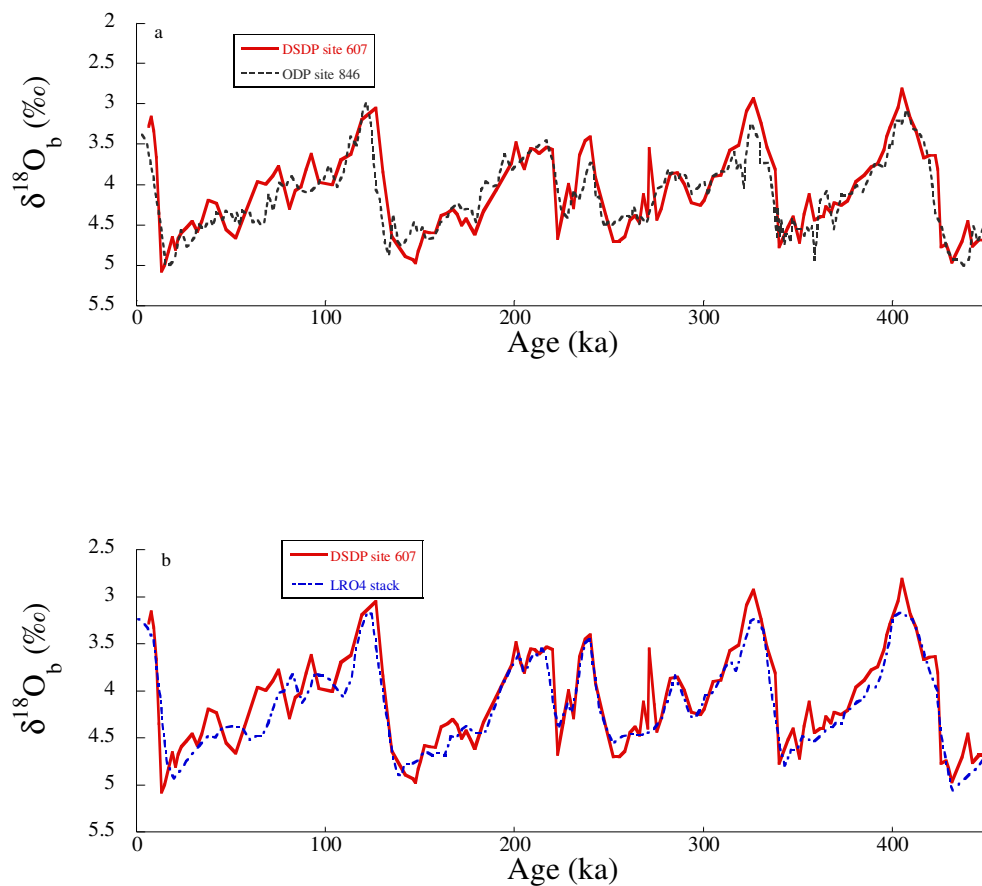
Figure 2.4 Benthic foraminiferal stable isotope data from DSDP site 607 from Ruddiman et al. (1989) and Raymo et al. (1989) and (a) ODP site 846 from Shackleton et al. (1995) and Mix et al. (1995) and (b) the LRO4 benthic stacked record from Lisiecki et al. (2005).
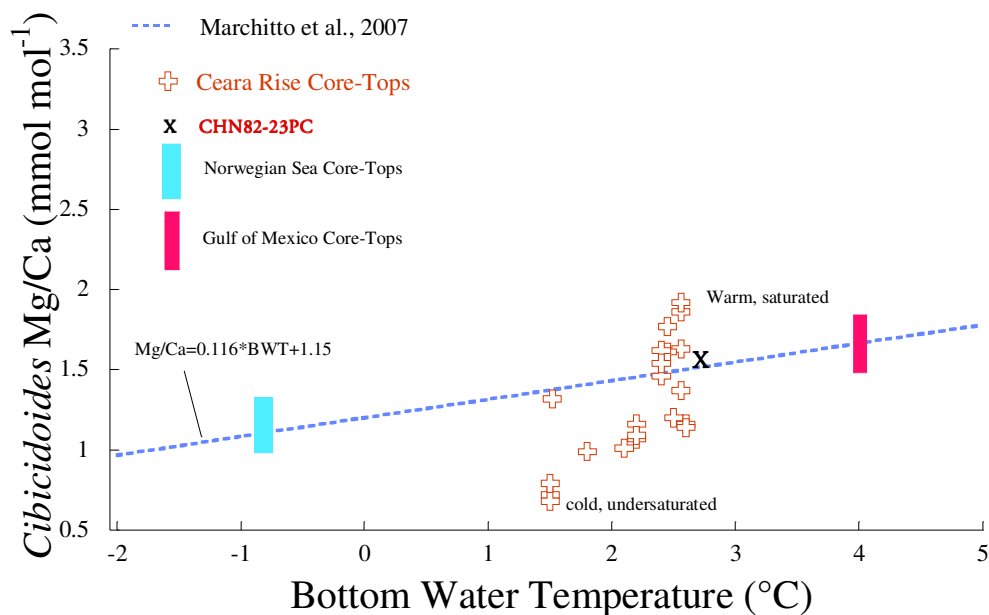
Figure 2.5 Dashed line represents extrapolation of Marchitto et al., (2007) *C. pachyderma* Mg/Ca-temperature calibration below 5°C. Plotted core-top Mg/Ca data from *Chain* 82-24-23PC, Norwegian Seas, and Gulf of Mexico fall along the Marchitto et al., (2007) calibration. Ceara Rise Mg/Ca core-top diverges from the expected relationship between temperature and Mg/Ca. Norwegian Sea and Gulf of Mexico Mg/Ca core-top data derive from Jordan (2008).
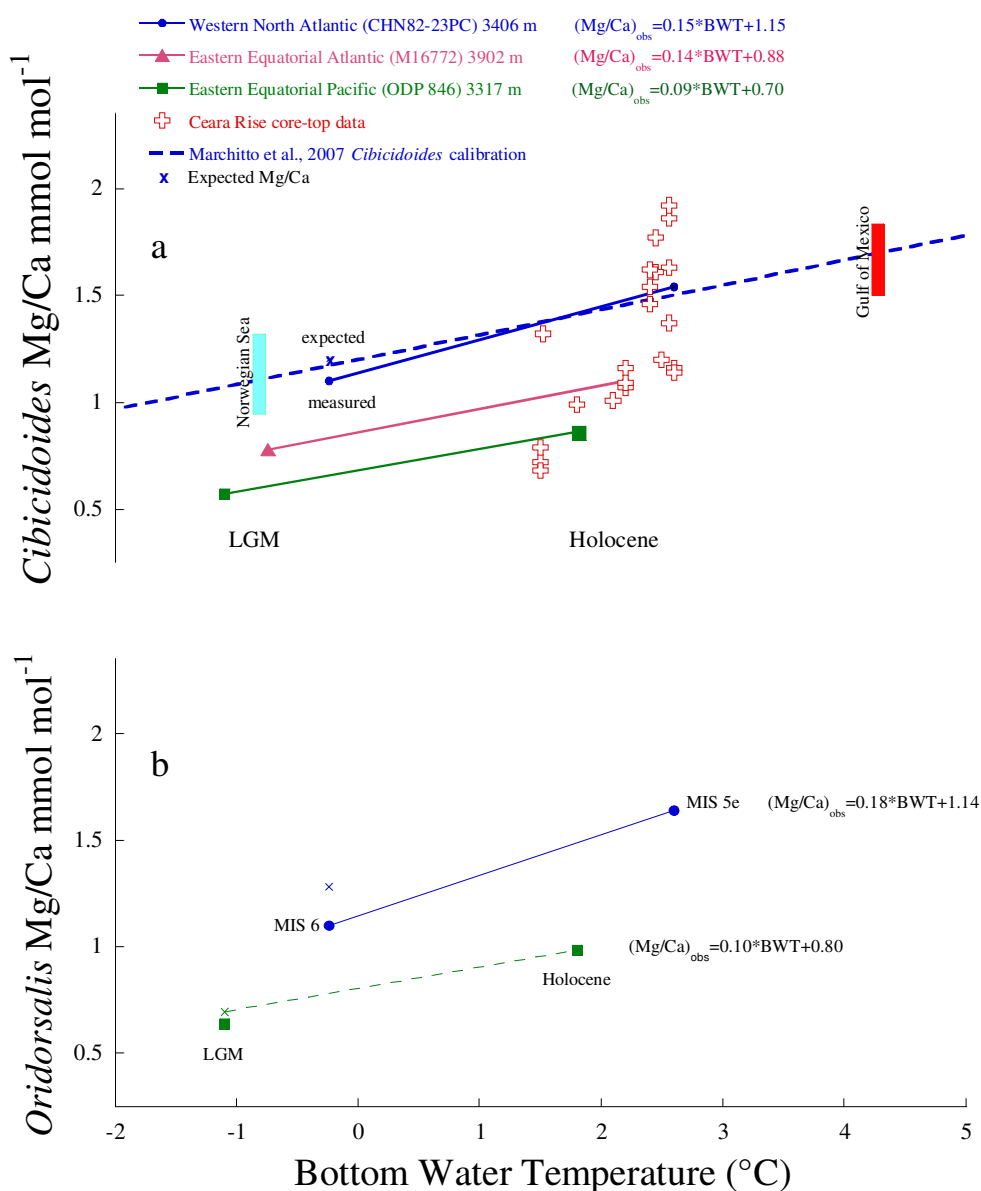
Figure 2.6 Mg/Ca of benthic foraminifera from the Holocene and LGM in cores from the Atlantic and Pacific for which LGM paleotemperatures have been estimated. (a) *C. wuellerstorfi* data from core *Chain* 82-24-23PC, M16772 (data from Martin et al., 2002), and ODP 846. Also shown are core top data from the Norwegian Seas, Gulf of Mexico, and Ceara Rise. The Marchitto et al., 2007 *Cibicidoides* calibration is shown for comparison. (b*) O. umbonatus* from core *Chain* 82-24-23PC and ODP 846. Note that MIS 5e and 6 are used instead of Holocene and LGM data in the Atlantic. Linear equations from observed data show distinct offsets in y-intercept and slope related to temperature and carbonate saturation effects. Expected glacial Mg/Ca estimates derived from assuming a 0.12 change in Mg/Ca per °C.
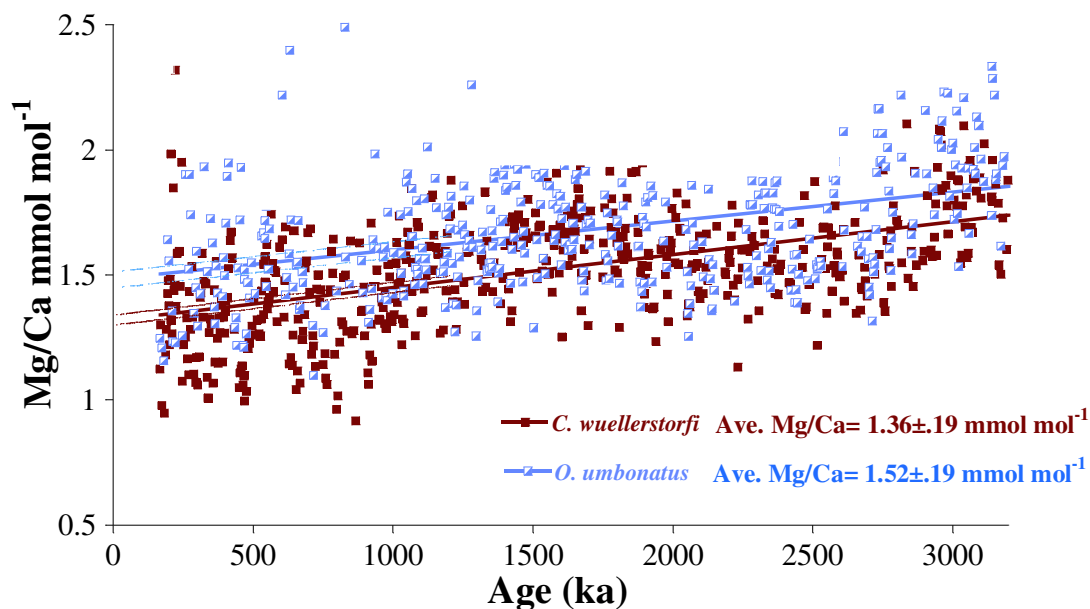
Figure 2.7 Mg/Ca records for two species *C. wuellerstorfi* and *O. umbonatus* show similar trends. The difference in Mg/Ca between species, 0.16 mmol mol^{-1} (p<0.001), is determined by calculating the difference in the whole-core mean from 0 to 3150 ka.
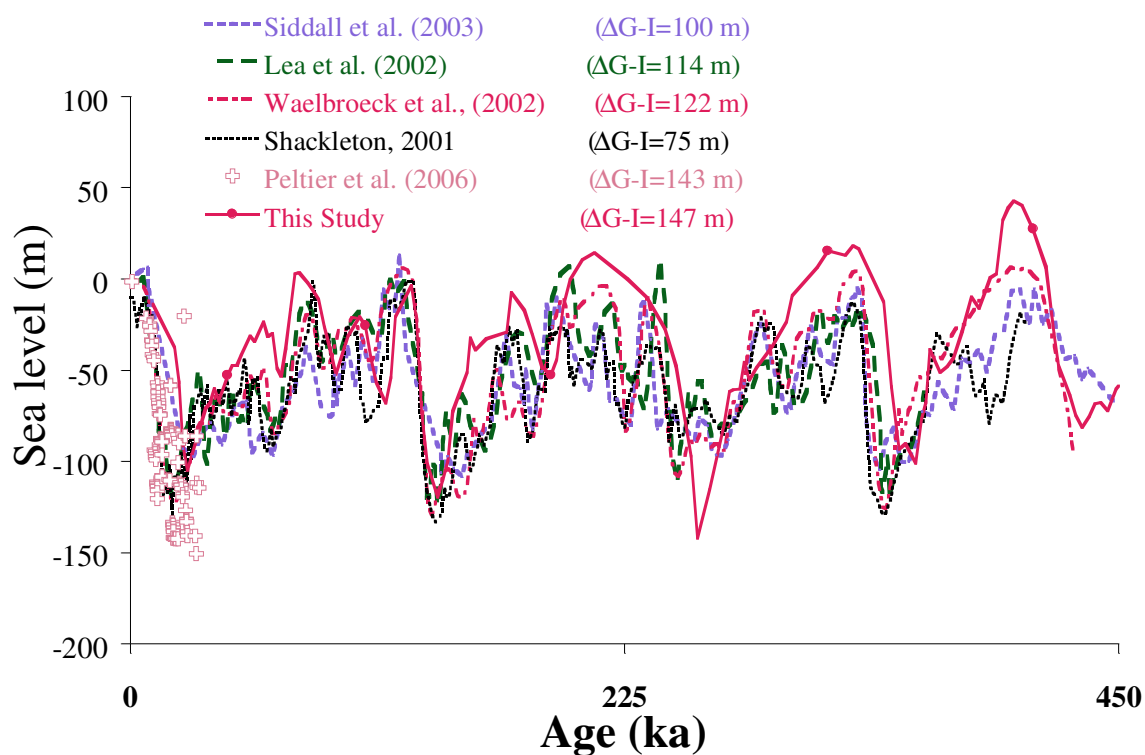
Figure 2.8 Sea level record derived from Mg/Ca-BWT estimates and $\delta^{18}O_b$ from *Chain* 82-24-23PC and DSDP site 607 compared with other published sea level records. The average glacial-interglacial sea level amplitude for all records is highlighted.
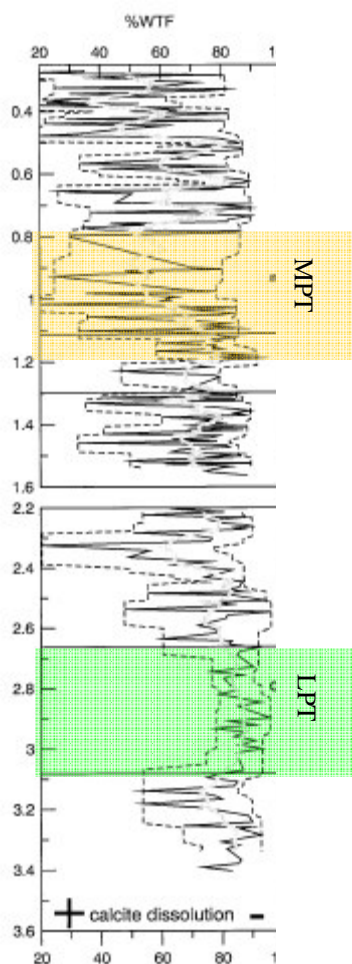
Figure 2.9 Pliocene-Pleistocene record of planktonic foraminiferal shell preservation, here represented as percentage whole-test foraminifera (%WTF) at ODP site 927 in the western Equatorial Atlantic. The figure and data is from Groger et al., (2003). The shaded regions represent the LPT and MPT.
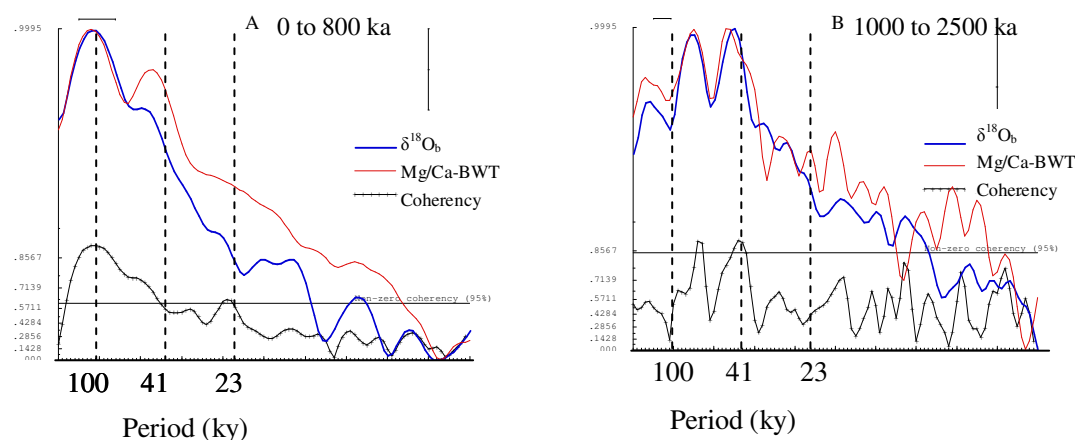
Figure 2.10 Comparison of spectral analysis of $\delta^{18}O_b$ and Mg/Ca-derived BWT records from DSDP site 607 in the late and early Pleistocene. (a) Time interval from 11 to 800 ka; (c) time interval from 1000 to 2500 ka. Panels also present the coherency from cross-spectral analysis between the DSDP 607 $\delta^{18}O_b$ and BWT for each period. The confidence interval at the 95% significance level and the bandwidth used for the spectral analysis are displayed.
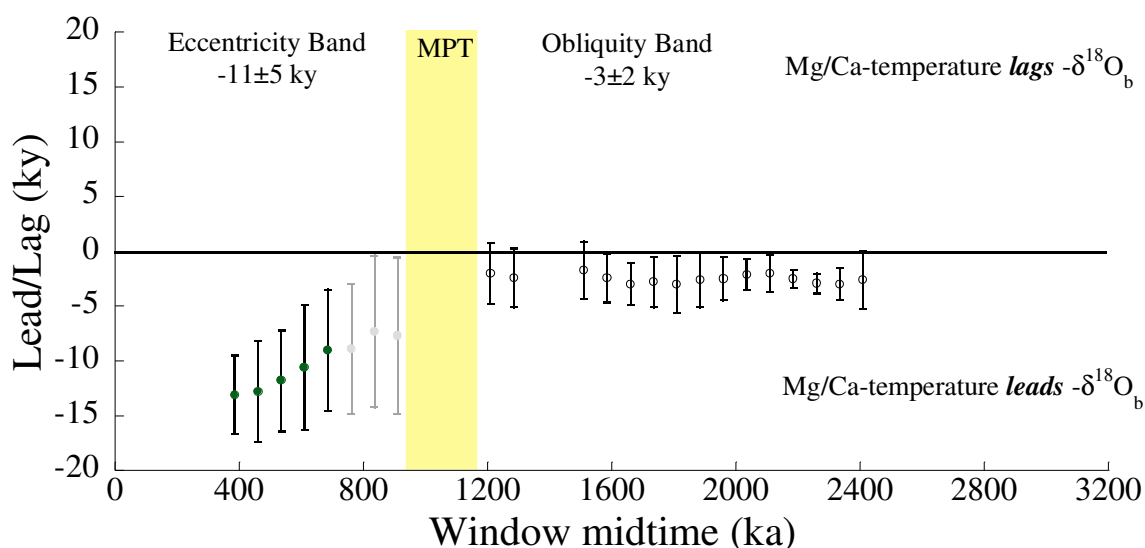
Figure 2.11 Eccentricity band (100-ky) and obliquity band (41-ky) phase and coherency relationship between benthic oxygen isotope record and Mg/Ca-BWT. Intervals that are coherent at 80% confidence level are shown with thick graybars and those that are coherent at 95% confidence level are with thin black bars. We use the inverse of benthic $\delta^{18}O_b$ record in our coherency analysis. Before coherency and phase analysis, all records were interpolated to even intervals of 3-ky resolution. Phases were computed with use of Arand program iterative spectra feature with a 300-kyr window and 250 lags.
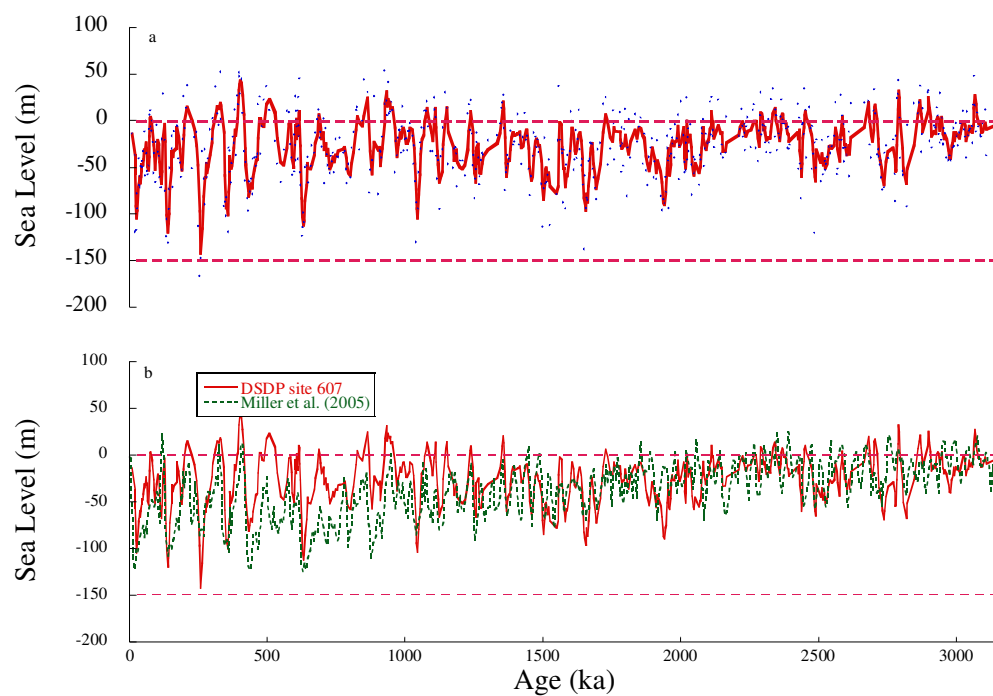
Figure 2.12 (a) DSDP site 607 sea level with a 3-point moving average applied; (b) Comparison between the smoothed DSDP site 607 sea level record and a sea level compilation record from Miller et al., (2005).
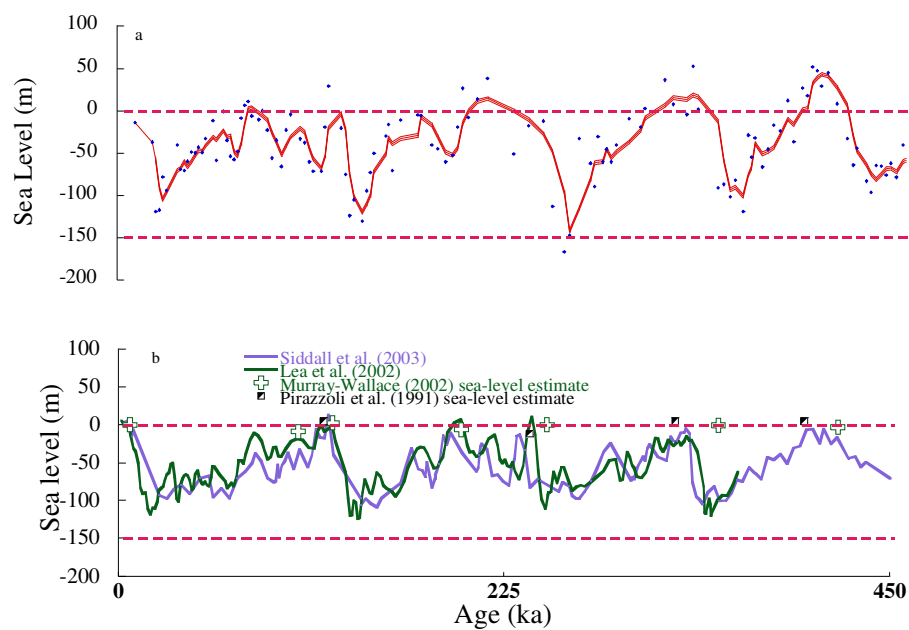
Figure 2.13 (a) DSDP site 607 sea level record across the last 4 glacial-interglacial cycles with 95% confidence intervals plotted; (b) Sea level records derived from Siddall et al., (2003), Lea et al., (2002), Murray-Wallace (2002), and Pirazzoli et al., (1991).
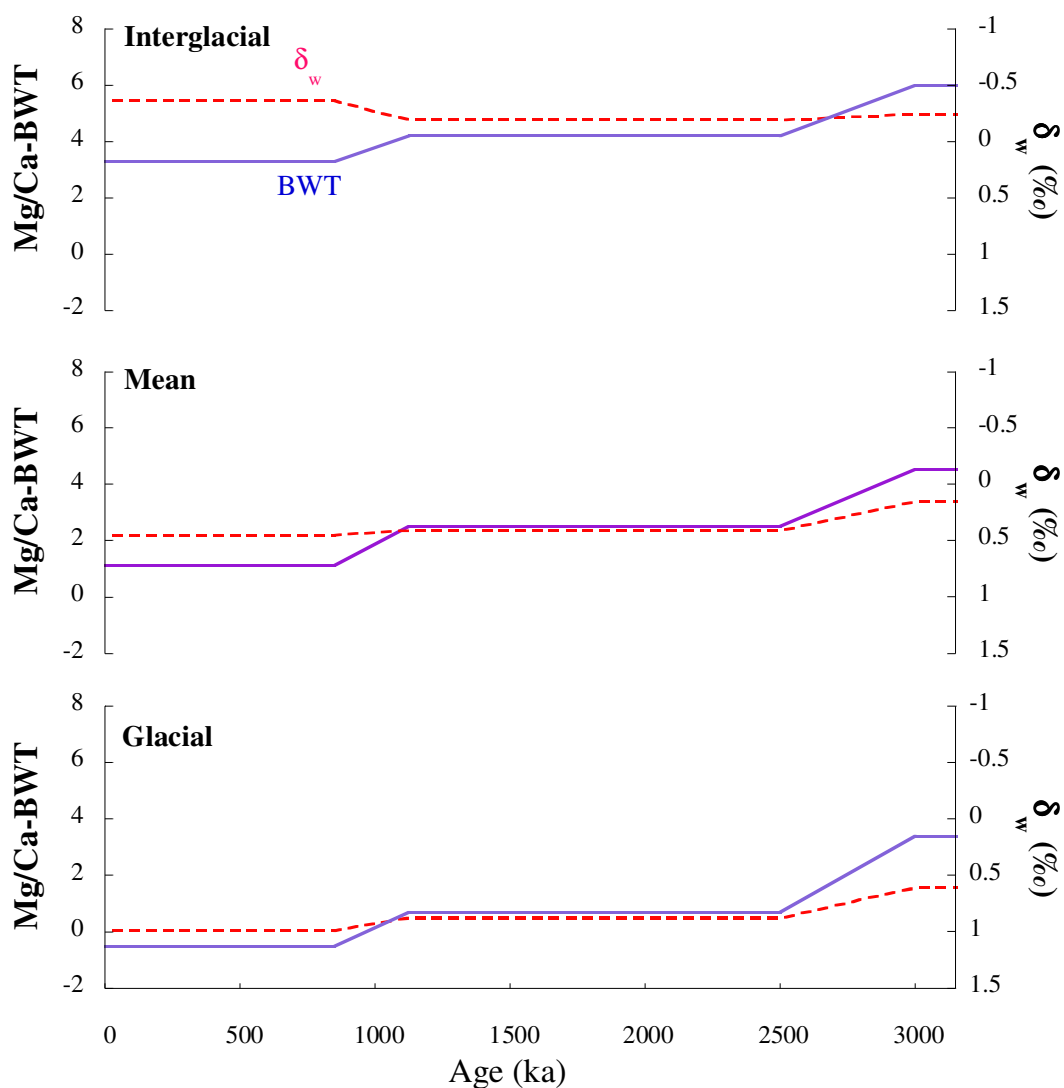
Figure 2.14 Schematic diagram of the mean, glacial, and interglacial long-term trends in Mg/Ca-BWT and the oxygen isotopic composition of seawater. Note the similarity in temperature and δ_ω across the LPT but divergence across the MPT. The MPT is associated with a decrease in mean temperature but an increase in glacial-interglacial δ_ω amplitude. Trendlines are based on average BWT and δ_ω data for each time interval.

Table 2.1 Average offset in Mg/Ca due to changes in the strength of the reducing agent. Note the offset translates into <0.5ºC which is within the uncertainty of the calibration. All concentration data in mmol mol^{-1}.

interval (Myr)	Mg/Ca $_{1:2}$	Mg/Ca $_{1:4}$	ΔMg/Ca
1.5-1.6	1.52	1.62	0.10
1.9-2.1	1.57	1.59	0.02
2.5-2.6	1.51	1.58	0.07
		mean offset	**0.06**

Table 2.2 Long-term analytical precision of laboratory internal consistency standards.

Consistency Standards	Statistic	^{25}Mg/^{43}Ca mmol mol^{-1}
CS1	Expected	1.246
	Mean	1.247
	±1s	0.016
	%RSD	**1.24%**
	Δ(meas-exp) %	0.12%
CS2	Expected	3.318
	Mean	3.325
	±1s	0.039
	%RSD	**1.16%**
	Δ(meas-exp) %	0.21%
CS3	Expected	7.504
	Mean	7.499
	±1s	0.043
	%RSD	**0.57%**
	Δ(meas-exp) %	-0.06%

Table 2.3 Location and hydrography for three core sites from the Atlantic and Pacific Ocean basins. *Cibicidoides* and *Oridorsalis* Mg/Ca data from each core site with detailed information from the downcore calibration analysis.

	Core		
	CHN82-23PC	**M16772**	**ODP 846**
Location	41ºN, 33ºW	1ºS, 11ºW	3ºS. 91ºW
Depth (m)	3406	3912	3296
BWT (°C)	2.7	2.3	1.5
ΔCO_3^{2-} (umol kg^{-1})	30	14	2
Cibicidoides **Mg/Ca data**			
Holocene Mg/Ca (mmol mol^{-1})	1.54	1.2	0.86
LGM Mg/Ca (mmol mol^{-1})	1.1	0.78	0.6
Expected LGM Mg/Ca (mmol mol^{-1})[a]	1.2	0.81	0.57
ΔMg/Ca$_{exp}$-Mg/Ca$_{obs}$	0.1	0.03	-0.03
$\Delta(\Delta CO32-)$[b]	12	3	-3
Observed equation	Mg/Ca=0.15*BWT+1.15	Mg/Ca=0.14*BWT+0.88	Mg/Ca=0.09*BWT+0.70
Expected equation	Mg/Ca=0.12*BWT+1.23	Mg/Ca=0.10*BWT+0.88	Mg/Ca=0.10*BWT+0.68
Oridorsalis **Mg/Ca data**			
Interglacial Mg/Ca (mmol mol^{-1})	1.64 (MIS 5e)	-	0.99 (H)
Glacial Mg/Ca (mmol mol^{-1})	1.1 (MIS 6)	-	0.69 (LGM)
Expected LGM Mg/Ca (mmol mol^{-1})[c]	1.28	-	0.64
ΔMg/Ca$_{exp}$-Mg/Ca$_{obs}$	0.18	-	-0.05
$\Delta(\Delta CO32-)$[d]	21	-	-6
Observed equation	Mg/Ca=0.18*BWT+1.14	-	Mg/Ca=0.10*BWT+0.80
Expected equation	Mg/Ca=0.12*BWT+1.31	-	Mg/Ca=0.12*BWT+0.77

a, c-Based on assuming 0.12 change in Mg/Ca per °C; b, d-calculated by converting the difference between expected and observed Mg/Ca into $\Delta CO32-$ using the carbonate sensitivity of 0.0086 from Elderfield et al., 2006;

Table 2.4 Statistical summary of the primary features of the Mg/Ca-bottom water temperature and δ_ω record, specifically the mean (M), glacial (G), and interglacial (I) trends, and glacial-interglacial Δ(G-I) amplitude from different time intervals.

Time Interval (kyr)	Mg/Ca-BWT				δ_ω (‰)			
	M	G	I	Δ(G-I)	M	G	I	Δ(G-I)
0 to 850	1.2	-0.5	3.3	3.9	0.45	0.91	-0.30	1.21
1150 to 2500	2.5	0.7	4.2	3.3	0.41	0.65	-0.05	0.70
3000 to 3150	4.5	3.4	6.0	2.0	0.15	0.35	-0.12	0.46

Chapter 3

3. The Mid-Pleistocene Transition: Trends and Mechanisms

3.1.Abstract

The mid-Pleistocene transition (Schrag et al.) (from ~1200 to 700 ka), is recorded in benthic foraminiferal oxygen isotope ($\delta^{18}O_b$) record as a shift in northern hemisphere glaciations from low amplitude 41-kyr periodicity to large amplitude 100-kyr glacial-interglacial cycles. The MPT has hypothetically been attributed to: (1) global cooling due to a long-term decreasing trend in greenhouse gases (Raymo, 1997); or (2) changes in internal ice sheets dynamics, independent of cooling (Clark and Pollard, 1998). However, evidence in support of either hypotheses is inconclusive. Here I present orbitally resolved Pleistocene bottom-water temperature and global ice-volume records that provide a new view of the origin of the 100-kyr climatic cycles. The record shows a cooling trend associated with an increase in the severity of glaciation and deglaciations across the MPT. The cooling trend is attributed to changes in insolation driven by a decrease in obliquity amplitude. Here, we re-analyze the BWT and sea level records together with sea surface temperature records and show that across the MPT: (1) the cooling trend is coherent with upwelling regimes and North and South Atlantic sites, (2) the frequency shift is expressed globally, (3) the phase relationship between temperature and $\delta^{18}O_b$ increases and (4) the meridional and zonal temperature gradient intensifies. The intensification of temperature gradients acts to decrease poleward heat transport to the high latitudes which could promote ice sheet growth. The increase in the phase relationship between BWT and $\delta^{18}O_b$ shows that the time constant of ice sheets changed due to the growth of thicker ice sheets. Therefore, we propose that the MPT is related to

a change in ice sheet dynamics, specifically growth of thicker ice sheets, and the high latitude cooling may have preconditioned the high latitudes for intensification of northern hemisphere glaciation but is not sufficient to explain the MPT.

3.2.Introduction

During the Pleistocene, climate underwent profound changes which led to the development of large-scale northern hemisphere (NH) glaciations following a 100-kyr pacing. The mid-Pleistocene transition (Schrag et al.), occurred from 1250 to 700 ka, marking a shift in frequency and intensity of northern hemisphere glaciations (Clark et al., 2006). In the early Pleistocene, small amplitude glacial-interglacial cycles were paced predominantly by changes in obliquity, at the 41-kyr period. Although, Raymo et al., (2006) proposed that glacial-interglacial cycles varied at 23-kyr due to changes in precession but due to the assymetrical response of the northern and southern hemisphere ice sheets to precessional forcing the signal canceled out leaving a strong obliquity signal. Following the MPT, ice sheets varied at the100-kyr period and the amplitude of glacial-interglacial variability increased implying growth of larger ice sheets. The emergence of 100-kyr cycles and increase in amplitude in the late Pleistocene, however, is poorly understood. A fundamental principle of Milanktovitch forcing is that changes in high latitude NH insolation control late Pleistocene ice ages. Although the 100-kyr pacing of the late Pleistocene glaciations is consistent with variations in Earth's eccentricity, the variation of insolation related to this orbital parameter is too weak and incapable of solely driving such ice ages (Imbrie et al., 1992). Additionally, the emergence of the 100-kyr cycles in the absence of any changes in orbital forcing rejects the possibility that variations in orbital parameters are the primary driver for the transition (Berger et al.,

1999). Therefore, in absence of direct forcing it has been often proposed that the MPT resides in the non-linear response of different components of the climate system (Berger et al., 1999). In chapter 2, I showed that although the deep ocean cooled across both the late-Pleistocene transition (LPT) and MPT, only the MPT is associated with a shift in frequency and amplitude of glacial-interglacial cycles. I suggest in chapter 2 that the LPT is a glaciation threshold response to a global cooling. The divergence in nature of the MPT and the LPT suggests that the entry into the 100-kyr world derives from some change internal to the climate system.

Several different hypotheses have been proposed to produce the non-linear transition. These can generally be classified into two groups: (1) external forcing and (2) ice sheet dynamics. The first group attributes the MPT to a global cooling, possibly caused by a secular decrease in greenhouse gases, specifically atmospheric carbon dioxide (pCO_2) (Raymo, 1997; Mudelsee and Schulz, 1997; Berger et al., 1999; Paillard, 1998). The basic idea in these hypotheses is that colder climate allows the growth of larger ice sheets, which consequently deglaciate only under maximum insolation forcing, while surviving through moderate insolation maxima, thereby giving a rise to the 100-kyr periodicity (e.g. Raymo, 1997; Berger et al., 1999; Tziperman and Gildor, 2003). Recently acquired CO_2 measurements from ice cores, dating back to 800,000 years ago, show no discernible decrease in pCO_2 but rather an increase in amplitude (Petit et al., 1999; Siegenthaler et al., 2005; Luthi et al., 2008). Current evidence to support the global cooling hypothesis is restricted to upwelling regimes, where cooling is evident across the MPT (Marlow et al., 2000; Liu and Herbert 2004; McClymont and Rossell-Mele, 2005). In contrast, sea surface temperature (SST) records from the western

Equatorial Pacific show no pronounced long term trend across the MPT (de Garidel-Thoron et al., 2005; Medina-Elizalde and Lea, 2005; McClymont and Rossell-Mele, 2005). The warm pool of the western Pacific (WPWP) is far from the influence of the continental ice sheets and should respond directly to the radiative forcing of changes in greenhouse gases (Lea, 2004). Thus, the relative long-term stability of the WPWP apparently challenges the decreasing pCO_2 scenario (de-Garidel Thoron et al., 2005). Both components of the MPT, a global cooling or a decrease in pCO2, are poorly understood.

The "*regolith hypothesis*" of Clark and Pollard (1998), argues that during the early Pleistocene the size of NH ice sheets was constrained by the occurrence of a relatively unstable regolith substrate, which could not support thick ice sheets. The exposure of Precambrian Shield bedrock by repeated glacial erosion allowed, however, the buildup of thicker ice sheets, which upon reaching a critical size started to respond non-linearly to eccentricity. In the latter hypothesis, the areal extent of ice sheets does not increase, as in the "cooling hypotheses" but rather the thickness of the ice sheet increases. The expansion of ice sheets, either areally or in height, in association with the MPT would have different impacts on climate via the ice-albedo effect. Recent studies suggest orbital obliquity as the primary driver of 41-kyr glacial-interglacial cycles in ice volume in the early Pleistocene and 80-120 kyr cycles in the late Pleistocene. After the MPT, climate skipped one or two obliquity beats before deglaciation and the response was channeled into 80- and 120-kyr cycles (Huybers and Wunsch, 2005; Huybers, 2006). Huybers (2007) proposed that the progression of Pleistocene G-I cycles is related to a threshold value corresponding to possibly a decrease in pCO_2, sea-ice variability, and ice

sheet dynamics. Alternatively, the trigger of the last several 100-kyr cycles in NH ice sheet variability has been linked to the influence of eccentricity through its modulation of orbital precession (Raymo, 1997; Kawamura et al., 2007). The relative importance of these processes is not well constrained and awaits development of unambiguous records of the high latitude climate change and global ice volume.

Deep sea records have provided a valuable window into high-latitude climate variability during the Pleistocene. The oxygen isotope composition ($\delta^{18}O$) of benthic foraminiferal shells is a recorder of changes in the deep ocean and is routinely used to understand transitions in climate. The isotopic composition from the deep ocean recorded in foraminifera is primarily a function of temperature of the ocean water in which the shells formed and the oxygen isotope composition of seawater (δ_ω), which depends on long-term changes in the extent of continental ice sheets and local changes in evaporation-precipitation. Thus, interpretation of $\delta^{18}O$ in terms of climate variability is limited by the lack of information of either temperature or δ_ω.

The global deep sea benthic foraminiferal oxygen isotope record shows a shift from a smaller amplitude ($\delta^{18}O_b$=1‰), 41-kyr glacial-interglacial cycles to larger amplitude ($\delta^{18}O_b$ =1.6‰) 100-kyr cycles, across the MPT (Fig. 3.1). The shift in average $\delta^{18}O_b$ is considered to the first order to represent an increase in polar ice volume which suggests the size of northern hemisphere ice sheets increased, although a component of the $\delta^{18}O_b$ signal might be a response to deep sea temperature variation.   The MPT began 1250 ka, identifiable by a gradual increase in the long-term average, the glacial-interglacial amplitude, and a shift to low-frequency variability, and reached completion by 700 ka. An independent paleothermometer is necessary to constrain the relative

contributions of ice volume and temperature to the $\delta^{18}O_b$ signal. Deep sea temperature estimates thus far has been controversial and limited. Emiliani (1955) suggested that the $\delta^{18}O_b$ record mainly reflect changes in deep sea temperature, whereas Shackleton (1967) later negated this claim and hypothesized that the $\delta^{18}O_b$ variability is primarily recording changes in ice volume, currently the general rule used when interpreting $\delta^{18}O_b$ records.

To circumvent these problems, several studies have implemented clever techniques to separate the $\delta^{18}O$ record into the relative contributions of temperature and ice volume. Approaches to directly resolve δ_ω and indirectly deep sea temperature, range from interpreting $\delta^{18}Ob$ records from regions presently near the freezing point of seawater (Labeyrie et al., 1987), modeling pore-water fluid chemistry (Schrag et al., 1996; Adkins et al., 2001; Schrag et al., 2002; Adkins et al., 2002), stacking benthic $\delta^{18}O$ records (Waelbroeck et al., 2002; Lisiecki and Raymo 2005), combining ice core and sediment records (Shackelton 2000), and using trace metal ratios in planktonic and benthic foraminifera (Lear et al., 2000; Martin et al., 2002; Lea et al., 2004).

To determine the magnitude of deep water cooling, Dwyer et al., (1995) used Mg/Ca ratios from ostracodes to reconstruct bottom water temperature (BWT) at Deep Sea Drilling Program (DSDP) site 607 in the North Atlantic, which currently is largely influenced by North Atlantic Deep water (NADW) formation. Note this Mg/Ca-BWT record is not continuous and covers only two intervals, the late Pleistocene (0-220 ka) and the late Pliocene (2200-3200 ka). The Mg/Ca-BWT shows an increase in the average Δ(G-I) amplitude from 3.6°C during the late Pliocene 41-kyr glaciations and a 4.5°C during the late Pleistocene 100-kyr glaciations (Fig. 3.2). This indicates that during the Pleistocene deep water was cooler than during the Pliocene. Subsequently, Martin et al.,

(2002), using benthic foraminiferal Mg/Ca show that both ocean basins cooled from ~2-4 °C during the last two glacial cycles in agreement with pore water records (Schrag et al., 1996; Adkins et al., 2002) (Fig. 3.2). However, the available records of deep sea temperature and ice volume change are limited to the last few glacial cycles and do not capture the nature of climate transition for the entire Pleistocene interval. To interpret and understand the climate transitions, an independent deep ocean temperature record documenting the Pleistocene is necessary.

Here, I focus on new, orbitally resolved records of BWT and global ice volume with the intent to understand the transition from 41-kyr to 100-kyr (G-I) cycles and the emergence of the climate into the modern 100-kyr regime. The high-resolution record of benthic foraminifera Mg/Ca from North Atlantic DSDP site 607 allows us to quantify the extent of global cooling and, paired with $\delta^{18}O_b$, to estimate the concomitant change in ice volume across the MPT. The BWT record is compared to newly, available high-resolution records of SST from Atlantic and Pacific Oceans to determine the global extent of cooling, commonality amongst the records, and examine changes in equator-pole temperature gradients. The 800,000 yr long record of pCO_2 variability presents an opportunity to evaluate high-latitude climate sensitivity to changes in radiative forcing and its role in BWT change. To constrain whether or not variation in ice sheet dynamics played a role in the MPT and entry of 100-kyr cycles, variations in Pleistocene global ice volume, derived from the Mg/Ca-BWT record, are evaluated within the context of available sea-level records. Here, I will demonstrate that the MPT was associated with a high-latitude cooling and a shift in the glacial-interglacial amplitude of ice volume. Following the MPT, glacial periods were cooler with more ice. Interglacial periods were

also cooler but with less ice. Therefore, I propose that although the cooling might have

been a precursor to the emergence of 100-kyr cycles, it is not sufficient to explain the

MPT. Instead, a change in ice sheet dynamics is necessary to explain the entry in the

100-kyr world.

3.3.Methods

A high resolution 1800 kyr record of past bottom water temperature variations in the deep

North Atlantic Ocean was obtained using Mg/Ca ratios in benthic foraminifera,

Cibicidoides wuellerstorfi and *Oridorsalis umbonatus* from DSDP site 607 (41°N, 32°W,

3427-m water depth) and *Chain* 82-24-23PC (43°N, 31°W, 3406-m water depth). Mg/Ca

measurements were done using a Finnigan Element-XR inductively coupled plasma mass

spectrometry (ICP-MS) following the analytical protocol detailed in Rosenthal et al.,

1999. The age model was constructed following the paleomagnetic time scale of Cande

and Kent (1992).

I compare the primary features (i.e. trend, amplitude, frequency, phase) of the

previously presented BWT record with newly available, orbitally resolved Pleistocene

SST records from multiple locations in the Pacific and Atlantic Ocean. The timescale

utilized for the SST records derives mainly from orbital tuning. Due to differences in age

models, there is an error of about 25-50 kyr associated with evaluating coherency among

temperature records.

Mean long-term trends in each dataset were determined using a Gaussian filter

with a 400-kyr cut-off frequency. To compute the interglacial and glacial trends in

temperature, I identify minimum glacial and maximum interglacial values in each marine

isotope stage and apply a curve fit to the data. Glacial-interglacial amplitude in temperature is determined by subtracting the glacial and interglacial trend in early and late Pleistocene intervals. The timing of shifts in mean, glacial, and interglacial trends was visually identified by the maximum shift in slope. Evolutionary spectral analysis was performed on the BWT record using the Arand Software Package using a time window of 300 kyr whereas evolutionary spectra performed on SST records derives from the analysis of Clark et al., (2006). Before spectral analysis was performed, the BWT record was resampled every 3 kyr using linear interpolation to obtain an evenly spaced record.

3.4. Bottom Water Temperature Record

In chapter 2, I have constructed a Mg/Ca downcore record from DSDP site 607 based on two benthic foraminifera species, *C. wuellerstorfi* and *O. umbonatus* (Fig. 3.3). DSDP site 607 is located in the sub-polar North Atlantic and is sensitive to changes in high latitude climate and NH ice sheet. Currently, DSDP site 607 resides in NADW, but intrusion of southern source waters during glacial periods makes this site sensitive to local water mass changes. Across the MPT, changes in the mean trend (MT), glacial (GT) and interglacial (IT) trends, glacial-interglacial amplitude Δ(G-I), and frequency shift represent the primary features of the Mg/Ca-BWT record (Table 3.1). To calculate the change in the temperature (MT, GT, IT) and Δ(G-I), I average the data from before the MPT (1150-1800ka) and after the MPT (0-850 ka) and subtract the two intervals from each other. The Mg/Ca-BWT record shows a long-term cooling of 1.4±1°C in the MT from 1150 to 850 ka and increase in Δ(G-I) from 3.3 to 4.3°C that begins following the initial cooling at ~900 ka. The GT and IT decrease concomitantly with the MT by

1.5±1°C and 0.9±1°C, respectively. The GT continues to decrease, following the MPT (1150 to 850 ka), until it reaches a plateau around 500 ka. Low-frequency variability emerges at 900 ka, following the cooling in the MT, and reaches full amplitude by 700 ka (Fig. 3b). The initial appearance of 100-kyr cyclity is characterized by a broadband power and evolves into a narrow, persistent band over the last 700 kyr. The BWT shift of 1.4°C from 1150 to 850 ka corresponds to an equivalent change in $\delta^{18}O_b$ of ~0.3‰. The actual shift in MT of $\delta^{18}O_b$ from 1150 to 850 ka is, however, ~0.3‰ which suggests the shift in $\delta^{18}O_b$ primarily represents a deep ocean cooling. The main features of the BWT record are similar to the $\delta^{18}O_b$ and suggest that temperature variation is a significant portion of the $\delta^{18}O_b$ signal.

As shown in chapter 2, the BWT record mainly reflects changes in polar surface ocean temperatures and to lesser extent water mass variability. To determine the global extent of cooling, I first compare the DSDP site 607 $\delta^{18}O_b$ record with the LRO4 stacked $\delta^{18}O_b$ record from Lisiecki and Raymo (2005) (Fig.3.1). The 607 $\delta^{18}O_b$ record represents a combination temperature, water mass, and ice volume effects. Variations in $\delta^{18}O_b$ are related to polar surface ocean temperature (where NADW forms), global ice volume, and local changes in temperature and δ_ω due to water mass variability. Across the MPT, part of the shift in $\delta^{18}O_b$ could be attributed to a regional change in temperature or δ_ω. The LRO4 $\delta^{18}O_b$ stack record represents $\delta^{18}O$ measurements from 57 sites and reflects changes in global deep water. From 1150 to 850 ka, the LRO4 and 607 $\delta^{18}O_b$ records increase by 0.18 and 0.27‰, respectively. The deep ocean might have cooled by a maximum of 0.8°C globally, assuming the 0.18‰ in LRO4 is solely related to temperature. The residual of 0.10‰ between LRO4 and 607 suggests that the additional

cooling of 0.6°C at site 607 is related to increased influence of AABW during glacial intervals. The relative Δ(G-I) in 607 $\delta^{18}O_b$ is greater than LRO4 in the early and late Pleistocene which implies that local changes in temperature during (G-I) periods are larger in the deep North Atlantic than in other regions (i.e. deep Pacific). The residual shows an average variability of ~±0.25‰ across the Pleistocene which suggests that the uncertainty related to influences due to changes in local δ_ω or local temperature of bottom water is ~1°C or 25-m of sea level similar to the uncertainty in the Mg/Ca-temperature calibration (See chapter 2). The uncertainty in temperature and sea level are calculated by assuming that a 1‰ change in $\delta^{18}O_b$ corresponds to a ~4.5°C change in temperature.

To independently evaluate the partitioning of BWT change between water mass changes and high latitude temperature, I use records of benthic foraminifera carbon isotopes, $\delta^{13}C_b$, and Cd/Ca ratios as tracers of paleocirculation at DSDP site 607. DSDP site 607 in the modern-day is saturated with NADW, but during the last glacial maximum, evidence suggests that the influence of AABW was larger (Boyle, 1982; Boyle and Keigwin 1985/86; Boyle and Keigwin, 1987; Oppo and Fairbanks, 1987; Raymo et al., 1997). During glacial periods, following the MPT, there was an increase in AABW influence. The $\delta^{13}C_b$ record, an indicator of water mass changes, shows a shift in periodicity and Δ(G-I) from 1050 to 1150 ka, similar to the Mg/Ca-BWT record mainly due to an increase in glacial minima (Raymo et al., 1997). The increase may additionally reflect the reduced contribution of southern source waters during deep water formation due to increased sea ice extent in the Southern Ocean. Here. I compare Cd/Ca ratios in benthic foraminifera to determine if the swings in $\delta^{13}C_b$ across the MPT are significantly influenced by ventilation changes in the Southern Ocean. In figure 3.4, a record of *C.*

wuellerstorfi Cd/Ca variability from DSDP site 607, is plotted with lower Cd/Ca (higher $\delta^{13}C_b$) values reflecting a higher proportion of NADW relative to AABW. The Cd/Ca record shows similarities to the $\delta^{13}C_b$ record both in MT and Δ(G-I) shift and suggests that across the MPT there was a major shift in AABW influence during glacial periods. Therefore, part of the increase in Δ(G-I) and decrease in the MT in the BWT record resulted from increased influence of the colder AABW.

To determine the magnitude of temperature change associated with (G-I) water mass variability, I model a temperature record based on a %NADW record at DSDP site 607 (Raymo et al., 1997). Assuming modern-day water mass properties (NADW T=2.7 ºC; AABW T=1ºC) and a simple mixing scenario, a %NADW-BWT record was calculated. This record has a (G-I) temperature range from ~1.5 to 2.6ºC and ~1 to 2.6ºC across 41-kyr and 100-kyr glacial-interglacial cycles, respectively (Fig.3.5). The Mg/Ca-BWT and modeled circulation driven ΔBWT records show an increase in Δ(G-I) BWT and long-term cooling in the MT across the MPT. However, the magnitude of cooling is much smaller in the %NADW-BWT record (~0.5ºC) than the Mg/Ca-BWT record (~1.4ºC). The subtraction of circulation driven BWT variability from the shift in BWT at this site leaves a residual cooling of 0.9ºC which is consistent with the estimate from residual $\delta^{18}O_b$. The BWT Δ(G-I) increases in both records, by 0.5ºC in the modeled-BWT and 1.0°C in the Mg/Ca record, which suggests the increase in Mg/Ca-BWT partially reflects an increase in AABW influence.

Another way to approach the question of how to distinguish between water mass mixing (local) and high-latitude climate change is to compare the IT and GT in BWT. During interglacial periods, site 607 is primarily bathed in NADW, a relatively saturated

water mass, while during glacial periods AABW, an undersaturated water mass, influences the region. Hence, the long-term GT reflects changes in carbonate saturation (see Chapter 2-Mg/Ca-temperature calibration), water mass mixing of southern source waters, and high latitude climate change. However, the IT will primarily reflect high latitude climate change and minimal carbonate saturation effects. The IT in BWT shows a 1°C cooling while the GT shows a larger 1.5°C cooling from 1150 to 850 ka (Fig.3.6). This offset in cooling trends is likely due to greater sensitivity to water mass mixing during glacial periods. Overall, from 1150 to 850 ka, the deep North Atlantic ocean cooled concomitantly with the high latitudes (Ruddiman et al., 1989; McClymont et al., 2008) and upwelling regimes (McClymont and Rosell-Mele, 2005; Lawrence et al., 2006). Assuming NADW formation across the last 1.8 Myrs, this Mg/Ca-BWT represents polar surface ocean temperatures and the cooling is a robust feature of the high latitudes independent of ocean circulation. The high latitude cooling is part of the long-term cooling of the Cenozoic associated with major climate transitions (Lear et al., 2000).

3.5. Comparison with other Temperature Records

To gain more perspective on whether DSDP 607 BWT record represents a global expression of the MPT, I compare the record to SST records from the tropical and subtropical Pacific and Atlantic Oceans (Table 3.2; Fig.3.7, 3.8). SST records from various locations have regional influences but also share commonality with the BWT record suggesting that high-latitude climate variability impacts and coeval with sub-tropical to tropical climate regimes. Pleistocene SST records derive from previously published studies from the North Atlantic (Ruddiman et al., 1989), South Atlantic (McClymont et al., 2005; Martinez et al., 2006), Eastern Equatorial Pacific (EEP)

(Lawrence et al., 2006; McClymont et al., 2005), Benguela upwelling regimes (Marlow et al., 2000; Durham et al., 2001) and WPWP (Medina-Elizalde and Lea, 2005; de Garidel Thoron 2005). Records from upwelling regimes Ocean Drilling Program (ODP) sites 846, 849, 1077, 1084 and the North Atlantic DSDP site 607 and South Atlantic ODP site 1087 (not shown in figure) reveal a long-term cooling in the MT across the MPT. In contrast, SST records from the WPWP (ODP site 806, core MD97-2140) show no discernible long-term trend associated with the MPT. The Mg/Ca-BWT trend is consistent with those sites influenced by upwelling and mid- to high latitude regions.

The initiation and culmination of the cooling trend is variable from site to site. However, the difference in timing of the transition amongst the temperature records are within the error of the reconstructions and various age models and points to a similar timing in the shift in temperature. DSDP 607 SST record shows a general cooling that began at ~1250 ka and reached a minimum value by 900 ka. Both SST records from the EEP decreased in the MT concomitantly from 1200 to 900 ka. ODP 1077, in the Benguela upwelling regime, agrees with the timing of the EEP shift, whereas ODP 1084 began at 1250 ka and ended at 825 ka. Thus, the decrease in SST, regardless of site, only slightly precedes the cooling in the BWT record by 50-100 ka and the termination of the cooling is relatively coherent with the BWT record (<25 ka). The presence of the cooling trend in regions remote from high latitudes and the commonality in timing of the decrease in temperature indicates that the cooling occurs at a large-scale.

Across the MPT, the BWT record shows an increase in Δ(G-I) that is pronounced in SST records from the mid to high latitudes and upwelling regimes (Fig.3.9).   The timing of the increase Δ(G-I) varies depending on region. To examine the shift in Δ(G-I),

I removed the trend from each temperature record and visually identified the main shift in amplitude. The BWT record from DSDP 607 and SST records from ODP 849 and 1077 show an overall correspondence in increase in Δ(G-I) occurring between 1000 to 900 ka. However, the shift in Δ(G-I) SST in DSDP 607 and ODP 846 precedes the shift in the BWT record transitioning at 1100 and 1250, respectively. This comparison indicates that before the MPT Δ(G-I) in temperature was smaller than following the transition and the timing of the actual shift varies depending on location. Unlike the shift in mean trends which occurred simultaneously, the increase in the amplitude shows a strong regional expression. The trend in temperature across the MPT is linked to a global forcing whereas the shift in amplitude is related a combination of local and global effects. Records from the WPWP show an increase in Δ(G-I) temperature amplitude but occur at 450 ka, much later than the other temperature records which suggests that this shift is not linked to the high latitudes (Fig. 3.10). The divergence in the timing of the Δ(G-I) shift implies that not one single mechanism can explain the features of temperature variability.

The shift in frequency observed in the BWT and $\delta^{18}O_b$ record, occurs in all records regardless of the distance from NH ice sheets. I peformed evolutionary spectra on the BWT record from this study (Fig. 3.3) (see Methods). The time frequency spectrograms based on the SST records derives from the analysis of Clark et al. (2006) in a review of the MPT (Fig. 3.11). In the early Pleistocene, SST records were dominated by 41-kyr cycles and 100-kyr cycles dominated in the late Pleistocene. The emergence of low frequency variability occurred simultaneously in all records except the DSDP site 607 SST. The BWT shows an increase in low frequency variability at ~900 ka characterized by a broadband of power becoming a narrow, persistent band of power at

~700 ka. Similarly, the, appearance of 100-kyr cycles in the tropical Pacific Ocean (ODP 806, 846, 849) and in the South Atlantic Ocean (ODP 1087) began at ~950 ka. The shift into 100-kyr cycles occurred at 1250 ka in the DSDP 607 SST record, earlier than BWT record or SST records from multiple regions. Clark et al., (2006) hinted that the early appearance of low-frequency variability in DSDP 607 SST record is related to sensitivity of this region to ice-sheet influences. However, if this were true I would expect the same low frequency variability to emerge in the BWT record. The DSDP 607 SST record is based on census counts and the discrepancy may stem from the uncertainty in the proxy application. Low frequency variability, in narrow band, increases in power at 450 ka in all records. The appearance of low-frequency variability in all records following the MPT, regardless of location, suggests a global forcing behind this response. The intensification of NH glaciation is accompanied by large scale changes in regions far from their influence.

Changes in SST and BWT are not synchronized with $\delta^{18}O_b$ record during the early or late Pleistocene. Orbital-scale BWT variability leads $\delta^{18}O_b$ in the early Pleistocene by 3±2 kyr in the obliquity band and by 10±5 kyr in the late Pleistocene in the eccentricity band (Fig. 3.12, 3.13). Changes in SST lead the $\delta^{18}O_b$ record by 3 kyr in the early Pleistocene from tropical Pacific Ocean (i.e. ODP 806 and 846) similar to BWT record. The lead of BWT and SST records increases in association with the emergence of 100-kyr cycles. The similar response in phase relationship of the high latitudes and tropical Pacific Ocean suggests a common link between the driver of long-term changes in both regions.

The coherency between the BWT and SST records in cooling, emergence of 100-kyr cycles, and increase in phase relationship suggests that the high latitudes are mechanistically linked to individual locations in different ways and there may exist important feedbacks between distant regions.   Today SST variability in upwelling region is tied to wind-driven thermocline depth changes, changes in temperature of surface water mid-latitude subduction sites (Harper, 2000), and deep ocean temperature variability (Philander and Federov, 2003). Thus, the SST records in upwelling regimes should partially reflect long-term trends in deep ocean variability and be modified by regional changes in wind strength of the source region. The WPWP is far from the influence of ice sheets and should reflect mainly direct effects of changes in radiative forcing, possibly greenhouse gases, but the shift in frequency from 41 to 100-kyr (G-I) cycles suggests a role for high latitude forcing. The mid to high latitude records are influenced by direct and high latitude climate variability related to ice sheet variations, shifts in Atlantic meridional overturning circulation, and upwelling intensity.

The decrease in temperature in high latitudes and upwelling regions in contrast to the long-term stability in the WPWP challenges the idea of decreasing pCO_2 across the Pleistocene as suggested by de Garidel-Thoron et al., (2005). The WPWP SST records show a shift in amplitude around 450 ka that is inconsistent with the EEP, mid-latitude, or high latitude SST records. (Fig. 3.10). The increase in WPWP SST amplitude, reflected by an increase in interglacial values, implies a change in the forcing. The pCO_2 record for the last 800 kyr shows an increase in Δ(G-I) across 450 ka similar to both western tropical Pacific temperature records. Atmospheric CO_2 changes have been proposed to be the dominant forcing in temperature variability in tropical ocean regions

(Crowley, 2000; Lea et al., 2004) and are forcing the (G-I) SST varability of the western tropical Pacific. High-latitude temperature did not respond to this shift in pCO_2, evident by the lack of increase in Δ(G-I) across 450 ka. The high latitudes may not be directly sensitive to pCO_2 variability, but rather respond to changes in glacial dynamics or insolation.

The increase in SST amplitude observed in the upwelling regimes ranges from 1250 to 900 ka depending on site. The increase in Δ(G-I) of pCO_2 at 450 ka is not shown in these SST records. The cooling and increase in SST amplitude in upwelling regions is forced by either changes in regional hydrographic conditions (e.g. wind strength) and/or high latitude climate variability. McClymont and Roselle-Mele (2005) suggested that cooling in the EEP is linked to changes in the equator-pole temperature gradients in the Southern Hemisphere in addition to the long-term trends in deep ocean temperature. Lawrence et al., (2006) proposed that the high latitudes modulate EEP conditions and there is a strong link in the obliquity band between the high and low latitudes. The synchronization in SST patterns from multiple upwelling regions on orbital timescales hints that changes in high latitude climate are driving upwelling regime temperatures. Regardless, of the mechanism of high latitude cooling, this signal seems to be imprinted in the Atlantic and Pacific surface ocean suggestive of a tight link to polar climate variability and a greater climate sensitivity than expected from a tropical regions remote from NH ice sheets.

3.6. Meridional Temperature Gradients

A progressive cooling in the high latitudes, as observed from the Mg/Ca-BWT record presented here, is paralleled by the intensification of the meridional and zonal SST

gradient that began about 1.2 Ma associated with the MPT (Fig. 3.14). Modification in

the meridional temperature gradient, defined here as the difference in SST between the

WPWP and high latitude surface ocean, could affect large-scale atmospheric dynamical

responses, such as changes in wind strength and moisture transport (Raymo and

Nisancioglu, 2003). To calculate the meridional ΔT and to assess its variability, I

subtracted the BWT record from the WPWP SST record from de Garidel-Thoron et al.,

(2005) and assumed that the cooling in the BWT record mainly reflects high latitude SST

patterns across the Pleistocene and that the WPWP is representative of the mean oceanic

response of the tropical ocean on long-time scales. Regardless of which WPWP SST

record, ODP 806 or MD97-2140, is used in the ΔT calculation the results are the same.

The meridional ΔT record shows a long-term intensification of the temperature gradient

which is largely driven by the progressive cooling of the high latitudes as the tropics

remain stable. Between 900 and 1000 kyr ago, Raymo et al., (1997) noted a pronounced

shift in $\delta^{13}C_b$ record suggesting weaker meridional overturning circulation possibly

related to reduced NADW production which would have resulted in less ocean heat

transport. Stronger winds are associated with an increase in temperature gradient as

suggested by modeling studies (Rind, 2000) and could subsequently impact the

development of upwelling regimes.

The similarity in the shift in meridional temperature gradient and upwelling

regimes suggest a tight link between extra-tropical and tropic ocean conditions.

Concomitant with the high latitude cooling is an increase in oceanic heat loss which is

linked to the development of the tropical thermocline until a new thermal balance is

achieved between the ocean and atmosphere (Philander and Federov, 2003; Boccaletti et

al., 2004); the high latitude oceanic heat loss is compensated by the increase in heat gain in the upwelling regions.

Across the MPT, the decrease in SSTs in upwelling regions has previously been associated with a decrease in deep ocean temperatures through the link between deep ocean stratification and shoaling of the thermocline (Philander and Federov, 2003). Deep ocean temperature variability, communicated through changes in the meridional temperature gradient, also, influence upwelling regimes through changes in wind strength which intensify upwelling and further cool SST.

Amid the cooling of the upwelling regimes, specifically in the eastern equatorial Pacific, and the attendant stability of SSTs in the WPWP, the zonal gradient in the tropical Pacific Ocean intensified. Proxy evidence shows that trade wind intensity, inferred from changes in mean grain size, increased across the MPT associated with the intensification of the zonal gradient (de Garidel-Thoron et al., 2005; McClymont et al., 2005). The reduction in heat flux and increase in moisture transport as suggested by McClymont et al. (2005), associated with an increase in the zonal gradient, to the high latitudes could act as a positive feedback on ice sheet development across the MPT (Molnar and Cane, 2002; Philander and Federov, 2003). An increase in moisture transport and decrease in heat flux would provide the precipitation source and favorable conditions for ice sheet growth that is necessary for the establishment of large ice sheets. The high latitude cooling and positive feedback related to the gradient shifts may have aided in maintaining or promoting the intensification of northern hemisphere glaciation.

3.7.Global Ice Volume

The use of an independent paleothermometer, such as Mg/Ca in benthic foraminifera, aids in constraining the relative contribution of ice volume and temperature to the benthic oxygen isotope record. This approach has been previously used in several studies (Dwyer et al., 1995; Lear et al., 2001; Martin et al., 2002; Billups et al., 2002) to determine the magnitude of changes in global ice volume and by inference sea level change. To illustrate this, I use the Mg/Ca-based temperatures and the following equation from Shackleton (1974): T=16.9 -4.0 (δ^{18}O$_{calcite}$-δ_ω) to calculate δ_ω, the oxygen isotopic composition of seawater which is based on empirical relationship between benthic foraminiferal (i.e. *Uvigerina peregrina*) δ^{18}O$_{calcite}$ and temperature.   The sea level estimates were based on assuming δ_ω variations represent changes in global ice volume and that 10 m change in sea level equates to a 0.0l ‰ change in δ_ω per meter sea level (Fairbanks, 1989) and the mean isotopic composition of ice sheets remained constant while they changed in size. The scaling of the δ_ω record to sea level uses an intermediate estimate between the upper value 0.011‰/m from Fairbanks and Matthews (1978) and the lower value of 0.008‰/m from Schrag et al., (1996). In addition to changes in δ_ω related to sea level and ice volume, local changes in δ_ω due to water mass variability and salinity end-member variations could influence this record

From marine isotope stage (MIS) 1 to 12, the sea level record (Fig. 3.15) shows similar glacial-interglacial variability with 100-kyr cyclity similar to other sea-level records (Shackleton, 2000; Waelbroeck et al., 2001; Lea et al., 2002; Siddall et al., 2003). The sea-level record is in good agreement in amplitude and trend, glacial-interglacial variability related to ice sheet development and retreat. However, the MT in both glacial

and interglacial periods from MIS 5e to 12 is offset from other estimates. The sea level record, derived from the Mg/Ca and $\delta^{18}O_b$ records, shows a considerable offset in interglacial high stand in comparison to sea level estimates from previous studies. For example, in a sea level compilation from Siddall et al. (2005), they showed that MIS 5e ranged from 0 to +6 m above present day sea level, wheras MIS 9 and 11 range from -3 to +4 and -1 to +4, respectively. Here, the sea level record shows much higher sea level estimates during MIS 9 and 11 by about +50-m and during MIS 5e and 7 by about +25-m. Part of this offset is attributable to the timing in the BWT and $\delta^{18}O_b$ records. BWT leads $\delta^{18}O_b$ by about 10 kyr and this phase relationship is evident across MIS 12 to 8 (Fig. 3.16). At peak interglacials, temperature has already began to decline while $\delta^{18}O_b$ has yet to reach full interglacial values and thus δ_ω estimates are higher than expected. In the sea level and deep sea temperature study, Waelbroeck et al., (2001) noted that the rate of buildup of ice sheets appear to have been slower the rate of decrease of local temperature. Lea et al., (2004) observed that tropical sea surface temperatures on average lead $\delta^{18}O_b$ by ~3kyr and significantly larger across terminations (e.g across termination-V by ~7-9 kyr). Martin et al., (2002) in their deep ocean temperature study, noted that the BWT temperature record leads changes in $\delta^{18}O_b$ the Atlantic Ocean. The lead of BWT over $\delta^{18}O_b$ seems to be a feature in the surface and deep ocean and in both the Atlantic and Pacific Ocean Basins.

Part of this offset derives from the uncertainty associated with using Mg/Ca-BWT estimates paired with $\delta^{18}O_b$ to estimate variations in the oxygen isotope composition of seawater and converting it to sea level. However, the similarity in the shape of glacial-interglacial variability of the 100-kyr cycles between previous estimates and the record

derived here suggests that the δ_ω record is largely reflecting changes in ice volume. Thus, I interpret large-scale changes in δ_ω and sea level. Aside from the offset, I compare changes in MT, GT, IT, Δ(G-I) and frequency. From 0 to 400 kyr, the record has a strong 100-kyr frequency associated with the ice volume changes and lags BWT changes by ~20 kyr. Following the MPT, around 700 ka, sea level amplitude increases from 70-90 m to 120-150 m in the late Pleistocene. Previous studies estimated a 100-140 m drop in eustatic sea level at the LGM and indicate that a similar range of sea level occurred over the last few glacial-interglacial cycles (Yokoyama et al., 2000; Shackleton, 2000; Lea et al., 2002; Waelbroeck et al., 2002; Siddall et al., 2003). Sea level estimates before MIS12 rely on snapshots of interglacial highstands (Pirazzoli et al., 1991; Murray-Wallace, 2002) which show the interglacial values decrease before 0.5 Ma to 20-30 m below present. These estimates correspond with the decrease in interglacial highstand between MIS 12 and MIS 20 shown in the earlier part of the Mg/Ca-derived sea level.

The lack of discernible trend in the sea level record but rather an increase in the amplitude suggests that much of the increase in the $\delta^{18}O_b$ MT is related to a deep ocean cooling. The change in Δ(G-I) in BWT corresponds with the increase in $\delta^{18}O_b$ amplitude (from 1.2 to 1.9 ‰) which means that relative contribution of temperature and ice volume to the $\delta^{18}O_b$ record is on average 50:50. These results are comparable to the studies of Dwyer et al. (1995), Adkins et al. (2002), Martin et al. (2002) and Shackleton (2000) who propose that half of the deep Atlantic 100-kyr signal in $\delta^{18}O_b$ record is driven by temperature.

The increase in the LRO4 $\delta^{18}O_b$ MT across MIS 22 to 28 of about 0.18 ‰ has been attributed to a lowering of sea level by 20-30 m (Kitamura and Kawagoe, 2006).

However, the Kitamure and Kawagoe (2006) estimate is based on sequence stratigraphy from shallow sediments and may reflect uncertainties related to quantifying local changes in uplift. The Mg/Ca-sea-level record shows no discernible lowering of sea level (~by 0±20 m) across MIS 22 to 28 with the full expansion of ice sheets not complete until MIS 12.

The sea level record, derived from the δ_ω record, might have a non-glacioeustatic component due to local changes in water mass mixing and changes in endmember character. Across glacial-interglacials and the MPT, changes in the mixing of northern and southern source waters may imprint the δ_ω record at this site. In the comparison between LRO4 $\delta^{18}O_b$ and the 607 $\delta^{18}O_b$ records (see figure 3.1), I calculated that residual 0.1‰ change $\delta^{18}O_b$ between LRO4 and 607 and determined that is was related to local changes in water mass mixing. The uncertainty in the global δ_ω change across the transition is ~<10 m due the influence of changes in local deepwater δ_ω. Regardless, the local δ_ω influence cannot account for the shift in the $\delta^{18}O_b$.

The MPT does not represent a shift in the ice volume MT, as previously thought, but rather an increase the Δ(G-I) of ice volume variations. Records of δ_ω from the WPWP show no discernible increase in ice volume across the MPT but rather an increase in the amplitude of the signal, similar to this study (de Garidel-Thoron et al., 2005; Medina-Elizalde and Lea, 2005). Evidence from sea level records show that sea level during MIS 13, 15, 17, and 19 stood lower than today's sea level (Shackleton, 1987) which suggests that prior to the development of the large saw-tooth pattern glacial-interglacial cycles of the last 500 ka, the sea level difference between interglacial-glacial

cycles was not as large. The findings of this study have implications for the understanding of the changes in glacial dynamics across the MPT.

3.8. Mechanisms of Glaciation

The main characteristics of the MPT, based on the $\delta^{18}O_b$ record, are a positive shift toward a cooler, more glaciated state, a shift into larger Δ(G-I), low-frequency variability, and asymmetric patterns of G-I variability. The intensification of NH glaciation has been linked to a threshold response to global cooling or a change in ice sheet dynamics. The "global cooling" hypotheses proposes that, due to a secular decrease in pCO_2, ice sheets became large enough, due to an increase in areal extent, to survive thru weak maxima in summer insolation (Raymo, 1997). On the other hand, the "ice sheet dynamics" hypothesis supports the idea that NH ice sheets reached a critical size, due to increase in ice sheet height, and survived through maxima in insolation. Predictions based on the "global cooling" hypotheses are that global temperature should decrease with a concomitant increase in Δ(G-I) due to an increase in the areal extent of ice sheets (i.e. increase in albedo). This follows the idea of Ashkenazy and Tziperiman (2004) who proposed that the Δ(G-I) of high latitude temperature is linked to changes in ice sheet albedo. According to the ice sheet dynamics hypothesis, predictions are that global temperatures should remain stable and Δ(G-I) in temperature should remain roughly the same before and after the MPT due to an increase in ice sheet thickness rather than a shift in areal extent (i.e. constant albedo).

The primary features of the BWT and global ice volume records, presented here, aid in evaluating the predictions based on the above hypotheses to understand the mechanism behind the MPT.   The BWT record, a high latitude climate signal, shows a

cooling, from 1150 to 825 ka, which slightly preceded the shift in the DSDP 607 $\delta^{18}O_b$ record. The cooling occurred in both the GT and IT and signals a shift in the mean climate state. SST records from the Atlantic and Pacific Oceans cooled along with the high latitudes and thus support the idea of a global cooling. However, the change in frequency, from 41 to 100-kyr, and the increase in Δ(G-I) does not occur simultaneously with the cooling. Low-frequency variability appears towards the end of the cooling trend and increases in power following 700 ka in all temperature records. The offset in the timing between the cooling trend and frequency shift suggests that a global cooling may not be sufficient to fully explain the MPT.

Did the areal extent of ice sheets change across the MPT? Evidence from the temperature records show an increase in Δ(G-I) but it occurs at variable timings depending on location. The BWT record displays an increase Δ(G-I) at ~900 ka but this increase is partially attributable to water mass changes and thus does not solely reflect ice driven albedo effects. SST records from upwelling regimes and North and South Atlantic respond early with a shift in Δ(G-I) across the MPT whereas WPWP SST records respond late with a shift in Δ(G-I) occurring at 450 ka. The separation of the timing between the amplitude shift in the high latitudes/upwelling regimes and WPWP suggest that they are responding to different forcings. The high latitudes/ upwelling regimes could be responding to a combination of ice-albedo effects, insolation forcing, and/or glacial dynamics but the WPWP is tightly linked to pCO_2 variability. Overall, the temperature records from high latitudes/upwelling regimes shows an increase in Δ(G-I) in temperature during the MPT but it difficult to ascertain if this is primarily a response to an increase in

areal extent of ice sheets. Other factors, highlighted above, could play a role in the increase in Δ(G-I).

The global ice volume record indicates that across the MPT there was no discernible shift in the MT. Around 700 ka, the record shows an increase in Δ(G-I) and is coherent with the increase in low-frequency variability. This suggests that despite the shift towards a cooler climate, deglaciations became more severe. An increase in the severity of deglaciations cannot be solely explained by a threshold response to global cooling and indicates that there was a change in ice sheet dynamics associated with the MPT.

Understanding the mechanism of temperature variation might help elucidate the role the cooling might have played in the MPT. The cooling trend in the high latitudes could be related to changes in glacial dynamics, decrease in pCO_2, and/or changes in insolation.

3.8.1. Glacial Dynamics

The global ice volume record, derived from using the Mg/Ca-BWT record in conjunction with the $\delta^{18}O_b$ record, suggests that ice sheets grew larger, in height, concomitant with the switch in frequency. A modeling study by Manabe and Broccoli (1987) determined that the presence of large ice sheets in the NH could disrupt atmospheric flow and shift wind patterns subsequently increasing cooling in the North Atlantic. In addition to the switch in ice sheet thickness, changes in the extent of sea ice during glacial periods could impact or enhance the decrease in high latitude temperature. Ganopolski et al. (1998), using a coupled global model of intermediate complexity, determined that during the last glacial maximum the sea ice margin in the North Atlantic migrated south and increased

albedo thereby enhancing high latitude cooling. Potentially the gradual cooling trend in the BWT record reflects the switch from thin to thick ice sheets and/or increase in sea ice extent. These mechanism could provide a link between the intensification of NH glaciation and high latitude cooling and increase in Δ(G-I). However, the shift in BWT began before the emergence of 100-kyr G-I cycles and cannot completely explain the cooling. Together the shift in glacial dynamics and sea ice extent might impact high latitude temperature patterns but are the not the primary drivers behind the MPT cooling.

3.8.2. Sensitivity to pCO_2

Changes in atmospheric greenhouse gases, specifically pCO_2, have been suggested to play a role in the MPT and drive changes in deep ocean temperature on (G-I) timescales (Mudelsee and Stattegger 1997; Mudelsee and Schultz 1997; Raymo et al.,1997; Berger et al. 1999; Shackleton, 2000). The BWT record shows that the deep ocean cooled and glacial-interglacial temperature amplitude intensified in association with the MPT. There are no available records of pCO_2 across the MPT but the ice core pCO_2 record from the last 800 ka shows glacial-interglacial variability with a strong ~100-kyr periodicity similar to the BWT record., The similarity between BWT and pCO_2 variations on (G-I) timescales suggests that pCO_2 could play a role in forcing deep ocean temperature (Shackleton, 2000; Martin et al., 2002).

Using ice core and sediment records, Shackleton (2000) established that pCO_2 is in phase with BWT but both lead ice volume by ~15 kyr and hypothesized that pCO_2 played a strong role in the ~100-kyr cycles of the late Pleistocene. In this study, the BWT record was not directly measured but based on deconvolving the oxygen isotope composition from the Vostok ice core record (Petit et al., 1999) into δ_ω and BWT changes. The large

lead of BWT and pCO_2 over changes in ice volume proposed by Shackleton (2000) is similar to that proposed by Weertman (1964) as the time constant of large ice sheets. Contrarily, Ruddiman (2003) argued against this idea by constructing a new age model and re-evaluated the leads/lags and determined a much smaller lead of 5kyr and proposed that pCO_2 plays a role in terminations and glaciations but through an ice-driven CO_2 feedback on ice volume. Using a coupled model, Stouffer and Manabe (2003) evaluated the sensitivity of the deep ocean temperature to changes in pCO_2 and determined that it would increase by $3°C$ for a doubling of pCO_2.

The construction of the Mg/Ca-BWT record provides a temporal link to ice core estimates of pCO_2 over the last 8 glacial-interglacial cycles to investigate the link and sensitivity between deep ocean temperature change and pCO_2. There is a strong correspondence between BWT and pCO_2 variability (Fig. 3.17) in frequency. The records diverge across MIS 11-13 where pCO_2 increases in amplitude but BWT amplitude remains constant and during MIS 14 where the BWT record does not respond to the decrease in pCO_2. The sensitivity of BWT to pCO_2 is similar in the two time intervals regardless of the switch in pCO_2 amplitude.

To understand the sensitivity of BWT variability to pCO_2, I follow the analysis of Lea (2004). To determine the equilibrium sensitivity of climate to pCO_2, Lea (2004) assumed that a SST record from the tropical Pacific ocean mainly reflected changes due to the radiative effect of greenhouse gases. The same approach is used in this study, but note that other forcings in addition to the greenhouse forcing influence the BWT record such as the size and distribution of NH ice sheets and ocean circulation. To define the climate sensitivity for the last 800 kyr, I use an expression from Ramaswamy et al., (2001) where

the greenhouse forcing is defined as $\Delta F = 4.841 \ln(C/Co) + 0.0906 (\sqrt{C} - \sqrt{Co})$ ($C = pCO_2$ at particular time; Co = pre-industrial pCO_2). The change in forcing (ΔF) per change in temperature (ΔT) is determined using maxima and minima in the bottom water temperature record assumed to be correlated to the peaks and valleys in the ice core-pCO_2 record. The correlation between forcing and temperature, for the last 800 kyr, has slope of $1.7\,(W\,m^{-2})^{-1}$. Note the intercept was fit thru zero to compare the climate sensitivity parameter λ to the slope. The λ value derived here are higher than previously proposed using a tropical sea surface temperature record and model-based results (Lea, 2004). The climate forcing of deep ocean temperature in the North Atlantic is not solely pCO_2 and the λ value is composed of other forcings which may lead to an overestimate of the climate sensitivity.

Using this climate sensitivity calculation, I calculate the expected change in pCO_2 associated with the high latitude cooling across the MPT. Assuming a high latitude cooling of ~1°C, determined from the Mg/Ca-BWT record, the ΔF expected from this cooling is ~0.2 W m^{-2}. Based on the BWT-pCO_2 sensitivity a change in ΔF of this magnitude would require a decrease in pCO_2 of 15 ppm. A decrease of 0.2 W m^{-2} or a decrease in pCO_2 of ~15 ppm, would be equivalent to a 0.7°C cooling in the Pacific surface ocean temperature across the MPT. However, across the MPT, there is no discernible trend in Mg/Ca-SST records which suggests that the pCO_2 did not decrease across the MPT. The uncertainty of the Mg/Ca-temperature calibration is ~±0.7°C and thus the expected decrease in Pacific SST is within the uncertainty. Overall, this analysis indicates pCO_2 variations cannot be the main driver in the high latitude cooling or the

transition as suggested by de Garidel- Thoron et al. (2005). The role pCO_2 plays in the MPT cooling and G-I variability may be as a feedback rather than the primary forcing.

3.8.3. Obliquity Modulation

Across the major climate transitions, changes in insolation have been invoked to explain development and intensification of glaciation. Specifically, several studies highlighted changes in obliquity, as the primary driver in the development of large-scale NH glaciation and Antarctic glaciation (Haug and Tiedemann, 1998; Coxall et al., 2005; Holbourn et al., 2005). These studies suggest that obliquity modulation plays a role in preconditioning the high latitudes for ice sheet development through a shift to colder summers. A long-term decrease in obliquity could act to cool the high latitudes, also. The cooling associated with the MPT occurs during an interval of transition from large to small amplitude obliquity cycles (Fig. 3.17). The decrease in obliquity amplitude began around 1250 ka and culminated at 825 ka similar to the cooling which occurs from 1150 to 825 ka. The coherency in timing suggests that obliquity driven changes in insolation might have induced the high latitude cooling. However, the trend in obliquity decreases during interglacials but increases during glacial periods. Overall, there is no long-term trend in obliquity which implies that obliquity-driven insolation variations are not driving the cooling assocatied with MPT. The decrease in obliquity during the interglacials indicates that the high latitudes experienced cooler NH summers which would promote ice sheet preservation whereas during glacial periods, warmer NH summers would persist in the high latitudes which would enhance ablation of ice sheets. Preservation of ice sheets during glacial periods plays a paramount role in the development of larger ice

sheets. Obliquity is not a likely candidate for preconditioning the high latitudes for intensification of NH glaciation.

3.9. Conclusions

The deep ocean cooling and increase in (G-I) temperature amplitude, observed in the Mg/Ca-BWT record across the MPT, represents a major shift in high latitude climate. Sea surface temperature records from upwelling regimes and mid-, high latitudes show a similar shift in temperature, while surface ocean conditions in the WPWP remained relatively stable. The divergence in the surface ocean records supports the idea that the deep ocean cooling is not related to a secular decrease in pCO_2 (de Garidel-Thoron et al., 2005). SST records from all regions show a coherent shift in the frequency of glacial-interglacial variability which is associated with glacial-interglacial variations in ice volume. This suggests that the changes in NH ice volume influences sites far from the high latitudes.

Associated with the high latitude cooling are changes in the meridional and zonal temperature gradients. The intensification of the meridional temperature gradient reduces oceanic heat transport providing a positive feedback on the high latitude cooling. Ocean circulation became sluggish along with the increase in ΔT which corresponds to a decrease in oceanic heat transport. The change in zonal ΔT could play a role in increasing the atmospheric moisture transport to high latitudes. The shift in high latitude temperature and increase in ΔT acts to promote ice sheet growth. These changes might precondition the high latitude climate for entry in the 100-kyr climate regime.

The high latitude cooling acted as a precursor to the expansion of NH ice sheets similar to the late Pliocene transition. However, the cooling is not sufficient to fully explain the features of glacial-interglacial variability in the late Pleistocene. The shift in frequency and development of asymmetric, G-I cycles in sea level did not occur until following the culmination of the cooling trend. The separation of the two transitions, cooling and frequency/sea level shift, points toward another mechanism to fully explain the shift in frequency and development of 100-kyr cycles in sea level and BWT.

Mechanisms that could explain the nature of transition are related to a change in ice sheet dynamics. Clark and Pollard (1998) propose that the transition is due to a shift from thin (2 km) to thick (3 km) ice sheets, where thick ice sheets begin to respond non-linearly to orbital forcing. Geological evidence shows that the pre-MPT areal extent of ice sheets was roughly the same as after the MPT (Clark and Pollard, 1998). This implies that ice sheets grew in height rather than areal extent. Clark and Pollard (1998) suggest that a change in basal substrate allowed for the growth of taller ice sheets, independent of a global cooling, which have internal mechanisms that lead to abrupt deglaciation and asymmetric G-I cycles.

The ice volume record supports the idea that MPT was a shift in the dynamics of ice sheets. The global cooling might have preconditioned the high latitude climate for growth of thicker ice sheets but did not primarily drive the transition. There are several lines of evidence that point toward a shift in ice sheet dynamics as the primary mechanism. First, following the MPT the structure of glacial-interglacial cycles in sea level became more asymmetric which implies that ice sheets abruptly deglaciated. Second, the 100-kyr G-I cycles are associated with a shift in the phase relationship

between BWT and $\delta^{18}O_b$, where the lead of BWT over $\delta^{18}O_b$ increases across the MPT. This implies an increase in the time constant of ice sheets which indicates that thicker ice sheets were more resistant to melting during insolation maxima. Third, the switch in frequency of sea level, from 41 to 100-kyr, indicates that the ice sheets persisted for much longer and grew in height and only deglaciated when the height of the ice sheet reached a critical value and at an insolation maxima. Fourth, the global ice volume record, following the MPT, shows an increase in (G-I) amplitude of ice volume variations, rather than a shift in the long-term trend. The amplitude increase represents the appearance of more severe glacial periods (more ice, colder) and less severe interglacial periods (less ice, colder). This shift implies that ice sheets grew in height rather than areal extent. All of these lines of evidence support the idea that thicker ice sheets developed following the MPT.

The evidence presented here suggests that the MPT represents a switch from thin to thick ice sheets driven by change in ice sheet dynamics and not a threshold response to a global cooling. This idea is supported by the difference in timing between the cooling trend and the frequency/sea level shift. The ice sheet dynamics mechanism explains the shift in frequency, increase in Δ(G-I) sea level amplitude, and appearance of asymmetric patterns in glacial cycles. Thus, the emergence of the 100-kyr cycles into the climates system is linked to a change in ice sheet dynamics and the high latitude cooling is a not sufficient to explain the MPT.

3.10 References

Ashkenazy, Y. and Tziperman, E., 2004. Are the 41 kyr glacial oscillations a linear response to Milankovitch forcing? Quaternary Science Reviews, 23: 1879-1890.

Berger, A., Li, X.S. and Loutre, M.F., 1999. Modelling northern hemisphere ice volume over the last 3 Ma. Quaternary Science Reviews, 18: 11.

Billups, K. and Schrag., D.P., 2002. Paleotemperatures and Ice-Volume of the Past 27 myr Revisited with Paired Mg/Ca and Stable Isotope Measurements on Benthic Foraminifera. Paleoceanography, 17, 10.1029/2000PA000567(1).

Boyle, E.A. and Keigwin, L.D., 1982. Deep circulation of the North Atlantic over the last 200,000 years: Geochemical evidence. Science, 218: 784-787.

Boyle, E.A. and Keigwin, L.D., 1985. Comparison of Atlantic and Pacific paleochemical records for the last 250,000 years: changes in deep ocean circulation and chemical inventories. Earth Planet. Sci. Lett., 76: 135-150.

Boyle, E.A. and Keigwin, L.D., 1987. North Atlantic thermohaline circulation during the last 20,000 years linked to high latitude surface temperature. Nature, 330: 35-40.

Cande, S. and Kent, D., 1992. A new geomagnetic polarity time scale for the late Cretaceous and Cenozoic. Journal of Geophysical Research, 97: 13917-13951.

Clark, P.U., Archer, D., D. Pollard, J.D. Blum, J.A. Rial, V. Brovkin, A.C. Mix, N. G. Pisias, and M. Roy, 2006. The Middle Pleistocene transition: Characteristics, mechanisms, and implications for long-term changes in atmospheric pCO2. Quaternary Science Reviews, 25: 3150-3184.

Clark, P.U. and Pollard, D., 1998. Origin of the Middle Pleistocene transition by ice sheet erosion of regolith. Paleoceanography, 13: 1-9.

de Garidel-Thoron, T., Rosenthal, Y., Bassinot, F. and Beaufort, L., 2005. Stable sea surface temperatures in the western Pacific warm pool over the past 1.75 million years. Nature, 433: 294-298.

Dwyer, G.S., Cronin, T.M., Baker, P.A., Buzas, M.E.R.J.S. and Correge, T., 1995. North Atlantic deepwater temperature change during late Pliocene and late Quaternary climatic cycles. Science, 270: 1347-1351.

Emiliani, C., 1955. Pleistocene temperatures. J. Geol., 63: 538-578.

Fairbanks, R.G., 1989. A 17,000-year glacio-eustatic sea level record: influence of glacial melting rates on the Younger Dryas event and deep-ocean circulation. Nature, 342: 637-642.

Fairbanks, R.G. and Matthews, R.K., 1978. The oxygen isotope stratigraphy of the Plesitocene reef tracts of Barbados, West Indies. Quaternary Research, 10(1): 181-196.

Flower, B.P. and Kennett, J.P., 1993. Relations between Monterey Formation deposition and middle Miocene global cooling: Naples Beach section, California. Geology, 21: 877-880.

Harper, S., 2000. Thermocline ventilation and pathways of tropical-subtropical water mass exchange. Tellus, Ser. A., 52: 330-345.

Huybers, P., 2006. Early Pleistocene glacial cycles and the integrated summer insolation forcing. Science, 313: 508-511.

Huybers, P. and Wunsch, C., 2005. Obliquity pacing of the late Pleistocene glacial terminations. Nature, 434: 491-494.

Huybers, P.J., 2007. Glacial variability over the last two million years: an extended depth-derived agemodel, continuous obliquity pacing, and the Pleistocene progression. Quaternary Science Reviews, 26(1-2): 37-55.

Imbrie, J. and al., e., 1992. On the structure and origin of major glaciation cycles: 1. Linear responses to Milankovitch forcing. Paleoceanog., 7: 701-738.

Imbrie, J. et al., 1993. On the Structure and Origin of Major Glaciation Cycles.2. The 100,000-Year Cycle. Paleoceanography, 8(6): 699-735.

Kawamura, K., et al., 2007. Northern Hemisphere forcing of climatic cycles in Antarctica over the past 360,000 years. Nature, 448: 912-917.

Kitamura, A. and Kawagoe, T., 2006. Eustatic sea-level change at the Mid- Pleistocene climate transition: new evidence from the shallow-marine sediment record of Japan. Quaternary Science Reviews, 25: 323-335.

Labeyrie, L.D., Duplessy, J.C. and Blanc, P.L., 1987. Variations in mode of formation and temperature of oceanic deep waters over the past 125,000 years. Nature, 327: 477-482.

Langdon, C. and (2000), o., 2000. Effect of calcium carbonate saturation state on the calcification rate of an experimental coral reef. Global Biogeochem. Cy., 14: 639-654.

Lawrence, K.T., Liu, Z. and Herbert, T.D., 2006. Evolution of the Eastern Tropical Pacific Through Plio-Pleistocene Glaciation. Science, 312: 79-83.

Lea, D.W., 2004. The 100 000-Yr Cycle in Tropical SST, Greenhouse Forcing, and Climate Sensitivity. J. Climate, 17: 2170-2179.

Lea, D.W., Martin, P.A., Pak, D.K. and Spero, H.J., 2002. Reconstructing a 350 ky history of sea level using planktonic Mg/Ca and oxygen isotope records from a Cocos Ridge core. Reconstructing a 350 ky history of sea level using planktonic Mg/Ca and oxygen isotope records from a Cocos Ridge core, 21: 283-293.

Lear, C.H., Elderfield, H. and Wilson, P.A., 2000. Cenozoic deep-sea temperatures and global ice volumes from Mg/Ca in benthic foraminiferal calcite. 287: 269-272.

Lisiecki, L.E. and Raymo, M.E., 2005. A Pliocene-Pleistocene stack of 57 globally distributed benthic d18O records. Paleoceanography, 20, PA1003, doi:10.1029/2004PA001071.

Liu, Z.H. and Herbert, T.D., 2004. High-latitude influence on the eastern equatorial Pacific climate in the early Pleistocene epoch. Nature, 427: 720-723.

Luthi, D., Le Floch, M., Bereiter, B. and al., e., 2008. High-resolution carbon dioxide concentration record 650,000-800,000 years before present. Nature, 453: 379-382.

Manabe, S. and Broccoli, A.J., 1985. The influence of continental ice sheets on the climate of an ice age. J. Geophys. Res., 90: 2167-2190.

Marlow, J.R., Lange, C.B., Wefer, G. and Rosell-Mele, A., 2000. Upwelling intensification as part of the Pliocene–Pleistocene climate transition. Science, 290: 2288–2291.

Martin, P.A. et al., 2002. Quaternary deep sea temperature histories derived from benthic foraminiferal Mg/Ca. Earth and Planetary Science Letters, 198(1-2): 193-209.

McClymont, E.L. and Rossel-Mele, A., 2005. Links between the onset of modern Walker circulation and the mid-Pleistocene climate transition. Geology, 33: 389-392.

Medina-Elizalde, M. and Lea, D.W., 2005. The mid-Pleistocene transition in the tropical Pacific. Science, 310: 1009–1012.

Molnar, P. and Cane, M.A., 2002. El Niño's tropical climate and teleconnections as a blueprint for pre-Ice Age climates. Paleoceanography, 17 (2): 10.1029/2001PA000663.

Mudelsee, M. and Schulz, M., 1997. The Mid-Pleistocene climate transition: onset of 100 ka cycle lags ice volume build-up by 280 ka. Earth And Planetary Science Letters, 151, 117-123., 151: 117-123.

Oppo, D.W. and Fairbanks, R.G., 1987. Variability in the deep and intermediate water circulation of the Atlantic Ocean during the past 25,000 years: Northern Hemisphere modulation of the Southern Ocean. Earth and Planetary Science Letters, 86: 1-15.

Paillard, D., The timing of Pleistocene glaciations from a simple multiple-state climate model. Nature, 391: 378-381.

Petit, J.R., Jouzel, J., Raynaud, D., Barkov, N.I. and J.-M. Barnola, I.B., M. Bender, J. Chappellaz, M. Davis, G. Delayque, M. Delmotte, V.M. Kotlyakov, M. Legrand, V.Y. Lipenkov, C. Lorius, L. Pépin, C. Ritz, E. Saltzman, and M. Stievenard., 1999. Climate and atmospheric history of the past 420,000 years from the Vostok ice core. Nature, 399: 429-436.

Philander, S.G. and Fedorov, A.V., 2003. Role of tropics in changing the response to Milankovich forcing some three million years ago. Paleoceanography, 18(2): 1045, doi:10.1029/2002PA000837.

Raymo, M.E., 1997. The timing of major climate terminations. Paleoceanography, 12: 577-585.

Raymo, M.E. and Nisancioglu, K., 2003. The 41 kyr world: Milankovitch's other unsolved mystery. Paleoceanography, 18.

Raymo, M.E., Oppo, D.W. and Curry, W.B., 1997. The mid-Pleistocene climate transition: a deep sea carbon isotope perspective. Paleoceanography, 12: 546-559.

Rind, D., 2000. Relating paleoclimate data and past temperature gradients: Some suggestive rules. Quaternary Science Reviews, 19: 381-390.

Rosenthal, Y., M. P. Field, and R. M. Sherrell, 1999. Precise determination of element/calcium ratios in calcareous samples using sector field inductively coupled plasma mass spectrometry. Analytical Chemistry, 71: 3248–3253.

Ruddiman, W.F., 2003. Orbital insolation, ice volume, and greenhouse gases. Quaternary Science Reviews, 22: 1597-1629.

Ruddiman, W.F., M.E. Raymo, D.G. Martinson, B.M. Clement, and J. Backman, 1989. Mid-Pleistocene evolution of Northern Hemisphere climate. Paleoceanography, 4: 353-412.

Shackleton, N.J., 1967. Oxygen isotope analyses and Pleistocene temperatures re-assessed. Nature, 215: 15-17.

Shackleton, N.J., 1974. Attainment of isotopic equilibrium between ocean water and the benthonic foraminifera genus Uvigerina: isotopic changes in the ocean during the last glacia. Colloques Internationaux du Centre National du Recherche Scientifique, 219: 203-210.

Shackleton, N.J., 1987. Oxygen isotopes, ice volume and sealevel. Quaternary Science Reviews, 6: 183-190.

Shackleton, N.J., 2000. The 100,000-year ice-age cycle identified and found to lag temperature, carbon dioxide, and orbital eccentricity. Science, 289: 1897-1902.

Siddall, M. et al., 2003. Sea-level fluctuations during the last glacial cycle. Nature, 423: 853-858.

Siegenthaler, U. and al, e., 2005. Stable carbon cycle–climate relationship during the late Pleistocene. Science, 310: 1313-1317.

Stouffer, R.J. and Manabe, S., 2003. Equilibrium response of thermohaline circulation to large changes in atmospheric CO2 concentration. Climate Dynamics, 20: 759-773.

Tziperman, E. and Gildor, H., 2003. On the mid-Pleistocene transition to 100-kyr glacial cycles and the asymmetry between glaciation and deglaciation times. Paleoceanography, 18(1): 1-8.

Waelbroeck, C. et al., 2002. Sea-level and deep water temperature changes derived from benthic foraminifera isotopic records. Quaternary Science Reviews, 21: 295-305.

Weertman, J., 1964. Journal of Glaciology, 38(145).

Yokoyama, Y., Lambeck, K., Deckker, P.P.J.D. and Fifeld, L.K., 2000. Timing of the last glacial maximum from observed sea-level minima. Nature, 406: 713-716.
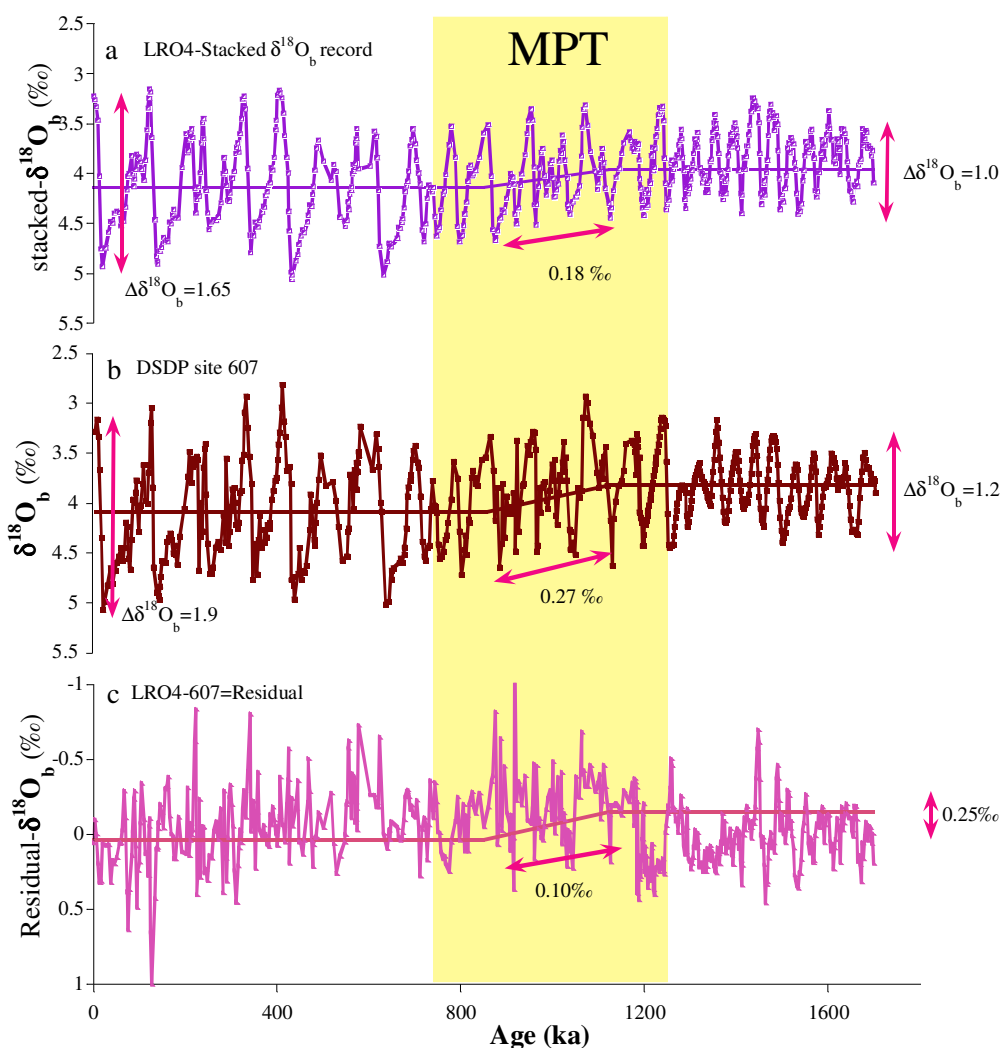
Figure 3.1 **(a)** LRO4 stacked benthic oxygen isotope record from Lisiecki and Raymo (2005); **(b)** DSDP Site 607 (this study) benthic oxygen isotope record; **(c)**Residual between the benthic oxygen isotope records in (a) and (b). The LRO4 record exhibits a smaller change in amplitude and trend across the MPT than the DSDP 607 record which suggests that DSDP 607 record represents local and global changes.
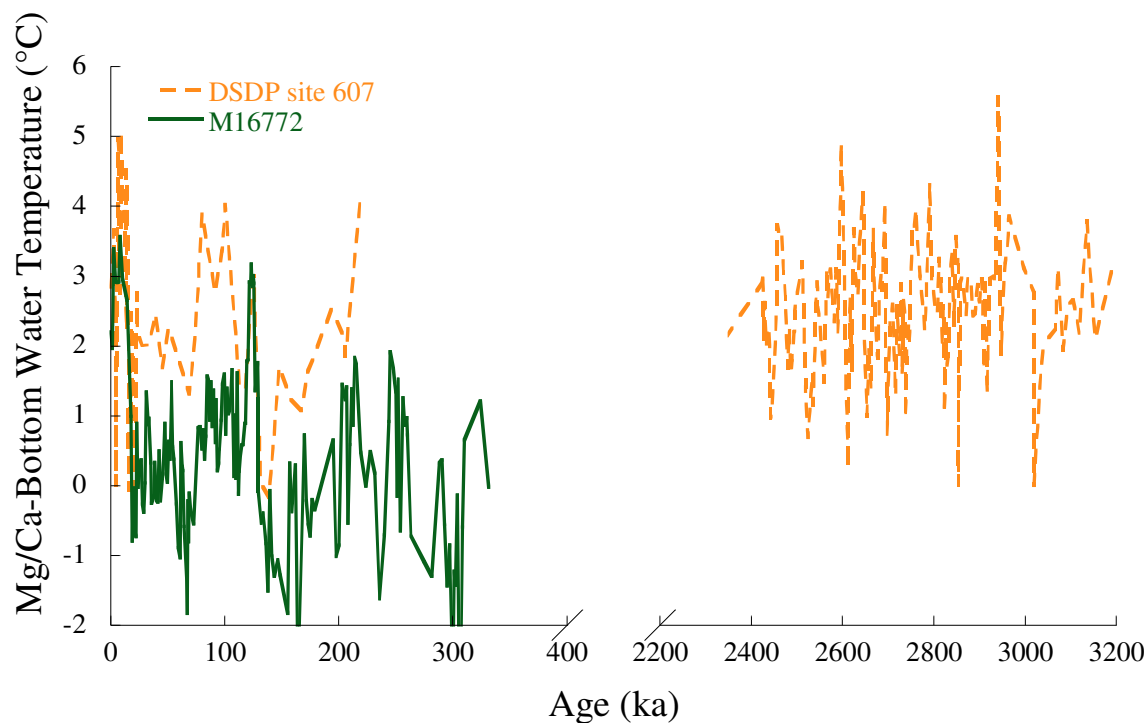
Figure 3.2 The bottom water temperature record for the last few glacial-interglacial cycles from DSDP site 607 and core M16772. The late Pliocene bottom water temperature record is from DSDP site 607. DSDP 607 BWT data derive from a Mg/Ca ostracod study by Dwyer et al., (1995) in the western north Atlantic. M16772 BWT record derive from a Mg/Ca benthic foraminifera study by Martin et al., (2002) in the eastern north Atlantic.
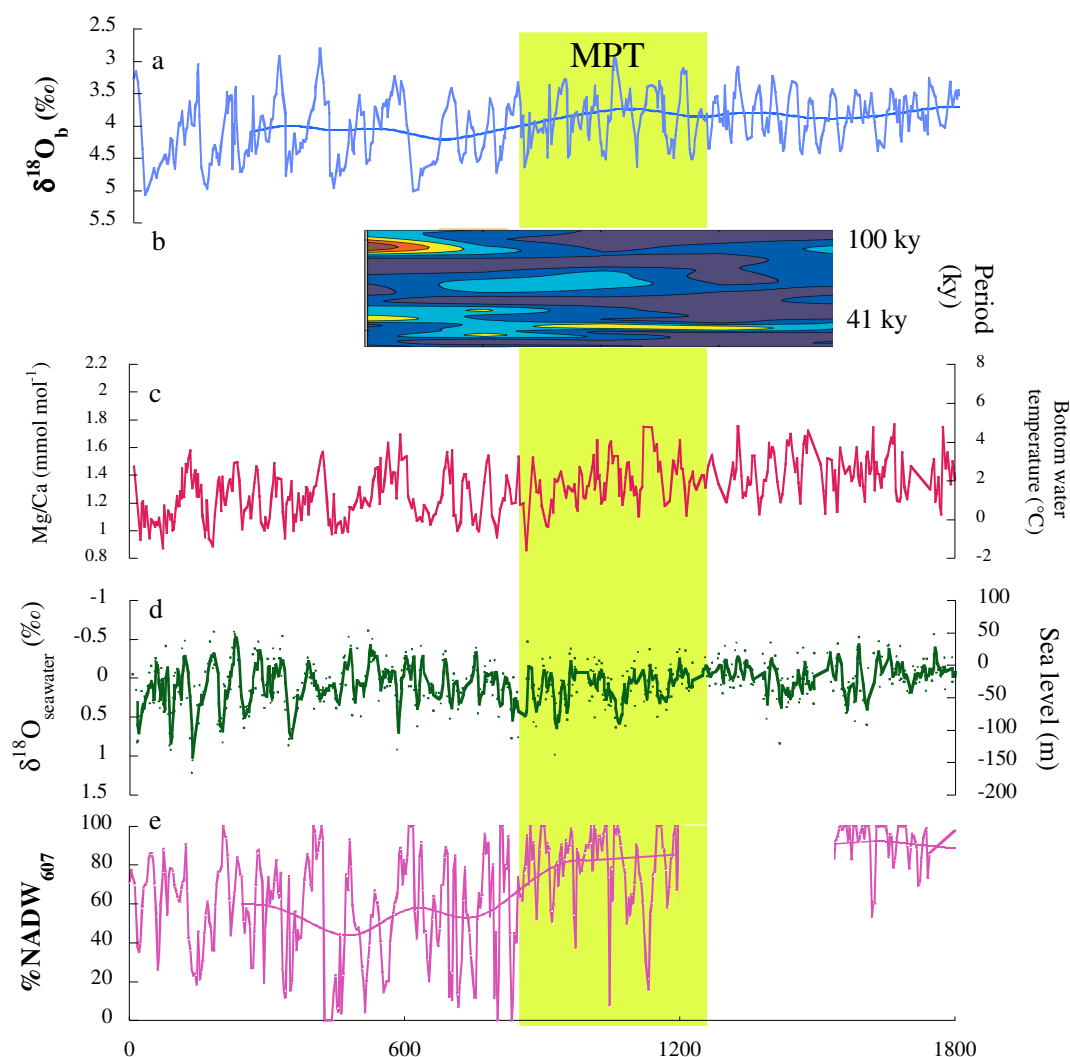
Figure 3.3 Western North Atlantic DSDP site 607 records based on the benthic foraminifera. **(a)** Previous reconstruction of benthic oxygen isotope record from Raymo et al., (1989) and Ruddiman et al., (1989); (b) Evolutionary spectra from 500 to 1500 ka; **(c)** Mg/Ca-derived BWT record. To convert Mg/Ca ratios to bottom water temperature the following equation was used: Mg/Ca=0.15*BWT+1.15; **(c)** δ_ω record, calculated by extracting the component in benthic $\delta^{18}O$ explained by the Mg/Ca-derived BWT using the paleotemperature equation from Shackleton (1973); The curve also represents a reconstruction of sea level relative to today calculated with the assumption that a 0.1‰ shift in δ_ω results from a 10-m change in sea level (11). **(e)** Percent NADW record as calculated by Raymo et al., (1997).
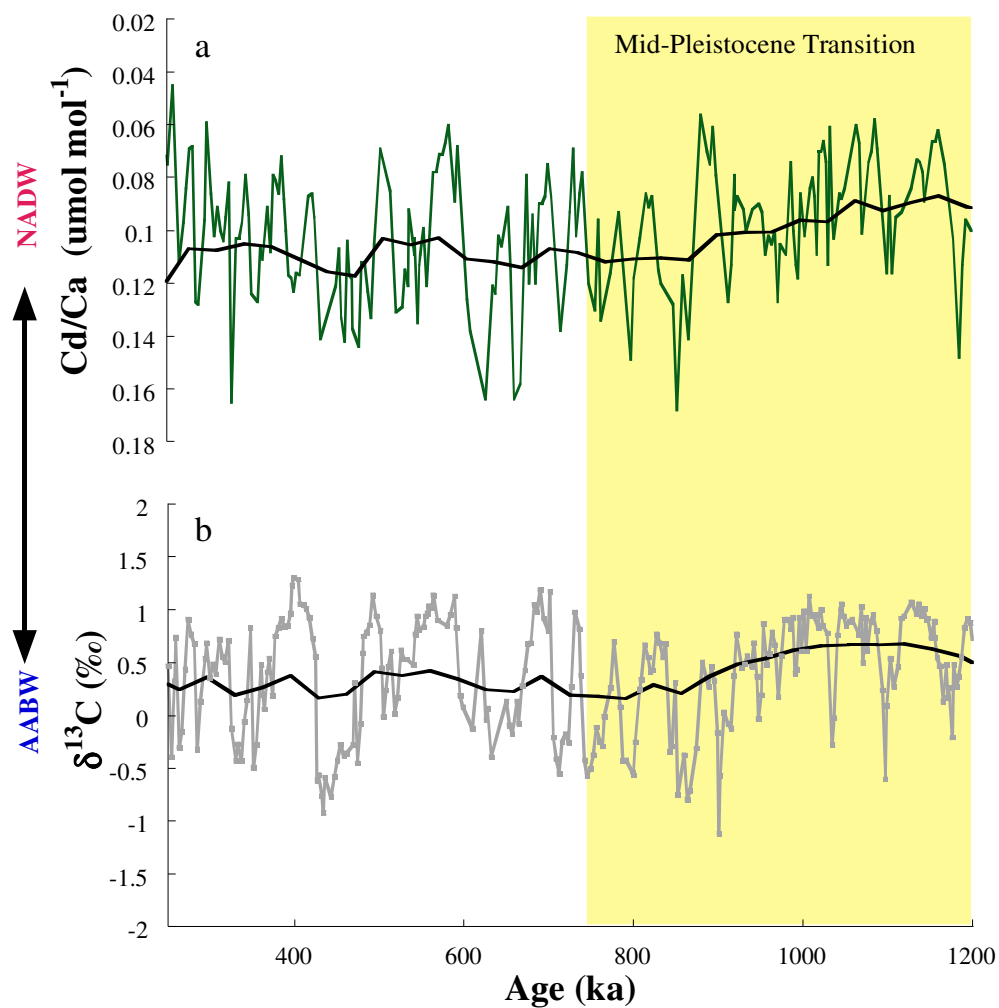
Figure 3.4 (a) DSDP site 607 benthic carbon isotope record from Ruddiman et al., (1989) and (b) Benthic foraminiferal Cd/Ca record from this study.
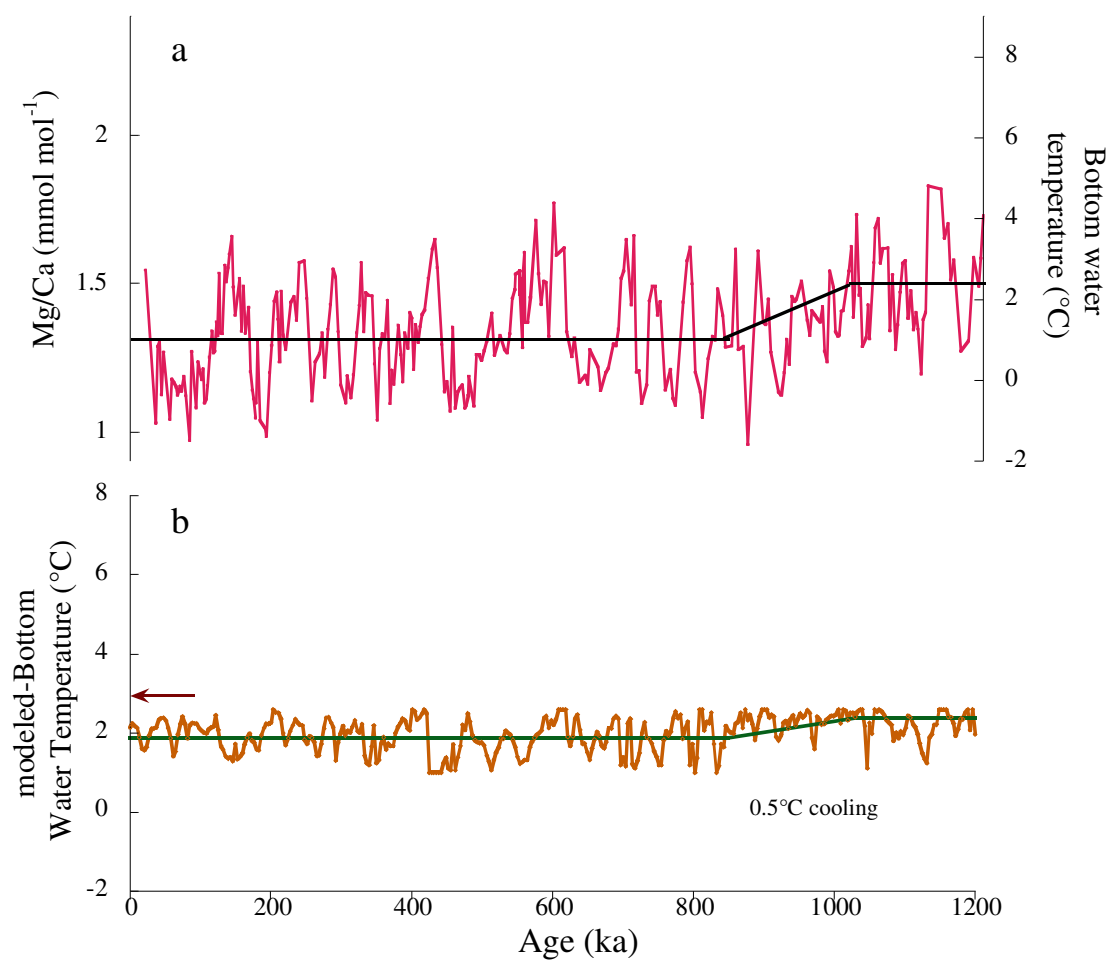
Figure 3.5 (a) Mg/Ca-BWT records versus (b) modeled BWT based on a simple water mass mixing scenario. The arrow in (b) indicates the present-day BWT at DSDP site 607. The cooling across the MPT is much larger in the Mg/Ca-BWT than the modeled-BWT record.
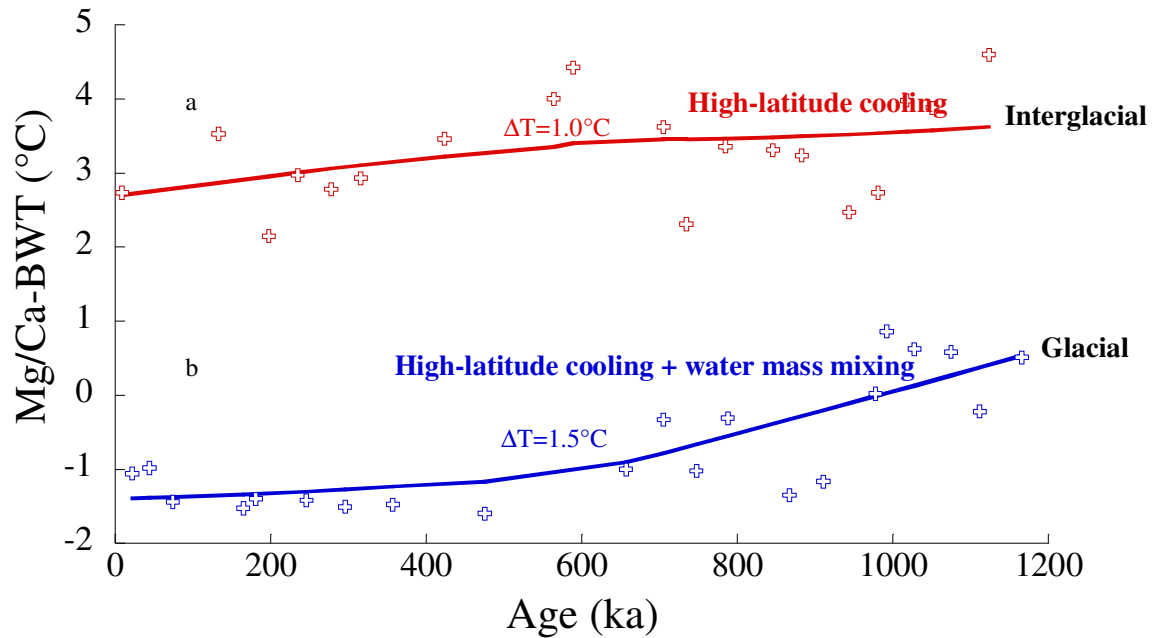
Figure 3.6 (a) Interglacial maxima and (b) glacial minima cooling trend. Interglacial trend represents high latitude cooling while glacial trend is a combination of high latitude cooling and water mass mixing.
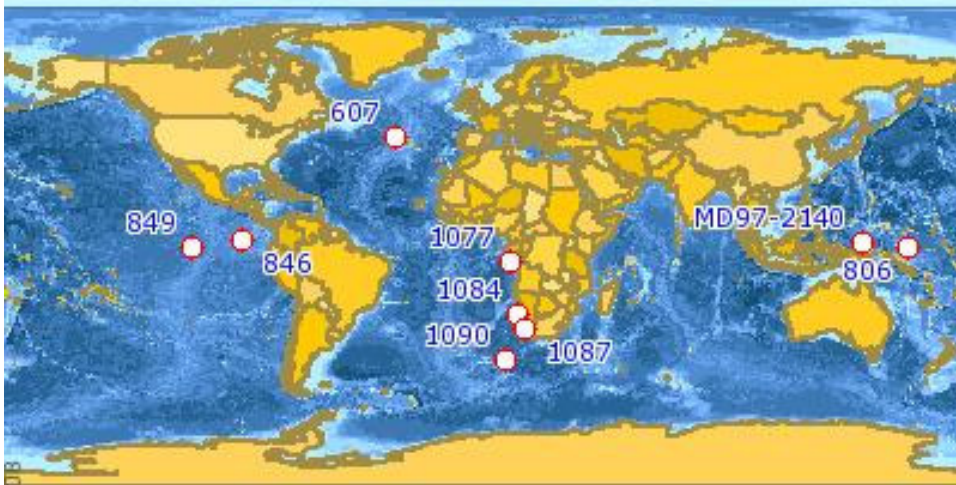
Figure 3.7 Location of core sites for the sea surface temperature records used in this analysis.
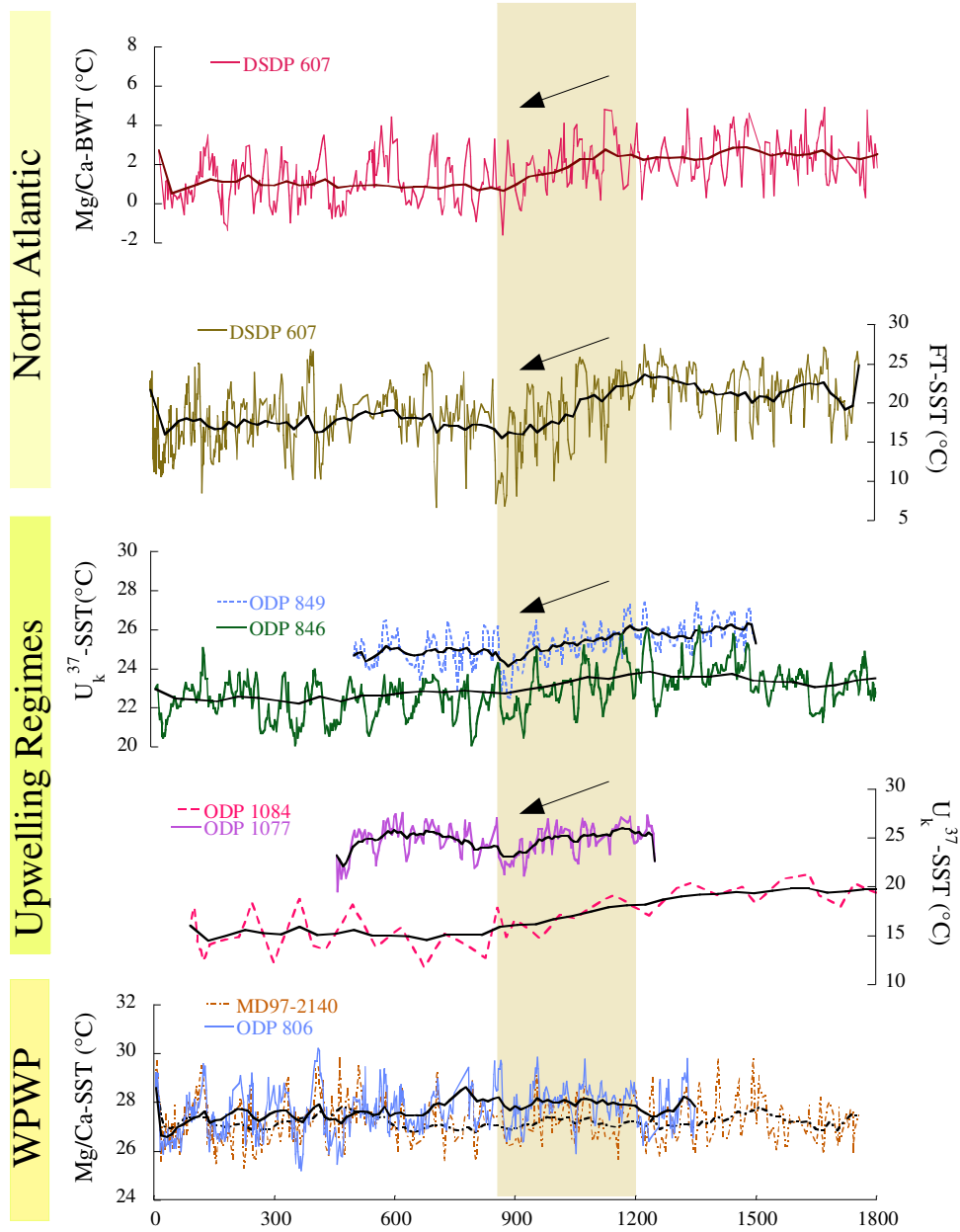
Figure 3.8 Temporal changes in the (a) Mg/Ca-bottom water temperature record (this study) and sea surface temperature records from (b) DSDP site 607, based on census counts of planktonic foraminifera, termed here faunal transfer (FT)-SST, (c) ODP sites 846 and 849, (c) ODP sites 1084 and 1077, (d) ODP site 806 and Core MD97-2140 for the Pleistocene. Trendlines were calculated with a Gaussian filter with a cutoff frequency of 400 ky. See Table 3.2 for site information.
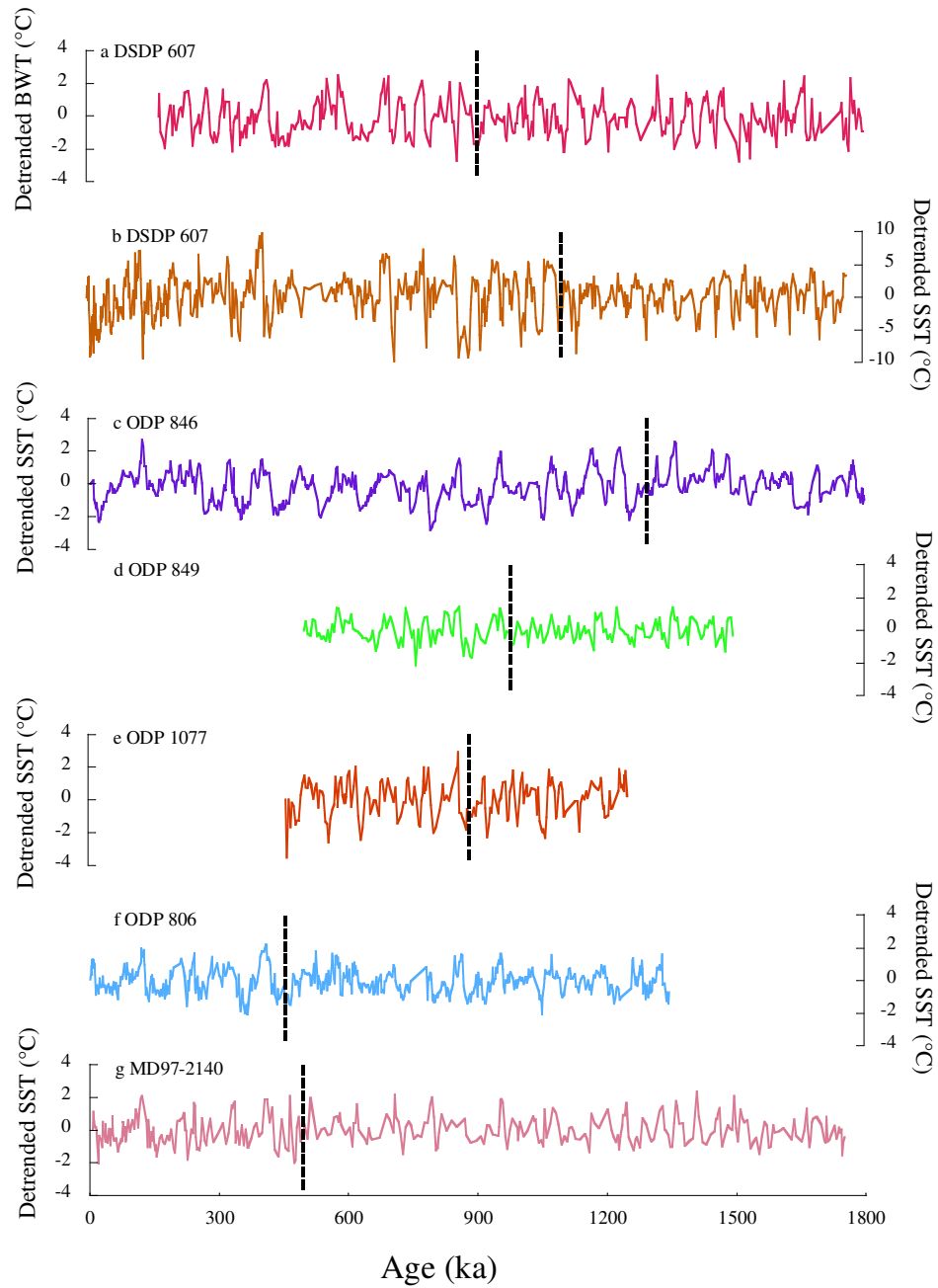
Figure 3.9 Detrended temperature records from figure 3.8. Note the increase in amplitude in the BWT record from (a)DSDP 607 and in the SST records from (b) DSDP 607, (c) ODP 846, (d)ODP 849 and (e) ODP 1077.
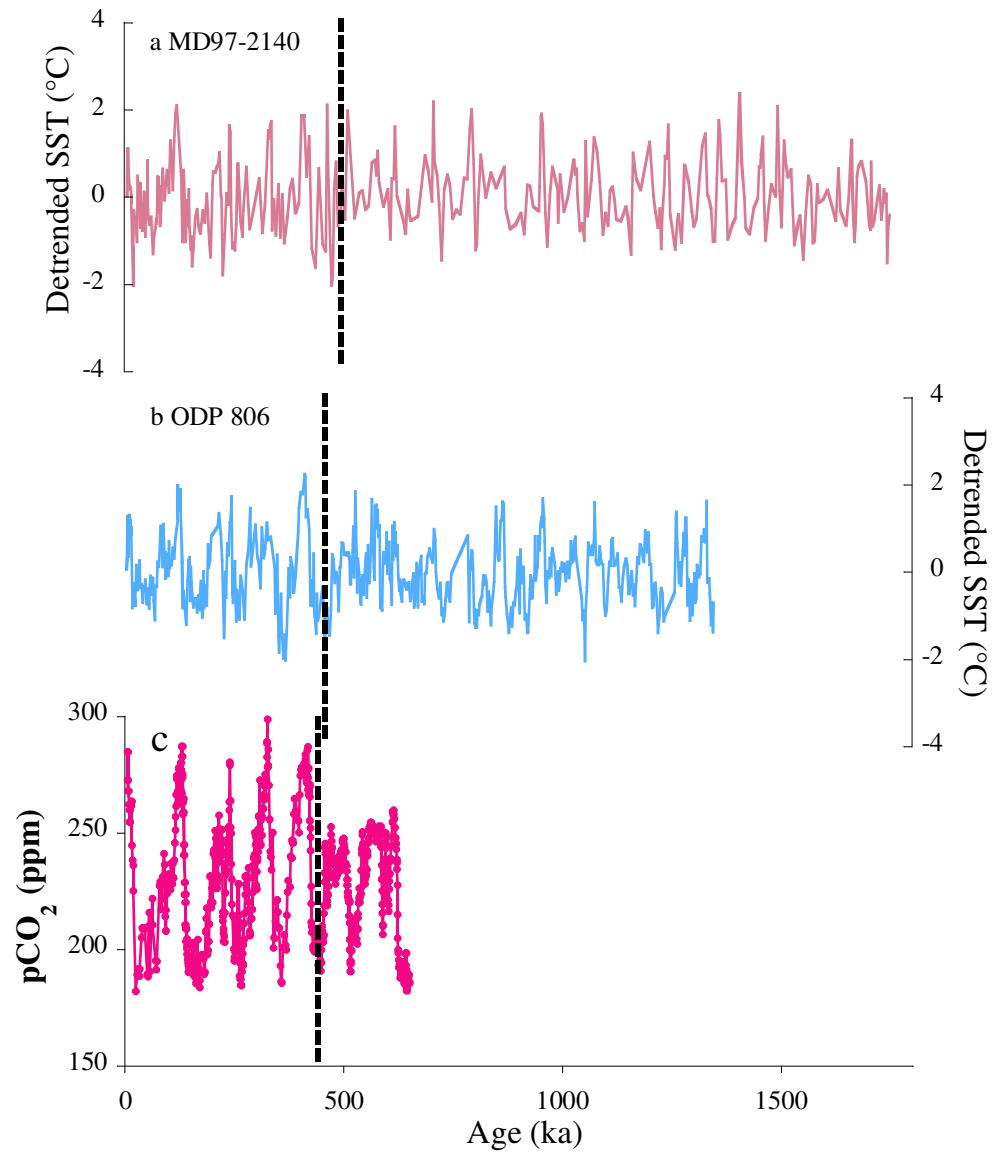
Figure 3.10 Detrended sea surface temperature records from western Pacific warm pool, specifically (a) Core MD97-2140 and (b) ODP 806 versus (c) atmospheric pCO_2. Note the increase in SST amplitude occurs following the MPT.
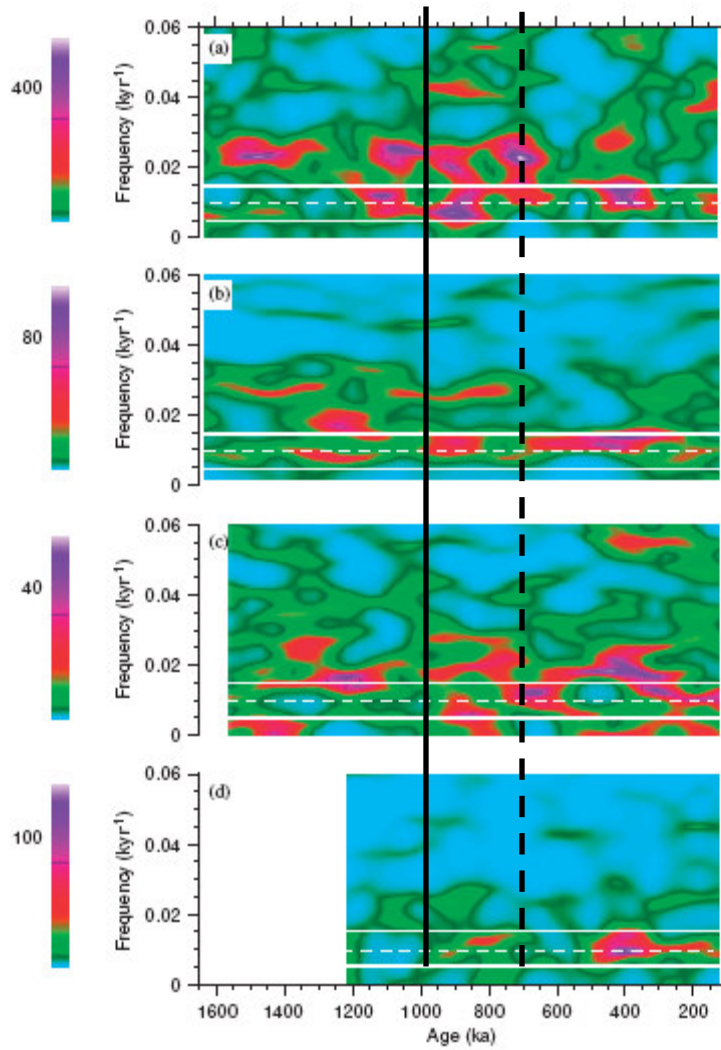
Figure 3.11 Evolutionary spectra of SST records from (a) DSDP site 607; (b) ODP site 846; (c) Core MD97-2140; (d) ODP site 806B. Modified figure from Clark et al., (2006). Solid line denotes first appearance of broad band low frequency variability in the BWT record. The dashed line corresponds to the emergenc of a narrow band of low frequency BWT variability.
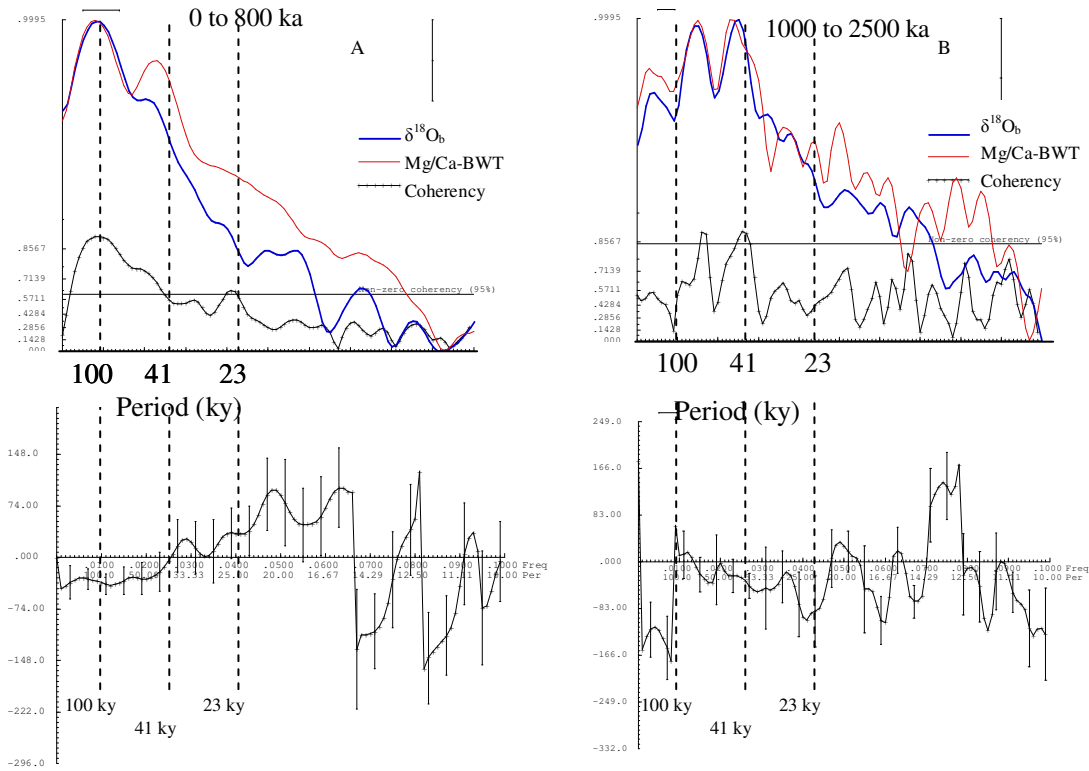
Figure 3.12 Comparison of spectral analysis of $\delta^{18}O_b$ and Mg/Ca-derived BWT records from DSDP 607 in the late and early Pleistocene. (a) Time interval from 11 to 800 ka; (b) time interval from 1000 to 2500 ka. Panels also present the coherency and phase relationship obtained from cross-spectral analysis between the DSDP 607 $\delta^{18}O_b$ and BWT for each period. The confidence interval (CI) at the 95% significance level and the bandwidth (BW) used for the spectral analysis are displayed.
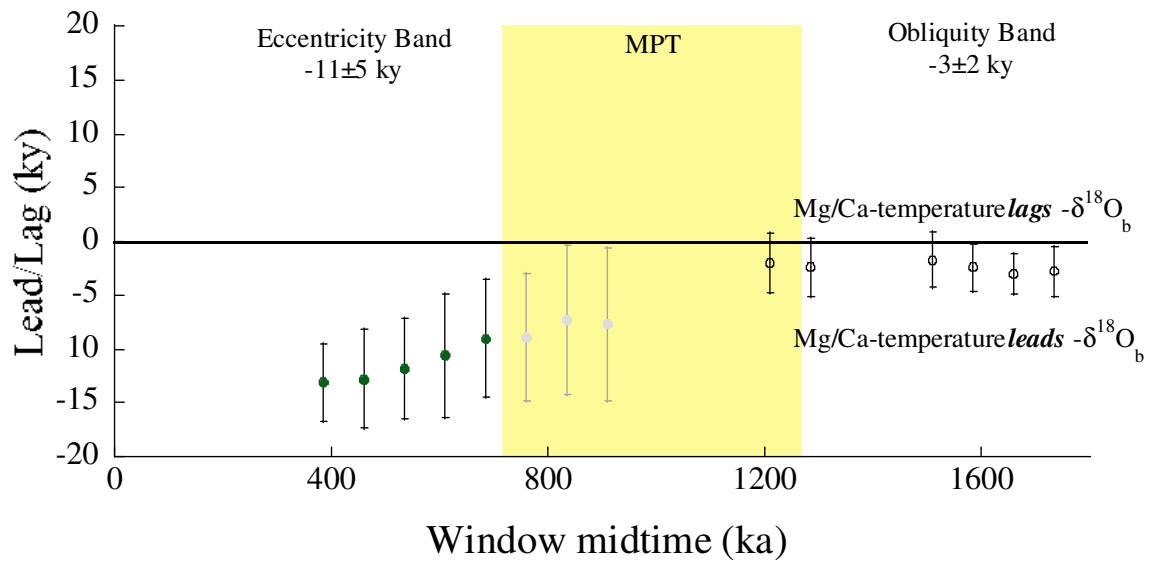
Figure 3.13 Eccentricity band (100-ky) and obliquity band (41-ky) phase and coherency relationship between benthic oxygen isotope record and Mg/Ca-BWT. Intervals that are coherent at 80% confidence level are shown with thick graybars and those that are coherent at 95% confidence level are with thin black bars. I use the inverse of benthic $\delta^{18}O_b$ record in our coherency analysis. Before coherency and phase analysis, all records were interpolated to even intervals of 3-ky resolution. Phases were computed with use of Arand program iterative spectra feature with a 300-kyr window and 250 lags.
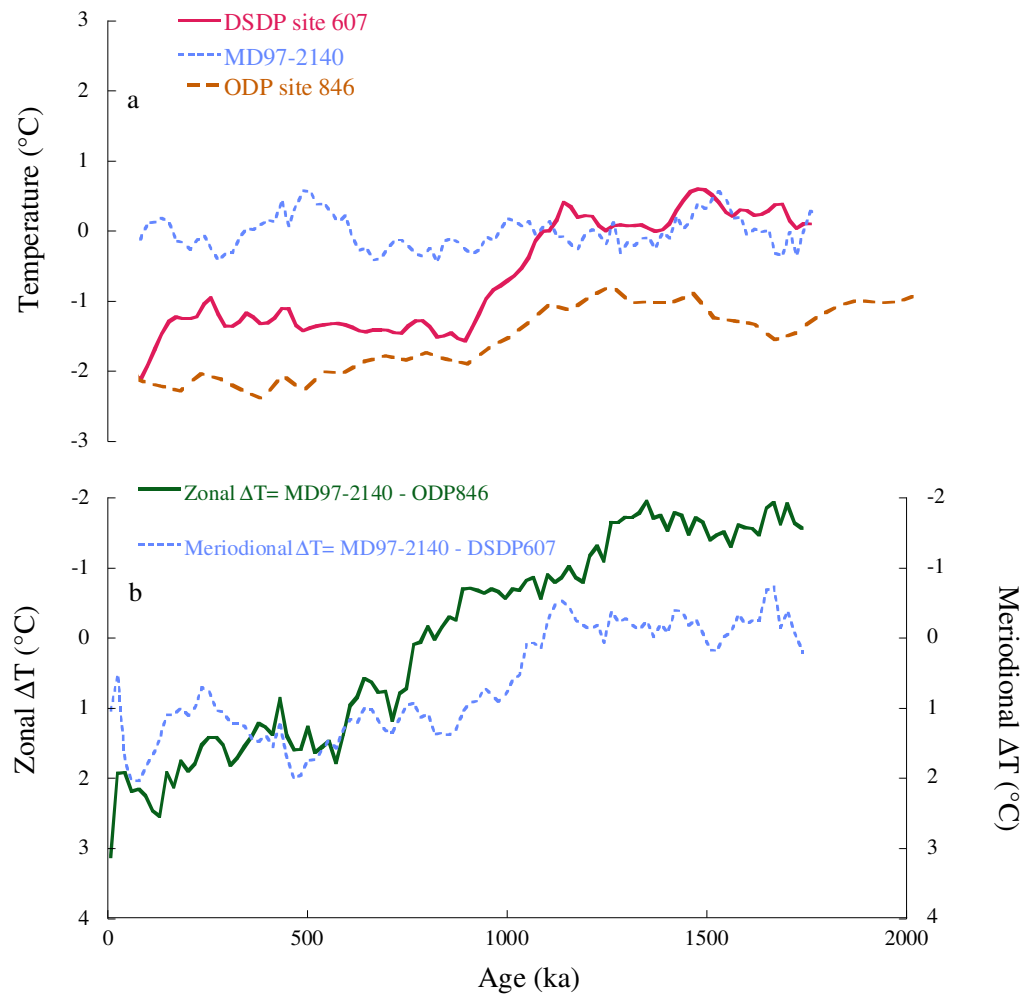
Figure 3.14 (a) Normalized temperature records from DSDP site 607 (Mg/Ca-BWT), MD97-2140 (Mg/Ca-SST), and ODP 846, (Uk37-SST). (b) Calculated meridional and zonal gradient.
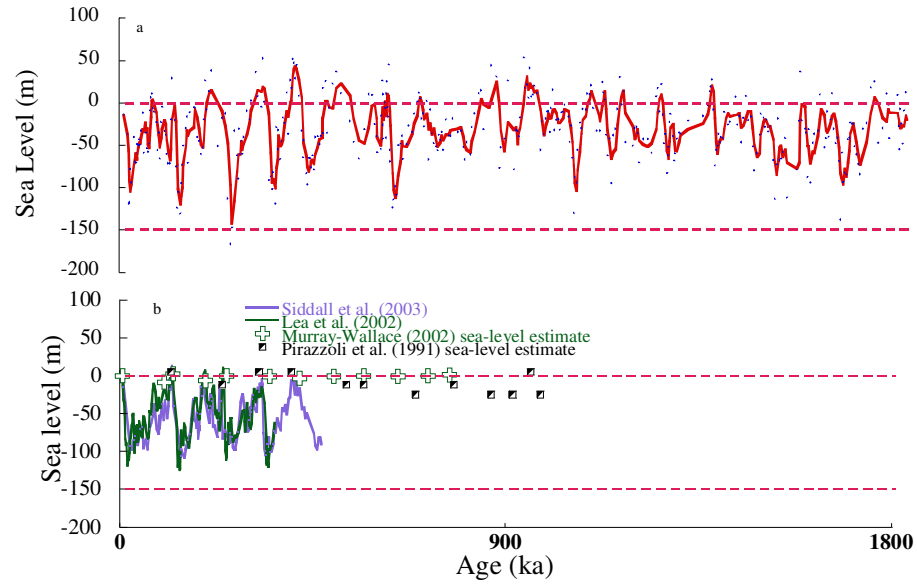
Figure 3.15 (a) Global ice volume and sea level record derived from this study compared to (b) sea level records from previous studies.
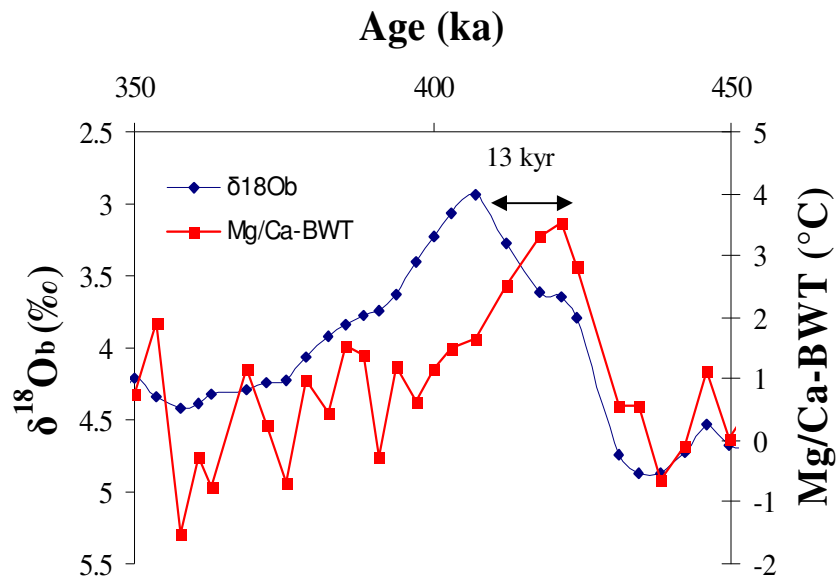
Figure 3.16 The benthic oxygen isotope and Mg/Ca-BWT record across MIS 12-10. Note the lead of BWT over $\delta^{18}O_b$.
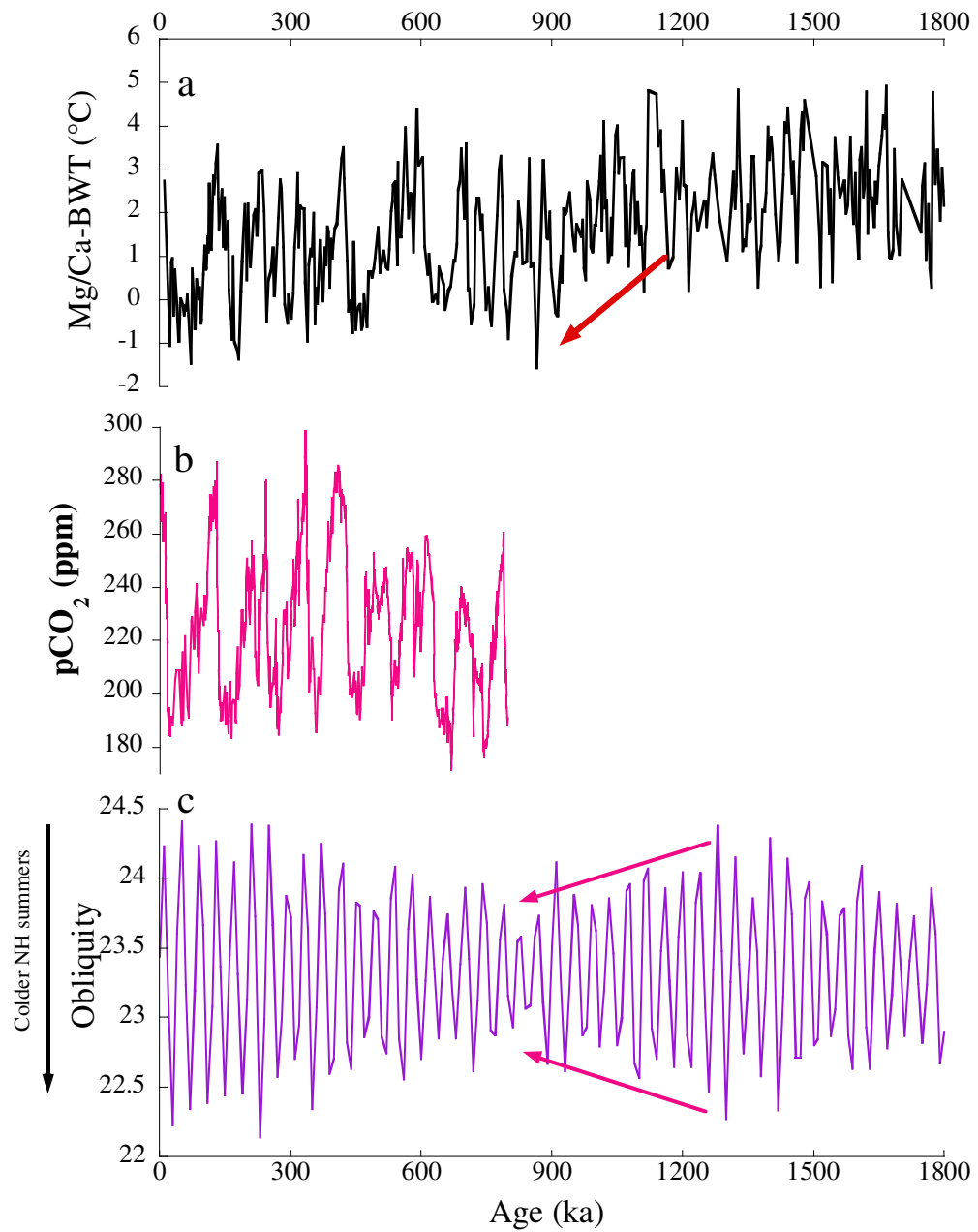
Figure 3.17 (a) Mg/Ca-BWT record; (b) pCO2 record from Vostok and Epica ice core data; (c) Obliquity variations across the Pleistocene.
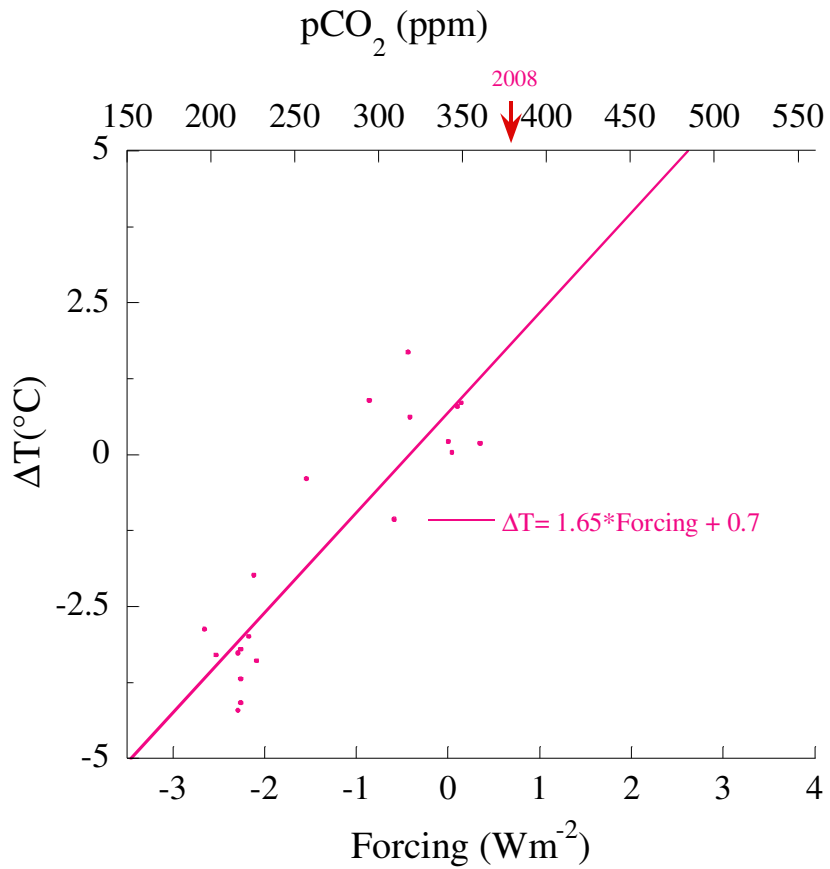
Figure 3.18 Greenhouse gas forcing (ΔF) plotted versus the response (ΔT) in bottom water temperature. The climate sensitivity (λ) is 1.65 °C per W m-2 which implies a 6.5°C change in bottom water temperature for a doubling of pCO_2.

Table 3.1 Statistical summary of the primary features of the Mg/Ca-bottom water temperature and δ_ω record, specifically the mean (M), glacial (G), and interglacial (I) trends, and glacial-interglacial Δ(G-I) amplitude from different time intervals.

	Mg/Ca-BWT				δ_ω (‰)			
Time Interval (kyr)	**M**	**G**	**I**	**Δ(G-I)**	**M**	**G**	**I**	**Δ(G-I)**
0 to 850	1.2	-0.5	3.3	3.9	0.45	0.91	-0.30	1.21
1150 to 1800	2.5	0.7	4.2	3.3	0.41	0.65	-0.05	0.70

Table 3.2 Site locations and supporting information on Pleistocene sea surface temperature records presented in Figure 3.2.

Site	Geographic region	Lat.	Long.	Water Depth (m)	TemperatureProxy	References
DSDP 607	North Atlantic	41 N	33 W	3427	Mg/Ca-BWT; Foram. transfer function	This Study; Ruddiman et al., 1989
ODP 846	Eastern Equatorial Pacific	3 S	91 W	3296	Alkenone Uκ'37	Liu and Herbert, 2004; Lawrence et a 2006
ODP 849	Eastern Equatorial Pacific	0 N	110 W	3839	Alkenone Uκ'37	McClymont et al., 2005
ODP 1077	Benguela Upwelling	5 S	10 E	2394	Alkenone Uκ'37	Durham et al., 2001
ODP 1084	Benguela Upwelling	25 S	13 E	1992	Alkenone Uκ'37	Marlow et al., 2000
ODP 1087	South Atlantic	31 S	15 E	1374	Alkenone Uκ'37	McClymont et al., 2005
ODP 1090	South Atlantic	42 S	8 E	3702	Alkenone Uκ'37	Martinez et al., 2006
ODP 806	Western Pacific	0 N	159 E	2520	Mg/Ca	Medina-Elizalde and Lea, 2005
MD97-2140	Western Pacific	2 N	142 E	2547	Mg/Ca	de Garidel-Thoron et al., 2005

Chapter 4

4. Sr/Ca Ratios in Marine Gastropods: Temperature Calibration and Growth Rate Effects

4.1 Abstract

Here we investigate the potential of Sr/Ca ratios in the marine gastropod *Conus ermineus*, for reconstructing sea water temperatures. We present annually resolved records of Sr/Ca and $\delta^{18}O$ for four shells collected alive from the Flower Garden Banks National Marine Sanctuary in the Gulf of Mexico. Our results show that variations in Sr/Ca and $\delta^{18}O$ co-vary with the *in situ* seasonal temperature cycle. Sr/Ca and temperature are positively correlated, in contrast with the inverse relationship found in inorganically precipitated aragonite. The seasonal Sr/Ca variability is superimposed on a long term trend of increasing Sr/Ca with age. Both the seasonal and long-term ontogenetic changes in Sr/Ca are associated with variations in growth rate, defined here as the shell linear extension rate (Siegenthaler et al.); the seasonal variability in LER is superimposed on a long term decrease with ontogeny. Thus, the covariance of Sr/Ca ratios with temperature and LER suggests that Sr incorporation is likely driven by temperature influence on growth rate, rather than by thermodynamic effects. Unlike the seasonal variability, the ontogenetic effect is characterized by inverse covariation between Sr/Ca and LER, suggesting that Sr/Ca variability is not controlled by growth rate alone, but probably by two different biomineralization mechanisms, one related to temperature and the other to age.

We use the seasonal Sr/Ca signal of four shells to construct a temperature calibration. To minimize the ontogenic effects, we separate the records into juvenile and adult growth stages and calculate the Sr/Ca-temperature (T) relationships:

Juvenile: Sr/Ca (mmol mol^{-1}) = (0.042 ±0.008) * T (ºC) + (0.24 ±0.21) (R^2 = 0.66)

Adult: Sr/Ca(mmol mol^{-1}) = (0.072 ±0.014) * T (ºC) – (0.05 ±0.34) (R^2 = 0.73)

Applying the calibration to a single specimen provides mean annual temperature estimates within ±1ºC of the in situ temperature record, but resolves the seasonal variability only within±3.5ºC. The large error in the seasonal estimates reflects the high variability among specimens. To reduce the uncertainty on seasonal temperatures, we propose combining records from multiple shells to generate an average temperature record. The potential of this approach needs, however, to be validated in other locations.

4.2 Introduction

Fundamental to reconstructing past climate is our ability to extract quantitative paleotemperatures from marine sediments. Many of these sediments consist of biogenic calcium carbonate (e.g. foraminifera, corals, and mollusks), which contains within the lattice trace elements that may record environmental conditions (e.g. Mg, Sr, Ba, Cd, and U). Corals and mollusks are particularly useful for isotopic and trace element studies because of their rapid skeleton accretion, which can provide a high-resolution archive of paleo-environmental variability. Mollusks, especially bivalves, have been rigorously studied for their ability to record past temperatures, salinity, and productivity (e.g., Dodd, 1965; Jones and Quitmeyer, 1996; Elliot et al., 2003; Ivany et al., 2004). Fewer studies, however, have investigated the isotope and trace metal composition of gastropods and their paleo-environmental applications (e.g., Buchardt and Fritz, 1978; Rosenthal and

Katz, 1989; Purton et al., 1999; Andreasson et al., 1999; Tripati and Zachos, 2002).

Among the latter are Kobashi et al. (2001), Kobashi and Grossman (2003), and Kobashi et al. (2004), who have examined isotopic records of fossil and modern *Conus ermineus* shells collected from different sites in the Gulf of Mexico. They note a good correlation between $\delta^{18}O$ and temperature, which suggests that $\delta^{18}O$ closely traces seasonal variations in seawater temperature. Using $\delta^{18}O$ records in fossil *Conus* shells, Kobashi et al. (2001) detail a record of cooling and increased seasonality in the U.S. Gulf Coast during the Tertiary. Interpretations of $\delta^{18}O$ in terms of paleotemperature variability might be limited, however, by lack of information about the oxygen isotopic composition of seawater (δ_w); variations in seawater δ_w are caused by both long term changes in the extent of continental ice sheets and local changes in freshwater input and evaporation. To circumvent this problem, the use of trace metal-temperature relations as a paleothermometer independent of salinity variations (e.g. Mg/Ca ratios in foraminifera (Nurnberg et al., 1996; Rosenthal et al., 1997) and coralline Sr/Ca (Weber, 1973; Beck et al., 1992) have been investigated. Such proxies allow us to estimate paleotemperatures, and combined with $\delta^{18}O$ measurements, to estimate δ_w and make inferences about continental ice volume and local salinity (e.g. Lear et al., 2000; Lea et al., 2000). In this study, we examine the effects of temperature and growth rate on Sr/Ca composition of *Conus* shells to refine their use as repositories of paleoenvironmental information.

Gastropods are widely distributed in the tropical and subtropical oceans. The high deposition rate of their shell along with their longevity (5-7 years) makes them potentially powerful archives of short term paleo-environmental variability (Kohn and Perron 1994). *Conus ermineus*, studied here, typically lives in the mixed layer and thus

records approximately sea surface temperatures (SST). Its shell consists of aragonite, and although aragonite is the less stable polymorph of $CaCO_3$ and may be altered to calcite during diagenesis, aragonite preservation offers a direct and simple way to identify diagenetic alteration in fossil samples (Kohn et al., 1979).

Mollusk biomineralization occurs at the mantle, a thin organic lining on the inner shell surface. Between the mantle and shell surface is the extrapallial fluid, which is an enclosed environment, isolated from seawater. Unlike corals, which crystallize directly from seawater, both gastropods and bivalves derive their shell substrate from the extrapallial fluid (Wilbur and Saleuddin, 1983; Cohen and McConnaughey, 2003). The crystallization process is highly mediated by physiology (Wada and Fujinuki, 1976). Thus, although thermodynamics play an important role in determining the shell Sr/Ca, biological effects such as ontogeny, metabolism, and growth rate must also be considered. A few studies have documented an apparent temperature effect on bivalve Sr/Ca, with increasing Sr/Ca at higher temperatures. Dodd (1965) reported that the Sr content of *Mytilus edulis* and *Mytilus californianus* vary seasonally with temperature. Likewise, in the bivalve *Mya arenaria*, Sr/Ca cycles positively correlate with seasonality in the environment and most likely are governed by temperature (Palacios et al., 1994). However, the results of Palacios et al. (1994) also indicate an ontogenetic effect related to growth rate and/or age. More recently, Gillikin et al. (2005) argue that Sr/Ca in the aragonitic bivalve *Saxidomus giganteus* is mainly controlled by biological processes that affect biomineralization, and thus growth rate. These authors note a significant positive correlation between mean annual Sr/Ca and growth rate, and a weak negative correlation between Sr/Ca and temperature. A similar correlation between Sr/Ca and growth rate

was found in the aragonitic bivalve, *Prototheca staminea* (Takesue and van Geen, 2004).

However, no correlation was found between Sr/Ca and growth rate or SST in *Mercenaria mercenaria* (Gillikin et al., 2005), in contrast to the observations of Stetcher et al. (1996).

The latter suggests that the biological imprint may vary among locations. In contrast with the observations of Gillikin et al. (2005) and Takesue and van Geen (2004), some studies have noted a negative correlation between growth rate and Sr/Ca, which they attribute to metabolic control on the composition of the extrapallial fluid. For example, Purton et al. (1999) observe in the aragonitic mollusks *Venericardia planicosta* and *Clavilithes macrospira* a trend of increased Sr/Ca with the age-related decrease in growth rate. Also, Klein et al. (1996) note large differences in mean Sr/Ca amongst different specimens of the calcitic bivalve *Mytilus trossulus*. In both studies, variations in Sr/Ca are attributed to variable mantle metabolic activity.   To overcome an ontogenetic/metabolic overprint, Goodwin et al. (2003) suggest using the juvenile portions of the bivalve record for paleoclimate reconstruction. These divergent observations for different species of aragonitic and calcitic mollusks attest to the complexity of using gastropod Sr/Ca as a temperature proxy, due to differences in taxonomy, mineralogy, biometry, and morphology. The problem is further confounded by the fact that, at least on seasonal time scales, the two factors that potentially most influence Sr/Ca ratios, temperature and growth rate, covary as organisms tend to grow slower and calcify less at lower temperatures (Lutz and Rhoads, 1980). These studies highlight the need to define taxon- and growth-stage specific trace metal paleothermometers.

4.3 Study Area and Samples

Four modern *Conus ermineus* shells were sampled from Stetson Bank in the Flower

Garden Banks National Marine Sanctuary (FGBNMS) (U. S. Gulf of Mexico) (Fig. 4.1).

Two live specimens (FGS2 and FGS3) and one that died shortly after collection (FGS1)

were collected on May 29, 2003. A fourth live specimen (FGS4) was collected on

September 4, 2003. All samples were collected at water depths between 21 and 26

meters.

Stetson Bank is a small clay/siltstone bank located 165 km south of the Texas-

Louisiana border on the outer continental shelf. This bank is elevated 50 m above the

seafloor and provides a habitat for a large fish community. The site is under the

influence of the subtropical climatic regime and is strongly affected by the Gulf Stream.

Large rivers and streams that flow into the Gulf of Mexico, most notably the Mississippi-

Achafalya River system, cause large seasonal fluctuations in sea surface salinity from 32

to 36 psu. Increased springtime precipitation along the southern U. S. results in

maximum river discharge and a coastal salinity minimum in the spring. High salinities

are caused by upcoast (eastward) flow in the summer, which confines Mississippi-

Achafalya discharge to the eastern Gulf. During non-summer months down-coast

(westward) flow carries this water to the Texas coast and shelf (LATEX, 1993).

The upper water column structure at Stetson Bank changes seasonally. During

spring and early summer, differences in temperature (~6ºC) between the surface and 24

m in the water column are most pronounced because low salinity waters inhibit vertical

mixing, and sea-surface warming precedes warming at depth by several months.

Maximum SSTs occur in early August, whereas the maximum temperature at 24 m

occurs in early September; minimum SSTs occur in early March. In the winter, the water column is well-mixed and therefore temperatures are constant with depth at this site.

4.4 Methods

4.4.1 Environmental Data from Stetson Bank

Hourly surface temperature and salinity recorded by automated recorders were collected at the sampling site from October 29, 2002 to December 12, 2003 and are available from Flower Gardens Banks National Marine Sanctuary. Unfortunately, this temperature record does not cover the entire duration of shell growth for the collected specimens. To construct a longer record which overlaps our gastropod records, spanning ~6-8 years prior to the collection in May 2003, we use SST data from the nearby buoy #42019 of the National Data Buoy Center (NDBC), 100 km west of Stetson Bank (http://www.ndbc.noaa.gov/index.shtml). NDBC buoy #42019 records sea surface conditions, whereas our gastropods were collected at a depth of ~24 m. Because stratification can result in temperature differences of 6ºC between the surface and 24 m during the mid-spring to summer interval, we apply an offset to the NDBC surface record to estimate temperatures at 24 m for that year (LATEX, 1993). The offset is based on temperature differences between sea surface and 24 m. The derived 24-m temperature record is shown in Figure 4.2.

4.4.2 Shell Sampling

Live *Conus ermineus* specimens were cleaned and polished with sandpaper at the spiral area of the cone shells to remove the periostracum, surface contamination, and encrusting organisms. Each sample was measured for height, width, and whorl length (linear length of the coils from the apex to the aperture) to approximate age (Table 4.1).

Live specimens were kept in aquaria following collection for observations and sampling. During sampling, the live specimens were removed from aquaria and wrapped in a wet towel for no longer than 20 minutes at a time. The shell surface and sampling drill were kept clean and dry with compressed air to prevent moisture intrusion and cross-contamination between samples. Linear sample grooves were milled parallel to growth banding using a 0.3-mm Brasseler carbide drill bit (Fig. 4.3). Initial sample intervals were 1 mm with a target resolution of 20 samples per annual cycle. We used 0.5-mm sample intervals for slow growth intervals (<20 mm yr^{-1}). Each groove was milled to a size approximately 0.3 mm deep, 0.3 mm wide and 3 mm long, sufficient to provide >500 μg of $CaCO_3$ powder. Half the powder from each sample was used for isotopic analysis and the other half for trace metal analysis. The dead specimen was sampled in a similar manner.

4.4.3 Isotopic and Trace Metal Analyses

For isotopic analysis, each sample was converted to CO_2 gas in a Finnigan Kiel II carbonate reaction system by adding 100% phosphoric acid at 70°C. The gas was subsequently analyzed on a Finnigan MAT 251 isotope-ratio mass spectrometer. Replicates were run on every fifth sample, with values obtained to an analytical precision of ±0.04‰ for δ^{13}C and ±0.07‰ for δ^{18}O. Results are reported relative to PDB by calibration to the NBS-19 reference standard (δ^{13}C = 1.95‰ PDB, δ^{18}O = -2.20‰ PDB).

For trace metal analyses, aragonite powder splits were progressively reacted with trace metal clean 0.065N HNO_3 (SEASTAR®), until complete dissolution was achieved. After a 10 minute centrifugation, 100 μl of the sample solution was further diluted with 300 μl of 0.5 N HNO_3 (SEASTAR®) to obtain a final Ca concentration ([Ca]) in the ~4 ±

1 mmol range. The progressive dissolution and dilution procedure ensured that [Ca] were kept relatively constant in order to minimize matrix effects (Rosenthal et al., 1999). The analytical method for measuring Sr/Ca by a Vista-Pro CCD Radial ICP-OES is based on the method outlined in Andreasen et al. (in press). Long-term precision for Sr/Ca, evaluated by repeatedly analyzing three consistency standard solutions in the range of 0.46 to 1.84 mmol mol^{-1} at the beginning and end of each run over the course of 3 years, is on average ± 1.5% (RSD).

4.5 Results

Paired measurements of Sr/Ca and $\delta^{18}O$ vs. in situ temperature are plotted as a function of distance from the apex (Fig. 4.4). Depicted this way, specimen age increases with increasing length (to the right in figure 4.44). All four gastropod records share several common features. First, in each record, Sr/Ca and $\delta^{18}O$ co-vary with the calculated seasonal record of seawater temperature at 24 m, showing between 6 and 8 cycles. Second, in each individual shell, both the mean annual and seasonal range of $\delta^{18}O$ are approximately constant throughout the record. In contrast, both the mean annual and seasonal amplitude of Sr/Ca increase with age. For example, the mean Sr/Ca ratio of FGS4 increases from about 1.4 mmol mol^{-1} near the apex to about 1.7 mmol mol^{-1} close to the aperture, with a concomitant increase in the seasonal amplitude from 0.8 to 1.0 mmol mol^{-1}. Third, there is a significant decrease in the width of the seasonal cycles with age (note that for FGS2 only the adult part of the shell was analyzed). Lastly, the $\delta^{18}O$ display similar ranges of values in all four shells: from -1.3‰ to 1.0‰ in FGS1, -1.1‰ to 1.3‰ in FGS3, -1.2‰ to 1.4‰ in FGS4, and -1.0‰ to 1.5‰ in FGS2 (excluding a single value of 2.1‰ that is likely an analytical artifact). There is significant variability in

Sr/Ca ratios among the four shells. Sr/Ca ratios range from 0.86 to 2.03 mmol mol^{-1} in FGS1, 1.14 to 2.56 mmol mol^{-1} in FGS2, 0.98 to 2.10 mmol mol^{-1} in FGS3, and 1.02 to 3.01 mmol mol^{-1} for FGS4.

4.6 Discussion

4.6.1 Age Model and Growth Rate

An age model has been constructed to convert whorl length to a time scale. As temperature and $\delta^{18}O$ are highly correlated ($R^2 = 0.84$), it is assumed that temperature is the primary control of the $\delta^{18}O$ record with only a minor influence from salinity (i.e. δ_ω) (Epstein et al., 1953; Grossman and Ku 1986; Kobashi et al., 2003; Gentry, 2005). The highest and lowest $\delta^{18}O$ values in the record represent peak winter and summer temperatures, respectively. In this site the lowest winter temperatures at 24 m depth typically occur in early March, whereas highest summer temperatures occur in early September. Because FGS1-FGS3 shells were collected on May 29, 2003 and FGS4 on September 24, 2003, we assume that the $\delta^{18}O$ maximum closest to the aperture coincides with early March 2003, whereas the preceding $\delta^{18}O$ minimum is identified as early September 2002. This anchor point method, applied in previous studies (e.g., Klein et al., 1996; Paillard et al., 1996), is used to establish the chronology of each record (Fig. 4.5a-b). Applying the $\delta^{18}O$ age model to the Sr/Ca record, Sr/Ca ratios of all four records correlate positively with temperature. Although the correlation between individual Sr/Ca records and temperature is good, the pooled correlation for all four records is not as good (Table 4.2). The cause of this discrepancy is the offset in mean Sr/Ca among different records, which might be related to natural variability within species. To assess whether the correlation between Sr/Ca and temperature could be improved, we tested an

alternative age model based on tuning Sr/Ca to temperature in a similar fashion as was done with $\delta^{18}O$. Whereas the latter age model slightly improves the individual correlations of Sr/Ca with temperature, there is no significant improvement for the pooled data; R^2 for the pooled data is 0.27 and 0.29 for the $\delta^{18}O$ and Sr/Ca age models, respectively (Table 4.2). Therefore, in the following discussion we use the $\delta^{18}O$ age model.

Using the $\delta^{18}O$ age model, we calculate linear extension rates (Siegenthaler et al.) (seasonal and mean annual) for each shell to determine if variations in extension rate affect the relationship between Sr/Ca and temperature. LER specifies the measured spiral length, between seasonal and annual tie points, with respect to time. For instance, mean annual LER is calculated from the distance between two annual extrema (i.e., the distance between two subsequent winter peaks). Note that LER is not directly proportional to calcification rate because shell length and wall thickness increase with ontogeny. Lorrain et al. (2005) used sclerochronology to determine the daily production of "surface of material" to quantify potential kinetic effects in the Sr/Ca of bivalve calcite. They suggest that the amount of $CaCO_3$ precipitated influences Sr/Ca ratios more than LER. In this study, LER is a rough estimate of growth rate and cannot be extended to calculate precipitation rate or the surface area of $CaCO_3$ precipitated. As the *Conus* shell grows, internal dissolution of the penultimate whorl occurs and shell material is added to the last whorl for defense against predators (Kohn et al., 1979). The remodeling of the shell as the gastropod ages makes it difficult to constrain surface area changes; therefore LER is only an approximation of growth rate. Two different stages of annual linear extension are evident: juvenile and adult (Fig. 4.6). The juvenile stage is marked by a fast LER

(>50 mm yr^{-1}) and typically extends over the first three years. LER during the adult stage

is slower (<50 mm yr^{-1}). Note that FGS1, FGS3, and FGS4 were sampled from the

juvenile to adult stages and therefore have similar growth patterns, whereas FGS2

includes only the slow-growing adult record of the shell. Mean annual Sr/Ca increases

with age as seen in shells FGS1, FGS3, and FGS4 (Fig.4.7). Here we refer to the age-

related decrease in mean annual LER and concomitant increase in mean annual Sr/Ca as

the ontogenetic effect.

Seasonal LERs are calculated from the distance between specific time points

associated with δ^{18}O extrema and the mid-points between these extrema. Hence, each

interval represents about a 3-month growth period. In the juvenile parts of the records,

δ^{18}O and Sr/Ca peaks are wider for the summer months than for the winter months,

indicating seasonal variability in LER (Fig. 4.5). This seasonal variability in LER is less

marked in the adult portion of the record, and is superimposed on a overall trend of

decreasing LER through the mollusk's life (Fig. 4.5). Other studies have suggesting that

the growth rate of some bivalve species slows considerably and the spacing between

annual peaks decreases with age (Stetcher et al., 1996; Gillikin et al., 2005).   On

seasonal time scales Sr/Ca positivitely covaries with changes in seasonal LER; Sr/Ca is

high during the summer when LER is high and low during the winter when LER is low.

Note however that although there is an apparent decrease in mean annual and seasonal

variability of LER (within the resolution of the sampling) the seasonal Sr/Ca cycle

remains relatively constant or slightly increases with age (i.e. Sr/Ca is also high when

growth slows with ontogeny).

4.6.2 Temperature and Growth Effects

The $\delta^{18}O$ data from all four gastropods shells are inversely correlated with

temperature yielding a slope of $\Delta\delta^{18}O/\Delta T = 0.19 \pm 0.01$ ($R^2 = 0.84$). The calculated

sensitivity of 0.19‰ per °C is close to the experimental relationship of 0.23‰ per °C for

aragonite (Grossman and Ku, 1986). The apparent consistency between these two results

suggests that temperature is the dominant control on $\delta^{18}O$ in the shells, whereas salinity-

related variability in δ_ω influences the $\delta^{18}O$ record to a lesser extent (Gentry, 2005). The

latter is likely the main cause for the small, albeit significant, discrepancy between the

gastropod and Grossman and Ku (1986) temperature sensitivity values.

Temperature control on Sr uptake into aragonite has been noted in inorganic

laboratory precipitates (Kinsman and Holland, 1969), corals (Beck et al., 1992), and

scelerosponges (Rosenheim et al., 1994). In these cases, Sr/Ca ratios exhibit an inverse

relationship with temperature, which is consistent with thermodynamic expectations. In

contrast, our data show a positive correlation between gastropod Sr/Ca and temperature.

Other studies of biogenic aragonite have also noted a positive relationship between Sr/Ca

and temperature: the aragonitic foraminifer *Hoeglundina elegans* (Rosenthal et al., 2006),

turritellid gastropods (Tripati and Zachos, 2000), and bivalves (Dodd, 1965; Stecher et

al., 1996; Takesue and van Geen, 2004; Gillikin et al., 2005). However, there is no

apparent relationship between temperature and Sr/Ca and in freshwater aragonitic

gastropods (Buchardt and Fritz, 1978). Thus, in contrast with corals Sr/Ca variations in

gastropod shells are likely driven by the influence of temperature on biological processes

(e.g., calcification rate or growth rate) rather than a thermodynamic effect on the

distribution coefficient. Zhong and Mucci (1989) show in inorganic precipitation

experiments that the distribution coefficient for Sr uptake in aragonite is independent of precipitation rate. Therefore, the growth rate related Sr discrimination mechanism has to be principally biological, either on the mineralization front (Gillikin et al., 2005) or during ion transport from the surrounding medium into the extrapallial fluid (Klein et al., 1996). Metabolic models of Sr incorporation suggest that Sr/Ca should be inversely related to growth rate, as seen in corals (de Villiers et al., 1995; Ferrier-Pages et al., 2002; Cohen and McConnaughey, 2003). Contrary to most bivalve studies, which demonstrate a positive correlation between Sr/Ca and growth rate, gastropod shells of the *Conus* species conform to the expected relationship of the metabolic models. Thus, the relationship between Sr/Ca and temperature is likely driven by temperature influence on growth rate.

The partition coefficient D_{Sr} for *Conus* gastropods varies from 0.1 at 18ºC to 0.3 at 30ºC (where $D_{Sr} = (Sr/Ca)_{shell}/(Sr/Ca)_{seawater}$). These values are comparable to the D_{Sr} for *H. elegans* for the same temperature range (Rosenthal et al., 2006), but are much lower than those obtained in coralline and inorganic aragonites (~1). This discrepancy supports our assumption that the relationship between temperature and Sr/Ca is mediated by biological processes. Given biological mediation, how constant is the relationship between Sr/Ca and temperature? The answer to this question determines the usefulness of gastropod Sr/Ca for paleotemperature reconstruction. Below we evaluate the fidelity of the relationship between Sr/Ca in *Conus* shells and temperature and LER.

Correlation among $\delta^{18}O$, Sr/Ca, and temperature are significant for most juvenile and adult portions of *Conus* shells, using both individual and pooled data ($R^2 > 0.50$) and show that Sr/Ca variability covaries with a temperature. However, juvenile and adult

stages yield Sr/Ca -δ^{18}O and Sr/Ca-temperature relations with different slopes and y-intercepts, indicating that juvenile and adult shells have different sensitivities to temperature (Table 4.3). Offset in Sr/Ca among the four records is related to the ontogenetic effect on Sr/Ca and is the main cause for the low correlation coefficient for the pooled Sr/Ca data set.

Above, we have shown that variations in LER occur throughout the gastropod's life as a function of age and also seasonally, particularly during the juvenile stage. Variations in LER affect the Sr/Ca record in two ways: (1) Mean annual Sr/Ca increases as a function of distance from the apex. The increase, which is not a function of temperature and not observed in the δ^{18}O records, suggests an ontogenetic effect of growth/metabolic processes on Sr/Ca; (2) Seasonal Sr/Ca amplitude increases in the later stages of the gastropod records. We note that the ontogenetic effect expressed by a decrease in LER and concomitant increase in Sr/Ca values is different from the effect of seasonal variations in LER on Sr/Ca values. For seasonal variations, a positive relationship is observed between LER and Sr/Ca values, in contrast with the negative correlation for the ontogenetic trend. This discrepancy suggests that seasonal and long term (ontogenetic) Sr/Ca variability is likely controlled by different mineralization mechanisms, and that the seasonal variability is more closely related to temperature. Therefore, we use the seasonal Sr/Ca signal to construct a temperature calibration.

4.7 Temperature Calibration

To minimize growth rate effects on the temperature calibration, we treat the data in the following ways before calculating the regression equations: (1) Divide each record into juvenile and adult portions to account for the increase in mean annual Sr/Ca seasonal

amplitude with age, and (2) Omit the first half year of juvenile growth to remove Sr/Ca variability associated with early stages of shell development. We find that treating the data this way yields more accurate temperature estimates than a multivariate regression of Sr/Ca, temperature, and growth rate. We propose two calibration equations, one for the juvenile and another for the adult stage. We use geometric mean regression (model II) of Sr/Ca against temperature (Laws, 1997). Using the geometric mean method, which normalizes the data to a zero intercept and equally weights errors in both variables, allows us to pool data from all samples despite offsets amongst the four shells (for examples see Rosenthal and Lohmann, 2002; Anand and Elderfield, 2003). The temperature (T) calibrations for all specimens are described by (Fig. 4.8):

Juvenile:

$$Sr/Ca \text{ (mmol mol}^{-1}) = (0.042 \pm 0.008) * T (^{\circ}C) + (0.24 \pm 0.21) \quad (R^2 = 0.66.) \quad (1)$$

Adult:

$$Sr/Ca \text{ (mmol mol}^{-1}) = (0.072 \pm 0.014) * T (^{\circ}C) - (0.05 \pm 0.34) \quad (R^2 = 0.68) \quad (2)$$

Using ANOVA, we calculate the standard deviations ($\pm 2\sigma$) of the slope and intercept. The juvenile and adult calibrations are significantly different beyond the 95% confidence interval of the calibration. The two calibrations are offset from each other due to the ontogenetic effect, which is not entirely eliminated by separating the record into juvenile and adult portions because variations in the seasonal amplitude within each growth stage are still present. There is relatively large scatter around the regression lines. Some of the scatter in the calibration might be related to: (1) error in the chronology of the Sr/Ca relative to the temperature record; (2) drilling the spire at different depths

leading to sampling aragonite deposited at different stages of growth; (3) instrumental error (±0.07°C); (4) error in the compilation of the temperature record, especially in converting SSTs to 24-m temperatures (±0.5°C); and (5) vertical migration during the gastropod's life. For example, a migration of ± 4 m from the collection depth of 24 m would result in a ± 0.7°C change and an 0.07 mmol mol^{-1} increase in Sr/Ca These uncertainties account for some of the scatter in our records, but the effects are likely small.

To test the applicability of Sr/Ca paleothermometry we use three (FGS2, FGS3, FGS4) of the four records to construct new calibration equations and then apply them to a fourth record (FGS1), which is excluded from and thus independent of the calibration. This is done for each combination of shells except for FGS2, which was sampled only in the adult portion. For each combination of shells, the juvenile and adult calibration equations are comparable to the calibrations for all four shells within 2σ and 3σ, respectively. The juvenile Sr/Ca-temperature calibration is applied to the juvenile portion of the FGS1 Sr/Ca record and the adult calibration to the adult portion. Thereafter, the two temperature reconstructions are spliced together to form a composite temperature record (Fig. 4.9). For this case study, the juvenile and adult temperature reconstruction accurately resolves the mean annual temperature (Fairbanks et al.) at 24 m within ±1°C for both juvenile and adult stages. However, estimates of the seasonal temperature amplitude are only accurate within ±3.5°C. The application of the model to other case studies, FGS3 and FGS4, resolves the MAT within ±1.5°C and ±1°C, and the seasonal temperature amplitude within ±4°C and ±3.5°C, respectively.

We test whether combining records from multiple shells to generate an average temperature record improves the accuracy of temperature estimates. For example, we calculate a pooled average by choosing two cycles from each growth stage that overlap amongst the shells and resampling each record at 0.1 yr interval. Subsequently, we combine the re-sampled Sr/Ca records and separate the record into juvenile and adult stages. The adult temperature reconstruction captures the mean annual temperature and seasonal range of the in situ temperature record within ±1°C. The juvenile reconstruction resolves the mean annual temperature within ±1°C, but the seasonal temperature range only to about ±4°C (Fig. 4.10). This approach needs to be further tested.

4.8 Summary and Conclusions

This study assesses the potential of using Sr/Ca ratios in the marine gastropod *Conus ermineus* for reconstructing sea surface temperature. Mollusk shells are potentially a very useful archive of paleo-climate, as their relatively fast growth rate provides seasonally resolved record of environmental changes. Results of this study show that Sr/Ca and $\delta^{18}O$ in the marine gastropod *Conus ermineus* co-vary with the seasonal cycle of *in-situ* water temperature. The seasonal variability is superimposed on a longer-term trend of increasing Sr/Ca with age. These changes in elemental ratios occur in association with changes in the shell linear extension rate (LER, used here as indicator of growth rate); LER exhibits cyclic seasonal variability superimposed on the long-term decrease with age (ontogenetic effect). The positive correlation between Sr/Ca and the seasonal temperature variability is in contrast with expectations from thermodynamics, inorganic precipitate experiments, and the behavior of Sr in coralline aragonite, thereby suggesting Sr/Ca variations are likely correlated with temperature through its influence

on growth rate, rather than a thermodynamic control on the distribution coefficient. The fact that seasonal variations in Sr/Ca are positively correlated with growth rate, in contrast with the negative correlation for the ontogenetic trend, suggests that Sr/Ca variability is not controlled by growth rate alone, but by two different biomineralization mechanisms. Of these, only the seasonal Sr/Ca variability is related to temperature.

We explored the utility of Sr/Ca for reconstructing sea surface temperature using four gastropod records. To minimize the ontogenetic effects on Sr/Ca we propose divide the records into juvenile (typically first three years) and adult sections. After accounting for the influence of the ontogenetic growth rate effect on Sr/Ca, we use the records to generate juvenile and adult Sr/Ca-temperature calibrations. Our findings show that application of the calibration to a single specimen resolves the mean annual temperature within ±1°C of the in situ temperature record, but overestimates seasonal temperature amplitude by ±3.5°C. The latter reflects the large variability in the seasonal Sr/Ca record among specimens. This variability is most likely due to variable growth rate effects among individual specimens. To improve the accuracy of the calibration, we propose using a combination of multiple shells to produce an average temperature record. Our study shows that a multi-specimen approach resolves the mean annual temperature within < ±1°C for both juvenile and adult calibration, and seasonal temperature amplitude within ±1°C for the adult calibration.

The results presented here suggest that the Sr/Ca-temperature calibration has the potential to reconstruct changes in mean annual temperature and seasonality in the past. This relationship is, however, influenced by biological processes linking temperature to growth rate. Therefore, caution should be taken before applying this calibration as the

relationship, which is biologically mediated, by may be both spatially and temporally variable.

4.9 References

Anand, P., H. Elderfield, and M. H. Conte (2003), Calibration of Mg/Ca thermometry in planktonic foraminifera from a sediment trap time series, *Paleoceanography*, *18*.

Andreasen, D., S. Sosdian, S. Perron-Cashman, C.H. Lear, T. Degaridel, P. Field, and Y. Rosenthal (in press), Fidelity of radial-viewed ICP-OES and magnetic-sector ICP-MS measurement of Mg/Ca and Sr/Ca ratios in marine biogenic carbonates: Are they trustworthy together? *Geochemistry Geophysics Geosystems*, *submitted*.

Andreasson, F., and B. Schmitz (1998), Tropical Atlantic seasonal dynamics in the early middle Eocene from stable oxygen and carbon isotope profiles of mollusc shells, *Paleoceanography*, *13*, 183-192.

Beck, W. J., L. R. Edwards, E. Ito, F. W. Taylor, J. Recy, F. Rougerie, P. Joannot, and C. Henin (1992), Sea-surface temperature from coral skeletal strontium/calcium ratios, *Science*, *257*, 644-647.

Buchardt, B., and P. Fritz (1978), Strontium uptake in shell aragonite from the freshwater gastropod *Limnaea stagnalis*, *Science*, *199*, 291-292.

Cohen, A. L., and T. A. McConnaughey (2003), Geochemical perspectives on coral mineralization, *Reviews in Mineralogy and Geochemistry*, *54*, 151-187.

DeVilliers, S., B. Nelson, and A. Chivas (1995), Biological controls on coral Sr/Ca and delta-O-18 reconstructions of sea surface temperatures, *Science*, *269*, 1247-1249.

Dodd, J. R. (1965), Environmental control of strontium and magnesium in Mytilus, *Geochimica et Cosmochimica Acta*, *29*, 385-398.

Elliot, M., P. B. de Menocal, B.K. Linsley, and S. S. Howe (2003), Environmental controls on the stable isotopic composition of *Mercenaria merceneria*: Potential application to paleoenvironmental studies, *Geochemistry Geophysics Geosystems*, *4*, 1056.

Epstein, S., R. Buchsbaum, H. Lowenstam, and H. Urey (1953), Revised carbonate-water isotopic temperature scale, *Geological Society of America, Bulletin*, *64*, 1315-1326.

Ferrier-Pages, C., F. Boisson, and D. Allemand (2002), Kinetics of strontium uptake in the scleractinian coral Stylophora pistillata, *Marine Ecology-Progress Series*, *245*, 93-100.

Gentry, K. (2005), Seasonal isotope and trace-metal profiles of serially sampled Conus gastropods: Proxies for paleoenvironmental change, M.S. thesis, 63 pp, Texas A&M.

Gillikin, D. P., A. Lorrain, J. Navez, J. Taylor, L. Andre, E. Keppen, W. Baeyens, and F. Dehairs (2005), Strong biological controls on Sr/Ca ratios in aragonitic marine bivalve shells, *Geochemistry Geophysics Geosystems*, *6*, 1-16.

Goodwin D.H., B. R. S., and D.L. Dettman (2003), Resolution and fidelity of oxygen isotopes as paleotemperature proxies in bivalve mollusk shells: Models and observations, *PALAIOS*, *18*, 110-125.

Grossman, E. L., and T. Ku (1986), Oxygen and carbon isotope fractionation in biogenic aragonite: Temperature effects, *Chemical Geology*, *59*, 59-74.

Ivany, L., B. Wilkinson, K. Lohmann, E. Johnson, B. McElroy, and G. Cohen (2004), Intra-annual isotopic variation in *Venericardia* bivalves: implications for early Eocene temperature, seasonality, and salinity on the U.S. Gulf Coast, *Journal of Sedimentary Research*, *74*, 7-19.

Ivany, L., S. Peters, B. Wilkinson, K. Lohmann, and B. Reimer (2004), Composition of the early Oligocene ocean from coral stable isotope and elemental chemistry, *Geobiology*, *2*, 97-106.

Jones, D. S., and I. R. Quitmyer (1996), Marking time with bivalve shells: Oxygen isotopes and season of annual increment formation, *Palaios*, *11*, 340-346.

Kinsman, D. J. J., and H. D. Holland (1969), The co-precipitation of cations with $CaCO_3$-IV. The co-precipitation of Sr^{2+} with aragonite between 16º and 96º degrees, *Geochimica et Cosmochimica acta*, *33*, 1-18.

Klein R., K. Lohmann, and C. W. Thayer (1996), Sr/Ca and C-13/C-12 ratios in skeletal calcite of Mytilus trossulus: Covariation with metabolic rate, salinity, and carbon isotopic composition of seawater, *Geochimica et Cosmochimica acta*, *60*, 4207-4221.

Kobashi, T., and E. L. Grossman (2003), The oxygen isotopic record of seasonality in *Conus* shells and its application to understanding late middle Eocene (38 Ma) climate, *Paleontological Research*, *7*, 343-355.

Kobashi, T., E. L. Grossman, D. T. Dockery, and L. C. Ivany (2004), Water mass stability recontructions from greenhouse (Eocene) to icehouse (Oligocene) for the northern Gulf Coast continental shelf (USA), *Paleoceanography*, *19*, 1022.

Kobashi, T., E. L. Grossman, T. E. Yancey, and D. T. Dockery (2001), Reevaluation of conflicting Eocene tropical temperature estimates: Molluskan oxygen-isotope evidence for warm low-latitudes, *Geology*, *29*, 983-986.

Kohn, A. J., E. R. Myers, and V. R. Meenakshi (1979), Interior remodeling of the shell by a gastropod mollusc, *Proc. Natl. Acad. Sci.*, *76*, 3406-3410.

Kohn, A. J., and F. E. Perron (1994), *Life History and Biogeography: Patterns in Conus*, 106 pp. pp., Oxford University Press, Oxford, UK.

LATEX (1997), Texas-Louisiana Shelf Circulation and Transport Processes Study, *NODC Project Code 0212*.

Laws, E. (1997), *Mathematical Methods for Oceanographers*, 343 pp., John Wiley, New York.

Lea, D., D. Pak, and H. Spero (2000), Climate impact of late Quaternary equatorial Pacific sea surface temperature variations, *Science*, *289*, 1719-1724.

Lear, C. H., H. Elderfield, and P. A. Wilson (2000), Cenozoic deep-sea temperatures and global ice volumes from Mg/Ca in benthic foraminiferal calcite, *Science*, *287*, 269-272.

Lorrain, A., D. P. Gillikin, Y. Paulet, L. Chauvaud, A. Lemercier, J. Navez, and L. Andre (2005), Strong kinetic effects on Sr/Ca ratios in the calcitic bivalve *Pecten maximus*, *Geology*, *33*, 965-968.

Lutz, R. A., and D. C. Rhoads (1980), *Growth Patterns within the Molluscan Shell: An Overview in Skeletal Growth of Aquatic Organisms*, 203-254 pp., Plenum Press, New York.

Nurnberg, D., J. Bijma, and C. Hemleben (1996), Assessing the reliability of magnesium in foraminiferal calcite as a proxy for water mass temperatures, *Geochimica et Cosmochimica acta*, *60*, 803-814.

Paillard, D., L. Labeyrie, and P. Yiou (1996), Macintosh program performs time-series analysis, *Eos Trans. AGU*, *77*, 379.

Palacios, R., J. Orensanz, and D. Armstrong (1994), Seasonal and life-long variation of Sr/Ca ratio in shells of *Mya arenaria* from Grays Harbor-an ancillary criterion in demographic studies, *Estuarine, Coastal, and Shelf Sciences*, *39*, 313-327.

Purton, L., G. Shields, M. Brasier, and G. Grime (1999), Metabolism controls Sr/Ca ratios in fossil aragonitic ontogenetic, *Geology*, *27*, 1083-1086.

Rosenheim, B. E., P. K. Swart, S. R. Thorrold, P. Willenz, B. Lorraine, and C. Latkoczy (2004), High-resolution Sr/Ca records in sclerosponges calibrated to temperature in situ, *Geology*, *32*, 145-148.

Rosenthal, Y., E. Boyle, and N. Slowey (1997), Temperature control on the incorporation of magnesium, strontium, fluorine and cadmium into benthic foraminiferal shells from Little Bahama Bank: Prospects for thermocline oceanography, *Geochimica et Cosmochimica Acta*, *61*, 3633-3643.

Rosenthal, Y., and A. Katz (1989), The applicability of trace elements in freshwater shells for paleogeochemical studies, *Chemical Geology*, *78*, 65-76.

Rosenthal, Y., C. Lear, D. Oppo, and B. Linsley. (2005), Temperature and carbonate Ion effects on Mg/Ca and Sr/Ca ratios in benthic foraminifera: The aragonitic species *Hoeglundina elegans*, *Paleoceanography*, *submitted*.

Rosenthal, Y., and G. P. Lohmann (2002), Accurate estimation of sea surface temperatures using dissolution-corrected calibrations for Mg/Ca paleothermometry, *Paleoceanography*, *17*.

Rosenthal, Y., P.Field, and R. M. Sherrell (1999), Precise determination of element/calcium ratios in calcareous samples using Sector Field Inductively Coupled Plasma Mass Spectrometry, *Analytical Chemistry*, *71*, 3248-3253.

Simkiss, K., and Wilbur, K. (1989), *Biomineralization: Cell Biology and Mineral Deposition*, 337 pp., Academic Press, Inc., San Diego, CA.

Stecher, H., D. Krantz, C. Lord, G. Luther, and K. Bock (1996), Profiles of strontium and barium in *Merceneria mercernaria* and *Spisula solidissima* shells, *Geochimica et Cosmochimica Acta*, *60*, 3445-3456.

Takesue, R., and A. VanGeen (2004), Mg/Ca, Sr/Ca, and stable isotopes in modern and holocene *Protothaca staminea* shells from a northern California coastal upwelling region, *Geochimica et Cosmochimica acta*, *68*, 3845-3861.

Tripati, A., J. Zachos, and (2002), Late Eocene tropical sea surface temperatures: A perspective from Panama, *Paleoceanography*, *17*, 1032.

Tripati, A., J. C. Zachos, and (2000), Paleocene and Eocene coastal ocean temperatures, *GFF*, *122*, 171-172.

Wada, K., Fujinuki, T., 1976. Biomineralization in bivalve mollusks with emphasis on the chemical composition of the extrapallial ̄uid. In: Watabe, N., Wilbur, K.M. (Eds.), The Mechanisms of Mineralization in Invertebrates and Plants. University of South Carolina Press, Columbia, pp. 175-190.

Weber, J. N. (1973), Incorporation of strontium into reef coral skeletal carbonate, *Geochimica et Cosmochimica Acta*, *37*, 2173-2190.

Wilbur, K.M., Salenddin, A.S.M., 1983. Shell formation. In: Wilbur, K.M. (Ed.), The Mollusca, Vol. 4. Academic Press, New York, pp. 235±287.

Zhong, S., and A. Mucci (1989), Calcite and aragonite precipitation from seawater solutions of various salinities: precipitation rates and overgrowth compositions, *Chemical Geology*, *78*, 283-299.
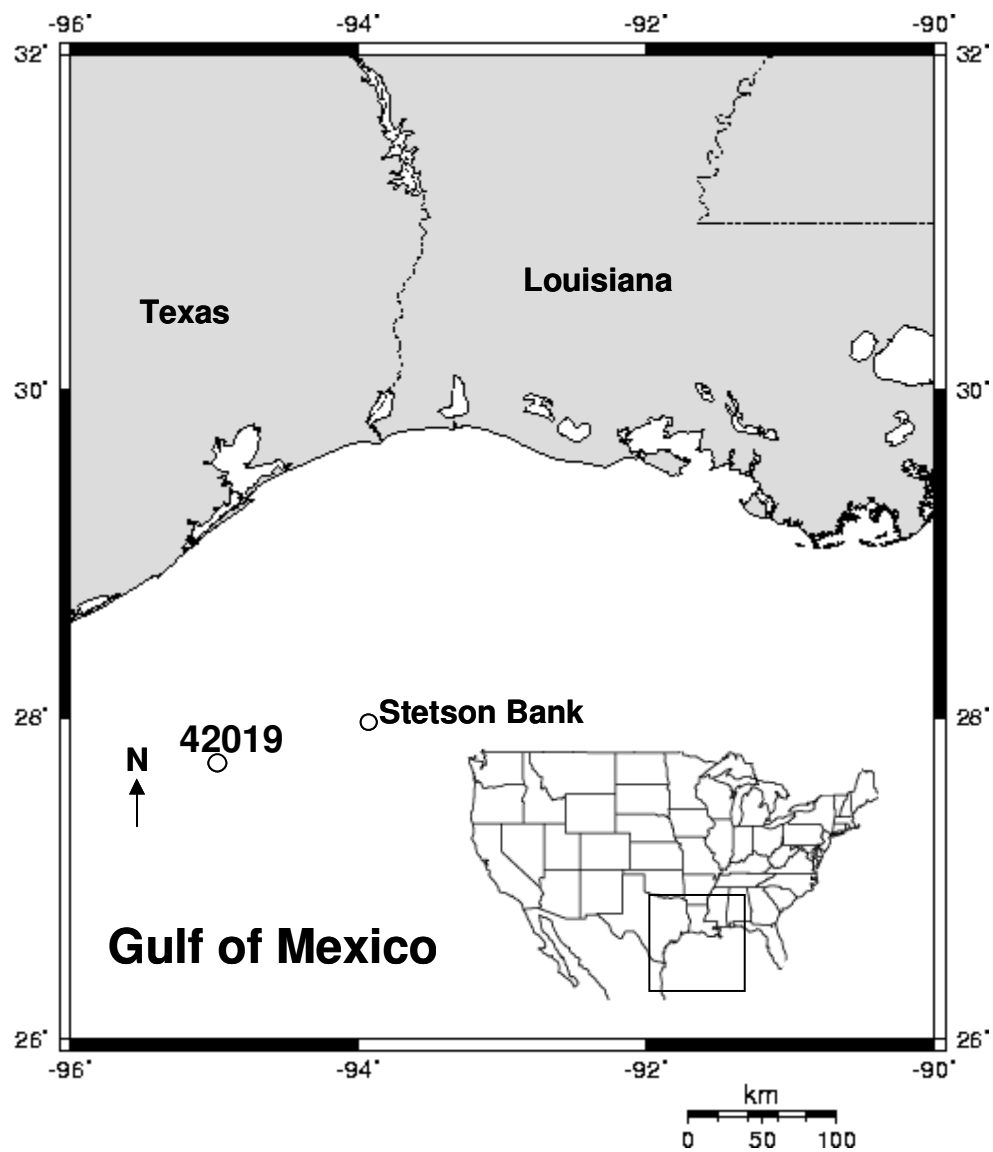
Figure 4.1 Map of U.S. Gulf Coast showing Flower Garden Banks National Marine Sanctuary, the location where *Conus ermineus* shells were collected and hydrographic parameters were measured. 100 km west of Stetson bank, the site of sample collection, is the NDBC #42019 which is used to extend the temperature record to earlier growth cycles.
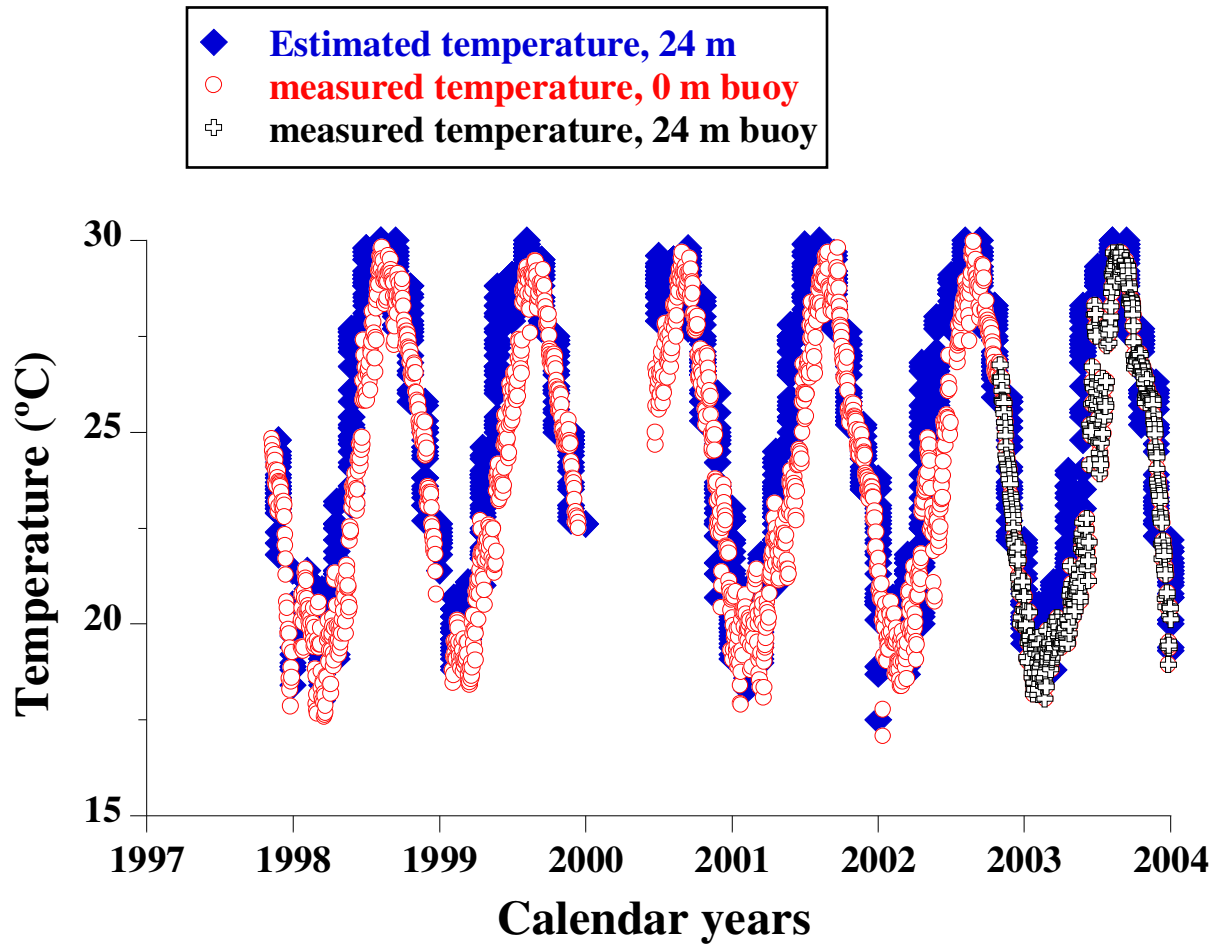
Figure 4.2 24 m Temperature record (circles) from 1997 to 2004 estimated from a compilation of SSTs (diamonds) and a nearby 24 m record (crosses), in the Stetson Bank, the collection site of *Conus* shells used in this calibration.
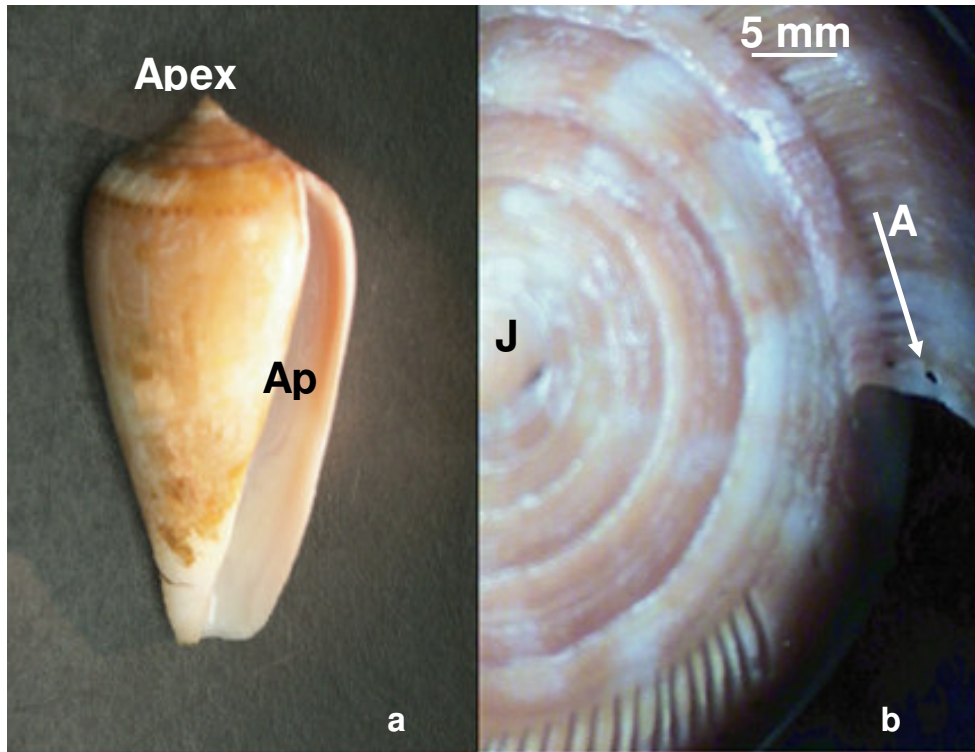
Figure 4.3 a) Picture of study specimen gastropod *C. ermineus* shell labeled from apex to aperture (Ap). (b) At a 1 mm sampling interval, samples were milled parallel to growth banding. The arrow indicates the direction of sampling. J = juvenile and A = adult.

Figure 4
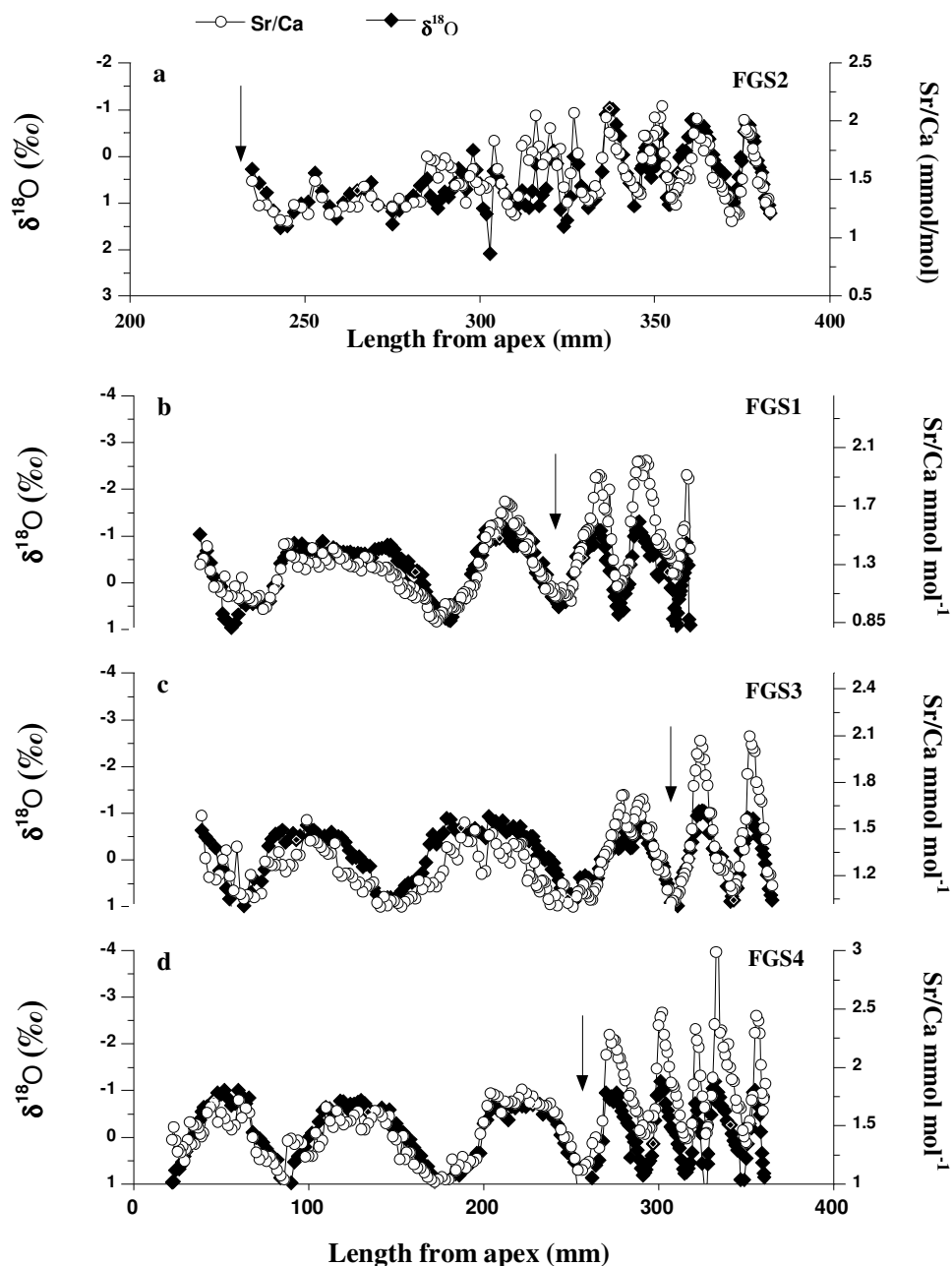
Figure 4.4 $\delta^{18}O$ and Sr/Ca records versus distance from apex and towards the aperture for modern shells FGS2, FGS1, FGS3, and FGS4. Note that the $\delta^{18}O$ scale has been inverted to correspond with temperature increasing upward, $\delta^{18}O$ and Sr/Ca scales are different in each panel, and x scale for FGS2 is different from the other three shells. The arrow indicates our placement of the transition zone from juvenile to adult. Direction of increasing age is the right and the entire record of FGS4 is not included.

139
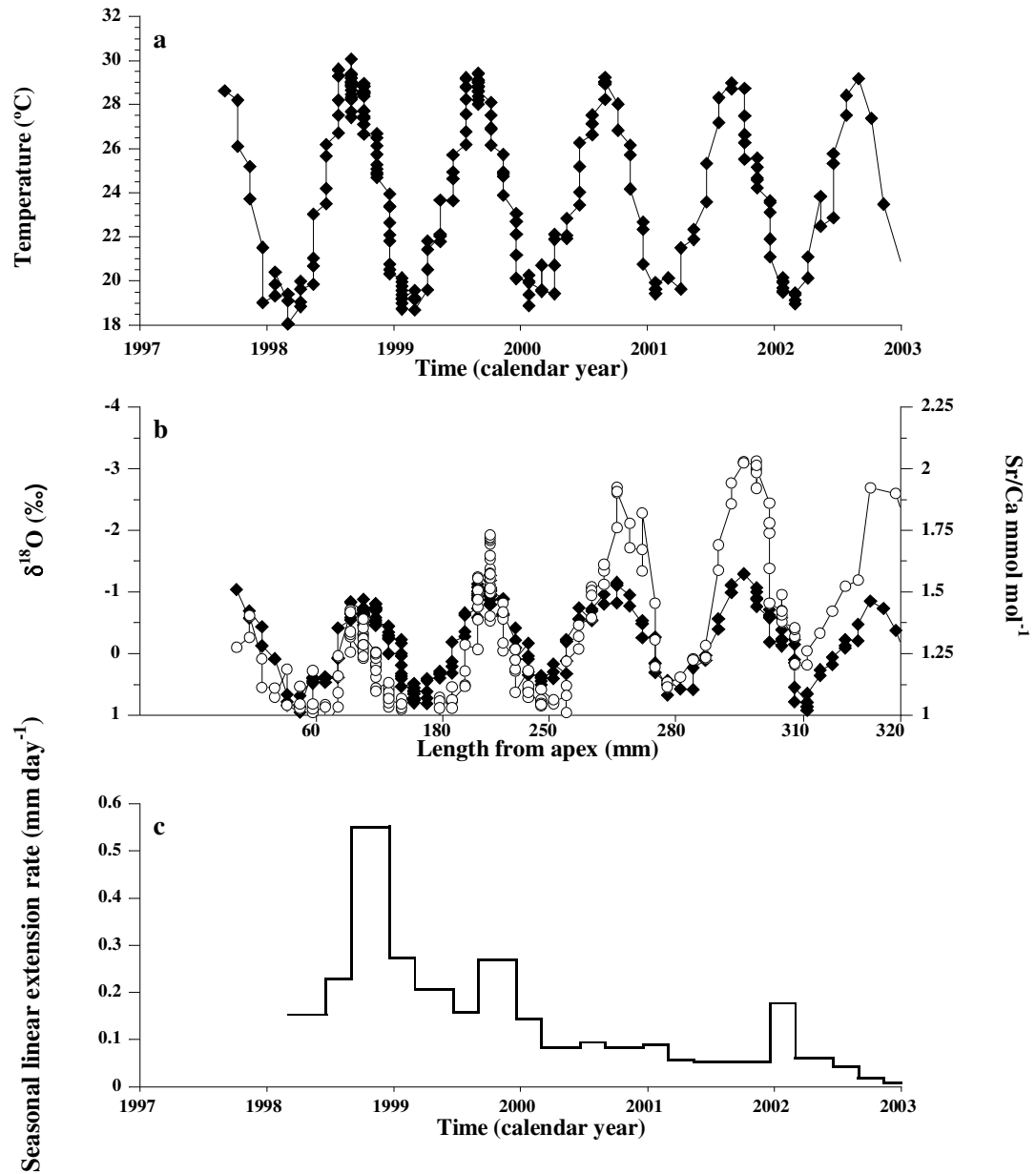
Figure 5

Figure 4.5 Example from FGS1 showing construction of the δ¹⁸O age model. (a) Temperature record versus calendar years from 1997 to 2003; (b) δ¹⁸O and Sr/Ca records from FGS1 versus length from the apex for corresponding years. Note the the x-axis for this plot is not linearly scaled; (c)Seasonal Linear extension rate (Siegenthaler et al.) versus calendar years. Seasonal LERs are calculated from the distance between specific time points associated with δ¹⁸O extrema and the mid-points between these extrema. A seasonal variation in linear extension rate is evident in the juvenile growth stage.
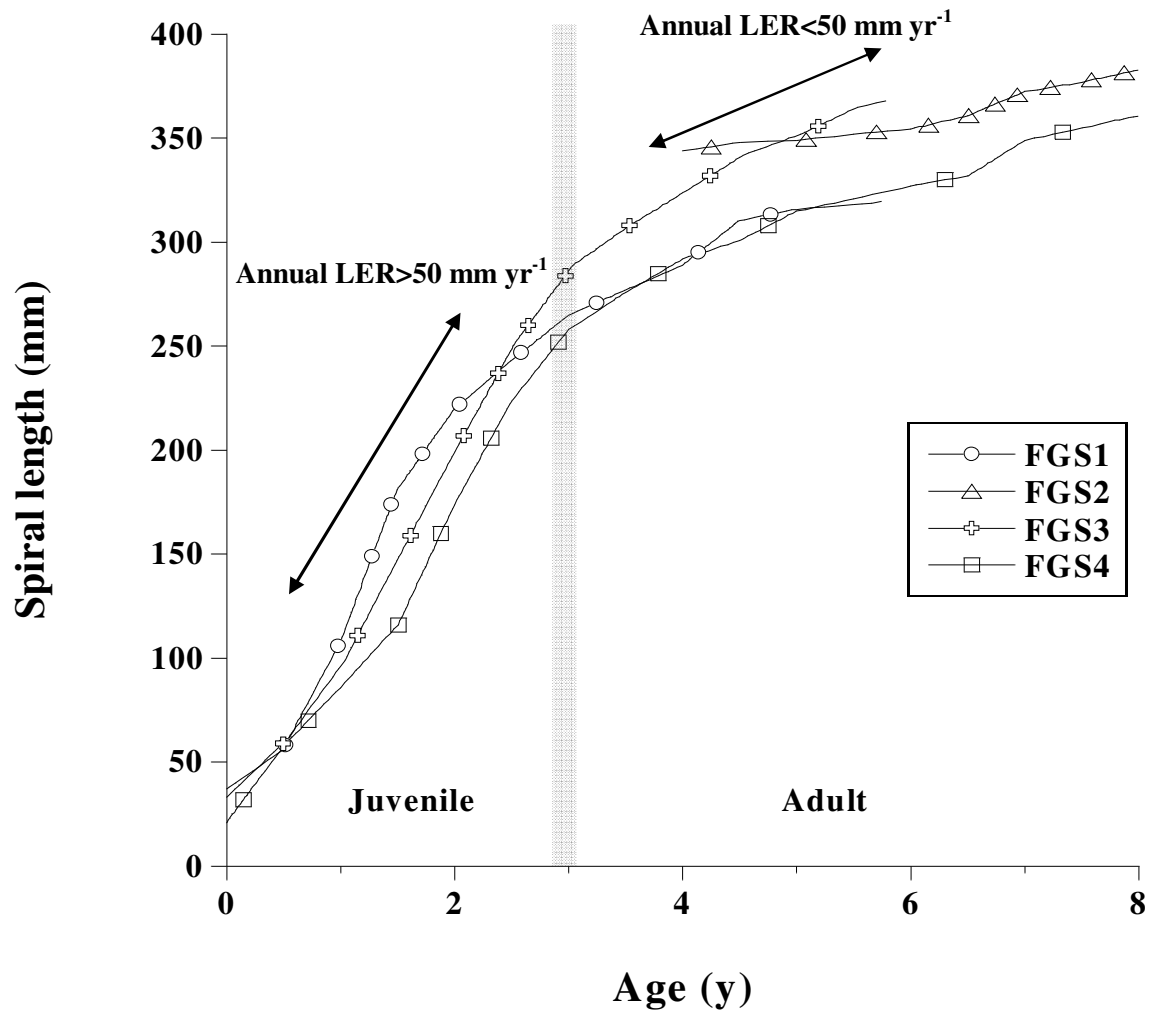
Figure 4.6 Mean annual Linear extension rate (Siegenthaler et al.) as a function of length along the spiral for specimens. Mean annual LER is calculated from the distance between two annual extrema (i.e., the distance between two subsequent winter peaks). Based on the variation of growth rate with age, two stages of growth were identified: juvenile and adult. The shaded region marks an adolescent zone, where the gastropod transitions from juvenile to adult. Typically the juvenile period is the first three years of growth followed by the adult. Note that only the adult portion of FGS2 was sampled.
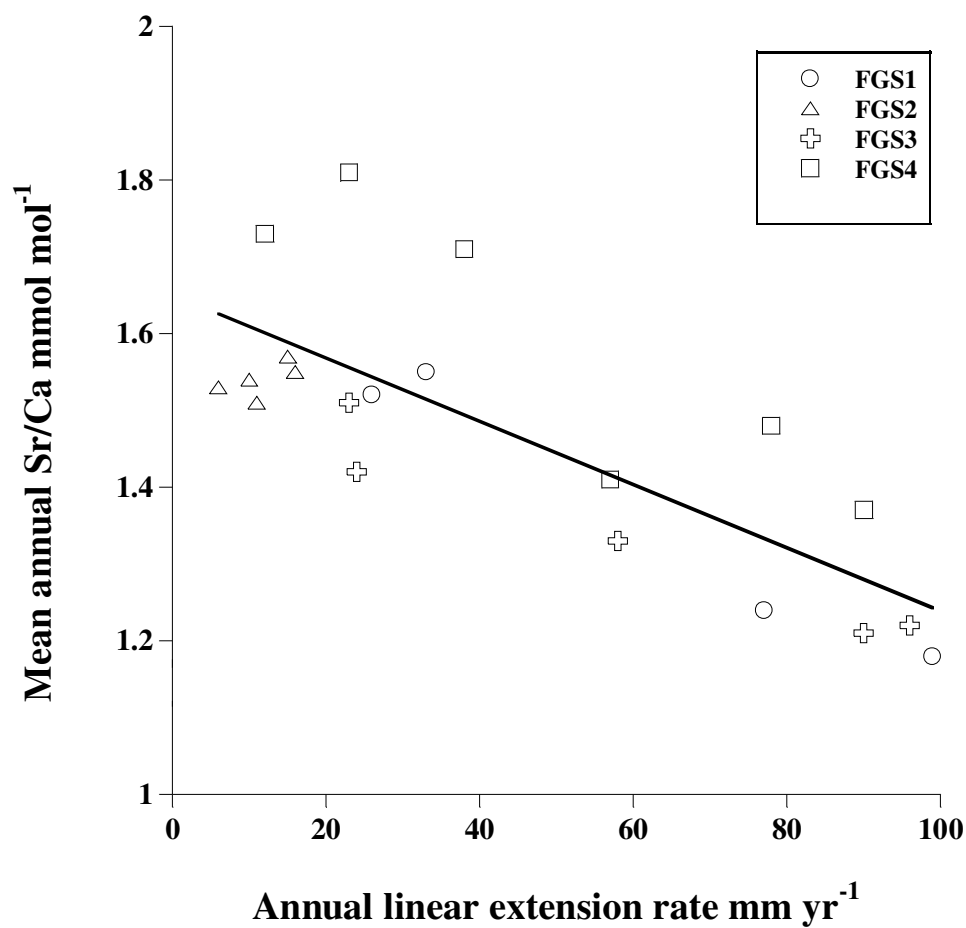
Figure 4.7 (a) Average annual Sr/Ca ratios (from data in figure 4) versus annual linear extension rates. Annually averaged Sr/Ca ratios are correlated with annual extension rate ($R^2 = 0.55$). Compiled from 4 modern shells FGS1(circles), FGS2 (triangles), FGS3 (crosses), and FGS4 (squares).

Figure 8
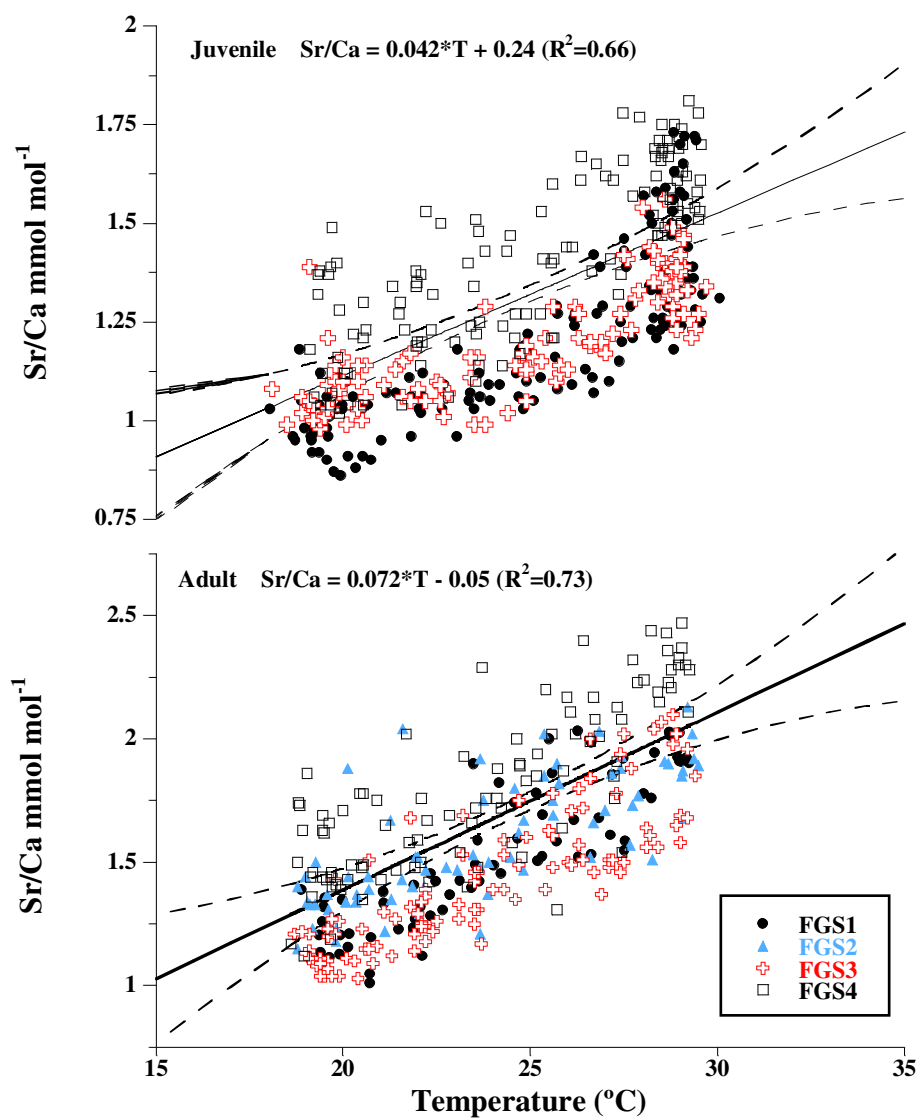
Figure 4.8 Regressions of the juvenile and adult Sr/Ca ratios versus temperature. 95% confidence intervals (dashed lines) are plotted. Note the regressions are significantly different within 2σ. Compiled from 4 modern shells FGS1(circles), FGS2 (triangles), FGS3 (crosses), and FGS4 (squares).
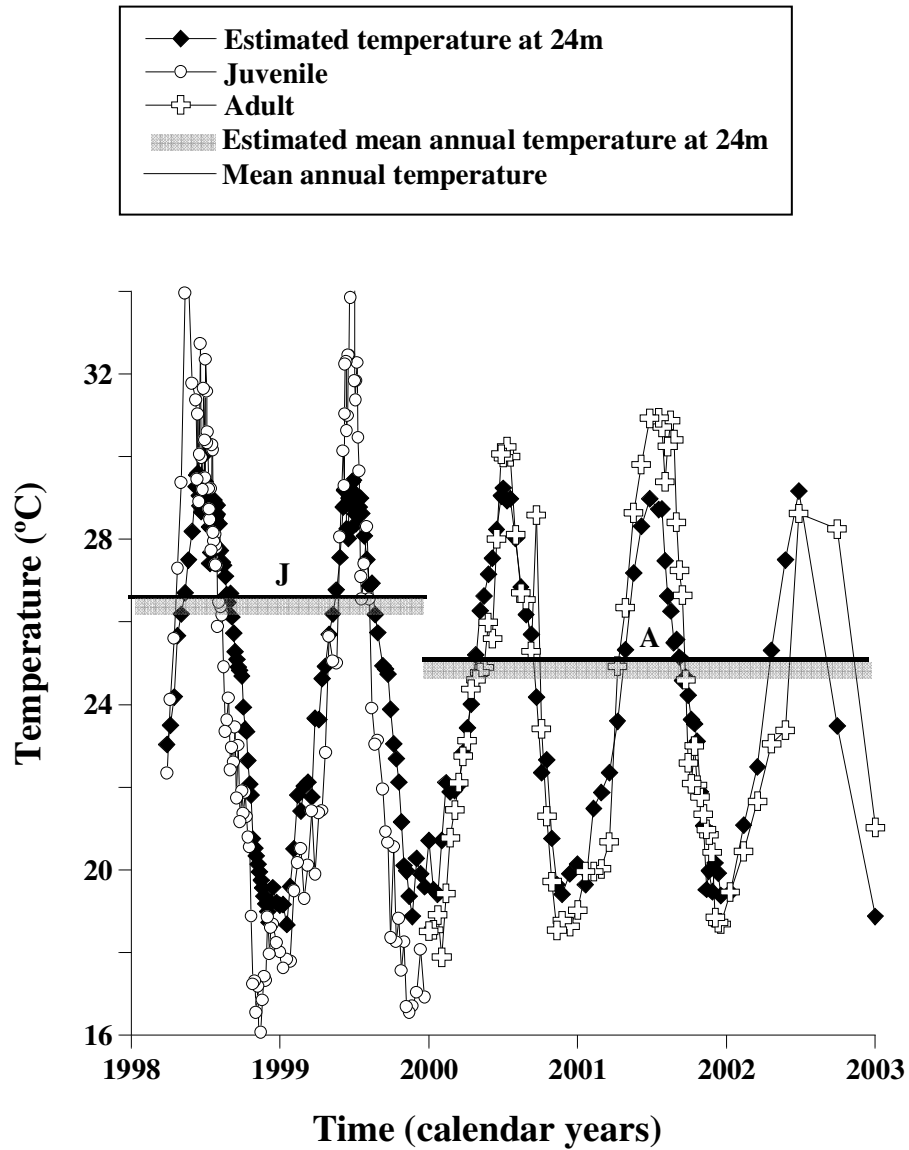
Figure 4.9 Temperature versus time in calendar years plotted for the estimated temperature at 24 m(diamonds) and juvenile (circles) and adult (crosses) temperature records. Note the juvenile and adult calibrations were applied to the FGS1 Sr/Ca record (omitted from calibration). Lines (A and J) indicate the mean annual temperature for the juvenile and adult temperature reconstructions. Shaded regions indicate the estimated mean annual temperature at 24m for these portions.
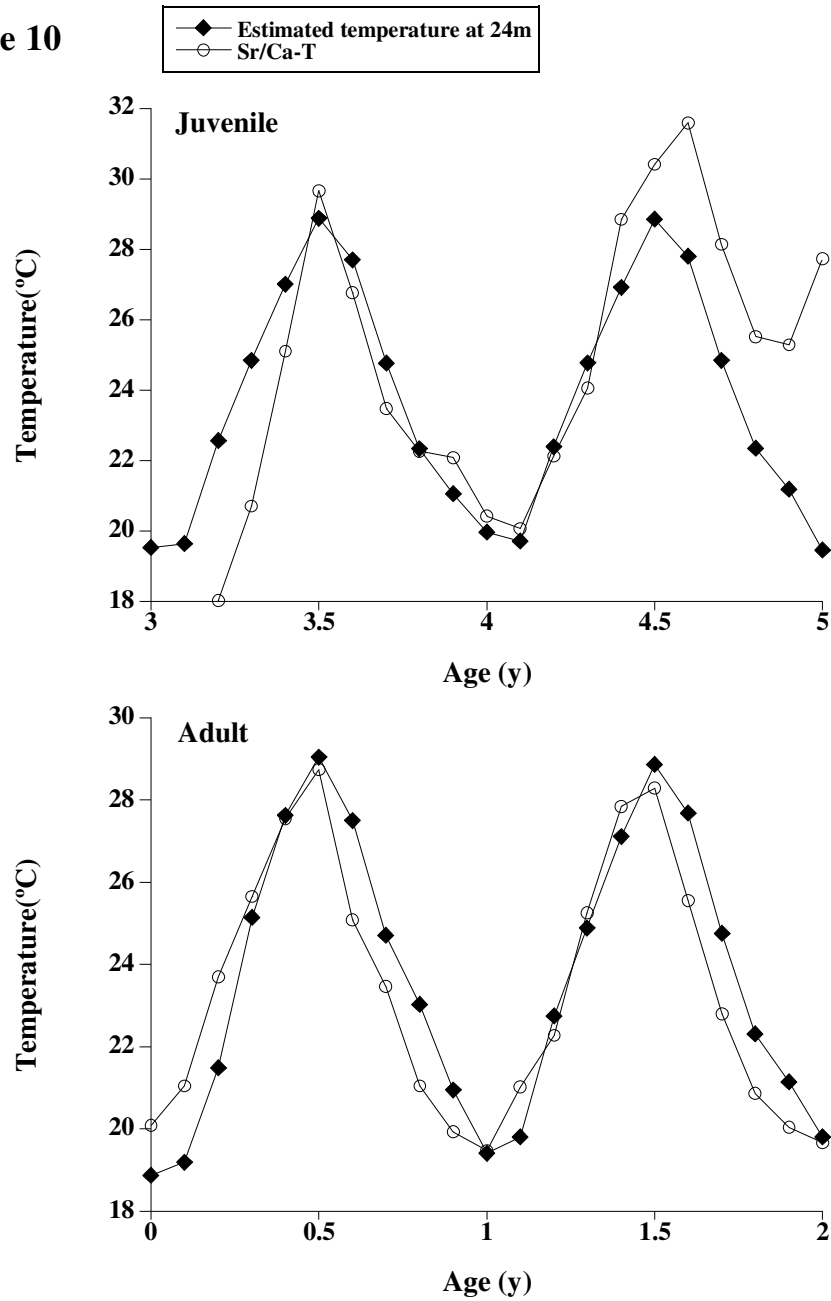
Figure 4.10 Pooled average juvenile and adult temperature reconstructions compared with the in situ temperature record. Note that the juvenile and adult reconstructions accurately reproduce the mean annual temperature of the in situ record, while the juvenile does not resolve the seasonal temperature variation.

Table 4.1 Data for size, whorl length, and age for *Conus* specimens. Note that several years of growth are in each whorl.

Specimen	FGS1	FGS2	FGS3	FGS4
Shell height (mm)	67	78	72	79
Shell width (mm)	39	44	41	46
Whorl length (mm)	320	385	369	360
Estimated life span (y)	5.8	12	5.8	8.8

Table 4.2 Coefficients of determination (R^2) from Sr/Ca and $\delta^{18}O$ versus temperature for the $\delta^{18}O$ and Sr/Ca age models.

Specimen		$\delta^{18}O$ age model Temperature	Sr/Ca age model Temperature
FGS1	Sr/Ca	**0.41**	**0.46**
	$\delta^{18}O$	0.80	0.83
FGS2	Sr/Ca	**0.68**	**0.80**
	$\delta^{18}O$	0.71	0.80
FGS3	Sr/Ca	**0.37**	**0.36**
	$\delta^{18}O$	0.83	0.83
FGS4	Sr/Ca	**0.56**	**0.67**
	$\delta^{18}O$	0.66	0.83
Pooled	Sr/Ca	**0.27**	**0.29**
	$\delta^{18}O$	0.74	0.82

Table 4.3 Statistics of $\delta^{18}O$-Sr/Ca and Sr/Ca-T regressions for individual and pooled Sr/Ca data for juvenile (J) portions, adult (A) portions, and the entire record (Siddall et al.). Note only adult portions of FGS2 were sampled. Included are slope (m), intercept (b) from the linear equation (y = mx + b) and coefficient of determination (R^2).

| Calibration		FGS1			FGS2	FGS3			FGS4			Pooled		
		all	J	A	all	all	J	A	all	J	A	all	J	A
$\delta^{18}O$-Sr/Ca	m	-0.35	-0.30	-0.43	-0.37	-0.31	-0.24	-0.47	-0.36	-0.28	-0.47	-0.30	-0.26	-0.40
	b	1.28	1.13	1.36	1.58	1.29	1.25	1.44	1.58	1.40	1.82	1.38	1.26	1.59
	R^2	0.54	0.72	0.68	0.80	0.54	0.52	0.85	0.41	0.67	0.71	0.33	0.47	0.51
Sr/Ca-T	m	0.046	0.044	0.081	0.061	0.042	0.034	0.082	0.053	0.048	0.085	0.047	0.045	0.079
	b	0.17	0.12	-0.41	0.10	0.30	0.42	-0.45	0.30	0.23	-0.21	0.26	0.17	-0.27
	R^2	0.37	0.64	0.76	0.77	0.37	0.45	0.75	0.28	0.62	0.63	0.28	0.51	0.56

Chapter 5

5. From Greenhouse to Icehouse: Insight from a Gastropod Shell

5.1 Abstract

From the greenhouse of the late Cretaceous to the icehouse of today, Earth's climate underwent dramatic changes across the Cenozoic. The early Eocene was a period of relative warmth with high global temperatures and lack of continental ice sheets. The Eocene-Oligocene transition (ca. 34 Ma), associated with onset Antarctic glaciation, has been attributed to opening of tectonic gateways, changes in ocean circulation, and decreasing levels of greenhouse gases. The tropical surface ocean response to Cenozoic climate change is not well understood. Evidence from the oxygen isotope records of planktonic foraminifera imply that the tropics were similar or cooler than today and did not show a change across the E-O transition. The interpretation of oxygen isotope records is limited due to the need to estimate changes in oxygen isotopic composition of seawater. Here, I utilize a new salinity independent paleothermometer, Sr/Ca ratios in marine gastropods, to reconstruct surface ocean temperature conditions, specifically mean annual and seasonal temperature variations, in the low latitudes. The Sr/Ca temperature calibration cannot be directly applied to the fossil gastropods Sr/Ca records due to an offset in fossil and modern shell Sr/Ca values. I discuss secondary effects that might influence fossil Sr/Ca, such as changes in seawater Sr/Ca and growth rate effects. Temperature is shown to be the primary control on strontium incorporation into the aragonitic fossil gastropod shells. Sea surface temperature records indicate that the low latitude ocean cooled along with the high latitudes throughout the Cenozoic. The low latitude cooling was associated with a long-term decrease in winter and summer

temperatures. This implies that the long-term Cenozoic climatic cooling trend occurred in the high and low latitudes.

5.2 Introduction

The Cenozoic climate is marked by distinct transitions, amidst the backdrop of a longterm cooling, identified by ice volume and temperature variations in proxy records. From the greenhouse climate in the late Cretaceous to the icehouse of the late Cenozoic, Earth's climate has evolved into a state of cyclic, global glaciation over the last ~65 Myr (Fig. 5.1). In the early Eocene greenhouse world (ca. 55 to 35 Ma), evidence from benthic foraminifera oxygen isotope and Mg/Ca records (Lear et al., 2000; Zachos et al., 1994), fauna and flora patterns (Axelrod, 1984), and Tex86-sea surface temperature records (Moran et al., 2006) suggest that high latitude temperatures were much warmer than today. Climate model simulations, with Eocene greenhouse gas concentration levels (i.e. 2x modern levels) (Pagani et al., 2005; Pearson et al., 1999) predict higher tropical and low-latitude temperatures along with high latitude warmth (Manabe et al., 1985;Sloan et al., 1995). Evidence from mollusk oxygen isotope records and faunal patterns indicated that low-latitude temperatures were warmer than present, in agreement with model predictions (Andreasson et al., 1998; Wilson, 1996; Yancey et al., 2003). In contrast, records of oxygen isotopic composition ($\delta^{18}O$) of planktonic foraminifera from low latitudes have been interpreted as representing similar or even cooler temperatures relative to today (Fig. 5.1) (Boersma, 1987; Bralower et al., 1995; Shackleton, 1981; Zachos et al., 1994).

In addition to temperature, the isotopic composition of foraminifera reflects changes in global ice volume, local salinity, and possibly altered by diagenesis. An

isotopic study of well-preserved planktonic foraminifera from Tanzania suggests that recrystallized material may have been overprinted by a component of diagenetic calcite precipitated in cold, deeper waters and propose that Eocene tropical temperature were >30°C (Pearson et al., 2001). The Eocene temperature estimates, however, derived from that study exceed present-day sea surface temperatures (SST) and contradict the current understanding of tropical climate stability. The higher than expected temperature estimates determined by Pearson et al., (2001) may be related to the marginal habitat of the planktonic foraminifera where local changes in hydrology could impact shell $\delta^{18}O$. An independent paleothermometer is necessary to unravel the cool tropics paradox and resolve this long-standing issue.

The Eocene-Oligocene (E-O) boundary (ca. 34 Ma) marks the transition from greenhouse to icehouse with rapid Antarctica glaciation and faunal overturn. Evidence from oxygen isotope records show that the ~1-1.5‰ isotopic excursion occurs in two main steps that represent some combination of ice growth and global cooling (Katz et al., 2008; Lear et al., 2008; Lear et al., 2004; Lear et al., 2004; Miller, 1987; Zachos et al., 2001). The nature and cause of this climatic transition has variably been linked to opening of marine gateways (Kennett, 1977; Kennett et al., 1976), decreasing atmospheric carbon dioxide (pCO_2) (Barron et al., 1985; Berner, 1991; DeConto et al., 2003; Pagani et al., 1999; Pearson et al., 2000; Sloan et al., 1992), and large-scale changes in ocean circulation (Barron, 1987; Rind et al., 1991). Records of high latitude temperature (Billups et al., 2003; Katz et al., 2008; Lear et al., 2008; Lear et al., 2000) from Mg/Ca paleothermometry show variable degrees of cooling associated with Antarctic ice sheet growth.

Low-latitude temperature estimates derived from the oxygen isotopic composition of planktonic foraminifera (Bralower et al., 1995; Pearson et al., 2001; Wade, 2000; Wright, 2001; Zachos et al., 1994), fish otoliths (Ivany et al., 2000) and mollusks (Kobashi et al., 2003; Kobashi et al., 2001) records are conflicting and highlight the need for further understanding of the climatic event. The interpretation of oxygen isotope records is complicated by the need to estimate the oxygen isotopic composition of local seawater (δ_{ω}). Low resolution tropical SST records compiled from the $\delta^{18}O$ of planktonic foraminifera for the last 65 Ma show cooler than expected temperatures and do not cover the E-O transition (Wright, 2001; Zachos et al., 1994). Using Mg/Ca ratios, Lear et al., (2008), observed a 2.5°C cooling in low-latitude SST from Tanzanian planktonic foraminifera. Ivany et al., (2001), using $\delta^{18}O$ measurements from aragonitic fish otoliths from the US Gulf Coast Plain, show little change in mean annual temperature (Fairbanks et al.) across the E-O transition but a significant increase in seasonality. Part of their interpretation relies on the assumption that changes in global $\delta^{18}O$, across the E-O, are related to a combination of changes in ice volume and cooling based on the study of Zacho et al., (1994). The partitioning of $\delta^{18}O$ between ice volume and temperature across the E-O is still under debate. Recently, Lear et al., (2008) proposed that the two tier step in $\delta^{18}O$ reflects a 70-m decrease in sea level whereas Katz et al., (2008) estimate that the $\delta^{18}O$ shift reflects a ~100-m decrease in sea level. Using $\delta^{18}O$ records in fossil gastropod shells from the US Gulf Coast, and global δ_{ω} estimates from Lear et al., (2000) which attribute the entire $\delta^{18}O$ shift to ice growth, Kobashi et al. (2001) indicate that seasonality increased across the E-O associated with a significant winter cooling in accord with Ivany et al., (2000). However, both studies rely on assumption about global and local

changes in δ_ω. A $\delta^{18}O$-independent paleotemperature reconstruction would aid in

evaluating the tropical surface ocean response to Cenozoic climate change, address the

issues of diagenetic overprints, and validate the study of Kobashi et al., (2001, 2003). An

independent lowlatitude SST record would provide an unambiguous record of Cenozoic

SSTs and be invaluable in resolving these long-standing issues.

Here, I construct a low resolution sea surface temperature record using Sr/Ca

ratios in marine gastropods to examine long-term changes in Cenozoic mean annual

temperature and seasonality. Gastropods have a long-life span (~yrs), deposit their shell

at high rates, and are ubiquitous in the tropical surface water which gives them value as a

recorder of tropical sea surface temperatures (Walls, 1977). Additionally, analysis of

growth bands provides records of seasonal temperature variations not obtainable from

foraminifera. The potential utility of Sr/Ca ratios in marine gastropods, *Conus ermineus*,

as an independent tropical paleothermometer is explored in Sosdian et al., (2006). In that

study, I have sampled four modern aragonitic gastropods for Sr/Ca and $\delta^{18}O$ analysis to

construct multi-year records for comparison to the *in situ* temperature record. My results

show that Sr/Ca and $\delta^{18}O$ positively co-vary with the *in situ* seasonal temperature cycle.

The temperature- Sr/Ca relationship is not straightforward, however. Although the Sr/Ca

record co-varies with temperature, there are additional trends, both seasonal and long-

term that are related to growth rate variations (Gentry et al., 2008; Sosdian et al., 2006).

Sosdian et al., (2006) conclude that Sr/Ca ratios in marine gastropods can quantify mean

annual temperature (Fairbanks et al.) within ±1°C. Seasonal temperatures are

quantifiable within ±1°C if the Sr/Ca data of adult growth stage from multiple specimens

are pooled. The Sr/Ca data from the juvenile portion of growth resolve MAT within ±1°C

but seasonal changes in temperature only within ±3.5°C. Here, I evaluate changes in the seasonal temperatures from the adult growth stages to quantify long-term oscillations in mean annual temperature and seasonality across the Cenozoic in the low latitude ocean. I will demonstrate that the low-latitude surface ocean experienced a long-term cooling along with high latitudes across the Cenozoic. Additionally, our results support the findings of Kobashi et al., (2000, 2003) that winter temperatures decreased from the early Eocene to the present concomitant with an increase in seasonality.

5.3 Methods

5.3.1 Study site and samples

Fossil shells were collected from the northern continental shelf of the Gulf of Mexico in the US (Fig. 5.2). This region is an ideal location to document Paleogene climate change due to its abundant fossiliferous strata formations. The modern Sr/Ca-temperature calibration study utilized *Conus ermineus* specimens from the U.S. Gulf Coast thus allowing for direct comparison to fossil specimens that lived in similar environments. The paleo-latitude, 30ºN, of these sites remained the same during the early Cenozoic which permits comparison of temperature estimates among different ages without concern of paleogeography. Moreover, oxygen isotope records were already acquired in previous studies (Kobashi et al., 2001; Kobashi and Grossman, 2003). For this study we collected and analyzed 12 *Conus sp.*, fossil shells from 8 formations covering the Eocene to mid-Miocene time interval (Table 5.1). All of the specimens came from Mississippi, except for Gosport Sand and Chipola formation shells which originated from Alabama and Florida, respectively. The paleodepth of each specimen was determined by the depositional environment. For example, the Yazoo and Red Bluff

formations represent a clay rich deep shelf environment whereas the other formations have a shallower paleodepth (Dockery, 1982). The Moody's Branch formation (MBC-2) represents a shallow marine waters near a retrograde shoreline and a paleo-water depth of 20-100m (Dockery, 1977). The paleo-water depth of most of the fossil specimens is shallow with the exception of RBC-1, RBC-3, and YCC-1 which derive from a deeper environment. Multiple specimens (1-3) were available for analysis in each time interval except the Miocene (17 Ma) and the mid-Eocene (38, 39 Ma). The species present in each interval are as follows, in order of increasing age: *Conus sulculus* (17 Ma), *Conus alveatus* (30, 32, 33 Ma), *Conus spp.*(36 Ma), *Conus tortilis*(38 Ma), and *Conus sauridens*(39, 42 Ma). The speciation of the specimens collected are different in each time interval, except across the E-O boundary region (30-33 Ma) and early Eocene where *Conus alveatus* and *Conus sauridens* were present and analyzed in consecutive time intervals. Each window of time where the same species are present should not be affected by potential species-specific Sr/Ca variations.

5.3.2 Sample Preparation and Analytical Method

Mollusc samples were prepared for sampling at Texas A&M University (TAMU). Isotopic and X-ray Diffraction (XRD) were completed at TAMU wheras trace metal analyses were performed at Rutgers University. Before sampling, mollusc shells were soaked in water overnight, cleaned by ultrasonification in distilled water, and dried at air temperature for about one day. If necessary, shells were polished with sandpaper to remove surface contamination. Each specimen was measured for height and width (Table 5.1). Linear sample grooves were milled parallel to growth banding using a 0.3-mm Brasseler carbide drill bit.

For trace metal analysis, aragonite powder splits were progressively reacted with trace metal clean 0.065N HNO_3 (SEASTAR®), until complete dissolution was achieved. After a 10 minute centrifugation, 100 μl of the sample solution was further diluted with 300 μl of 0.5 N HNO_3 (SEASTAR) to obtain a final Ca concentration ([Ca]) in the ~4 mM range. The progressive dissolution and dilution procedure ensured that [Ca] were kept relatively constant in order to minimize matrix effects . The analytical method for measuring Sr/Ca by a Vista-Pro CCD Radial ICP-OES is based on the method outlined by Andreasen et al. [2006]. Long-term precision for Sr/Ca, evaluated by repeatedly analyzing three consistency standard solutions in the range of 0.46 to 1.84 mmol mol^{-1} at the beginning and end of each run over the course of 3 years, is on average ±1.5% (RSD).

Before trace element analysis, fossil shells were tested for diagenetic alteration or presence of secondary calcite, using XRD. Although the XRD results demonstrate that the fossils are ~99% aragonite, Ragland et al., (1979) show evidence pointing to pre-recrystallization changes in the composition of shell material. To further assess if any of the specimens underwent diagenetic changes, Mg/Ca and Mn/Ca data are evaluated. Fossil specimens BFC-1 and BFC-3 have elevated levels of Mn and Mg, about 2x higher than the average of other specimens. Therefore, the Sr/Ca data for these two specimens are considered as potentially altered by diagenesis and are not used to interpret temperature variations.

5.4 Results

Paired measurements of Sr/Ca and $\delta^{18}O$ are plotted as a function of distance from apex (Fig.5.3; 5.4). Depicted this way, specimen age increases with increasing length. All the gastropods share several common features with each other and the modern *Conus*

ermineus specimen, FGS-1 (plotted in figure 5.3). Fossil Sr/Ca shows a distinct cyclicity similar to $\delta^{18}O$ (R^2 ranges from 0.25 to 0.90, Table 5.1). The seasonal variations in $\delta^{18}O$ (Kobashi et al., 2001, 2003) are replicated in the intra-shell Sr/Ca records and are consistent in fossil and modern shells. Higher Sr/Ca occurs in warmer temperatures with lower $\delta^{18}O$ values whereas lower Sr/Ca is associated with colder temperatures. The covariance of $\delta^{18}O$ and Sr/Ca is consistent with a temperature influence on Sr incorporation into aragonitic gastropod shells.

In addition to the temperature influence, growth rate plays a role in Sr/Ca variations (Sosdian et al., 2006). The fossil specimen, MBC-2 (38 Ma) plotted in figure 5.4, is representative of the typical Sr/Ca and $\delta^{18}O$ profile found in the modern marine gastropods ($R^2=0.45$). On the basis of the variation of growth rate with age, two stages of growth were identified: juvenile and adult (Fig. 5.4). Sosdian et al., (2006) suggests that the juvenile section, or the first three years of growth, has a typical growth rate of >50 mm yr^{-1}. Seasonal variability in growth is less marked in the slow growing (<50 mm yr^{-1}) adult section of the record, and is superimposed on an overall trend of decreasing growth rate through the mollusk's life. Growth rate also varies seasonally, higher in the summer and lower into the winter, as expressed by a significant decrease in the width of $\delta^{18}O$ and Sr/Ca seasonal cycles during winter intervals. As the gastropod ages, the Sr/Ca amplitude and mean Sr/Ca increases concomitantly with the decrease in growth rate. For example, in the juvenile stage of MBC-2, Sr/Ca varies between winter and summer months from 2.0 to 2.65 mmol mol^{-1} whereas in the adult stage it varies from 2.1 to 3.1 mmol mol^{-1}. The mean ontogenetic change in Sr/Ca is in the summer maxima but the winters are consistent between juvenile and adult growth stages. Consequently, the mean

annual Sr/Ca increases from 2.39 to 2.48 mmol mol^{-1}, between the juvenile and adult stages, respectively.

To minimize the ontogenetic effects, I use only the adult/slow growing stages of growth (LER<50 mm yr^{-1}), to evaluate changes in seasonality and mean annual temperature. Table 5.1 highlights the main features (i.e. maximum, minimum, mean, and correlation between $\delta^{18}O$ and Sr/Ca) of the fossil shells. The fossil shells, except for BFC-3, MSC-1, RBC-3, YCC-1, and GSC-1, exhibit a significant correlations between Sr/Ca and $\delta^{18}O$ ($R^2>0.5$). Specimens that are not significantly correlated with $\delta^{18}O$ ($R^2<0.5$) still exhibit Sr/Ca cyclity. In the 33 Ma time interval, fossil specimens, RBC-1 and RBC-3, display similar range of Sr/Ca variability regardless of the weak correlation between $\delta^{18}O$ and Sr/Ca for RBC-3. RBC-1 and -3 both have similar mean, maximum, minimum, and amplitude which imply that they reflect similar environmental variability. Here, fossil Sr/Ca records with a strong correlation between Sr/Ca and $\delta^{18}O$ ($R^2>0.50$) are only used in the temperature evaluation.

5.5 Discussion

Sosdian et al., (2006) observe a positive relationship between Sr/Ca and temperature and suggest that the Sr/Ca dependence on temperature in marine gastropods, specifically *Conus ermineus*, is driven by the influence of temperature on biological processes (e.g. calcification rate or growth rate) rather than a direct thermodynamic effect on the distribution coefficient (Carre et al., 2008). In their study, they also observe long-term ontogenetic effect characterized by an age-related decrease in growth rate and concomitant increase in mean annual Sr/Ca. To minimize ontogenetic effects, they construct specific calibrations for the juvenile and adult stages of growth. The

application of these calibrations to fossil specimens of the genus *Conus,* is, however, not straightforward.   In the modern calibration, adult Sr/Ca values range below ~2.25 mmol mol^{-1} (1 to 2.25 mmol^{-1}), whereas Sr/Ca values in the fossil specimens exceed 2.25 mmol mol^{-1} (1.9 to 3.1 mmol mol^{-1}) (i.e. assuming no change in seawater Sr/Ca values). The Sr/Ca-paleotemperature equation constructed by Sosdian et al., 2006 may not directly applicable to the fossil specimens because the range of Sr/Ca variability is much higher in than the modern Sr/Ca range. Taking the fossil Sr/Ca at face value and applying the modern calibration results in mean annual temperatures that exceed 35°C in some intervals.   Tropical paleotemperature estimates from the early Eocene (ca. 50 Ma), a period of extreme warmth, and across the E-O transition, fall within the temperature range of 32-35°C and 28-32°C, respectively (Pearson et al., 2007). Paleotemperature estimates from the δ^{18}O record (Kobashi et al., 2001, 2003) indicate that temperatures ranged from 20 to 28°C across the Cenozoic. The difference between modern and fossil Sr/Ca values cannot purely be related to temperature variations.

However, the Sr/Ca records of the fossil specimens support the idea that Sr incorporation into the aragonitic crystal lattice is related to temperature. Consistent seasonal signals from the δ^{18}O and Sr/ca intra-shell records are present in the fossil specimens which is consistent with the temperature dependence of Sr/Ca. The intra-shell Sr/Ca- δ^{18}O relationship is consistent in the Eocene, Oligocene, and Miocene shells. Variations in δ^{18}O with Sr/Ca, plotted in figure 5.5 for modern and fossil shells, show a similar relationship which suggests that temperature sensitivity in modern and fossil shells is similar. Variations in δ^{18}O are related to temperature and the oxygen isotopic composition of seawater. To determine if the modern and fossil shells have the same

Sr/Ca-temperature relationship, I use two fossil specimens from the mid-Eocene, a relatively ice free environment, and convert $\delta^{18}O$ to temperature assuming the δ_w was -0.06‰, based on Lear et al., (2000) estimates corrected for latitudinal differences in surface δ_w (Zachos et al., 1994). The slope, derived from DBC-2 and DBC-4, gives 0.10 ± 0.02 mmol mol^{-1} per °C (1σ) change in Sr/Ca per °C in DBC-2 and DBC-4 (Table 5.2). The modern Sr/Ca-temperature calibration based on the adult growth portions has a slope of 0.072 ± 0.014 mmol mol^{-1} per °C (1σ) and within the estimates from the fossil specimens. This suggests that temperature sensitivity from the modern calibration is applicable to the fossil Sr/Ca records.

The offset in mean Sr/Ca between the modern and fossil calibration lines must be attributable to non-temperature related effects,. such as growth rate or seawater Sr/Ca variations, which might play a role in influencing fossil shell Sr/Ca variability (Dodd, 1965; Gillikin et al., 2005; Klein et al., 1996; Palacios et al., 1994; Purton et al., 1999; Stecher et al., 1996; Takesue et al., 2004). Potentially, inter-species Sr/Ca offsets might account for the higher mean Sr/Ca in the fossil shells. Seawater Sr/Ca (Sr/Ca$_{sw}$) variations across the Cenozoic might affect the fossil long-term Sr/Ca record but not on seasonal time scales unless there is a strong local effect (e.g. salinity). Below, I discuss the potential controls on fossil Sr/Ca and examine whether they can account for the offset in mean Sr/Ca.

5.5.1. Secular variations in sawater Sr/Ca

The distribution coefficient (D_{Sr}) for Sr^{2+} in the *Conus* gastropod shell is defined as $D_{Sr}= (Sr/Ca)_{shell}/(Sr/Ca)_{seawater}$. The absolute values of Sr/Ca-derived paleotemperatures (as opposed to relative changes) depend on assumptions about the contemporaneous

Sr/Ca composition of seawater in which the gastropod calcified. The residence time of Sr and Ca in seawater is ~3 and ~1 Myr, respectively (Broecker et al., 1982; Palmer et al., 1992). Major sources of Sr and Ca to the oceans are rivers and a major sink of both is biogenic carbonate production (M.L. Delaney, 1988; Turekian, 1964). Hydrothermal activity is a significant source of Ca (Elderfield et al., 1996). Cenozoic records of seawater Sr/Ca have been derived from calcitic planktonic foraminiferal Sr/Ca (Graham et al., 1982) and benthic foraminiferal Sr/Ca (Lear et al., 2003). The planktonic records show considerable scatter and might be affected by other factors such as diagenesis and inter-species offsets. The compiled Cenozoic seawater Sr/Ca (Lear et al., 2003) is based on the analysis of well-preserved calcitic benthic foraminifera (Fig. 5.6). Using this compilation, I adjust the *Conus* Sr/Ca record for secular variations in seawater Sr/Ca. Plotted in figure 5.6b is the mean Sr/Ca from each time interval corrected and uncorrected for seawater Sr/Ca variations. The corrected record has a higher mean Sr/Ca and the change in mean Sr/Ca across the record is larger, especially in the mid-Eocene. The corrected fossil Sr/Ca values exceeds the modern *Conus* Sr/Ca range which suggests that either the benthic foraminiferal Sr/Ca record underestimates seawater Sr/Ca variations or the fossil Sr/Ca is higher due to inter-species offsets (i.e. growth rate, size, habitat).

Secular changes in carbonate saturation might affect the benthic foraminiferal Sr/Ca record. Lear et al., (2003) observed a depth-dependent increase strontium incorporation(i.e. 0.101 mmol mol^{-1} change in Sr/Ca per km) into benthic foraminiferal calcite, which has been partially attributed to saturation effects (Elderfield et al., 1996; Rosenthal et al., 1997; Stoll et al., 1998). An increase in carbonate saturation [$\Delta CO_3^=$] of

~40 umol/kg would lower the benthic foraminiferal Sr/Ca by 0.4 mmol mol^{-1}, assuming

that the entire shift in Sr/Ca with depth is due to carbonate saturation changes. Lear and

Rosenthal (2006) document significant changes in carbonate saturation across the

Cenozoic from a Li/Ca benthic foraminiferal record (Fig. 5.7). The Li/Ca record shows

a large shift from the mid-Eocene to the early Oligocene of ~3 umol mol^{-1} which might

indicate that $\Delta CO3=$ increased by 40 umol kg^{-1}. Such an increase in ΔCO_3 would

potentially increase foraminiferal Sr/Ca by ~0.4 mmol mol^{-1} and seawater Sr/Ca by ~2

mmol mol^{-1}. However, this saturation driven change in Sr/Ca is not large enough to

offset fossil Sr/Ca from the modern by the observed amount of 1 mmol mol^{-1}.

Were seawater Sr/Ca ratios much higher in the Eocene and Oligocene thus

contradicting benthic foraminifera data? An abstract by Averyt and Paytan (2003), using

deep-sea, marine barite to reconstruct seawater Sr/Ca variations, suggests that seawater

Sr and Ca concentrations varied by greater than 2x modern concentrations through the

Cenozoic. The barite Sr/Ca record predicts larger variations than the foraminiferal Sr/Ca

record. To evaluate potential Sr/Ca$_{sw}$ variability, I calculate seawater Sr/Ca ratios from

δ^{18}O-paleotemperature and the Sr/Ca-paleotemperature equations. Using the fossil shell

δ^{18}O data from Kobashi et al., (2001), I determined temperature using the Grossman and

Ku (1989) paleotemperature equation and δ_ω estimates from Lear et al., (2000) corrected

for latitude following Zachos et al., (1994). The distribution coefficient, D$_{Sr}$, for modern

Conus gastropods varies from 0.1 at 18°C to 0.3 at 30°C. The calculated Sr/Ca$_{sw}$ record,

determined by combining δ^{18}O-temperature estimates and utilizing the distribution

coefficient, is offset from the foraminiferal Sr/Ca record (Fig. 5.8). δ^{18}O-

paleotemperatures and Sr/Ca ratios yield high seawater Sr/Ca in the Paleogene. The

gastropod-derived seawater Sr/Ca averages ~19 mmol mol^{-1} across the Eocene to mid-Miocene, whereas the foraminiferal seawater Sr/Ca averages ~8 mmol mol-1. Also, the gastropod derived record shows larger swings in seawater Sr/Ca than the foraminiferal record which might be related to local effects. Could the gastropod D_{Sr} be affected by changes in carbonate saturation? Bailey and Lear (2006) evaluated whether Sr incorporation into freshwater aragonitic mollusks may be influnced by the degree of carbonate saturation and determined that Sr uptake in aragonitic bivalve shells is not affected by the degree of saturation of water. However, Rosenthal et al., (2006) observed that carbonate saturation affects Sr uptake in aragonitic benthic foraminifera but below a saturation level of 15 umol kg^{-1}. The influence of carbonate saturation changes on trace metal uptake in marine gastropods is minimal and does not drive the shell Sr/Ca variations.

Carbonate saturation effects on Sr/Ca benthic foraminiferal calcite cannot account for the entire offset in modern and fossil shell Sr/Ca. Although, validation of the Cenozoic seawater Sr/Ca record is necessary to determine if Eocene seawater Sr/Ca values were much higher than the present contrary to the Lear et al., (2003) record. Potentially, differences in the growth rate of the modern and fossil specimens might be the cause for the offset in long-term Sr/Ca$_{sw}$ between the fossil data and the benthic foraminifera record.

5.5.2 Does growth rate affect fossil Sr/Ca? Are there inter-species or intra-species differences in the Sr/Ca ratios of *Conus*?

Using the Sr/Ca record as a seasonal marker, I calculate linear extension rates (Siegenthaler et al.), as an indicator of growth rate, for each shell. LER specifies the

measured spiral length, between annual tie points, with respect to time. MBC-2, a large specimen, similar in size to the modern specimens, shows comparable changes in LER to the modern specimen, FGS-1. Both show the transition from the fast growing (>50 mm yr^{-1}), juvenile stage to the slow growing (<50 mm yr^{-1}), adult stage. However, the remaining fossil specimens exhibit growth rates below 50 mm yr^{-1} in most cases and do not exhibit a distinct juvenile-adult transition (Fig. 5.9).

The modern *Conus* specimens are relatively large and have higher growth rates in comparison to the fossil shells (Table 5.1). Could the higher fossil Sr/Ca values be related to the distinct offset in shell size and growth rate relative to the modern shells? The fossil specimens are offset from the modern specimens in mean Sr/Ca and size (Fig. 5.10). Among the fossil specimens, size and Sr/Ca, however, do not covary suggesting the fossil Sr/Ca variations are not driven by size.

Annual and sub-annual variations in LER have been shown to influence Sr/Ca variations in mollusk shells (Gillikin et al., 2005). Here, mean annual LER is not correlated with mean Sr/Ca in the fossil specimens (Fig. 5.11) which suggests that differences in ontogenetic growth rate variations are not the primary control on fossil Sr/Ca. Comparing Sr/Ca ratios and seasonal growth rates in all fossil specimens results in a insignificant correlation between seasonal LER and seasonal Sr/Ca (R^2=0.2) in the winter and fall. Growth rate cannot explain the Sr/Ca variability in the fossil specimens which suggests that Sr/Ca ratios are not under direct control of growth rate.

In addition to growth rate variations, differences in mean Sr/Ca can be related to habitat differences (Gillikin et al., 2005) such as nutrient availability and other site-specific variables. The modern *Conus* specimens, used in the Sr/Ca-temperature

calibration, originate from Stetson Bank in the Gulf of Mexico. However, in the fossil record, specimens are derived from Mississippi, Florida, and Alabama stratigraphic formations. The habitat of the fossil specimens could affect the Sr/Ca ratios. To fully understand the driver behind differences in mean fossil Sr/Ca, I evaluate changes in fossil carbon isotopic composition. The δ^{13}C record in modern *Conus ermineus* primarily reflects seasonal variations in the δ^{13}C of the dissolved inorganic carbon (DIC) pool (i.e. due to salinity, seasonal stratification, nutrient concentration) and long-term variations in ontogeny (e.g. metabolic efficiency) (Gentry et al., 2008). Variations in δ^{13}C could be used to infer whether a large specimen with more rapid growth inhabited a nutrient-rich or less saline environment. Habitat and growth rate differences in δ^{13}C are superimposed on the long-term Cenozoic changes in δ^{13}C $_{DIC}$ (Fig. 5.12). The four shells used in the modern calibration are offset from each other by about ±0.27‰. In each time slice, fossil specimens deviate from the mean by the same amount indicating that their habitat was similar. However, YCC-1 (36 Ma) is significantly offset from the long-term record suggesting that it grew in a low salinity and/or higher nutrient environment or experienced metabolic efficiency. In this time slice, there are no large swings in seawater δ^{13}C (Zachos et al., 2001). Contrastly, the YCC-1 Sr/Ca is not offset in a similar way suggesting that changes in δ^{13}C either may be difficult to use as a habitat proxy or Sr/Ca is not influenced largely by habitat differences. The correlation between δ^{18}O and Sr/Ca is weak which suggests that a variable other than temperature is driving Sr/Ca variations.

The δ^{13}C analysis does not resolve habitat induced changes in Sr/Ca and to fully answer this question a modern case study is necessary. The modern calibration is based on *Conus ermineus* specimens and is valid for application to the same species in similar

habitat. The fossil *Conus sp.*, are from various locations and of different species which requires an evaluation of modern *Conus* specimens from different habitats and species to determine if changes in fossil Sr/Ca are primarily controlled by temperature.

Across the 30-33 Ma interval, the Sr/Ca data are derived from the same species, *Conus alveatus* (BFC-1, BFC-3, MSC-1, MSC-2, RBC-1, RBC-3) and represent an interval to assess intra-species Sr/Ca variability in other *Conus* species (Fig. 5.12). In each time interval, similar mean, minimum, and maximum Sr/Ca ratios are resolved in two fossil specimens, but maximum and minimum values from BFC-1 and BFC-3 are offset by 0.28 mmol mol^{-1}. The cause of this discrepancy might be related to variable growth habitats, in addition to diagenetic alteration. The δ^{13}C record of BFC-1 has an asymmetric sawtooth pattern indicative of offshore, spring upwelling regime, while BFC-3 has a cuspate pattern which represents a nearshore regime with continental cold fronts. Their calcification depth, habitat and seasonal range in temperature could differ which may account for offset in the Sr/Ca maxima and minima, even though the mean Sr/Ca is similar. A detailed study documenting how habitat differences could affect Sr/Ca variability in various *Conus* species is needed to fully quantify its effect on fossil shell Sr/Ca.

5.6 Cenozoic Low-Latitude Climate Variations

5.6.1 δ^{18}O and Sr/Ca variability

Comparison of the δ^{18}O and Sr/Ca variability, with their similar and contrasting controls, can aid in interpreting the fossil Sr/Ca dataset. δ^{18}O and Sr/Ca records are plotted in figure 5.14 with an increase in temperature indicated by a decrease in δ^{18}O and increase in Sr/Ca values along the calibration line. Offsets from the calibration line,

which affect either Sr/Ca independent of δ^{18}O or vice versa, may be due to several nontemperature related effects: 1) variations in seawater Sr/Ca, or growth rate; and 2) decrease/decrease in ice volume, and/or changes in local salinity. From 42 to 38 Ma, both the δ^{18}O and Sr/Ca shift toward more positive and lower values, respectively. The covariance between these climate indicators suggest that the climate cooled during the late Eocene. From 38 to 33 Ma the main trend is a > 1‰ positive shift in δ^{18}O signaling an increase in ice volume across the E-O transition. The Eocene-Oligocene transition marks beginning of Antarctic glaciation and icehouse conditions of the late Cenozoic. A cooling in the low latitude surface waters is supported by concomitant faunal overturn and mollusk mass extinction associated with a colder climate or increase in seasonality. Between 36 and 32 Ma, Sr/Ca variations are small indicating small non-unidirectional changes in surface temperature. From 32 to 17 Ma, we see a trend of warming and less continental ice. This comparison shows that low latitudes cooled in association with the high latitudes. Part of the non-temperature related shift in δ^{18}O might be related to a change in the δ_ω of the riverine water. Presently in the Gulf of Mexico, salinity variations can affect the isotopic temperature determinations by ~0.5°C per ppt (Kirby et al., 1998). Interpretation of δ^{18}O records with an independent temperature record is necessary to evaluate changes in local and global δ_ω.

5.6.2 Seasonality

Across the Eocene-Oligocene transition, proxy evidence from the oxygen isotopes of fish otoliths and mollusks indicate that the low-latitude experienced an increase in seasonality mainly due to cooling of winters (Ivany et al., 2000; Kobashi et al., 2001). The low-latitude climate changed from the Eocene to Oligocene. Changes in seasonality

have been suggested as a trigger for ice sheet buildup and cause of related extinctions. The development of the Sr/Ca ratios in marine gastropods as a salinity independent paleothermometer (Sosdian et al., 2006) provides a means to constrain changes in seasonality across the transition without the secondary influences of local salinity variations on the δ^{18}O record.

In the modern calibration study, there is inter-specimen variability in the seasonal Sr/Ca amplitude not related to temperature and estimation of seasonality is limited. For example, Sosdian et al., (2006) determined that the adult section resolve the seasonal temperature within ±1°C when >3 specimens are pooled but only to about ±4°C with one specimen. In the fossil record, in most intervals only 1-2 specimen are available and thus interpretation of the Sr/Ca-seasonal temperature record is limited. Here to convert Sr/Ca ratios to temperature I used the modern calibration slope an interpret relative changes in temperature to evaluate the large-scale variations in seasonality from the adult section with the understanding that there is considerable uncertainty (±4°C) in its application to accurately record temperature seasonality.

The overall trend in Sr/Ca-derived seasonal temperatures shows a long-term winter cooling trend from the early Eocene into the Miocene similar to the findings of Kobashi et al., (2001) (Fig. 5. 15). Summer temperatures decrease from the early Eocene into the Oligocene and then begin to increase into the Miocene. The corresponding δ^{18}O-temperature data shows a similar long-term shift. However, the records diverge in magnitude of these changes. From the early Eocene to the Miocene, the seasonal temperature amplitude, derived from δ^{18}O-temperature, increases in contrast to the Sr/Ca-temperature record which shows no overall increase or decrease in seasonal amplitude.

To explain the divergence between the Sr/Ca and $\delta^{18}O$ records either changes in growth rate are influencing the Sr/Ca record and the change in seasonality is unresolvable within the uncertainty of the calibration or the $\delta^{18}O$ variations are related to salinity changes which acts to decrease/increase $\delta^{18}O$ similar to a warming/cooling.

In the modern calibration study of stables isotopes in marine gastropods, Gentry et al., (2008) notes that the influence of low salinity riverine waters from the late spring to early summer can affect the structure of the $\delta^{18}O$ record, however, during the peak summer and winter temperatures salinity is constant and thus the *Conus* $\delta^{18}O$ - temperature extremes will be unaffected by variable salinity. The winter and summer $\delta^{18}O$ -temperature should not be heavily influenced by salinity variations unless there is shift in the time of freshwater discharge.

These lines of evidence suggest that the divergence in Sr/Ca and $\delta^{18}O$ temperature estimates is driven by growth rates variations on maximum and minimum Sr/Ca values amongst different specimens. The fine-scale changes in seasonality are not resolvable within the uncertainty of the Sr/Ca-temperature calibration.

5.6.3 Low-latitude sea surface temperature variability

Sr/Ca ratios, for the last 42 Myrs, were analyzed for *Conus sp*., and mean Sr/Ca values are plotted in Figure 5.16**.** The low resolution gastropod Sr/Ca records, compiled from 10 fossil shells, show three major intervals I) late Eocene cooling without major change in continental ice volume; II) Eocene-Oligocene transition characterized primarily by increase in ice volume and small changes in sea surface temperatures; III) Oligocene to mid-Miocene warming and a decrease in the extent of continental ice. The corrected Sr/Ca record, for changes in seawater Sr/Ca using the Lear et al., (2003) record shows a

comparable long-term variability but the variations are relatively larger. Also, at 32 Ma the Sr/Ca value is less than at 42 Ma which suggests that temperatures were warmer in the Eocene greenhouse. The Lear et al., (2003) record used to correct the Sr/Ca record may be biased by carbonate saturation changes and give higher paleotemperatures than expected, so I evaluate the uncorrected Sr/Ca record with the caveat that the mean Sr/Ca values may be offset. The decrease in mean Sr/Ca from the early Eocene (42 Ma) to the Oligocene (36 Ma) suggests the tropics experienced a long-term cooling of about~5°C along with the high latitudes during this interval (Fig. 5.16). Polar temperatures, inferred from bottom water temperature records, display a general cooling trend from 42 to 36 Ma (Fig. 5.16). This suggests that during the greenhouse interval of the early Eocene, the tropics were cooler than today, in contrast to the results from oxygen isotope records of planktonic foraminifera. Following this cooling phase, temperature returned partially to Eocene-like climate with a 4°C warming. This partial return indicates that the transition between climate states occurs in multiple steps. The second cooling phase from 33 Ma, to 32 Ma when temperature decreased by 4°C occurred in association with the E-O transition when Antarctica became glaciated. Due to the low resolution of the SST record, the timing of the cooling could have occurred between 36 and 33 Ma. Following this cooling phase, temperatures increased into the Miocene by ~5°C from 32 to 17 Ma, returning to climate conditions similar to before the E-O transition. From the Miocene to present-day, temperature decreased as part of long-term cooling trend.

Relative SST changes inferred from gastropod Sr/Ca ratios are generally consistent with other low-resolution records of Cenozoic temperatures. Sea surface temperature records from Eocene to Miocene derived mainly from $\delta^{18}O$ records fish

otoliths (Ivany et al., 2000), fossil *Conus sp.* (Kobashi et al., 2003), and planktonic foraminifera (Zachos et al., 1994) (Fig. 5.17). Across 42 to 36 Ma, sea surface temperature record from otoliths and planktonic foraminifera show a ~1 and ~3°C cooling, respectively. These estimates contrast the results from gastropod $\delta^{18}O$ and Sr/Ca records which exhibit a larger cooling of 6°C. The $\delta^{18}O$ -temperature estimates from otoliths and planktonic foraminifera records might have overestimated the cooling by 3°C, due to uncertainties in estimation of changes in $\delta^{18}O$. Across the E-O (from 33-32), the otolith and $\delta^{18}O$ *Conus* records shows no cooling but rather an increase in seasonality with winters getting colder. The Zachos et al, (1994) record shows no discernible change and suggest that the tropics did not respond to high latitude climate change. Recent studies using Mg/Ca ratios in foraminifera indicate that low-latitude ocean response to the E-O transition occurred in distinct cooling steps ranging from 2-5°C (Katz et al., 2008; Lear et al., (2008). The Sr/Ca-temperature record shows a 4°C cooling from 33 to 32 Ma in accord with the Mg/Ca-temperature records. The *Conus* temperature record documents the E-O at low resolution with samples at 36, 33, and then 32 Ma. The Sr/Ca24 temperature cooling trend may represent the endpoint of a cooling trend that started between 33 and 36 Ma. The divergence between the $\delta^{18}O$ and elemental ratio (i.e. Mg/Ca and Sr/Ca) temperature estimates implies that the estimate of utilized in the $\delta^{18}O$ study overestimates the increase in ice volume associated with Antarctic glaciation.

The temperature trends derived from fossil *Conus* Sr/Ca are comparable to other temperature records from the Cenozoic. Aside from the potential complications of growth rate effects and Cenozoic seawater Sr/Ca variations, to the first order Sr/Ca ratios in fossil Conus shells document mean annual temperature change. The record presented

here suggests that the tropical latitudes were responsive to high latitude climate change and varied along with them rather than remaining constant. The equator-pole thermal gradient seems to be relatively constant across the Cenozoic in contrast to the results of Wright (2001).

5.7 Conclusions

Gastropod Sr/Ca paleothermometry is applicable to reconstruct relative changes in MAT and seasonality in the past. Our results indicates that low-latitude sea surface temperature during the early Eocene were warmer than today. The late Eocene cooling occurred without major change in continental ice volume. MAT decreased towards the Oligocene concomitant with winter and summer cooling along with the increase in continental ice volume, associated with the Eocene-Oligocene transition. Our record suggests that the results of Kobashi et al., (2001, 2003) are relatively robust. Sr/Catemperature estimates are generally consistent with other low resolution sea surface temperature records from the tropical ocean. Our findings suggest that large-scale changes occurred in the low latitudes, along with the high latitudes, in response to the transition from an ice-free greenhouse world to today's icehouse world.

5.8 References

Barker, S. and Elderfield, H., 2002. Foraminiferal calcification response to glacial-interglacial changes in atmospheric CO_2. Science, 297: 833-836.

Becquey, S. and Gersonde, R., 2002. Past hydrographic and climatic changes in the Subantarctic Zone of the South Atlantic: the Pleistocene record from ODP Site 1090. Palaeogeography, Palaeoclimatology, Palaeoecology, 182: 221-239.

Billups, K., and D.P. Schrag, 2003. Application of foraminiferal Mg/Ca ratios to questions of Cenozoic climate change. Earth and Planetary Science Letters, 209(1-2): 181-195.

Billups, K. and Schrag., D.P., 2002. Paleotemperatures and Ice-Volume of the Past 27 myr Revisited with Paired Mg/Ca and Stable Isotope Measurements on Benthic Foraminifera. Paleoceanography, 17, 10.1029/2000PA000567(1).

Boyle, E.A., and L.D. Keigwin., 1985/6. Comparison of Atlantic and Pacific paleochemical records for the last 215,000 years: Changes in deep ocean circulation and chemical inventories. Earth and Planetary Science Letters, 76: 135-150.

Broecker, W.S. and Peng, T.H., 1982. Tracers in the Sea. Eldigio Press, Palisades, New York.

Bryan, S.P. and Marchitto, T.M., 2008. The Mg/Ca - temperature proxy in benthic foraminifera: New calibrations from the Florida Straits and a hypothesis regarding Mg/Li. Paleoceanography.

Clark, P.U. and Pollard, D., 1998. Origin of the Middle Pleistocene transition by ice sheet erosion of regolith. Paleoceanography, 13: 1-9.

Cronin, T.M., Kitamura, A., Ikeya, N., Watanabe, M. and Kamiya, T., 1994. Late Pliocene climate change 3.4   2.3 Ma: paleoceanographic record from the Yabuta Formation, Sea of Japan. Palaeogeography, Palaeoclimatology, Palaeoecology, 108: 437-455.

Crowley, T.J., 1985. Late Quaternary carbonate changes in the North Atlantic and Atlantic/Pacific comparisons. In: E. Sundquist, and W.S. Broecker (Editor), The Carbon Cycle and Atmospheric CO_2: Natural Variations Archean to Present. Geophysical Monograph Series, AGU, Washington, DC, pp. 271-284.

de Garidel-Thoron, T., Rosenthal, Y., Bassinot, F. and Beaufort, L., 2005. Stable sea surface temperatures in the western Pacific warm pool over the past 1.75 million years. Nature, 433: 294-298.

Dockery, D.T., 1982. Lower Oligocene Bivalvia of the Vicksburg group in Mississippi. Mississippi Bureau of Geology, Geological Survey Division, Bulletin, 123: 261 pp.

Dockery, D.T.I., 1977. Mollusca of the Moodys Branch Formation, Mississippi. Mississippi Bureau of Geology, Geological Survey Division, Bulletin, 120: 7-20.

Dodd, J.R., 1965. Environmental control of strontium and magnesium in Mytilus. Geochim. Cosmochim. Acta, 29: 385-398.

Dowsett, H.J. and Cronin, T.M., 1990. High eustatic sea level during the middle Pliocene: evidence from southeastern U.S. Atlantic coastal plain. Geology, 18: 435-438.

Dwyer, G.S., Cronin, T.M., Baker, P.A., Buzas, M.E.R.J.S. and Correge, T., 1995. North Atlantic deepwater temperature change during late Pliocene and late Quaternary climatic cycles. Science, 270: 1347-1351.

Elderfield, H., Bertram, C.J. and Erez, J., 1996. Biomineralization model for the incorporation of trace elements into foraminiferal calcium carbonate. Earth and Planetary Science Letters, 142(3-4): 409-423.

Elderfield, H., Yu, J., Anand, P., Kiefer, T. and Nyland, B., 2006. Calibrations for benthic foraminiferal Mg/Ca paleothermometry and the carbonate ion hypothesis. Earth and Planetary Science Letters, 250(3-4): 633-649.

Fairbanks, R.G., 1989. A 17,000-year glacio-eustatic sea level record: influence of glacial melting rates on the Younger Dryas event and deep-ocean circulation. Nature, 342: 637-642.

Fairbanks, R.G., 1989. 17,000 year glacio-eustatic sea level record: influence of glacial melting rates on the Younger Dryas event and deep ocean circulation. Nature, 342: 637-642.

Fairbanks, R.G. and Matthews, R.K., 1978. The oxygen isotope stratigraphy of the Plesitocene reef tracts of Barbados, West Indies. Quaternary Research, 10(1): 181-196.

Gillikin, D.P. et al., 2005. Strong biological controls on Sr/Ca ratios in aragonitic marine bivalve shells. Geochemistry Geophysics Geosystems, 6.

Graham, D.W., Bender, M.L., Williams, D.F. and Keigwin, L.D., 1982. Strontium-calcium ratios in Cenozoic planktonic foraminifera. Geochim. Cosmochim. Acta, 46: 1281-1292.

Harper, S., 2000. Thermocline ventilation and pathways of tropical-subtropical water mass exchange. Tellus, Ser. A., 52: 330-345.

Haug, G. and Tiedemann, R., 1998. Effect of the formation of the isthmus of panama on the Atlantic Ocean thermohaline circulation. Nature, 393: 673-676.

Jordan, K., 2008. Mg/Ca-Temperature Calibration. Master Sc. Thesis, Rutgers, The State University of New Jersey, New Brunswick.

Kennett, J.P. and Hodell, D.A., 1993. Evidence for relative climatic stability of Antarctica during the early Pliocene: A marine perspective. Geografiska Annaler, 75: 205-220.

Kitamura, A. and Kawagoe, T., 2006. Eustatic sea-level change at the Mid- Pleistocene climate transition: new evidence from the shallow-marine sediment record of Japan. Quaternary Science Reviews, 25: 323   335.

Klein, R.T., Lohmann, K.C. and Thayer, C.W., 1996. Sr/Ca and C-13/C-12 ratios in skeletal calcite of Mytilus trossulus: Covariation with metabolic rate, salinity, and carbon isotopic composition of seawater. Geochimica Et Cosmochimica Acta, 60(21): 4207-4221.

Labeyrie, L.D., Duplessy, J.C. and Blanc, P.L., 1987. Variations in mode of formation and temperature of oceanic deep waters over the past 125,000 years. Nature, 327: 477-482.

Lawrence, K.T., Liu, Z. and Herbert, T.D., 2006. Evolution of the Eastern Tropical Pacific Through Plio-Pleistocene Glaciation. Science, 312: 79-83.

Lea, D.W., Martin, P.A., Pak, D.K. and Spero, H.J., 2002. Reconstructing a 350 ky history of sea level using planktonic Mg/Ca and oxygen isotope records from a Cocos Ridge core. Reconstructing a 350 ky history of sea level using planktonic Mg/Ca and oxygen isotope records from a Cocos Ridge core, 21: 283-293.

Lear, C.H., Elderfield, H. and Wilson, P.A., 2000. Cenozoic deep-sea temperatures and global ice volumes from Mg/Ca in benthic foraminiferal calcite. 287: 269-272.

Lear, C.H., Elderfield, H. and Wilson, P.A., 2003. A Cenozoic seawater Sr/Ca record from benthic foraminiferal calcite and its application in determining global weathering fluxes. Earth and Planetary Science Letters, 208(1-2): 69-84.

Lear, C.H., Y. Rosenthal, and N. Slowey, 2002. Benthic foraminiferal Mg/Capaleothermometry: A revised core-top calibration. Geochimica et Cosmochimica Acta, 66: 3375-3387.

Lisiecki, L.E. and Raymo, M.E., 2005. A Pliocene-Pleistocene stack of 57 globally distributed benthic d18O records. Paleoceanography, 20, PA1003, doi:10.1029/2004PA001071.

Luthi, D., Le Floch, M., Bereiter, B. and al., e., 2008. High-resolution carbon dioxide concentration record 650,000-800,000 years before present. Nature, 453: 379-382.

M.L. Delaney, E.A.B., 1988. Tertiary paleoceanic chemical variability: unintended consequences of simple geochemical models. Paleoceanography, 3: 137-156.

Marchitto, T.M., Bryan, S.P., Curry, W.B. and McCorkle, D.C., 2007. Mg/Ca temperature calibration for the benthic foraminifer Cibicidoides pachyderma. Paleoceanography, 22(1): doi:10.1029/2006PA001287.

Marchitto, T.M. and deMenocal, P.B., 2003. Late Holocene variability of upper North Atlantic Deep Water temperature and salinity. Geochemistry, Geophysics, Geosystems, 4(12).

Marchitto, T.M., Oppo, D.W. and Curry, W.B., 2002. Paired benthic foraminiferal Cd/Ca and Zn/Ca evidence for a greatly increased presence of Southern Ocean Water in the glacial North Atlantic. Paleoceanography, 17, doi:10.1029/2000PA000598.

Marlow, J.R., Lange, C.B., Wefer, G. and Rosell-Mele, A., 2000. Upwelling intensification as part of the Pliocene Pleistocene climate transition. Science, 290: 2288 2291.

Martin, P.A. et al., 2002. Quaternary deep sea temperature histories derived from benthic foraminiferal Mg/Ca. Earth and Planetary Science Letters, 198(1-2): 193-209.

McClymont, E.L. and Rossel-Mele, A., 2005. Links between the onset of modern Walker circulation and the mid-Pleistocene climate transition. Geology, 33: 389-392.

Medina-Elizalde, M. and Lea, D.W., 2005. The mid-Pleistocene transition in the tropical Pacific. Science, 310: 1009 1012.

Mudelsee, M. and Raymo, M.E., 2005. Slow dynamics of the Northern Hemisphere Glaciation. Paleoceanography, 20, PA4022, doi:10.1029/2005PA001153.

Palacios, R., Orensanz, J.M. and Armstrong, D.A., 1994. SEASONAL AND LIFELONG VARIATION OF SR/CA RATIO IN SHELLS OF MYA-ARENARIA FROM GRAYS-HARBOR (WASHINGTON) - AN ANCILLARY CRITERION IN DEMOGRAPHIC-STUDIES. Estuarine Coastal and Shelf Science, 39(4): 313-327.

Palmer, M.R. and Edmond, J.M., 1992. Controls over the strontium
isotope composition of river water. Geochim. Cosmochim. Acta, 56: 2099-2111.

Pearson, P.N. et al., 2007. Stable warm tropical climate through the Eocene Epoch. Geology, 35(3): 211-214.

Peltier, W.R. and Fairbanks, R.G., 2006. Global glacial ice volume and Last Glacial Maximum duration from an extended Barbados sea level record. Quaternary Science Reviews, 25: 3322-3337.

Purton, L.M.A., Shields, G.A., Brasier, M.D. and Grime, G.W., 1999. Metabolism controls Sr/Ca ratios in fossil aragonitic mollusks. Geology, 27(12): 1083-1086.

Raitzsch, M., Kuhnert, H., Groeneveld, J. and Bickert, T., 2008. Benthic foraminifer Mg/Ca anomalies in South Atlantic core top sediments and their implications for paleothermometry. Geochemistry, Geophysics, Geosystems, 9: doi:10.1029/2007GC001788.

Raymo, M.E., B. Grant, M. Horowitz, and G. H. Rau, 1996. Mid-Pliocene warmth: stronger greenhouse and stronger conveyor. Marine Micropaleontology, 27: 313-326.

Raymo, M.E., D. W. Oppo, and W. Curry, 1997. The mid-Pleistocene climate transition: a deep sea carbon isotopic perspective. Paleoceanography, 12: 546 559.

Rind, D., 2000. Relating paleoclimate data and past temperature gradients: Some suggestive rules. Quaternary Science Reviews, 19: 381-390.

Rosenthal, Y., Boyle, E.A. and Slowey, N., 1997. Temperature control on the incorporation of magnesium, strontium, fluorine, and cadmium into benthic foraminiferal shells from Little Bahama Bank: Prospects for thermocline paleoceanography. Geochimica Et Cosmochimica Acta, 61(17): 3633-3643.

Rosenthal, Y., Boyle, E.A. and Slowey, N., 1997. Temperature control on the incorporation of Mg, Sr, F and Cd into benthic foraminiferal shells from Little Bahama Bank: prospects for thermocline paleoceanography. Geochimica et Cosmochimica Acta, 61: 3633-3643.

Ruddiman, W.F., M.E. Raymo, D.G. Martinson, B.M. Clement, and J. Backman, 1989. Mid-Pleistocene evolution of Northern Hemisphere climate. Paleoceanography, 4: 353-412.

Ruddiman, W.F. and Raymo, M.E., 1988. Northern hemisphere climate regimes during the past 3 Ma: possible tectonic connections. In: N.J. Shackleton, R.G. West, and D.Q. Bowen (Editor), The Past Three Million Years: Evolution of Climatic Variability in the North Atlantic Region. University Press, Cambridge, pp. 227-234.

Russell, A.D., S. Emerson, B.K. Nelson, J. Erez, and D.W. Lea, D.W., P. A. Martin, D. K. Pak, and H. J. Spero, 1995. Uranium in foraminiferal calcite as a recorder of seawater uranium concentrations. Geochimica et Cosmochimica Acta, 58: 671-681.

Schefus, E., Damste, J.S.S. and Jansen, J.H.F., 2004. Forcing of tropical Atlantic sea surface temperatures during the mid-Pleistocene transition. Paleoceanography, 19, PA4029, doi:10.1029/2003PA000892.

Schrag, D.P., Hampt, G. and Murray, D.W.S., 1996. Pore fluid constraints on the temperature and oxygen isotopic composition of the glacial ocean. Science, 272: 1930-1932.

Schrag, D.P., J. F. Adkins, K. McIntyre, J. L. Alexander, D. A. Hodell, C. D. Charles, and J. F. McManus, 2002. The oxygen isotopic composition of seawater during the Last Glacial Maximum. Quaternary Science Reviews, 21: 331-342.

Shackleton, N.J., 1974. Attainment of isotopic equilibrium between ocean water and the benthonic foraminifera genus Uvigerina: isotopic changes in the ocean during the last glacia. Colloques Internationaux du Centre National du Recherche Scientifique, 219: 203-210.

Shackleton, N.J., 1987. Oxygen isotopes, ice volume and sealevel. Quaternary Science Reviews, 6: 183-190.

Shackleton, N.J., 2000. The 100,000-year ice-age cycle identified and found to lag temperature, carbon dioxide, and orbital eccentricity. Science, 289: 1897-1902.

Shackleton, N.J. and Opdyke, N.D., 1973. Oxygen isotope and paleomagnetic stratigraphy of Equatorial Pacific core V28-238: oxygen isotope temperatures and ice volumes on a 10^5 and 10^6 year scale. Quaternary Research, 3: 39-55.

Siddall, M. et al., 2003. Sea-level fluctuations during the last glacial cycle. Nature, 423: 853-858.

Siegenthaler, U. and al, e., 2005. Stable carbon cycle   climate relationship during the late Pleistocene. Science, 310: 1313-1317.

Stecher, H.A., Krantz, D.E., Lord, C.J., Luther, G.W. and Bock, K.W., 1996. Profiles of strontium and barium in Mercenaria mercenaria and Spisula solidissima shells. Geochimica Et Cosmochimica Acta, 60(18): 3445-3456.

Stoll, H.M. and Schrag, D.P., 1998. Effects of Quaternary sea level cycles on strontium in seawater. Geochimica Et Cosmochimica Acta, 62(7): 1107-1118.

Takesue, R.K. and Van Geen, A., 2004. Mg/Ca, Sr/Ca, and stable isotopes in modern and holocene Protothaca staminea shells from a northern California coastal upwelling region. Geochimica Et Cosmochimica Acta, 68(19): 3845-3861.

Turekian, K.K., 1964. The marine geochemistry of strontium. Geochim. Cosmochim. Acta, 28: 1479-1496.

Tziperiman, E. and Gildor, H., 2003. On the mid-Pleistocene transition to 100- kyr glacial cycles and the asymmetry between glaciation and deglaciation times. Paleoceanography, 18.

Waelbroeck, C. et al., 2002. Sea-level and deep water temperature changes derived from benthic foraminifera isotopic records. Quaternary Science Reviews, 21: 295-305.

Yokoyama, Y., Lambeck, K., Deckker, P.P.J.D. and Fifeld, L.K., 2000. Timing of the last glacial maximum from observed sea-level minima. Nature, 406: 713-716.

planktonic
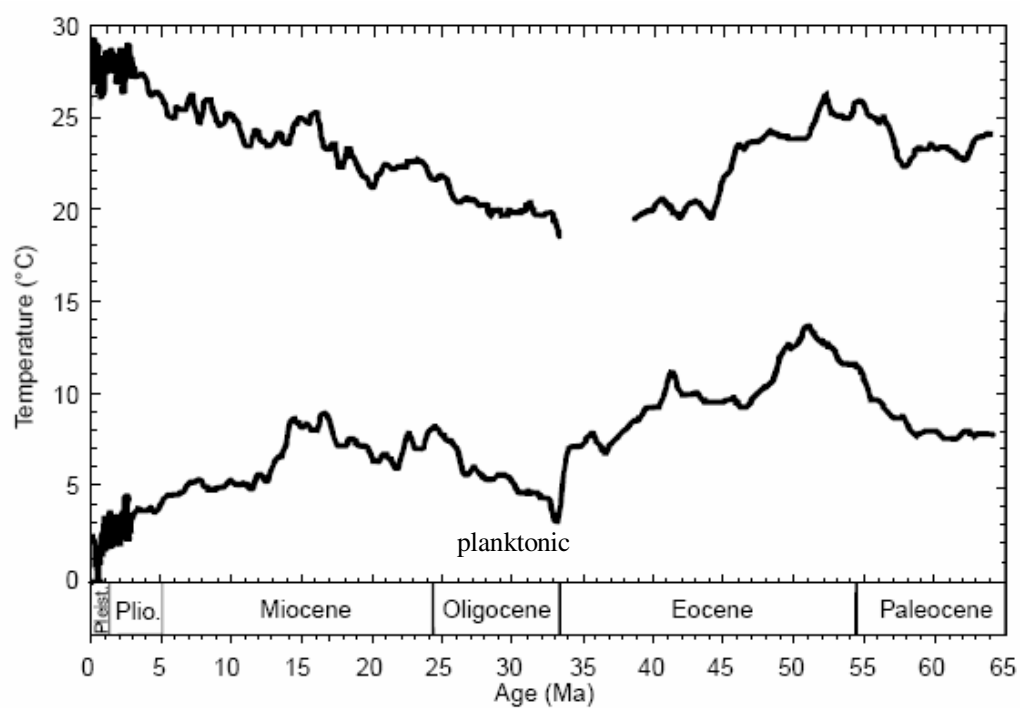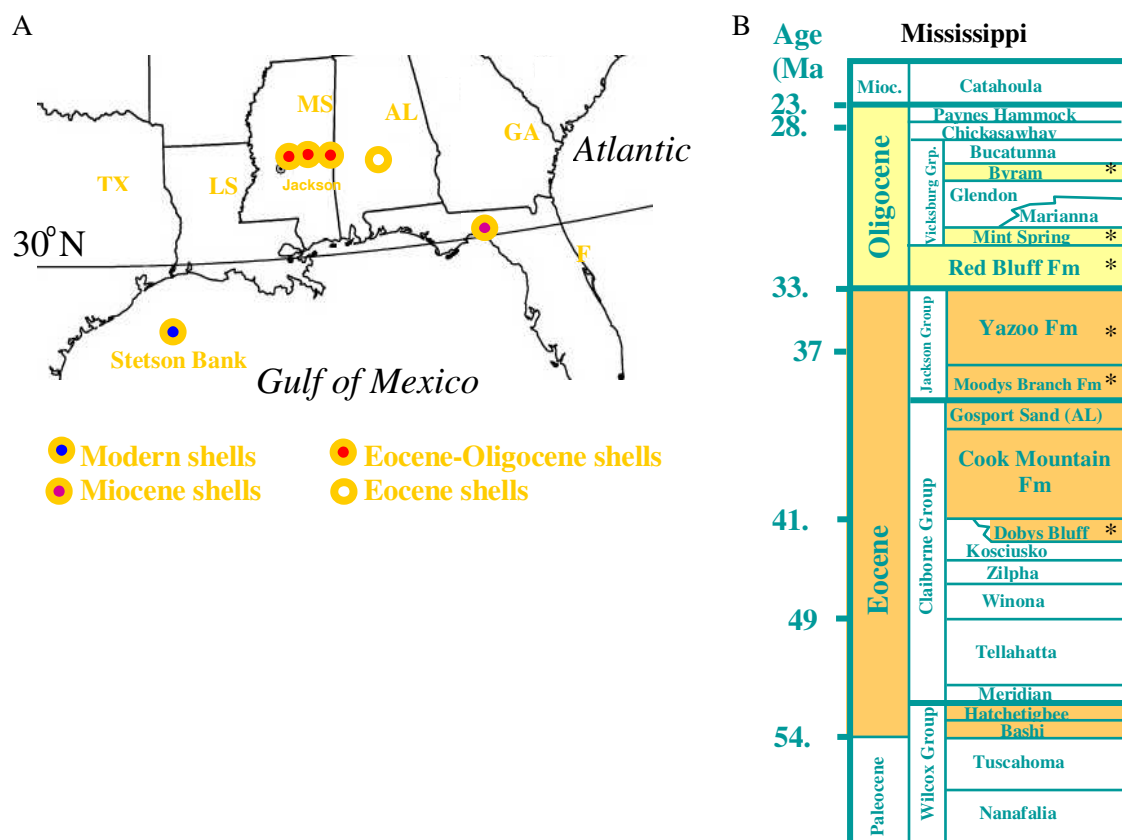
Figure 5.2 (a)Map of U.S. Gulf Coast (figure from Kobashi et al., 2004.) Circles represent the sampling sites for mollusks. (b)Age and stratigraphic formation information from Dockery (1980, 1996). Miocene *Conus* specimens collected from Florida are not included in this diagram. Asterisks highlight sample collection sites.
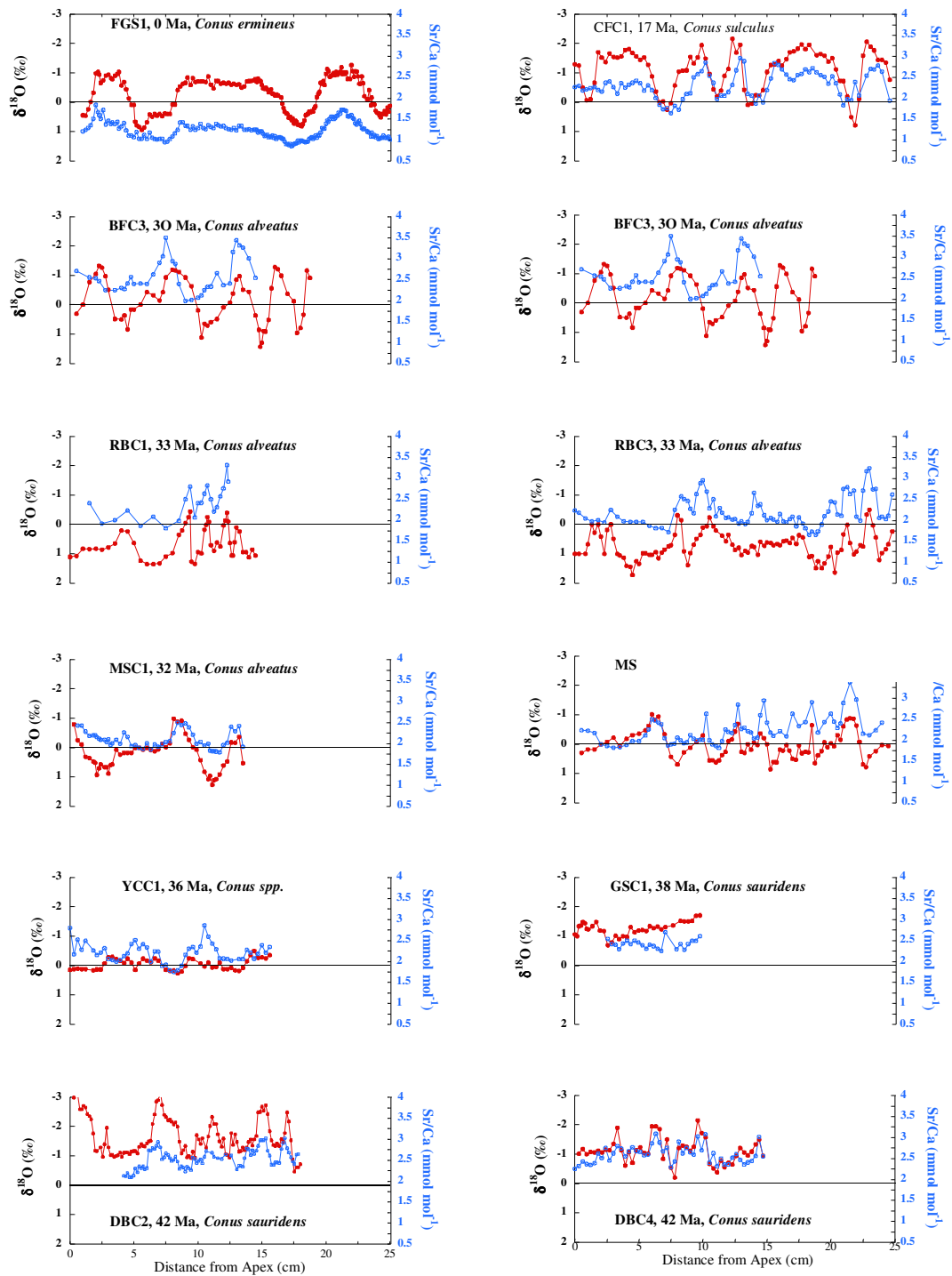
Figure 5.3 Oxygen and Sr/Ca profiles of *Conus sp.* from modern and fossil specimens. Sr/Ca range is converted into relative change in temperature (ΔT) using the modern calibration Solid line denotes δ^{18}O=0‰ and Sr/Ca=2 mmol mol^{-1}
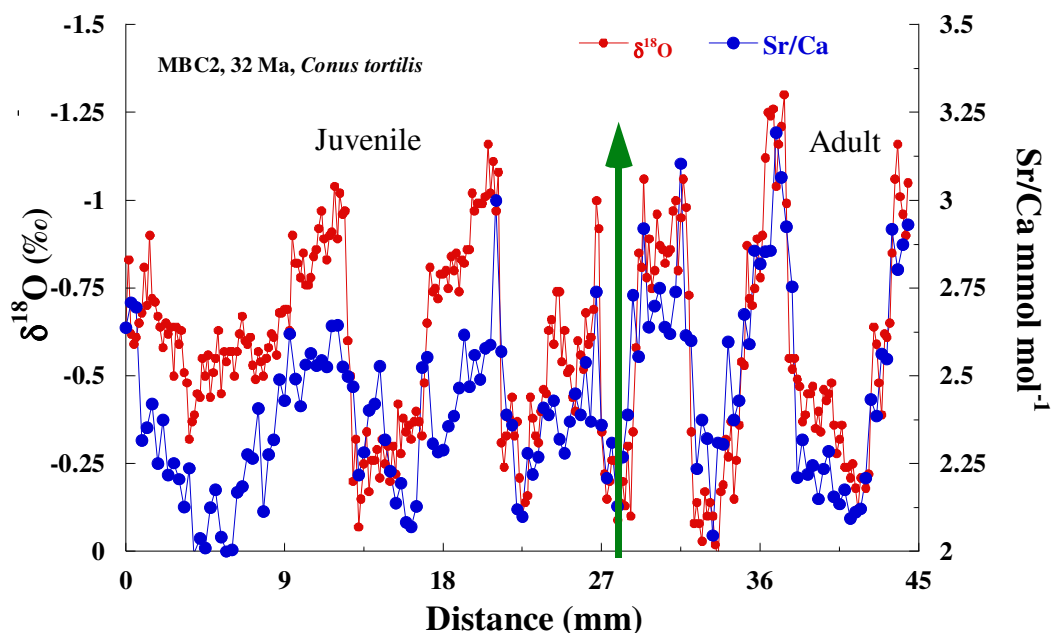
Figure 5.4 Oxygen and Sr/Ca profiles of Moody's Branch *Conus tortilis* shell, MBC-2. Note the covariance of both records throughout the lifespan of the specimen and the increasing summer Sr/Ca maxima with age. The green arrow denotes the transition between the juvenile to adult growth stage.
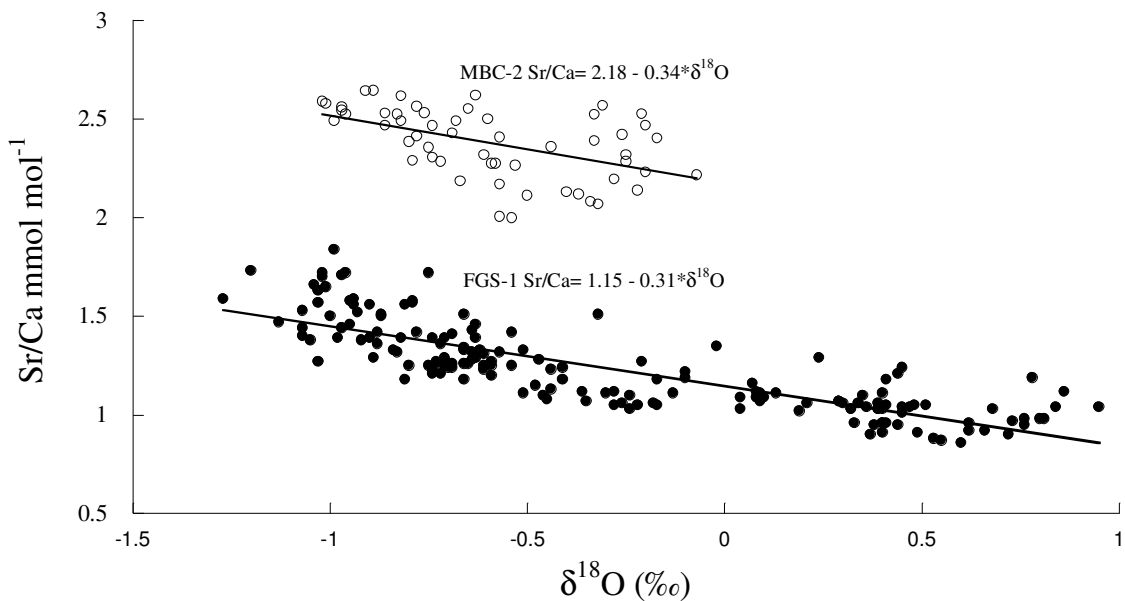
Figure 5.5 Sr/Ca plotted versus $\delta^{18}O$ for two gastropod shells, one modern (FGS-1) and a fossil (MBC-2). The arrow diagram illustrates the potential mechanisms that could explain changes in Sr/Ca and $\delta^{18}O$.
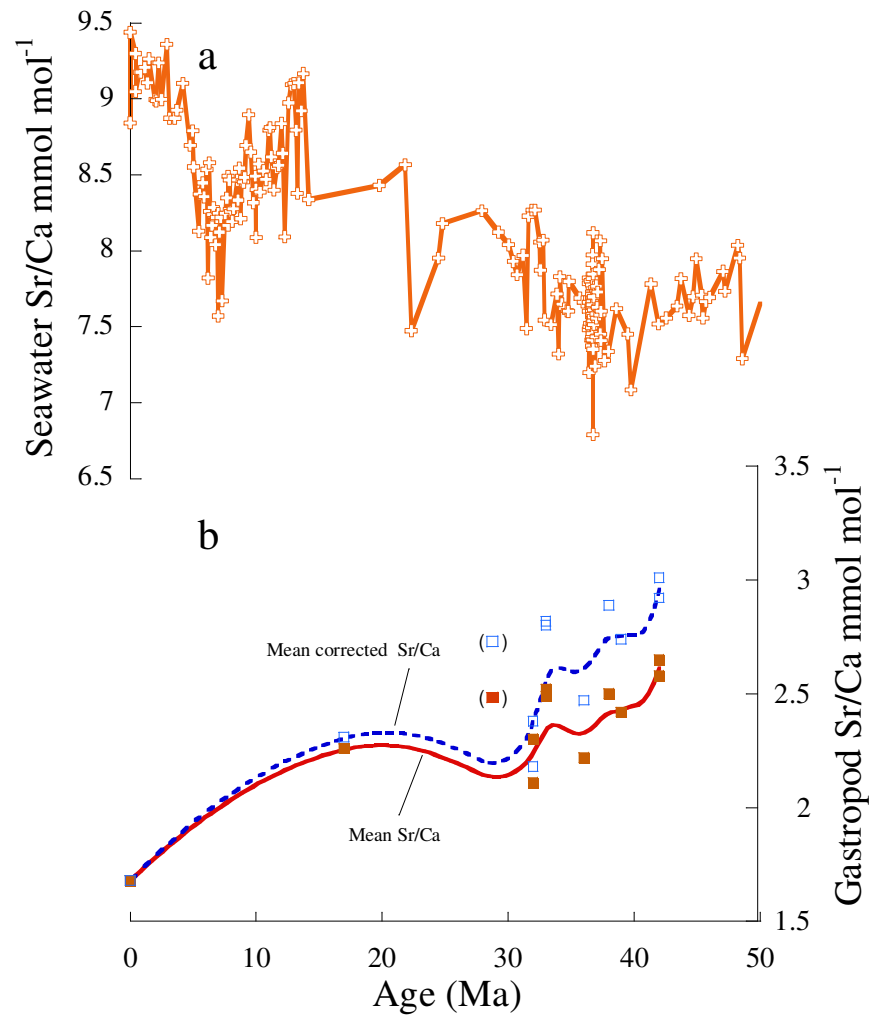
Figure 5.6 (a) Seawater Sr/Ca record for the Cenozoic from Lear et al., (2003). **(b)**Mean Sr/Ca constructed from gastropod record. Uncorrected data shown in solid squares whereas data corrected for changes in seawater composition are shown in open squares. Sr/Ca data from BFC-1 and BFC-3 (30 Ma) is excluded due to diagenetic alteration.
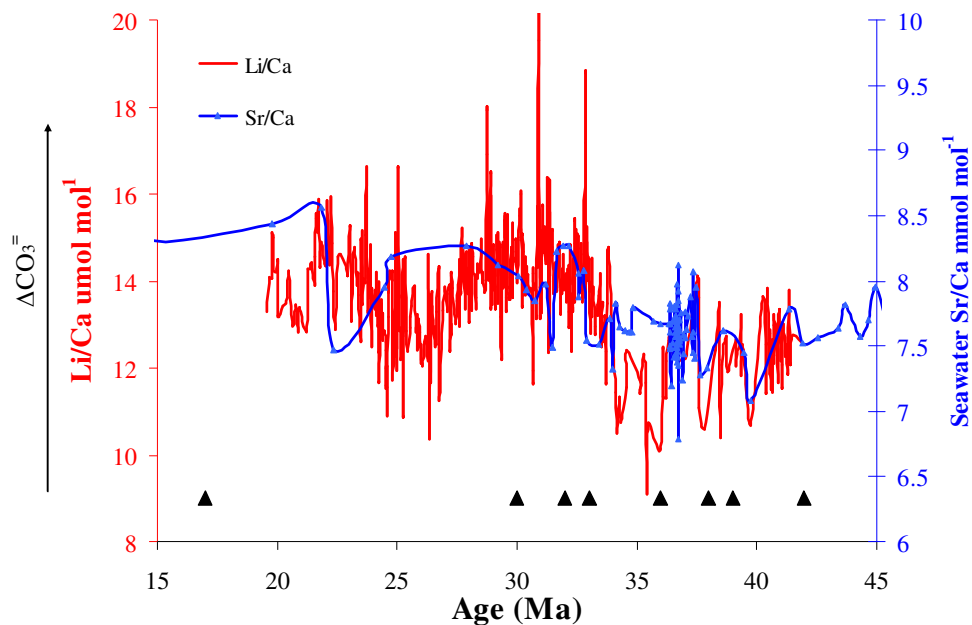
Figure 5.7. Foraminiferal Li/Ca and Sr/Ca (triangles) vs. age. Li/Ca data are from Lear and Rosenthal (2006) and seawater Sr/Ca data from Lear et al., (2003). Li/Ca decreases with decreasing carbonate saturation. Note the large oscillations in Li/Ca across the Eocene-Oligocene. Black triangles represent interval where fossil *Conus* shells are present.
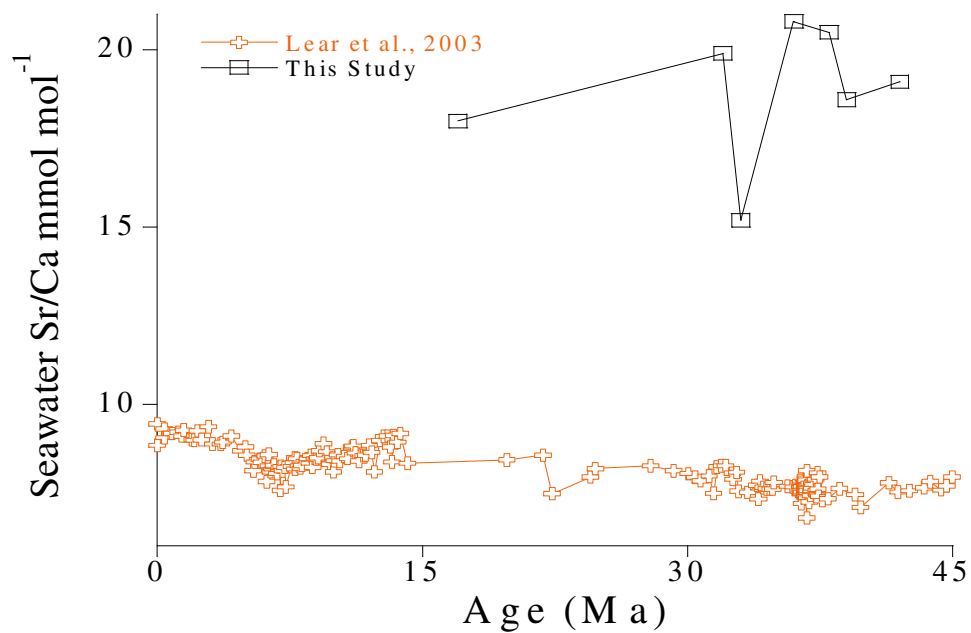
Figure 5.8 Seawater Sr/Ca variations determined from benthic foraminifera (Lear et al., 2003) and marine gastropods (this study).
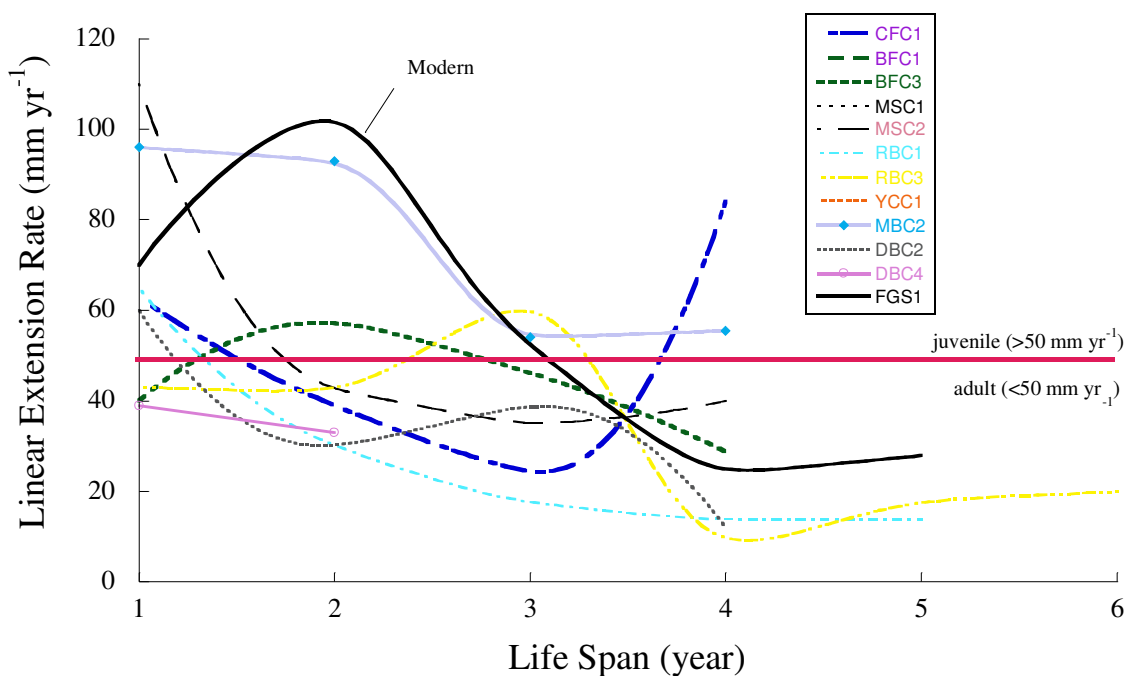
Figure 5.9 Linear extension rate (Siegenthaler et al.) across the life span of the gastropod shell. Specimen FGS-1, a modern *Conus,* shows a distinct transition in LER from juvenile to adult growth stages. MBC-2 and BFC-1 show similar variations in LER whereas the remaining fossil specimens exhibit adult-like LER (<50 mm yr^{-1}) throughout their life span.
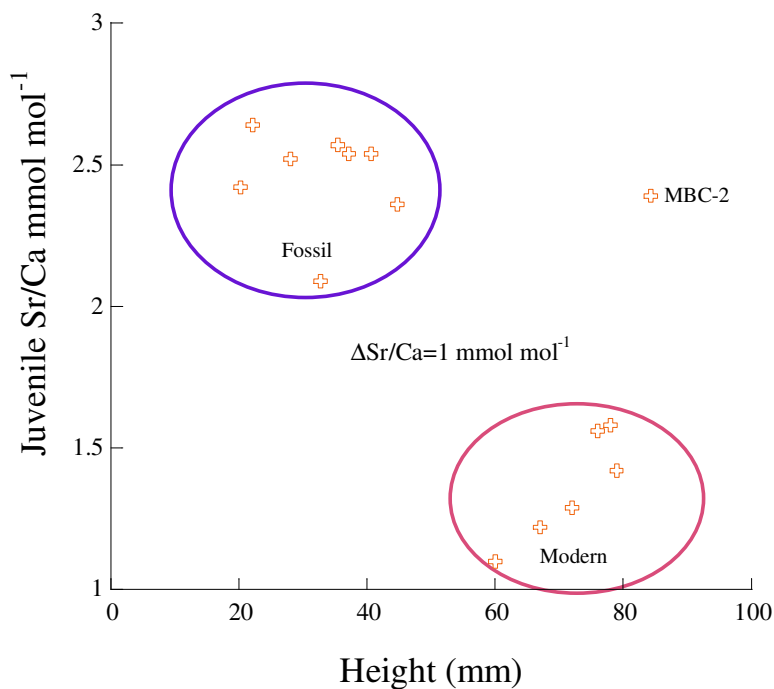
Figure 5.10 Difference in shell size, here height (mm), between fossil and modern *Conus* specimens. The average offset in mean Sr/Ca is ~ 1 mmol mol^{-1} between the two size groups. Note that MBC-2, a large, long-lived specimen, is part of the fossil group.
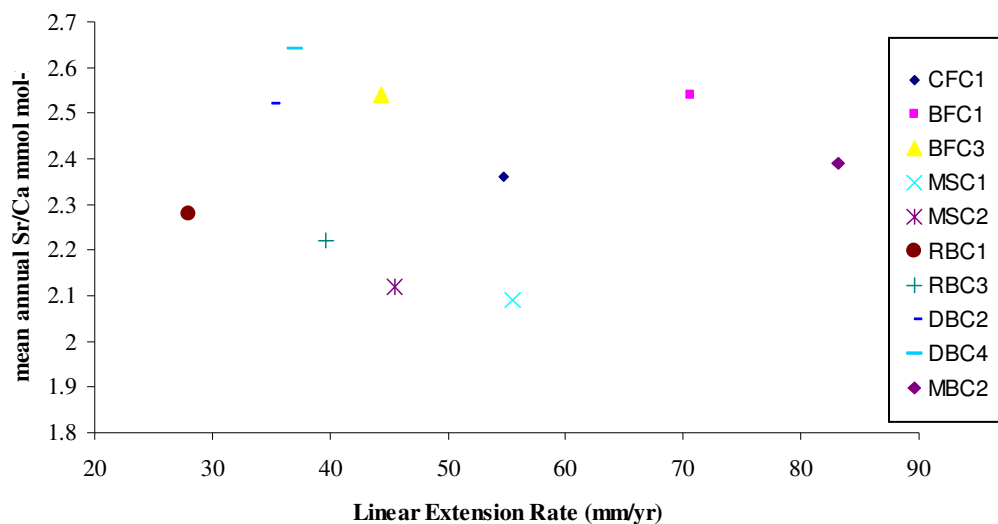
Figure 5.11 Average mean annual LER versus mean Sr/Ca for all fossil specimens. There is no distinct trend between the mean Sr/Ca and annual LER which suggests that growth rate variations are not driving Cenozoic fossil Sr/Ca variations.
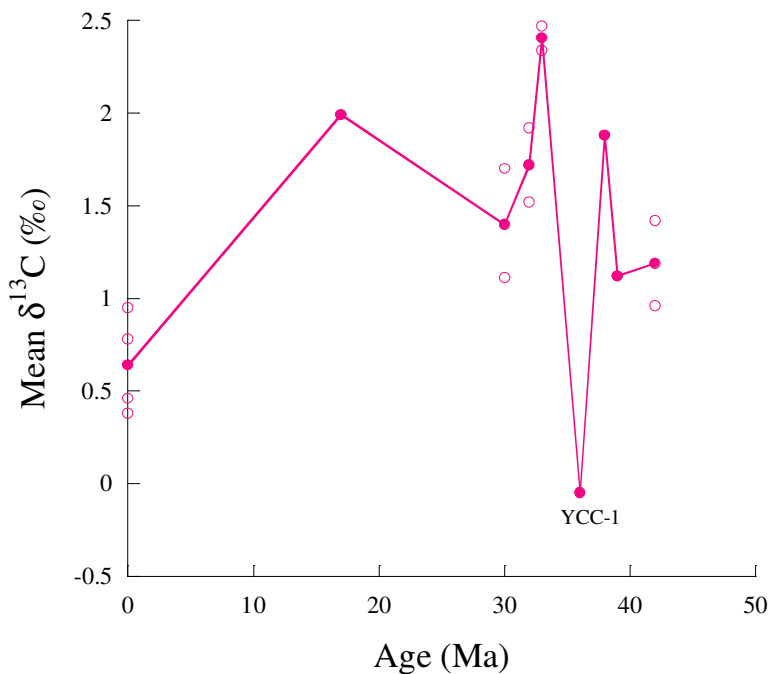
Figure 5.12 Fossil gastropod $\delta^{13}C$ variations across the Cenozoic. Note the sharp excursion at 36 Ma with specimen YCC-1.
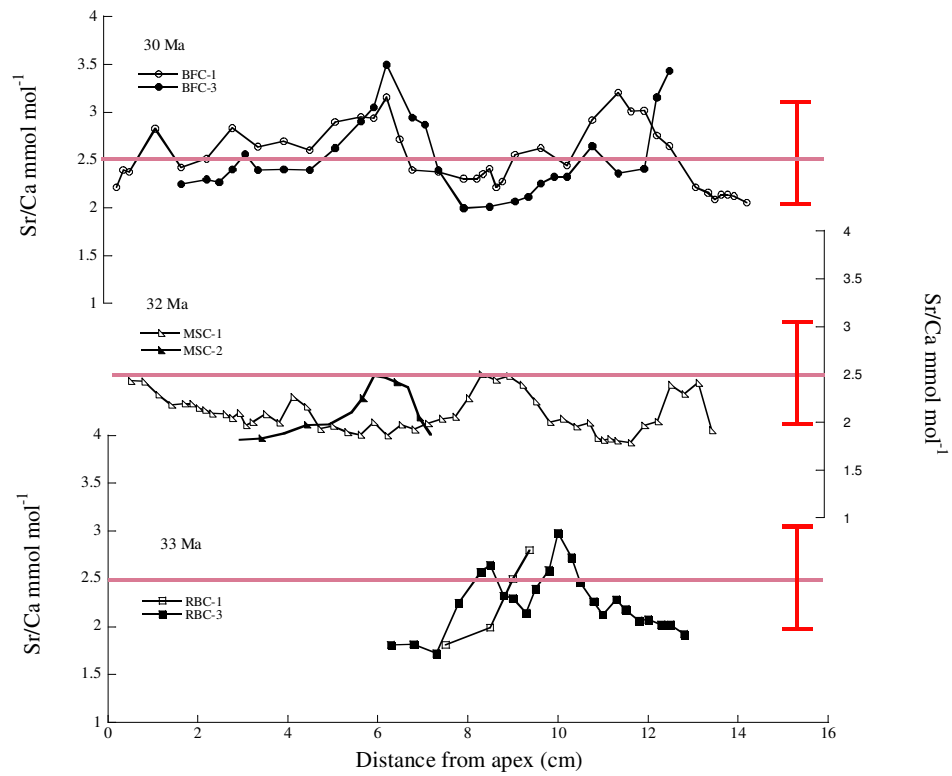
Figure 5.13 Sr/Ca profiles versus spiral distance of fossil specimens *Conus alveatus* from three time intervals. The red brackets denote a 10°C temperature range.
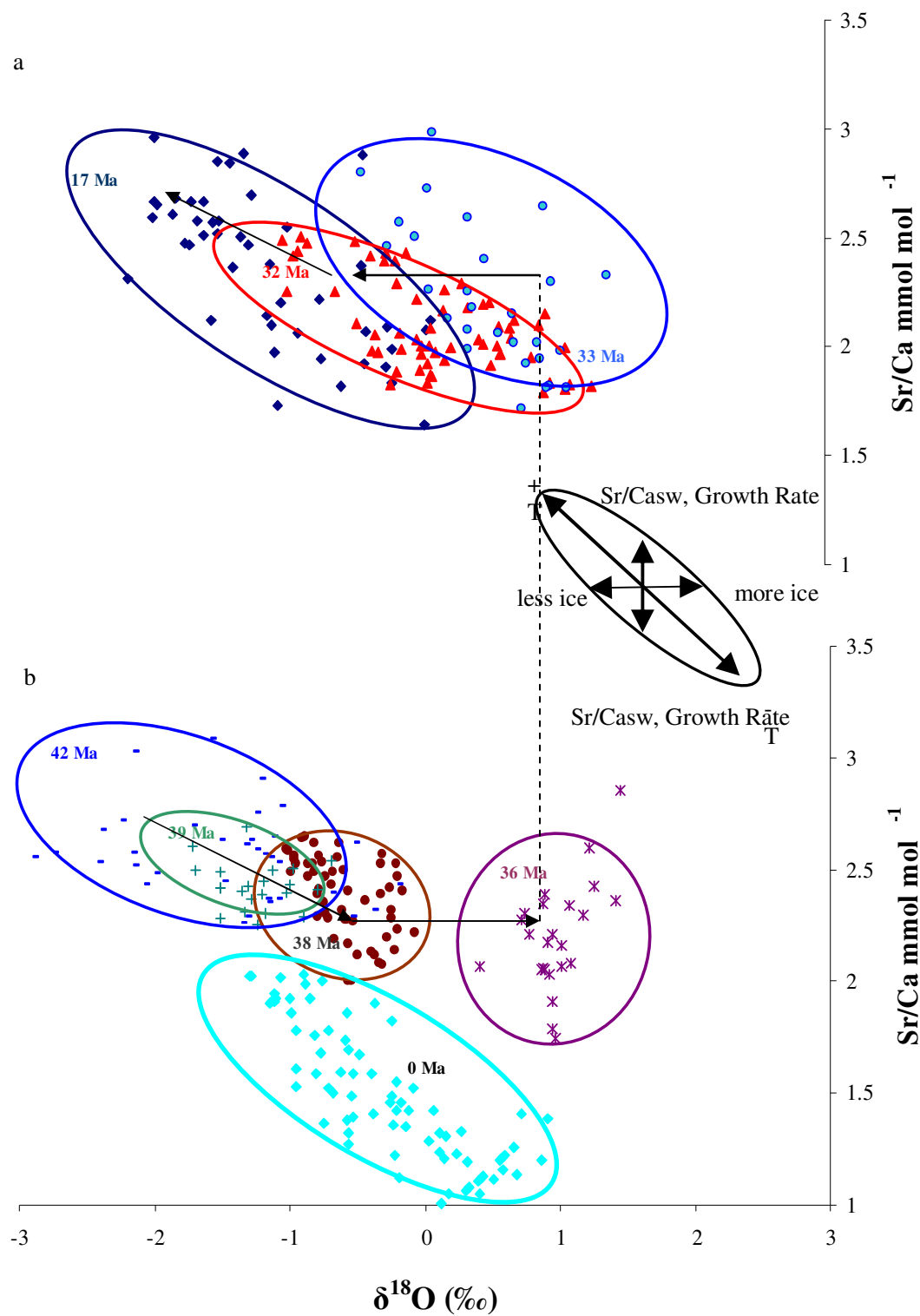
Figure 5.14 Gastropod shell δ¹⁸O and Sr/Ca variations from fossil specimens. (a) Late Eocene to Miocene data; (b) Early to late Eocene data.
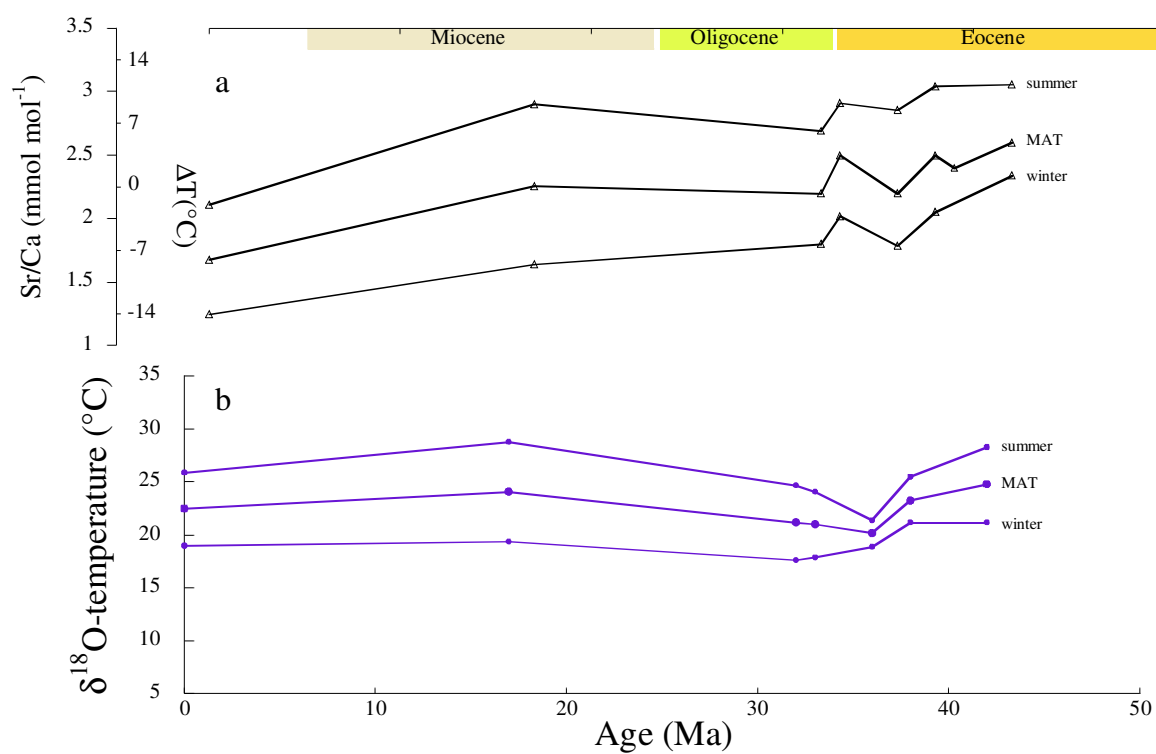
Figure 5.15 (a) Sr/Ca and (b) oxygen isotope paleotemperatures (from Kobashi et al., 2001) change of gastropods through the Cenozoic. Upper, middle, and lower curves represent summer, mean, and winter Sr/Ca values and δ^{18}O-paleotemperatures. Changes in temperature are scaled on the Sr/Ca y-axis using the modern calibration slope.
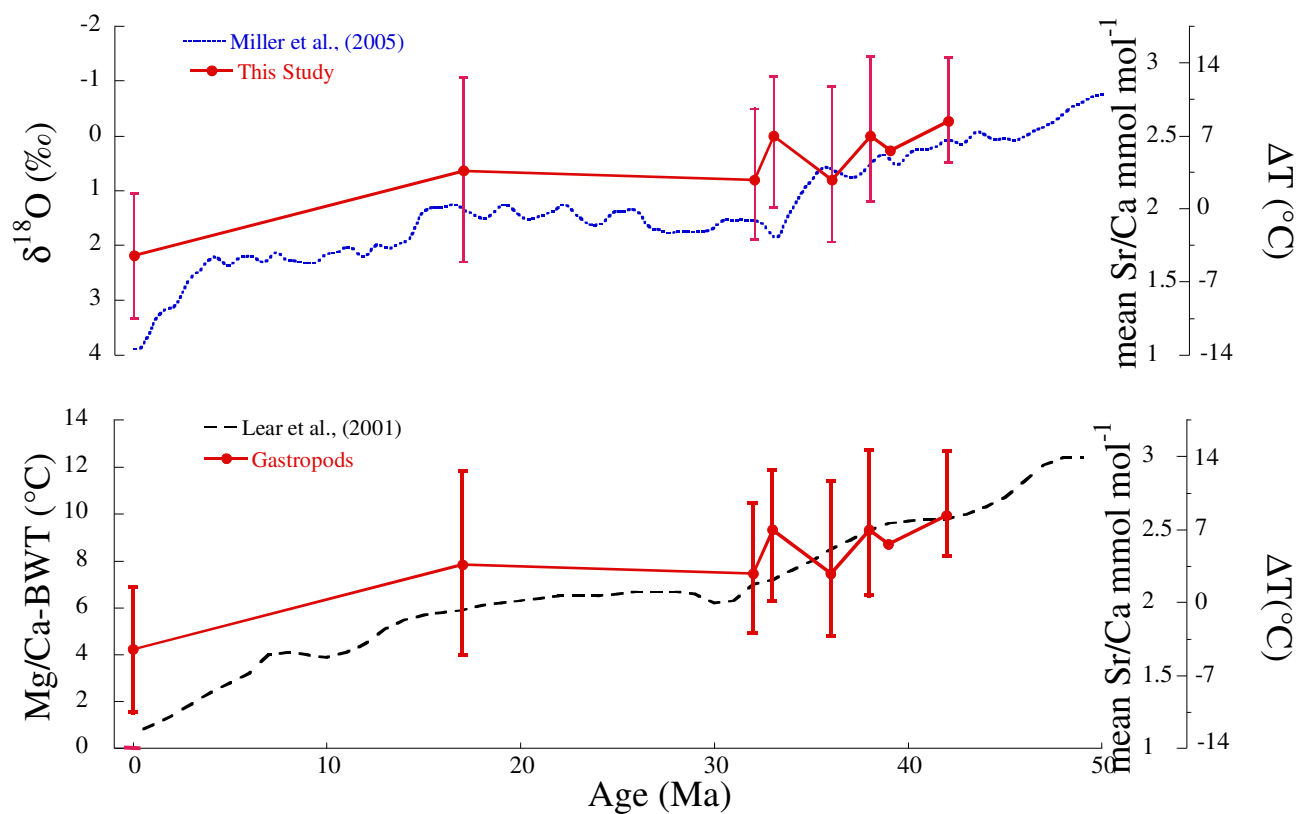
Figure 5.16 (a)Benthic oxygen isotope record from Miller et al., 2005 and (b) bottom water temperature record from Lear et al., (2000) versus the Mean Sr/Ca record and inferred change in temperature from the fossil gastropods. The modern calibration sensitivity of ~1 mmol mol-1 per 10°C is applied to determine the change in temperature from the Sr/Ca data. Red bars represent the average seasonal amplitude for the time interval.
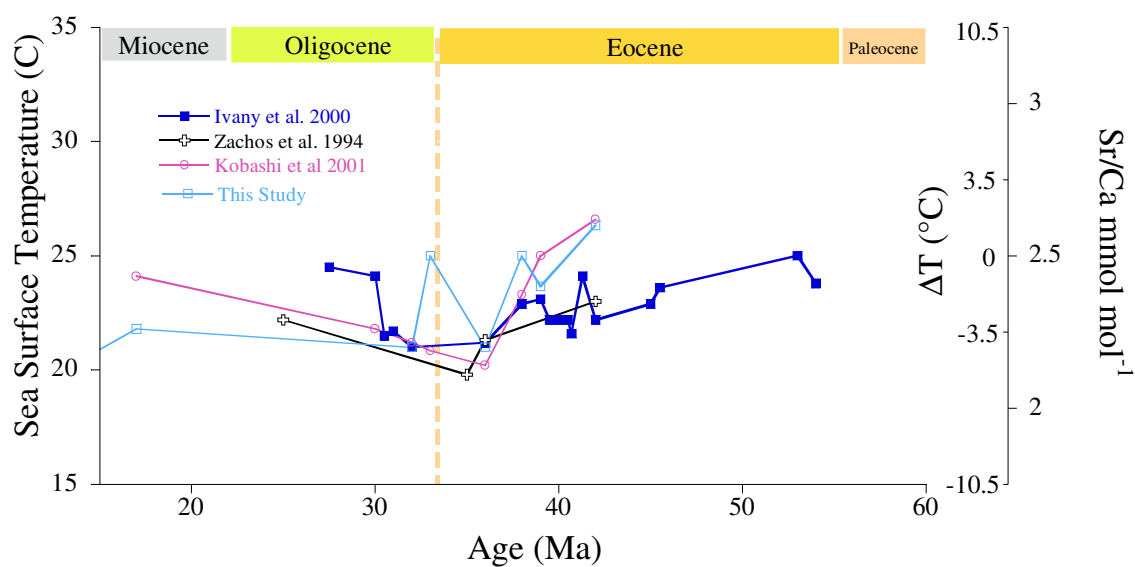
Figure 5.17. Sea surface temperature records from oxygen isotopic composition of otoliths, planktonic foraminifera, and mollusks (Ivany et al., 2000; Zachos et al., 1994; Kobashi et al., 2001).

Table 5.1 Data for size, Sr/Ca compositions, and collection site for *Conus* specimens.

Sample ID	Formation name	Species	Age (Ma)	Height (cm)	Width (cm)	δ^{18}O-Sr/Ca Correlation, R^2	Paleodepth
FGS1	Stetson Bank, (present)	*Conus Ermineus*	0	67	39	0.64	shallow
CFC-1	Chipola fm., FL	*Conus sulculus*	17	44.7	27.3	0.50	shallow
BFC-1	Byram fm., MS	*Conus alveatus*	30	40.65	20.4	0.67	shallow
BFC-3	Byram fm., MS	*Conus alveatus*	30	37.15	20.4	0.25	shallow
MSC-1	Mint Spring fm., MS	*Conus alveatus*	32	32.7	11.6	0.68	shallow
MSC-2	Mint Spring fm., MS	*Conus alveatus*	32			0.94	shallow
RBC-1	Red Bluff fm., MS	*Conus alveatus*	33	32	16	0.90	deeper
RBC-3	Red Bluff fm., MS	*Conus alveatus*	33			*0.28*	deeper
YCC-1	Yazoo fm., MS	*Conus spp*	36			*0.25*	deeper
MBC-2	Moodys Branch fm., MS	*Conus tortilis*	38	87	50	0.45	shallow
GSC-1	Gosport Sand, AL	*Conus sauridens*	39		10.8	*0.01*	shallow
DBC-2	Dobys Bluff fm., MS	*Conus sauridens*	42	36	16	0.67	shallow
DBC-4	Dobys Bluff fm., MS	*Conus sauridens*	42		11.8	0.67	shallow

Sample ID	Formation name	Sr/Ca mmol mol^{-1}			
		Mean	Maximum	Minimum	Amplitude
FGS1	Stetson Bank, (present)	1.22	1.73	0.86	0.87
CFC-1	Chipola fm., FL	2.36	2.89	1.88	1.02
BFC-1	Byram fm., MS	2.54	3.19	2.14	1.05
BFC-3	Byram fm., MS	2.54	3.47	2.13	1.35
MSC-1	Mint Spring fm., MS	2.09	2.45	1.83	0.62
MSC-2	Mint Spring fm., MS	2.12	2.48	1.85	0.64
RBC-1	Red Bluff fm., MS	2.28	2.80	1.81	0.99
RBC-3	Red Bluff fm., MS	2.22	2.82	1.83	0.99
YCC-1	Yazoo fm., MS	2.21	2.86	1.89	0.98
MBC-2	Moodys Branch fm., MS	2.39	2.63	2.07	0.56
GSC-1	Gosport Sand, AL	2.42			
DBC-2	Dobys Bluff fm., MS	2.52	2.93	2.12	0.82
DBC-4	Dobys Bluff fm., MS	2.64	3.08	2.29	0.79

Table 5.2 Calculation of temperature sensitivity for fossil specimens.

Specimen	Age (Ma)	Sr/Ca mmol mol^{-1}		δ^{18}O-T[1] (°C)		ΔSr/Ca/ΔT (mmol mol^{-1} °C^{-1})
		maximum	minimum	maximum	minimum	
DBC-2	42	3.0	2.3	31.8	24.1	0.09
DBC-4	42	3.1	2.3	27.8	21.8	0.12

[1]Assuming dw=-0.06‰ from Lear et al., (2001) corrected for latitude (Zachos et al., 1994) and using the) paleotemperature equation of Grossman and Ku (1989

Chapter 6

6. Conclusions and Future Directions

In chapter 2, I utilized Mg/Ca benthic foraminiferal paleothermometry to reconstruct, at an orbital scale resolution, long-term changes in deep ocean temperature across the Pliocene-Pleistocene in the deep North Atlantic. The Mg/Ca-bottom water temperature (BWT) record derived from Deep Sea Drilling Project site 607 in the sub-polar North Atlantic shows two main cooling phases associated with the development and intensification of large-scale northern hemisphere glaciation (NHG). Superimposed on the cooling trend, glacial-interglacial variability in BWT changes from small amplitude, high frequency to large amplitude, low frequency cycles. The changes in BWT are coherent with the major features of the benthic oxygen isotope record ($\delta^{18}O_b$) at this site which indicates that a significant portion of the $\delta^{18}O_b$ record is related to change in temperature. Using paired $\delta^{18}O_b$ and Mg/Ca-BWT records, I evaluated the nature of changes of global ice volume variations across each major climate transition in the Pliocene-Pleistocene. I highlight the divergent in the sea level history between the late Pliocene transition (LPT) and the mid-Pleistocene transition (Schrag et al.). Across the LPT, sea level decreased in association with the development of large-scale NHG. However, across the MPT there is no discernible change in sea level associated with the intensification of NHG. Rather, the amplitude of glacial-interglacial sea level estimates increases indicating that glacial and interglacial periods became more severe. The major features of the BWT and sea level records suggest that the LPT is likely related to the glaciation threshold response to a global cooling whereas the MPT represents a change in ice sheet dynamics.

In chapter 3, I focus on the primary features of the BWT and sea level record across the MPT. The cooling trend in the deep North Atlantic Ocean represents high latitude cooling that is expressed in regions remote from NH ice sheet variability. Sea surface temperature (SST) records from upwelling regimes and the North and South Atlantic Ocean show a coherent decrease in temperature and shift in frequency and amplitude similar to the BWT record presented in chapter 2. The coherency in temperature variability suggests that cooling is a global signal. However in the western equatorial Pacific Ocean, SST records show no long-term change associated with the MPT. Temperature at this site is mainly driven by variations in atmospheric carbon dioxide (pCO_2). Thus, the long-term stability of this region implies that pCO_2 is not driving the decrease in temperature in the high latitudes and upwelling regimes. This contradicts the global cooling hypothesis which proposes that the global cooling coherent with the MPT was driven by a secular decrease in greenhouse gases. I hypothesize that the cooling across the MPT is not sufficient to fully explain the features of the MPT. The switch in frequency from 41 to 100-kyr glacial-interglacial cycles, increase in phase relationship between BWT and $\delta^{18}O_b$, increase in severity of glacial-interglacial cycles did not occur until the culmination of the cooling trend. Part of the MPT is related to a switch in ice sheet dynamics, specifically a transition from thin to thick ice sheets.

In chapter 4, I developed a new salinity independent low-latitude paleothermometer from a modern calibration study using Sr/Ca ratios in marine gastropods. The proxy has potential to reconstruct changes in mean annual and seasonal temperature variations within ±1°C. In chapter 5, I apply the calibration to fossil gastropod Sr/Ca records and evaluate changes in low-latitude SST across the Cenozoic.

The temperature record shows a long-term trend toward cooler conditions in the tropics which suggests that the low latitudes responded to Cenozoic climate change concomitant with the high latitudes.

In addition to the major findings of each chapter, uncertainties associated with each proxy, Mg/Ca benthic foraminiferal and Sr/Ca marine gastropod paleothermometry, need to be more fully explored. The Mg/Ca-temperature record constructed from the deep North Atlantic shows long-term and orbital-scale changes related to high latitude climate changes, water mass mixing, and carbonate saturation. Ideally, an intermediate water depth Mg/Ca-temperature record would better represent solely changes in the North Atlantic Ocean regardless of changes in ocean circulation or deep ocean carbonate saturation. Another record would assist in determining the effects of carbonate saturation on the Mg/Ca-temperature calibration and separate the local from global temperature effects. Additionally, using the Mg/Ca-temperature record to deconvolve the $\delta^{18}O_b$ into its temperature and ice volume components is useful for the evaluation long-term changes in sea level variability but does not resolve finescale changes across glacial-interglacial cycles. Replicate analysis in certain time intervals would minimize the error associated with this proxy and allow for accurate comparison of interglacial and glacial periods. Regardless, the record presented in chapter 2 shows the utility of Mg/Ca ratios in benthic foraminifera to provide a high-resolution record of NHG and associated climate variability.

The Sr/Ca gastropod chapters highlight the potential utility of this temperature proxy to infer past changes in low latitude temperature and global ice volume. However, future work is necessary to fully quantify long-term controls on fossil gastropod Sr/Ca.

To determine if Cenozoic variations in *Conus* Sr/Ca are influenced by vital effects (e.g. habitat, inter-species variability) or changes seawater Sr/Ca a complimentary study of various Conus sp., specifically (*Conus spurious* and *Conus floridanus*) would be beneficial to further the interpretation of this study. Sr/Ca data from these species could be compared to the modern calibration based on *Conus ermineus* to evaluate species-specific and habitat. This comparison will allow us to establish if changes in fossil Conus Sr/Ca are primarily recording temperature.

7. Appendices

Table 7.1 Benthic foraminiferal stable isotope data from *Chain* 82-24-23 Piston Core. Species analyzed were *Cibicidoides wuellerstorfi* and *Uvigerina species.* All isotope data is referenced to *Pee Dee Belemnite* (PDB).

Depth interval (cm)	$\delta^{13}C$ (‰)	$\delta^{18}O$ (‰)	Species
25	0.96	3.01	*C. wuellerstorfi*
30	1.22	3.65	*C. wuellerstorfi*
40	0.48	4.54	*C. wuellerstorfi*
45	0.68	4.30	*C. wuellerstorfi*
50	0.63	4.44	*C. wuellerstorfi*
55	0.45	4.49	*C. wuellerstorfi*
60	0.67	4.37	*C. wuellerstorfi*
65	0.59	4.56	*C. wuellerstorfi*
70	1.16	4.24	*C. wuellerstorfi*
75	0.87	4.54	*C. wuellerstorfi*
80	1.15	4.44	*C. wuellerstorfi*
85	1.02	4.42	*C. wuellerstorfi*
90	1.02	4.41	*C. wuellerstorfi*
95	1.06	4.04	*C. wuellerstorfi*
100	0.47	4.18	*C. wuellerstorfi*
105	1.09	4.31	*C. wuellerstorfi*
110	0.98	4.22	*C. wuellerstorfi*
115	1.12	3.93	*C. wuellerstorfi*
125	1.18	4.20	*C. wuellerstorfi*
130	1.20	4.04	*C. wuellerstorfi*
135	1.20	4.05	*C. wuellerstorfi*
140	1.22	4.02	*C. wuellerstorfi*
145	1.18	3.94	*C. wuellerstorfi*
150	1.22	3.85	*C. wuellerstorfi*
155	1.22	4.03	*C. wuellerstorfi*
160	1.25	3.78	*C. wuellerstorfi*
165	1.18	3.90	*C. wuellerstorfi*
170	1.01	3.62	*C. wuellerstorfi*
175	0.48	3.56	*C. wuellerstorfi*
180	1.18	3.57	*C. wuellerstorfi*
185	1.11	3.66	*C. wuellerstorfi*
190	0.79	3.42	*C. wuellerstorfi*
195	1.38	3.22	*C. wuellerstorfi*
200	1.40	3.62	*C. wuellerstorfi*
205	1.32	3.37	*C. wuellerstorfi*
210	1.48	3.20	*C. wuellerstorfi*
215	1.37	3.66	*C. wuellerstorfi*

220	1.24	3.44	*C. wuellerstorfi*
225	0.98	3.45	*C. wuellerstorfi*
230	1.13	2.74	*C. wuellerstorfi*
235	0.89	3.32	*C. wuellerstorfi*
240	1.16	3.10	*C. wuellerstorfi*
245	0.87	3.39	*C. wuellerstorfi*
250	1.07	3.38	*C. wuellerstorfi*
255	0.97	2.92	*C. wuellerstorfi*
260	1.13	2.87	*C. wuellerstorfi*
265	1.11	2.77	*C. wuellerstorfi*
270	1.08	2.53	*C. wuellerstorfi*
275	1.06	2.44	*C. wuellerstorfi*
280	0.74	2.67	*C. wuellerstorfi*
285	0.45	3.01	*C. wuellerstorfi*
290	0.71	3.43	*C. wuellerstorfi*
295	0.78	3.79	*C. wuellerstorfi*
300	1.08	2.76	*C. wuellerstorfi*
310	0.15	4.19	*C. wuellerstorfi*
315	-0.68	4.44	*Uvigerina sp.*
320	-0.85	4.67	*Uvigerina sp.*
325	0.99	3.92	*C. wuellerstorfi*
330	0.35	3.87	*C. wuellerstorfi*
335	-0.77	4.49	*Uvigerina sp.*
340	0.28	4.17	*C. wuellerstorfi*
345	0.07	3.90	*C. wuellerstorfi*
350	0.46	3.82	*C. wuellerstorfi*
355	0.35	4.00	*C. wuellerstorfi*
360	0.59	3.27	*C. wuellerstorfi*
365	0.41	3.46	*C. wuellerstorfi*
370	0.65	3.79	*C. wuellerstorfi*
375	0.32	3.95	*C. wuellerstorfi*
380	0.93	3.31	*C. wuellerstorfi*
385	0.95	3.50	*C. wuellerstorfi*
390	0.99	2.99	*C. wuellerstorfi*
395	0.99	2.87	*C. wuellerstorfi*
400	0.98	2.96	*C. wuellerstorfi*
405	0.90	2.73	*C. wuellerstorfi*
410	0.91	3.12	*C. wuellerstorfi*
415	0.68	3.11	*C. wuellerstorfi*
420	0.83	3.06	*C. wuellerstorfi*
425	0.88	3.82	*C. wuellerstorfi*
430	0.50	2.99	*C. wuellerstorfi*
435	0.24	2.63	*C. wuellerstorfi*

440	0.69	3.51	*C. wuellerstorfi*
450	0.93	3.51	*C. wuellerstorfi*
455	-0.34	4.38	*Uvigerina sp.*
460	0.69	3.85	*C. wuellerstorfi*
465	0.77	4.04	*C. wuellerstorfi*
470	0.40	3.91	*C. wuellerstorfi*
475	0.18	3.97	*C. wuellerstorfi*
480	0.60	3.57	*C. wuellerstorfi*
485	0.57	3.20	*C. wuellerstorfi*
490	0.71	3.16	*C. wuellerstorfi*
495	0.67	3.61	*C. wuellerstorfi*
500	0.90	3.62	*C. wuellerstorfi*
505	1.03	2.99	*C. wuellerstorfi*
510	1.05	3.27	*C. wuellerstorfi*
515	0.95	2.98	*C. wuellerstorfi*
520	1.07	2.98	*C. wuellerstorfi*
525	0.97	3.45	*C. wuellerstorfi*
530	0.72	3.27	*C. wuellerstorfi*
535	0.99	3.07	*C. wuellerstorfi*
540	0.90	2.81	*C. wuellerstorfi*
545	0.90	2.55	*C. wuellerstorfi*
550	1.05	2.61	*C. wuellerstorfi*
555	1.13	2.48	*C. wuellerstorfi*
560	0.94	2.62	*C. wuellerstorfi*
565	0.79	2.28	*C. wuellerstorfi*
585	-0.17	4.27	*C. wuellerstorfi*
590	-0.23	4.32	*C. wuellerstorfi*
595	0.72	3.78	*C. wuellerstorfi*
605	0.46	3.86	*C. wuellerstorfi*
610	0.67	3.74	*C. wuellerstorfi*

Table 7.2 Benthic foraminiferal stable isotope data from DSDP site 607. Species analyzed were *Cibicidoides wuellerstorfi* and *Uvigerina species.* All isotope data is referenced to *Pee Dee Belemnite* (PDB).

Site	Hole	Core	Section	Interval (cm)	Composite depth (m)	$\delta^{13}C$ (‰)	$\delta^{18}O$ (‰)	Species
607	A	2	3	74-76	962	-0.79	4.97	*Uvigerina sp.*
607	A	2	3	89-91	977	-0.43	5.03	*Uvigerina sp.*
607	A	2	3	104-106	992	-0.60	4.64	*Uvigerina sp.*
607	A	2	3	119-121	1007	0.07	4.73	*Uvigerina sp.*
607	*	2	1	51-53	1050	-0.38	4.60	*Uvigerina sp.*
607	*	2	1	69-71	1068	-1.13	4.71	*Uvigerina sp.*
607	*	2	1	82-84	1081	-1.04	4.49	*Uvigerina sp.*
607	*	2	1	102-104	1101	-0.02	4.39	*Uvigerina sp.*
607	*	2	1	114-116	1113	0.81	3.42	*C. wuellerstorfi*
607	*	2	1	130-132	1129	0.74	3.32	*C. wuellerstorfi*
607	*	2	1	145-147	1144	0.87	3.18	*C. wuellerstorfi*
607	*	2	2	24-26	1173	-0.32	3.71	*C. wuellerstorfi*
607	*	2	2	54-56	1203	-0.24	4.62	*Uvigerina sp.*
607	*	2	2	64-66	1213	1.12	3.51	*C. wuellerstorfi*
607	*	2	2	101-103	1250	0.23	3.16	*C. wuellerstorfi*
607	*	2	2	116-118	1265	0.48	3.10	*C. wuellerstorfi*
607	*	2	2	145-147	1294	0.83	2.72	*C. wuellerstorfi*
607	*	2	3	9-11	1308	1.00	2.56	*C. wuellerstorfi*
607	*	2	3	21-23	1320	0.04	2.87	*C. wuellerstorfi*
607	*	2	3	70-72	1369	-1.08	4.99	*Uvigerina sp.*
607	*	2	3	85-87	1384	-1.17	5.08	*Uvigerina sp.*
607	*	2	3	101-103	1400	-0.56	4.96	*Uvigerina sp.*
607	*	2	3	117-119	1416	-0.24	4.64	*Uvigerina sp.*
607	*	2	3	145-147	1444	-0.81	4.76	*Uvigerina sp.*
607	*	2	4	11-13	1460	-0.65	4.72	*Uvigerina sp.*
607	*	2	4	23-25	1472	-0.11	4.67	*Uvigerina sp.*
607	*	2	4	33-35	1482	0.27	3.93	*C. wuellerstorfi*
607	*	2	4	57-59	1506	0.76	3.79	*C. wuellerstorfi*
607	*	2	4	71-73	1520	-0.49	4.44	*Uvigerina sp.*
607	*	2	4	84-86	1533	-0.05	4.40	*Uvigerina sp.*
607	*	2	4	98-100	1547	1.00	3.41	*C. wuellerstorfi*
607	*	2	4	113-115	1562	0.51	3.18	*C. wuellerstorfi*
607	*	2	4	125-127	1574	0.81	3.39	*C. wuellerstorfi*
607	*	2	4	147-149	1596	0.62	3.20	*C. wuellerstorfi*
607	*	2	5	9-11	1608	0.09	3.57	*Uvigerina sp.*
607	*	2	5	23-25	1622	1.24	2.73	*C. wuellerstorfi*
607	*	2	5	35-37	1634	1.24	2.65	*C. wuellerstorfi*
607	*	2	5	47-49	1646	1.22	2.74	*C. wuellerstorfi*

607	*	2	5	64-66	1663	1.26	2.56	*C. wuellerstorfi*
607	*	2	5	84-86	1683	1.00	2.70	*C. wuellerstorfi*
607	*	2	5	107-109	1706	0.98	2.92	*C. wuellerstorfi*
607	*	2	5	123-125	1722	0.47	3.17	*C. wuellerstorfi*
607	*	3	3	12-14	2007	1.14	3.25	*C. wuellerstorfi*
607	*	3	3	27-29	2022	0.23	3.56	*Uvigerina sp.*
607	*	3	3	57-59	2052	-0.38	3.88	*Uvigerina sp.*
607	*	3	3	72-74	2067	-0.82	4.60	*Uvigerina sp.*
607	*	3	3	102-104	2097	-0.55	4.56	*Uvigerina sp.*
607	*	3	3	146-148	2141	-1.08	4.34	*Uvigerina sp.*
607	*	3	4	11-13	2156	0.61	3.40	*C. wuellerstorfi*
607	*	3	4	26-28	2171	1.13	2.91	*C. wuellerstorfi*
607	*	3	4	42-44	2187	-0.08	3.56	*Uvigerina sp.*
607	*	3	4	69-71	2214	0.85	3.29	*C. wuellerstorfi*
607	*	4	1	11-13	2216	0.85	3.08	*C. wuellerstorfi*
607	*	4	3	11-13	2514	-0.87	4.74	*Uvigerina sp.*
607	*	4	3	88-90	2591	-0.93	4.50	*C. wuellerstorfi*
607	*	4	3	117-119	2620	-0.06	4.30	*C. wuellerstorfi*
607	*	4	4	41-43	2694	0.17	4.03	*C. wuellerstorfi*
607	*	4	4	58-60	2711	-1.13	4.54	*Uvigerina sp.*
607	*	4	4	72-74	2725	-1.00	4.18	*Uvigerina sp.*
607	*	4	4	116-118	2769	0.68	3.48	*C. wuellerstorfi*
607	*	4	5	11-13	2814	1.17	3.02	*C. wuellerstorfi*
607	*	4	5	26-28	2829	0.97	3.06	*C. wuellerstorfi*
607	*	4	5	70-72	2873	0.49	2.88	*C. wuellerstorfi*
607	*	4	5	85-87	2888	-1.08	3.97	*Uvigerina sp.*
607	*	4	5	117-119	2920	-1.75	4.54	*Uvigerina sp.*
607	*	4	5	132-134	2935	-0.08	4.10	*C. wuellerstorfi*
607	*	4	5	146-148	2949	-1.49	4.42	*Uvigerina sp.*
607	*	4	6	11.5-13.5	2965	-0.44	4.16	*Uvigerina sp.*
607	*	4	6	27-29	2980	0.70	3.45	*C. wuellerstorfi*
607	*	4	6	42-44	2995	0.94	3.28	*C. wuellerstorfi*
607	*	4	6	57-59	3010	-0.83	4.00	*Uvigerina sp.*
607	*	4	6	72-74	3025	-1.22	4.17	*Uvigerina sp.*
607	*	4	6	103-105	3056	-1.56	4.58	*Uvigerina sp.*
607	*	4	6	132-134	3085	-0.98	4.36	*Uvigerina sp.*
607	*	4	6	146-148	3099	-1.22	4.28	*Uvigerina sp.*
607	*	4	7	11-13	3114	-1.07	4.23	*Uvigerina sp.*
607	*	5	1	101-103	3348	-0.29	3.47	*Uvigerina sp.*
607	*	5	2	26-28	3423	0.68	3.02	*C. wuellerstorfi*
607	*	5	2	47-49	3444	0.62	2.47	*C. wuellerstorfi*
607	*	5	2	56-58	3453	-0.16	2.91	*C. wuellerstorfi*
607	*	5	2	102-104	3499	-0.59	4.14	*C. wuellerstorfi*

607	*	5	2	117-119	3514	-1.44	4.76	*Uvigerina sp.*
607	*	5	3	11-13	3558	-1.28	4.44	*Uvigerina sp.*
607	*	5	3	26-28	3573	-0.75	4.05	*C. wuellerstorfi*
607	*	5	3	56-58	3603	-0.93	4.58	*Uvigerina sp.*
607	*	5	3	86-88	3633	0.66	3.39	*C. wuellerstorfi*
607	*	5	3	102-104	3649	0.50	3.42	*C. wuellerstorfi*
607	*	5	4	26-28	3723	-1.06	4.29	*Uvigerina sp.*
607	*	5	4	41-43	3738	-0.13	3.85	*C. wuellerstorfi*
607	*	5	4	57-59	3754	-0.02	3.55	*C. wuellerstorfi*
607	*	5	4	87-89	3784	0.37	3.25	*C. wuellerstorfi*
607	*	5	4	102-104	3799	0.28	3.14	*C. wuellerstorfi*
607	*	5	4	117-119	3814	0.82	2.85	*C. wuellerstorfi*
607	*	5	4	131-133	3828	0.76	2.57	*C. wuellerstorfi*
607	*	6	5	39-41	4941	-0.64	4.06	*Uvigerina sp.*
607	*	6	5	84-86	4986	-0.22	3.76	*Uvigerina sp.*
607	*	6	5	114-116	5016	0.78	2.59	*C. wuellerstorfi*
607	*	6	6	9-11	5061	0.05	2.71	*C. wuellerstorfi*
607	*	6	6	39-41	5091	-1.10	4.18	*Uvigerina sp.*
607	*	6	6	68-70	5120	-1.14	4.35	*Uvigerina sp.*
607	*	6	6	97.5-99.5	5150	-0.56	3.72	*Uvigerina sp.*
607	*	6	6	129-131	5181	0.98	3.07	*C. wuellerstorfi*
607	A	7	5	24-26	5249	0.47	3.68	*C. wuellerstorfi*
607	*	7	1	9.5-11.5	5294	0.29	4.00	*Uvigerina sp.*
607	*	7	1	39-41	5324	1.00	2.99	*C. wuellerstorfi*
607	*	7	1	54-56	5339	0.95	2.83	*C. wuellerstorfi*
607	*	7	1	99-101	5384	0.92	3.39	*C. wuellerstorfi*
607	*	7	2	9-11	5444	-0.84	3.97	*Uvigerina sp.*
607	*	7	2	54-56	5489	1.01	3.07	*C. wuellerstorfi*
607	*	7	2	84-86	5519	0.65	2.59	*C. wuellerstorfi*
607	*	7	2	129-131	5564	0.92	2.98	*C. wuellerstorfi*
607	*	9	1	39-41	7310	1.11	2.76	*C. wuellerstorfi*
607	*	9	1	71-73	7342	1.06	3.02	*C. wuellerstorfi*
607	*	9	1	84-86	7355	0.97	3.23	*C. wuellerstorfi*
607	*	9	1	99-101	7370	0.20	3.26	*C. wuellerstorfi*
607	*	9	1	112-114	7383	-0.86	4.14	*Uvigerina sp.*
607	*	9	1	144-146	7415	-0.11	4.08	*Uvigerina sp.*
607	*	9	2	9-11	7430	-0.11	3.63	*Uvigerina sp.*
607	*	9	2	39-41	7460	0.18	3.34	*Uvigerina sp.*
607	*	9	3	9-11	7580	0.55	3.11	*C. wuellerstorfi*
607	*	9	3	24-26	7595	-0.34	3.93	*Uvigerina sp.*
607	*	9	3	54-56	7625	0.81	3.00	*C. wuellerstorfi*
607	*	9	3	69-71	7640	0.63	3.10	*C. wuellerstorfi*

607	*	9	3	83-85	7654	1.13	2.92	*C. wuellerstorfi*
607	*	9	3	100-102	7671	0.93	3.04	*C. wuellerstorfi*
607	*	9	3	144-146	7715	0.98	2.85	*C. wuellerstorfi*

Table 7.3 Late Pliocene-Pleistocene benthic foraminiferal Mg/Ca data for (a) *C. wuellerstorfi* from *Chain* 82-24-23 Piston Core; (b) *C. wuellerstorfi* from DSDP site 607; (c) *Oridorsalis umbonatus* from DSDP site 607; (d) Composite Mg/Ca data from both *Chain* 82-24-23 Piston Core and DSDP site 607. Composite Mg/Ca data are on the LRO4 age model (See chapter 2). MCD is meters composite depth.

a)

	Chain 82-24-23PC
Depth (cm)	*C. wuellerstorfi* **Mg/Ca**
26.5	1.56
40	1.11
45	1.32
50	1.33
55	1.18
60	1.30
75	1.12
80	1.22
85	1.22
90.000	1.20
95.000	1.18
100.000	1.21
105.000	1.19
110	1.23
115	1.18
125	1.07
130	1.30
140	1.15
145	1.27
150	1.24
155	1.22
160	1.25
165	1.16
170	1.17
175	1.21
180	1.28
190	1.36
195	1.30
200.000	1.30
205	1.39
210	1.35
215	1.55

220	1.36
225	1.35
235	1.57
240	1.52
245	1.57
250	1.61
260	1.68
265	1.50
270	1.41
285	1.53
290	1.36
295	1.50
300	1.35
310	1.43
315	1.25
320	1.20
325	1.17

b)

	DSDP site 607
MCD	*C. wuellerstorfi* Mg/Ca
691	1.30
706	0.98
743	0.95
763	1.18
775	1.28
790	1.43
803	1.48
811	1.38
820	1.22
828	1.48
841	1.32
856	1.27
886	1.44
901	1.46
916	1.37
931	1.59
962	1.59
977	1.45
1007	1.08
1023	1.22
1049	1.25
1067	1.33
1080	1.16
1100	1.10
1112	1.43
1128	1.28
1143	1.53
1159	1.33
1172	1.10

1202	1.07
1212	1.17
1232	1.06
1249	1.17
1264	1.41
1279	1.43
1293	1.59
1307	1.33
1319	1.48
1333	1.47
1353	1.46
1368	1.09
1383	1.01
1399	1.27
1415	1.32
1428	1.30
1459	1.07
1481	1.15
1519	1.25
1532	1.15
1546	1.33
1561	1.27
1573	1.40
1585	1.38
1595	1.15
1607	1.33
1621	1.27
1633	1.35
1645	1.39
1662	1.41
1682	1.53
1705	1.64
1721	1.67
1731	1.57
1759	1.28
1835	1.05
1850	1.11
1863	1.12
1878	1.14
1892	1.06
1901	1.10
1913	1.10
1915	1.00
1945	1.03
1959	1.21
1975	1.25
1990	1.23
2006	1.26
2021	1.30
2051	1.40

2096	1.32
2125	1.27
2140	1.26
2155	1.32
2170	1.44
2183	1.34
2186	1.54
2213	1.58
2215	1.47
2230	1.46
2238	1.62
2243	1.36
2259	1.39
2274	1.41
2304	1.74
2320	1.55
2335	1.43
2350	1.52
2364	1.51
2380	1.31
2410	1.81
2423	1.61
2469	1.64
2483	1.33
2559	1.15
2591	1.17
2606	1.14
2620	1.26
2664	1.04
2679	1.12
2694	1.32
2725	1.07
2754	1.24
2769	1.27
2784	1.34
2799	1.53
2814	1.56
2829	1.67
2858	1.43
2873	1.69
2888	1.18
2904	1.26
2920	1.22
2949	1.13
2964	1.45
2980	1.50
2995	1.50
3010	1.39
3025	1.44
3056	1.14

3085	1.19
3099	1.09
3114	1.06
3158	1.44
3182	1.59
3211	1.51
3199	1.64
3228	1.18
3259	0.96
3274	1.02
3304	1.23
3334	1.31
3349	1.30
3364	1.49
3394	1.50
3409	1.28
3470	1.64
3485	1.27
3515	1.28
3544	0.92
3604	1.63
3634	1.35
3650	1.36
3664	1.45
3679	1.26
3724	1.11
3739	1.06
3755	1.18
3770	1.30
3785	1.15
3815	1.45
3829	1.45
3859	1.52
3891	1.32
3906	1.32
3921	1.41
3939	1.39
3954	1.37
3969	1.31
3983	1.42
3995	1.29
4025	1.54
4056	1.49
4072	1.33
4087	1.31
4101	1.32
4116	1.41
4144	1.34
4178	1.55
4193	1.63

4208	1.39
4223	1.46
4238	1.74
4253	1.47
4268	1.49
4283	1.51
4298	1.22
4312	1.32
4327	1.31
4338	1.31
4372	1.58
4384	1.56
4404	1.67
4431	1.62
4461	1.85
4476	1.44
4489	1.55
4521	1.26
4536	1.48
4553	1.71
4566	1.69
4596	1.48
4612	1.35
4627	1.47
4639	1.36
4658	1.44
4686	1.50
4733	1.61
4761	1.81
4776	1.82
4790	1.52
4798	1.66
4836	1.61
4852	1.58
4866	1.59
4896	1.27
4941	1.28
4971	1.59
4986	1.44
5003	1.67
5031	1.73
5046	1.74
5061	1.88
5076	1.39
5120	1.44
5136	1.28
5150	1.39
5166	1.49
5234	1.78
5249	1.47

5264	1.38
5294	1.59
5324	1.60
5339	1.66
5506	1.56
5519	1.58
5534	1.44
5549	1.54
5564	1.83
5579	1.45
5594	1.64
5684	1.43
5699	1.55
5714	1.52
5802	1.39
5834	1.49
5864	1.62
5879	1.71
5894	1.63
5923	1.45
5954	1.32
5969	1.36
5984	1.73
5999	1.67
6014	1.70
6029	1.72
6044	1.62
6059	1.61
6072	1.74
6087	1.51
6149	1.63
6164	1.71
6179	1.67
6194	1.65
6207	1.80
6318	1.66
6331	1.75
6349	1.48
6378	1.69
6393	1.70
6423	1.52
6438	1.57
6454	1.51
6485	1.56
6498	1.87
6513	1.50
6528	1.65
6543	1.51
6573	1.43
6588	1.68

6603	1.62
6618	1.66
6634	1.68
6648	1.91
6678	1.51
6693	1.70
6708	1.64
6723	1.25
6738	1.60
6753	1.73
6768	1.73
6783	1.67
6813	1.54
6828	1.67
6843	1.73
6858	1.76
6873	1.57
6888	1.75
6901	1.68
6918	1.67
6933	1.73
6948	1.78
6963	1.85
6978	1.80
6993	1.93
7008	1.36
7023	1.51
7038	1.48
7053	1.60
7068	1.73
7083	1.50
7113	1.30
7128	1.64
7143	1.76
7325	1.49
7342	1.63
7355	1.77
7383	1.57
7445	1.92
7460	1.69
7474	1.81
7489	1.75
7520	1.52
7535	1.67
7550	1.63
7565	1.51
7595	1.29
7609	1.64
7625	1.59
7640	1.57

7654	1.65
7671	1.56
7685	1.69
7700	1.61
7715	1.81
7730	1.59
7790	1.91
7835	2.00
7865	1.91
7895	1.67
7910	1.72
7940	1.51
7955	1.54
7970	1.95
7985	1.37
8000	1.43
8015	1.49
8030	1.47
8045	1.53
8060	1.59
8075	1.58
8105	2.09
8135	1.37
8150	1.37
8180	1.23
8264	1.60
8294	1.62
8339	1.50
8355	1.57
8369	1.42
8384	1.31
8399	1.64
8414	1.60
8429	1.63
8442	1.77
8489	1.55
8504	1.73
8519	1.83
8549	1.54
8564	1.69
8579	1.67
8669	1.79
8684	1.34
8699	1.51
8714	1.38
8730	1.37
8759	1.53
8774	1.54
8787	1.60
8819	1.54

8849	1.55
8864	1.43
8879	1.65
8894	1.41
8909	1.62
8939	1.43
8984	1.53
8999	1.66
9014	1.48
9028	1.55
9119	1.44
9164	1.70
9291	1.51
9305	1.50
9335	1.42
9351	1.57
9365	1.60
9379	1.55
9395	1.66
9408	1.78
9425	1.46
9453	1.40
9500	1.13
9500	1.48
9515	1.71
9558	1.60
9575	1.53
9605	1.60
9665	1.32
9695	1.59
9725	1.65
9755	1.62
9770	1.62
9815	1.48
9845	1.36
9905	1.72
9933	1.66
9978	1.53
10055	1.56
10086	1.60
10100	1.43
10130	1.53
10145	1.42
10175	1.52
10190	1.54
10329	1.47
10344	1.46
10494	1.71
10539	1.53
10554	1.60

10569	1.82
10584	1.36
10599	1.37
10644	1.46
10734	1.87
10779	1.22
10854	1.56
10869	1.69
10884	1.69
10914	1.53
10929	1.35
10947	1.61
10959	1.69
11004	1.66
11019	1.43
11049	1.54
11064	1.78
11081	1.51
11094	1.59
11109	1.58
11142	1.49
11176	1.52
11189	1.68
11202	1.40
11353	1.71
11367	1.35
11406	1.58
11428	1.36
11444	1.45
11459	1.44
11488	1.53
11501	1.48
11526	1.42
11634	1.50
11698	1.58
11751	1.92
11764	1.39
11778	1.36
11804	1.64
11831	1.53
11844	1.53
11858	1.68
11871	1.45
11900	1.78
11942	1.72
11956	1.70
12016	1.55
12089	2.10
12104	1.49
12149	1.59

12164	1.69
12179	1.45
12194	1.91
12224	1.54
12314	1.56
12332	1.60
12384	1.82
12419	1.59
12435	1.60
12449	1.57
12482	1.65
12497	1.79
12510	1.58
12524	1.93
12539	1.84
12554	2.08
12568	2.07
12579	2.02
12592	1.84
12645	1.86
12660	1.78
12676	1.66
12714	1.90
12764	1.80
12795	1.77
12810	1.88
12826	1.88
12855	1.55
12869	1.58
12883	1.78
12896	2.10
12914	1.69
12932	1.82
12946	1.57
12960	1.59
12977	1.93
12989	1.96
13007	1.69
13020	1.67
13036	1.88
13051	1.91
13085	1.83
13126	1.89
13146	1.81
13188	2.02
13294	1.81
13299	1.80
13312	1.96
13351	1.86

c)

DSDP site 607

MCD	*O. umbonatus* Mg/Ca
683	1.25
706	1.21
736	1.16
790	1.64
811	1.56
856	1.36
866	1.24
901	1.23
1007	1.26
1100	1.52
1128	1.74
1172	1.35
1202	1.45
1212	1.59
1232	1.30
1264	1.42
1368	1.51
1415	1.73
1443	1.63
1471	1.37
1481	1.31
1505	1.53
1519	1.43
1595	1.41
1607	1.57
1621	1.50
1645	1.71
1662	1.90
1682	1.95
1773	1.29
1788	1.33
1805	1.22
1820	1.53
1892	1.22
1901	1.21
1913	1.48
1915	1.52
1945	1.26
1959	1.47
1990	1.41
2006	1.55
2066	1.42
2140	1.82
2170	1.66
2183	1.67
2213	1.72
2215	1.65

2228	1.45
2230	1.77
2259	1.52
2274	1.68
2514	1.42
2529	1.49
2559	1.58
2591	1.72
2620	1.45
2664	1.54
2679	1.55
2694	1.72
2711	1.36
2725	1.38
2754	1.51
2769	1.47
2904	1.30
2920	1.10
3056	1.27
3085	1.38
3259	1.44
3394	1.57
3445	1.46
3634	1.56
3650	1.43
3739	1.31
3755	1.36
3785	1.45
3800	1.64
3815	1.61
3891	1.60
3939	1.41
3954	1.57
3969	1.61
3995	1.41
4009	1.40
4025	1.75
4116	1.43
4131	1.59
4268	1.74
4283	1.51
4298	1.58
4327	1.44
4338	1.41
4384	1.87
4404	1.90
4416	1.75
4461	1.65
4476	1.85
4489	1.65

4509	1.46
4521	1.53
4536	1.80
4553	1.52
4566	1.50
4581	1.57
4627	1.61
4639	1.46
4658	1.81
4672	1.56
4686	1.52
4702	2.01
4821	1.89
4836	1.77
4896	1.51
4941	1.51
4956	1.55
4971	1.37
4986	1.74
5003	1.59
5016	1.77
5046	1.69
5061	1.82
5076	1.55
5091	1.38
5120	1.27
5136	1.38
5150	1.49
5166	1.68
5181	1.57
5234	1.70
5249	1.85
5264	1.66
5294	1.61
5324	1.64
5339	1.80
5384	1.61
5429	1.26
5444	1.36
5459	1.48
5489	1.61
5506	1.60
5534	1.67
5579	1.99
5594	1.52
5609	1.51
5624	1.55
5638	1.53
5654	1.55
5654	1.76

5669	1.53
5669	1.68
5684	1.61
5699	1.89
5714	1.91
5759	1.39
5774	1.51
5788	1.53
5802	1.71
5819	1.63
5834	1.72
5849	1.90
5864	1.94
5879	1.84
5894	1.85
5954	1.47
5969	1.60
5999	1.65
6014	1.94
6029	1.86
6044	1.96
6059	1.92
6102	1.79
6119	1.62
6134	1.47
6149	1.67
6164	1.59
6179	1.94
6302	1.29
6331	1.90
6349	1.64
6360	1.49
6378	1.89
6407	1.78
6423	2.04
6438	1.57
6454	1.91
6468	1.51
6498	1.86
6543	1.86
6588	1.78
6603	1.64
6618	1.66
6648	1.83
6663	1.76
6693	1.81
6708	1.54
6723	1.72
6738	1.99
6753	1.94

6768	1.63
6783	1.77
6798	2.10
6813	1.60
6843	1.62
6858	1.60
6873	1.60
6888	1.71
6901	1.64
6918	1.88
6933	1.90
6963	2.02
7008	1.77
7023	1.48
7038	1.51
7053	1.44
7068	1.91
7083	1.70
7113	1.72
7128	1.62
7143	1.71
7355	1.82
7370	1.58
7383	1.48
7400	1.75
7415	1.56
7430	1.48
7460	1.97
7474	1.66
7550	1.72
7565	1.71
7580	1.62
7595	1.47
7625	2.25
7640	1.87
7654	1.78
7805	2.25
7895	1.61
7910	1.61
7925	1.47
7940	1.37
7955	1.43
7970	1.73
7985	1.70
8000	1.47
8015	1.79
8030	1.69
8045	1.81
8060	2.06
8105	1.85

8120	1.47
8135	1.82
8310	1.64
8339	1.79
8355	1.53
8669	1.68
8684	1.51
8699	1.35
8714	1.25
8730	1.38
8744	1.46
8759	1.86
8774	1.71
8787	1.62
8924	1.63
8939	1.49
9028	1.84
9044	1.56
9059	1.48
9074	1.36
9089	1.36
9104	1.54
9119	1.44
9395	1.93
9453	1.40
9515	1.94
9635	1.68
9650	1.53
9665	1.50
9680	1.46
9695	1.78
9710	1.78
9725	1.88
9740	1.78
9800	1.58
9830	1.82
9875	1.52
9905	1.87
9919	1.77
9933	1.83
9950	1.83
9978	1.48
9995	1.60
10010	1.51
10025	1.45
10039	1.63
10055	1.77
10069	1.83
10086	1.76
10100	1.87

10114	1.76
10130	1.88
10161	1.69
10175	1.75
10344	2.08
10359	1.44
10374	1.52
10389	1.70
10404	1.58
10419	1.39
10434	1.44
10449	1.58
10464	1.39
10479	1.50
10614	1.99
10629	1.48
10659	1.64
10749	1.49
10764	1.54
10779	1.52
10794	1.53
10809	1.55
10827	1.55
10839	1.54
10869	1.96
10884	1.93
10914	1.94
10947	1.76
11034	1.89
11049	1.83
11064	1.95
11081	1.88
11094	2.07
11176	1.53
11189	2.07
11202	1.68
11394	1.61
11444	1.59
11459	1.65
11488	1.77
11526	1.65
11538	1.56
11551	1.45
11566	1.42
11592	1.32
11608	1.57
11620	1.51
11634	1.54
11646	1.68
11659	1.91

11670	2.07
11683	2.16
11698	2.17
11706	1.95
11721	1.96
11737	2.07
11790	1.93
11817	2.01
11831	1.84
11844	1.61
11858	1.52
11871	1.65
11885	1.75
12003	2.22
12016	1.97
12149	1.66
12164	1.58
12179	1.71
12209	1.91
12350	2.16
12370	1.90
12466	1.85
12482	1.74
12539	2.04
12579	2.01
12592	2.12
12616	2.23
12676	2.23
12697	1.81
12728	2.00
12742	2.03
12764	1.72
12780	1.94
12795	2.16
12810	1.75
12826	1.53
12869	1.93
12896	2.21
12946	1.85
12960	1.93
12977	1.67
13036	1.92
13051	2.01
13066	1.91
13085	2.13
13111	2.10
13146	1.96
13178	1.87
13294	1.74
13299	2.33

13312	2.28
13335	2.22
13351	1.88
13365	1.90

<u>d)</u>

Age (ka)	Composite Mg/Ca
10.4	1.57
20.0	1.08
22.0	1.30
24.1	1.32
26.1	1.16
28.1	1.29
34.2	1.09
36.2	1.20
38.3	1.20
40.3	1.18
42.3	1.16
44.4	1.18
46.4	1.17
48.4	1.21
50.4	1.16
54.5	1.04
56.5	1.29
60.6	1.12
62.6	1.26
64.6	1.23
66.7	1.20
68.7	1.23
70.7	1.14
72.8	1.15
74.8	1.19
76.8	1.27
80.9	1.35
82.9	1.28
85.6	1.29
88.3	1.38
90.9	1.34
93.6	1.55
96.3	1.35
99.0	1.34
104.3	1.58
107.0	1.52
109.7	1.57
111.9	1.63
116.4	1.70
118.6	1.50
120.8	1.41
127.9	1.54
130.3	1.35

132.7	1.51
135.1	1.35
140.0	1.43
142.3	1.23
144.5	1.17
146.8	1.15
153.5	1.10
154.8	1.04
157.2	1.29
162.0	1.11
171.5	1.08
173.6	1.05
179.5	1.16
183.1	1.27
187.6	1.44
191.5	1.48
194.2	1.37
197.2	1.20
200.3	1.48
205.8	1.31
211.3	1.25
226.3	1.44
235.1	1.46
243.3	1.37
248.5	1.60
255.2	39.43
258.3	39.89
263.9	40.73
270.2	41.68
272.7	42.06
274.5	42.33
277.3	42.75
279.3	43.05
281.9	43.44
285.0	43.90
292.1	44.97
298.9	45.99
301.5	46.37
312.8	48.07
317.5	48.78
325.4	49.96
329.0	50.49
331.7	50.90
342.9	52.59
346.6	53.14
350.0	53.65
352.9	54.08
357.6	54.80
360.4	55.20
362.4	55.51

364.1	55.76
368.5	56.43
371.7	56.91
374.8	57.37
378.7	57.95
383.1	58.61
386.4	59.11
391.6	59.89
394.2	60.27
397.1	60.72
399.7	61.10
402.2	61.48
406.0	62.04
411.1	62.82
417.0	63.69
420.4	64.21
422.5	1.58
427.9	1.27
430.5	1.27
433.4	1.13
436.6	1.19
439.1	1.34
441.8	1.20
444.9	1.27
448.7	1.10
453.9	1.11
458.7	1.20
461.7	1.22
465.7	1.25
466.2	1.14
472.4	1.03
475.5	1.23
480.8	1.23
488.0	1.21
497.0	1.24
507.0	1.28
527.4	1.39
536.1	1.23
548.7	1.31
561.3	1.25
570.5	1.24
578.4	1.31
584.3	1.45
588.7	1.49
589.6	1.55
598.2	1.57
598.8	1.47
601.9	1.26
602.2	1.53
603.5	1.64

604.2	1.36
606.2	1.36
607.6	1.46
610.1	1.77
611.5	1.55
612.7	1.43
614.0	1.52
615.1	1.52
616.4	1.30
618.9	1.84
620.1	1.63
625.4	1.66
627.1	1.32
631.3	1.22
633.5	1.30
637.9	1.12
643.6	1.15
646.4	1.11
649.0	1.25
657.7	1.18
661.3	1.09
670.3	1.16
674.5	1.18
682.2	1.27
685.3	1.27
688.3	1.33
691.4	1.53
694.4	1.56
697.6	1.69
703.6	1.43
707.3	1.71
711.1	1.16
715.0	1.17
718.6	1.20
724.5	1.27
727.8	1.44
731.2	1.50
734.5	1.50
737.8	1.39
741.1	1.44
746.8	1.09
753.4	1.17
757.4	1.22
762.2	1.19
775.1	1.44
781.6	1.61
786.2	1.66
789.5	1.51
794.1	1.16
802.4	1.27

805.5	1.17
812.3	1.21
821.8	1.30
827.1	1.29
832.9	1.49
845.5	1.38
851.1	1.26
863.1	1.27
869.2	1.65
872.8	1.25
880.6	1.26
888.3	1.06
902.3	1.64
908.0	1.36
910.9	1.35
913.3	1.45
916.0	1.24
924.7	1.08
928.0	1.07
932.0	1.16
935.8	1.29
939.1	1.19
942.2	1.46
945.3	1.44
948.2	1.45
954.4	1.52
963.3	1.36
967.0	1.31
970.5	1.41
974.6	1.39
978.2	1.37
981.6	1.36
984.9	1.42
987.7	1.24
990.8	1.20
994.0	1.57
999.6	1.50
1003.6	1.32
1007.7	1.30
1011.3	1.31
1014.7	1.40
1017.8	1.40
1026.8	1.56
1029.9	1.65
1032.9	1.39
1036.0	1.47
1039.0	1.76
1042.0	1.47
1045.1	1.49
1048.1	1.28

1053.9	1.31
1056.9	1.43
1059.3	1.31
1066.9	1.59
1070.2	1.71
1075.6	1.75
1078.9	1.58
1082.9	1.64
1091.2	1.64
1095.5	1.34
1099.2	1.54
1104.5	1.27
1107.0	1.36
1110.0	1.48
1113.3	1.58
1116.6	1.59
1120.5	1.38
1124.9	1.48
1129.9	1.34
1134.6	1.40
1138.3	1.34
1144.3	1.18
1148.4	1.38
1152.6	1.40
1156.9	1.87
1174.5	1.86
1178.5	1.68
1182.6	1.73
1185.4	1.52
1188.6	1.60
1198.4	1.26
1208.1	1.30
1216.8	1.60
1227.5	1.50
1231.4	1.60
1235.6	1.76
1239.2	1.55
1242.4	1.54
1245.4	1.39
1248.0	1.18
1252.2	1.44
1254.4	1.48
1256.0	1.52
1258.0	1.43
1259.6	1.39
1266.3	1.49
1268.5	1.49
1270.5	1.40
1274.8	1.56
1280.3	1.65

1283.8	1.58
1300.6	1.43
1334.7	1.28
1345.2	1.43
1349.2	1.49
1352.1	1.59
1355.5	1.46
1358.7	1.54
1361.8	1.87
1364.7	1.64
1367.6	1.49
1370.4	1.32
1373.4	1.36
1376.0	1.34
1379.5	1.48
1383.0	1.42
1386.9	1.43
1391.2	1.64
1395.9	1.64
1409.0	1.19
1413.4	1.32
1417.5	1.34
1421.5	1.46
1427.0	1.45
1432.4	1.52
1438.0	1.74
1443.6	1.63
1448.1	1.71
1452.1	1.67
1457.8	1.44
1463.8	1.29
1466.7	1.35
1472.7	1.58
1475.8	1.76
1479.5	1.72
1483.4	1.81
1487.5	1.70
1495.5	1.52
1498.9	1.62
1502.3	1.44
1505.5	1.28
1508.7	1.57
1512.7	1.73
1517.1	1.79
1521.8	1.67
1525.9	1.84
1548.3	1.57
1554.1	1.37
1556.1	1.20
1559.6	1.62

1568.0	1.61
1570.6	1.38
1573.1	1.53
1575.3	1.21
1579.9	1.71
1585.1	1.57
1587.9	1.50
1597.5	1.56
1601.0	1.45
1604.5	1.48
1611.6	1.71
1615.2	1.49
1618.7	1.41
1622.3	1.59
1625.8	1.41
1629.5	1.29
1633.7	1.63
1638.0	1.67
1642.0	1.50
1645.5	1.55
1648.9	1.86
1652.0	1.38
1655.1	1.59
1658.3	1.50
1661.7	1.50
1665.2	1.40
1668.5	1.55
1671.2	1.48
1674.7	1.61
1677.8	1.65
1681.0	1.71
1684.6	1.78
1688.9	1.74
1693.6	1.88
1699.5	1.38
1708.2	1.30
1717.5	1.29
1726.5	1.32
1735.3	1.67
1744.1	1.41
1754.4	1.31
1757.1	1.44
1759.4	1.56
1779.4	1.39
1781.7	1.54
1783.6	1.62
1785.6	1.29
1787.6	1.35
1790.5	1.48
1794.1	1.26

1798.3	1.19
1802.8	1.86
1807.4	1.66
1811.7	1.55
1817.4	1.67
1833.3	1.42
1841.6	1.60
1848.4	1.53
1854.7	1.42
1860.8	1.42
1866.9	1.27
1872.6	1.66
1879.2	1.86
1885.0	1.65
1890.2	1.64
1896.5	1.58
1901.2	1.71
1906.1	1.63
1910.6	1.85
1914.7	1.59
1928.3	1.96
1931.0	2.11
1936.1	2.05
1940.5	1.96
1944.9	1.56
1947.1	1.59
1949.3	1.28
1951.5	1.34
1953.9	1.39
1956.5	1.78
1959.3	1.45
1962.3	1.35
1965.3	1.56
1968.3	1.49
1971.4	1.59
1975.0	1.76
1978.7	1.58
1986.3	1.70
1989.6	1.28
1992.5	1.51
1995.2	1.36
2000.1	1.22
2009.7	1.62
2012.6	1.64
2014.1	1.46
2016.8	1.57
2018.3	1.46
2019.7	1.42
2021.1	1.30
2022.6	1.66

2024.5	1.62
2026.6	1.64
2028.4	1.80
2035.2	1.56
2037.5	1.76
2040.0	1.87
2045.2	1.55
2047.8	1.71
2050.4	1.70
2066.2	1.66
2069.2	1.32
2072.2	1.33
2075.1	1.21
2078.3	1.27
2081.2	1.26
2084.2	1.62
2087.2	1.54
2089.7	1.52
2095.9	1.54
2102.0	1.55
2105.0	1.43
2108.1	1.67
2111.2	1.40
2114.2	1.64
2117.4	1.45
2120.6	1.57
2136.2	1.48
2144.1	1.62
2148.1	1.37
2151.8	1.29
2161.2	1.35
2164.5	1.39
2209.8	1.52
2213.4	1.50
2220.2	1.41
2223.3	1.58
2225.7	1.61
2228.2	1.56
2230.9	1.73
2233.3	1.81
2236.5	1.46
2241.7	1.29
2253.4	1.76
2261.5	1.61
2265.0	1.54
2272.1	1.61
2279.1	1.51
2282.6	1.34
2286.1	1.31
2289.7	1.27

2293.0	1.61
2296.4	1.61
2299.7	1.70
2303.1	1.62
2306.5	1.65
2309.9	1.64
2316.6	1.39
2320.0	1.48
2323.4	1.66
2326.8	1.36
2333.8	1.32
2340.5	1.73
2343.4	1.59
2346.1	1.60
2349.5	1.69
2355.1	1.42
2358.4	1.42
2361.4	1.32
2364.4	1.25
2367.2	1.45
2370.4	1.59
2373.5	1.66
2377.3	1.60
2380.3	1.57
2383.5	1.60
2386.8	1.63
2389.7	1.42
2392.6	1.52
2394.9	1.57
2423.5	1.47
2426.6	1.70
2429.2	1.24
2431.8	1.33
2434.4	1.53
2437.3	1.39
2440.2	1.19
2443.1	1.25
2445.9	1.40
2448.7	1.19
2451.5	1.31
2454.7	1.73
2466.0	1.54
2469.9	1.62
2473.8	1.85
2477.4	1.35
2480.5	1.36
2483.4	1.85
2486.3	1.28
2489.1	1.46
2492.0	1.46

2508.3	1.92
2512.5	1.29
2516.5	1.35
2520.1	1.26
2523.1	1.34
2526.1	1.36
2529.9	1.36
2533.3	1.35
2537.8	1.57
2542.5	1.76
2547.2	1.75
2556.6	1.66
2560.6	1.34
2565.0	1.61
2567.5	1.71
2576.2	1.68
2579.1	1.43
2582.1	1.73
2585.0	1.60
2587.8	1.81
2590.9	1.62
2593.1	1.77
2595.7	1.59
2601.8	1.50
2609.2	1.43
2612.1	1.82
2615.7	1.45
2665.9	1.43
2680.0	1.41
2683.8	1.48
2689.3	1.60
2696.0	1.47
2698.3	1.38
2701.0	1.25
2704.0	1.22
2713.2	1.38
2715.8	1.32
2718.6	1.35
2721.4	1.51
2724.7	1.76
2728.0	1.93
2731.9	2.04
2736.5	2.04
2739.1	1.80
2744.8	1.81
2751.4	1.93
2771.2	1.78
2774.6	1.66
2777.2	1.87
2780.0	1.61

2783.0	1.48
2786.2	1.51
2789.1	1.46
2792.2	1.58
2795.5	1.81
2804.0	1.74
2806.5	1.73
2817.9	2.10
2821.0	1.69
2846.4	1.49
2859.9	1.54
2864.1	1.56
2867.9	1.49
2871.1	1.96
2874.4	1.75
2877.6	1.55
2895.2	1.57
2898.5	1.61
2901.9	2.03
2905.9	1.75
2909.4	1.85
2919.1	1.60
2923.5	1.61
2927.3	1.58
2931.9	1.69
2935.4	1.62
2938.5	1.82
2941.1	1.59
2943.9	1.98
2946.9	1.89
2949.8	2.15
2952.5	2.14
2954.5	1.97
2957.0	1.93
2962.7	2.12
2970.2	1.90
2973.8	1.81
2977.3	1.90
2982.0	1.65
2985.7	1.94
2988.9	1.86
2991.9	1.89
2997.1	1.69
3000.8	1.79
3004.4	1.92
3009.0	1.75
3014.0	1.63
3022.5	1.56
3026.5	1.68
3030.4	1.81

3033.6	2.17
3038.0	1.72
3042.6	1.86
3046.2	1.63
3049.8	1.69
3053.8	1.73
3056.4	2.01
3060.2	1.71
3063.1	1.69
3066.5	1.85
3070.2	1.91
3074.1	1.75
3079.2	1.94
3085.9	1.97
3089.5	1.93
3094.4	1.83
3103.9	1.72
3107.0	2.08
3145.5	1.71
3146.7	2.03
3149.6	2.09
3154.1	2.10
3157.3	1.81
3160.1	1.75

8.**Curriculum Vita**

 8.1 Colleges Attended
Ph.D**.** Rutgers University (2008) Institute of Marine and Coastal Sciences, New Jersey, USA, Title: Climate Transitions across the Cenozoic, Advisor: Dr. Yair Rosenthal, Committee: Dr. Tony Broccoli, Dr. Ken Miller, Dr Jim Wright, and Dr. Maureen Raymo

B.Sc. cum laude Monmouth University (2008), New Jersey, major in chemistry

8.2 Professional Experience
2007-2008   USSSP Schlanger Ocean Drilling Fellow
2004-2007   Graduate Assistant, Institute of Marine and Coastal Sciences, *Rutgers University*
2007   Summer Graduate student participant, Focus: Culturing planktonic foraminifera, USC Wrigley Institute of Environmental Studies, Catalina, CA
2003   Summer Graduate student participant, Focus: Paleoclimate: combining observations and dynamics, *Grand Combin Summer School*, Aosta, Italy
2003-2004   Teaching Assistant, Chemical Oceanography, Institute of Marine and Coastal Sciences, *Rutgers University*
2002-2003   Graduate Assistant, Institute of Marine and Coastal Sciences, *Rutgers University*
2001   Summer Undergraduate Research Fellow, Advisor: Dr. Lisa Tauxe, Focus: Paleomagnetism, Scripps Institution of Oceanography, *University of California, San Diego*

8. 3 Publications
M. Greaves, N. Caillon, H. Rebaubier, G. Bartoli, S. Bohaty, I. Cacho, L. Clarke, M. Cooper, C. Daunt, M. Delaney, P. deMenocal, A. Dutton, S. Eggins, H. Elderfield, D. Garbe-Schoenberg, E. Goddard, D. Green, J. Groeneveld, D. Hastings, E. Hathorne, K. Kimoto, G. Klinkhammer, L. Labeyrie, D. W. Lea, T. Marchitto, M. A. Martínez-Botí, P. G. Mortyn, Y. Ni, D. Nuernberg, G. Paradis, L. Pena, T. Quinn, Y. Rosenthal, A. Russell, T. Sagawa, **S. Sosdian**, L. Stott, K. Tachikawa, E. Tappa, R. Thunell, P. A. Wilson, (2008), Interlaboratory comparison study of calibration standards for foraminiferal Mg/Ca thermometry, *Geochem. Geophys. Geosyst,* 9, Q08010, doi:10.1029/2008GC001974

Gentry, D. K., **S. Sosdian,** E.L. Grossman, Y. Rosenthal, D. Hicks, and C.H. Lear (2008), Stable Isotope and Sr/Ca Profiles from the Marine Gastropod Conus ermineus: Testing a Multi-proxy Approach for Inferring Paleotemperature and Paleosalinity, *Palios,* 23, 195-209

Sosdian S., D. K. Gentry, C. H. Lear, E. L. Grossman, D. Hicks, Y. Rosenthal (2006), Strontium to calcium ratios in the marine gastropod Conus ermineus : Growth rate effects and temperature calibration, *Geochem. Geophys. Geosyst*., 7, Q11023, doi:10.1029/2005
Andreasen D. H**., S. Sosdian**, S. Perron-Cashman, C. H. Lear, T. deGaridel-Thoron, P. Field, Y. Rosenthal (2006), Fidelity of radially viewed ICP-OES and magnetic-sector

ICP-MS measurement of Mg/Ca and Sr/Ca ratios in marine biogenic carbonates: Are they trustworthy together?, Geochem. Geophys. Geosyst., 7, Q10P18, doi:10.1029/2005GC001124.